JACC
Basic to Translational Science

A Journal of the American College of Cardiology

JACC
Basic to Translational Science
A Journal of the American College of Cardiology

CORRESPONDENCE FOR AMERICAN COLLEGE OF CARDIOLOGY

All correspondence for the College, other than that related to *JACC: Basic to Translational Science* should be sent to Resource Center, American College of Cardiology, 2400 N Street, NW, Washington, DC 20037

JACC: BASIC TO TRANSLATIONAL SCIENCE VOL. 4, NO. 4, 2019

PRECLINICAL RESEARCH

Female Authorship in Preclinical Cardiovascular Research

Temporal Trends and Influence on Experimental Design

Alisha Labinaz,[a,b,c] Jeffrey A. Marbach, MBBS,[a,d] Richard G. Jung, BSc,[a,b,e,f] Robert Moreland, MD,[a,g] Pouya Motazedian, MD,[a,h] Pietro Di Santo, MD,[a,d,i] Aisling A. Clancy, MD, MSc,[j,k] Zachary MacDonald, MD,[l] Trevor Simard, MD,[a,b,d,e] Benjamin Hibbert, MD, PhD,[a,b,d,e] F. Daniel Ramirez, MD[a,d,i]

VISUAL ABSTRACT

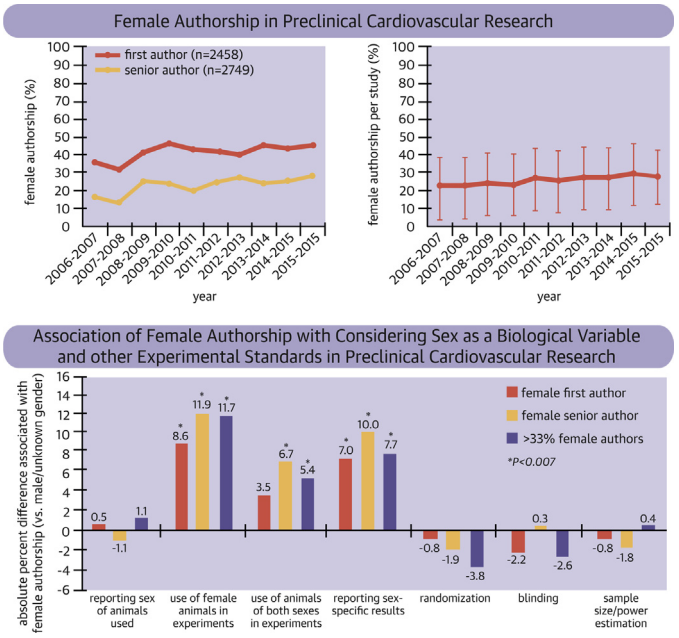

Labinaz, A. et al. J Am Coll Cardiol Basic Trans Science. 2019;4(4):471–7.

HIGHLIGHTS

- **In this analysis of 3,396 preclinical studies published in 5 leading cardiovascular journals over a 10-year period, women accounted for 24 ± 17% of authors per manuscript.**
- **Female authorship is increasing in preclinical cardiovascular science, but the proportions of articles with first and senior authors of different sex have remained unchanged, which suggests that segregation by sex in mentorship relationships exists and persists.**
- **In preclinical studies that reported the sex of the animals used, female authorship was positively associated with studying female animals, using animals of both sexes, and reporting sex-specific results, which are findings that persisted in adjusted and sensitivity analyses.**
- **Author sex was not associated with other measures of methodological rigor or with 60-month citation counts.**

From the [a]CAPITAL Research Group, University of Ottawa Heart Institute, Ottawa, Ontario, Canada; [b]Vascular Biology and Experimental Medicine Laboratory, University of Ottawa Heart Institute, Ottawa, Ontario, Canada; [c]Faculty of Science, University of Ottawa, Ottawa, Ontario, Canada; [d]Division of Cardiology, University of Ottawa Heart Institute, Ottawa, Ontario, Canada; [e]Department of Cellular and Molecular Medicine, University of Ottawa, Ottawa, Ontario, Canada; [f]Faculty of Medicine, University of Ottawa, Ottawa, Ontario, Canada; [g]Department of Radiology, Brigham and Women's Hospital, Harvard Medical School, Boston, Massachusetts; [h]Department of Medicine, University of Calgary Cumming School of Medicine, Calgary, Alberta, Canada; [i]School of Epidemiology and Public Health, University of Ottawa, Ottawa, Ontario, Canada; [j]Department of Obstetrics and Gynecology, University of Ottawa, Ottawa, Ontario, Canada; [k]Department of Epidemiology, Harvard T.H. Chan School of Public Health, Boston, Massachusetts; and the [l]Department of Emergency Medicine, University of Ottawa, Ottawa, Ontario, Canada. Dr. Jung was supported by the Canadian Institutes of Health Research (CIHR). Dr. Ramirez was supported by CIHR, the University of Ottawa Heart Institute Foundation, the Ernest and Margaret Ford Research Endowed Fund, and the Cardiac Arrhythmia Network of Canada (CANet) as part of the Networks of Centres of Excellence. All other authors have reported that they have no relationships relevant to the contents of this paper to disclose.

ISSN 2452-302X https://doi.org/10.1016/j.jacbts.2019.04.004

ABBREVIATIONS AND ACRONYMS

CI = confidence interval

NIH = National Institutes of Health

OR = odds ratio

SUMMARY

In this analysis of 3,396 preclinical cardiovascular studies, women were first, senior, and both first and senior authors in 41.3%, 20.7%, and 11.0% of the studies, respectively. Female authorship increased over a 10-year period. However, the proportion of studies with first and senior authors of differing sex was low and stable, suggesting that segregation by sex in mentorship relationships exists and persists. Female authors were more likely to consider sex as a biological variable, but author sex was not associated with other measures of experimental rigor or research impact, indicating that women's underrepresentation was not due to differences in research capacity or impact. (J Am Coll Cardiol Basic Trans Science 2019;4:471–7)

The now outdated axiom that cardiovascular disease is a disease of men began to be meaningfully challenged in the 1980s, with considerable effort focused on adequately representing women in clinical trials. Central to many of these initiatives was (and continues to be) the recognition that fundamental yet poorly understood differences exist between men and women, and that these differences could engender health disparities if ignored. However, this "revolution" has not permeated preclinical stages of research, which serve to inform clinical trials. The preferential use of male animals and a lack of sex-disaggregated reporting is increasing in cardiovascular science (1), despite the emphasis of the National Institutes of Health (NIH) on considering sex in preclinical research as important for advancing the health of women (2) and despite its feasibility in most research settings (3). This bias has the potential to undermine advances made in clinical trial design by skewing our understanding of disease processes and the effectiveness of potential therapies (4).

SEE PAGE 478

It has been argued that the participation of women in research enhances knowledge outcomes and scientific progress (5), in part via enhanced exploration of sex differences (6). If true, sex gaps in medicine and research—including the underrepresentation of women in fields such as cardiology (7) and the relative lack of adequate mentorship for women (8)—would not only have important societal implications but also meaningful scientific ramifications. Recognizing this possibility, the NIH has emphasized their commitment to diversity in the biomedical research workforce (including better representation of women) and identified assessing the impact of this diversity on the quality and outputs of research as 1 of 4 major diversity challenges facing the biomedical "ecosystem" (9).

We therefore examined a large body of leading preclinical cardiovascular research to explore potential differences in experimental rigor between male and female researchers, focusing on the inclusion of female animals in experiments and on analyses of sex differences. Temporal trends in female authorship and patterns in mentorship relationships by sex were examined as secondary analyses. We hypothesized that female authorship and mentorship relationships between men and women had both increased, but that these would not be associated with increased consideration of sex as a biological variable or with other measures of experimental rigor.

METHODS

As described (10), all preclinical studies published between July 2006 and June 2016 in *Circulation*; *Circulation Research*; *Hypertension*; *Stroke*; and *Arteriosclerosis, Thrombosis, and Vascular Biology* were reviewed. Studies were included if they reported original data from in vivo experiments using nonhuman mammals and proposed therapeutic applications or implications to specific human disorders. Pre-specified variables collected included the disease studied, the animal model(s) used and their sex, and whether any study result was reported by sex. Because of the possibility that differences in female animal inclusion or sex-specific analyses might be attributable to broader differences in experimental design, we also analyzed whether animals were randomized, whether blinding was used (concealed allocation or

The authors attest they are in compliance with human studies committees and animal welfare regulations of the authors' institutions and Food and Drug Administration guidelines, including patient consent where appropriate. For more information, visit the *JACC: Basic to Translational Science* author instructions page.

Manuscript received March 13, 2019; revised manuscript received April 22, 2019, accepted April 27, 2019.

blinded outcome assessment), and whether sample size and/or power estimations were performed.

Study author names were extracted from Scopus. Author sex was determined using the online database genderize.io, which included >216,000 first names across 79 countries and 89 languages when queried. The database determines the sex of a name with an associated certainty factor. First authors are generally considered to have executed most of the published work, whereas senior authors are usually the study supervisors or principal investigators, and are generally considered to have contributed most to study planning and design (11,12); therefore, these were selected as our primary analyses. Female authorship as a proportion of all authors per manuscript was examined as a secondary analysis (per 10% increase and dichotomized as ≥33% of authors). Scopus was also queried to determine citation counts at 60 months for articles published between July 2006 and June 2011, as described (10). Post hoc analyses of mentorship relationships by sex were performed, with senior authors designated as mentors and first authors as mentees. A certainty factor of ≥70% was used to assign author sex for all analyses, otherwise sex was considered unknown. Articles with authors of unknown sex were excluded in primary analyses but were included in secondary and post hoc analyses to minimize missing data. Sensitivity analyses using a certainty factor of ≥90% for author sex and of sex-specific reporting restricted to studies in which animals of both sexes were used were performed.

Categorical variables are reported as number (percentage) and were compared using chi-square tests. Continuous variables are reported as mean ± SD or median with interquartile range (25th to 75th percentiles) (IQR) and were compared using Student's *t*-tests or Mann-Whitney U tests, respectively. Temporal trends were assessed using Cochran-Armitage tests or Spearman's rank-order correlation (ρ) using 12-month intervals. The associations of author sex with factoring sex of the animals studied in the reporting, design, and analysis of experiments and with the implementation of other study design elements were examined using chi-square tests (reported as absolute percent differences in study characteristics) and via simple and multivariable logistic regression (reported as odds ratios [ORs] with 95% confidence intervals [CIs]). Citation count comparisons were performed via stratification and multivariable linear regression. All analyses were performed using SAS version 9.4 (SAS Institute, Inc., Cary, North Carolina) using a 2-tailed α level of 0.05 (corrected using the Bonferroni method to account for multiple comparisons when specified).

RESULTS

Of 28,636 articles screened, 3,396 met the study inclusion criteria (**Figure 1**). Women accounted for 24 ± 17% of authors per manuscript, with 542 articles (16.0%) not including any female authors and none being authored solely by women. After excluding articles with authors of unknown sex, women were identified as first authors of 1,016 of 2,458 articles, senior authors of 569 of 2,749 articles, and both first and senior authors of 235 of 2,135 preclinical studies (41.3%, 20.7%, and 11.0%, respectively). The distribution of observed mentorship relationships differed from the expected distribution, with disproportionately high numbers of same-sex mentorships identified ($p < 0.001$), including a relative 50% greater than expected frequency of male to male mentorships. No difference was observed in the number of coauthors of articles with female versus male first or senior authors (9.6 vs. 9.6; $p = 0.864$; and 9.2 vs. 9.5; $p = 0.075$; respectively). Five-year citation counts were comparable between female and male authors (21 [interquartile range (IQR): 13 to 31] vs. 20 [IQR: 12 to 33]; $p = 0.509$ for first authors; 18 [IQR: 12 to 30] vs. 20 [IQR: 13 to 31]; $p = 0.170$ for senior authors). Author sex was similarly not predictive of citation counts in multivariable models that adjusted for cardiovascular disease studied, publication date, and journal.

Temporal analyses over 10 years indicate that the proportions of female first and senior authors each increased, with women accounting for between 32.3% and 46.3% of first authors and between 11.8% and 26.1% of senior authors (**Figure 2A**). There was a corresponding temporal increase in the proportion of manuscripts with women as both first and senior authors (full range: 5.5% to 14.9%; $p_{trend} = 0.001$). The proportions of articles with first and senior authors of differing sex did not change (full range: 28.5% to 34.3%; $p_{trend} = 0.663$ for female first and male senior authorship; full range: 5.5% to 14.9%; $p_{trend} = 0.184$ for male first and female senior authorship). Per article, the mean proportion of female authors slightly increased (full range: 21.4% to 26.8%; $p < 0.001$) (**Figure 2B**).

Female and male authors were equally likely to report the sex of animals used in preclinical experiments (815 of 1,016 [80.2%] vs. 1,150 of 1,442 [79.8%]; $p = 0.776$ for first authors; 455 of 569 [80.0%] vs. 1,767 of 2,180 [81.1%]; $p = 0.556$ for senior authors). However, when the sex of the animals was reported, women were more likely to have used female animals in their experiments (292 of 815 [35.8%] vs. 313 of 1,150 [27.2%], $p < 0.001$ for first authors; 181 of 455 [39.8%] vs. 492 of 1,767 [27.8%]; $p < 0.001$ for senior

FIGURE 1 Literature Search

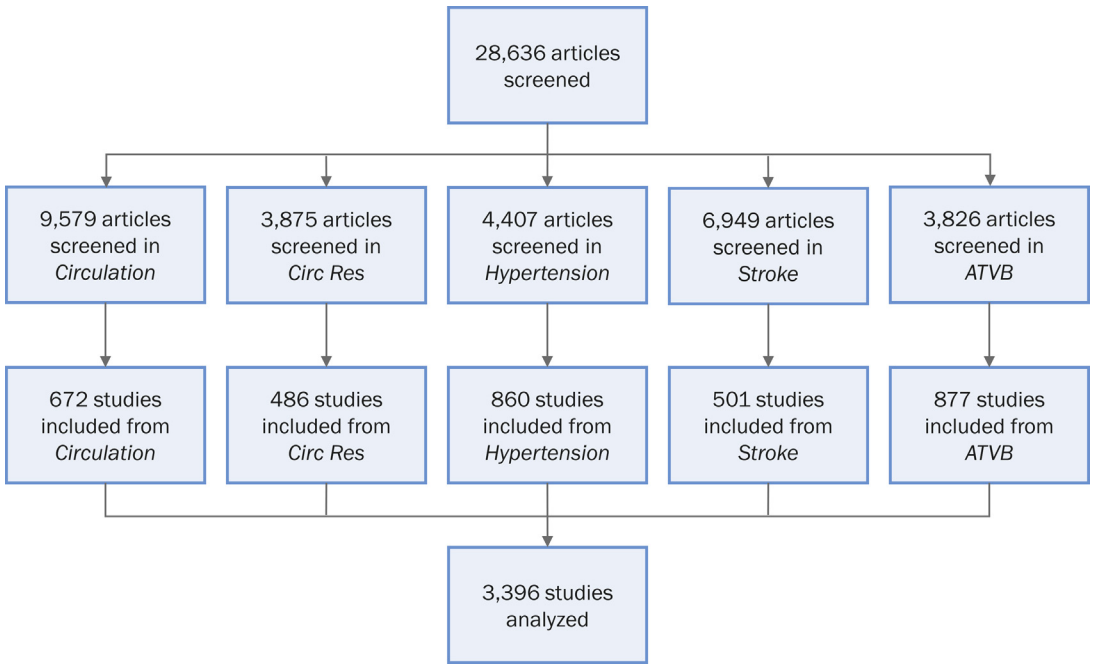

Literature search. *ATVB* = *Arteriosclerosis, Thrombosis and Vascular Biology*; *Circ Res* = *Circulation Research*. Modified from Ramirez et al. (10).

authors), to have used animals of both sexes (156 of 815 [19.1%] vs. 179 of 1,150 [15.6%]; p = 0.038 for first authors; 98 of 455 [21.5%] vs. 262 of 1,767 [14.8%]; p < 0.001 for senior authors), and to have reported sex-specific results (326 of 815 [40.0%] vs. 380 of 1,150 [33.0%]; p = 0.002 for first authors; 199 of 455 [43.7%] vs. 597 of 1,767 [33.8%]; p < 0.001 for senior authors). Similar findings were observed when female authorship was examined as a proportion of all authors per manuscript. In contrast, female authorship was not associated with randomization, blinding, or sample size estimation after correcting for multiple

FIGURE 2 Female Authorship in Preclinical Cardiovascular Research

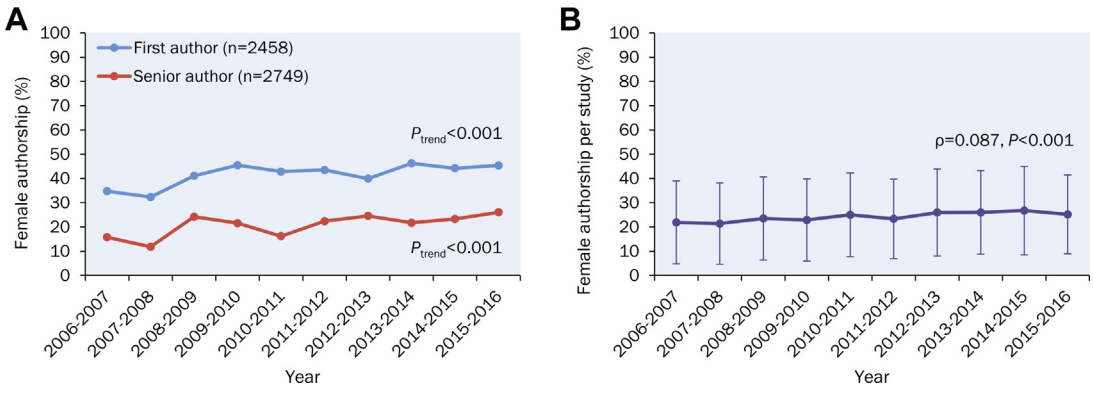

(A) Proportion of women as first and senior authors. **(B)** Mean proportion of women as authors per study. Error bars depict SD.

FIGURE 3 Association of Female Authorship With Considering Sex as a Biological Variable and Other Experimental Standards in Preclinical Cardiovascular Research

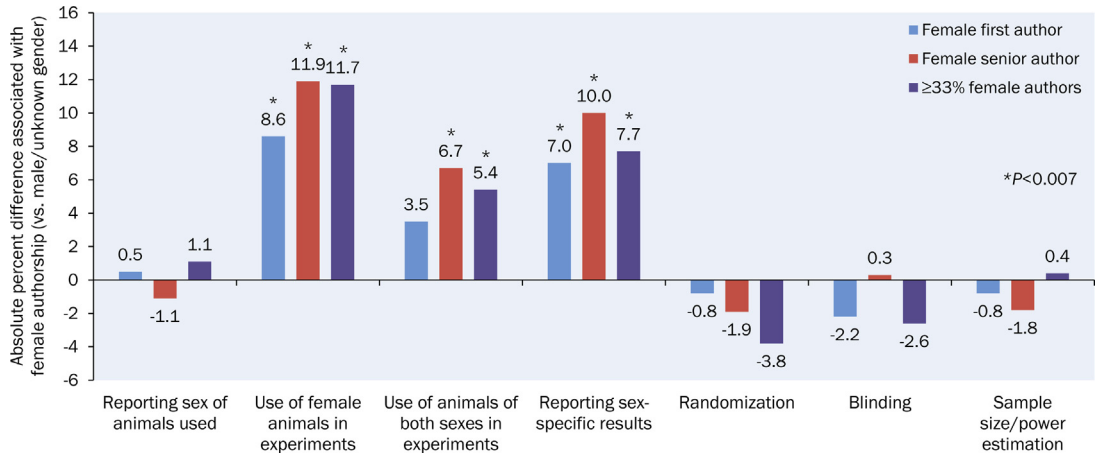

Absolute percent differences shown for first, senior, and ≥33% female authorship. *Corrected using the Bonferroni method to account for multiple comparisons ($\alpha = 0.05$ divided by 7).

comparisons (Figure 3). The preceding differences persisted when female authorship was examined on an interval scale (per 10% increase) and after adjusting for pre-specified potential confounders (Table 1). All findings were also comparable in sensitivity analyses using a minimum certainty factor of 90% for author sex. When restricted to studies that included both male and female animals (N = 335 to 421), female senior authorship (but not first or cumulative authorship) remained associated with reporting sex-specific results after adjusting for pre-specified potential confounders (OR: 2.2; 95% CI: 1.1 to 4.4; p = 0.036).

DISCUSSION

Sex differences in innate scientific ability have long ago been refuted (13); however, career trajectories and personal and professional experiences often differ between male and female academics (8,13), which may influence researchers' priorities and practices. Although there are clear societal benefits to promoting sex inclusivity in research, its impact on the quality and impact of research remains unexplored (9). Our analysis of preclinical cardiovascular research demonstrates that: 1) approximately 41% of first authors and 21% of senior authors over a recent 10-year period were women; 2) although female authorship is increasing, segregation by sex in mentorship relationships exists and persists; and 3) when women influence experimental design and reporting or are a larger proportion of the research team, studies are more likely to include female animals and to explore sex-based differences, but author sex is not associated with other measures of methodological rigor or research impact.

Preclinical research using animal models often precedes and informs clinical trials. However, important and remediable methodological shortcomings remain prevalent in preclinical cardiovascular research (10), including a tendency to exclude females in animal experiments and to ignore the potential influence of sex on study outcomes (1). Women's perspectives have been suggested to uniquely promote scientific progress in general and advances in women's health in particular, in part due to their greater tendency to explore the effects of gender and sex (5,6). Our data suggest that women are indeed more attuned to considering sex as a biological variable in preclinical experiments, but that male and female researchers are more alike than they are different when broader measures of scientific rigor and research impact are considered.

A corollary to the previously described findings is that the persistent underrepresentation of women in preclinical cardiovascular research is highly unlikely to be attributable to differences in research capacity or potential impact. Rather, systemic factors are probably influential. For instance, although modern scientific endeavors are increasingly reliant on research teams and networks—settings in which a diversity of viewpoints and experiences are sought

TABLE 1 Association Between Female Authorship and Experimental Design Characteristics in Preclinical Cardiovascular Studies

	N*	Crude OR (95% CI)	Adjusted OR (95% CI)†	p Value†
Female first author				
Reporting sex of animals	2,458	1.03 (0.84–1.26)	0.96 (0.77–1.19)	0.698
Inclusion of female animals‡	1,965	1.49 (1.23–1.81)	1.60 (1.30–1.96)	<0.001
Inclusion of animals of both sexes‡	1,965	1.28 (1.01–1.63)	1.29 (1.01–1.66)	0.046
Sex-specific reporting of results‡	1,965	1.35 (1.12–1.63)	1.33 (1.10–1.62)	0.004
Randomization	2,458	0.95 (0.78–1.16)	1.03 (0.83–1.28)	0.776
Blinding	2,458	0.91 (0.76–1.08)	0.95 (0.79–1.15)	0.608
Sample size estimation	2,458	0.70 (0.41–1.20)	NR	
Female senior author				
Reporting sex of animals	2,749	0.93 (0.74–1.18)	0.83 (0.65–1.07)	0.153
Inclusion of female animals‡	2,222	1.71 (1.38–2.12)	1.81 (1.43–2.28)	<0.001
Inclusion of animals of both sexes‡	2,222	1.58 (1.22–2.04)	1.58 (1.20–2.08)	0.001
Sex-specific reporting of results‡	2,222	1.52 (1.24–1.88)	1.44 (1.16–1.79)	0.001
Randomization	2,749	0.90 (0.71–1.12)	0.88 (0.68–1.13)	0.308
Blinding	2,749	1.02 (0.84–1.23)	1.14 (0.92–1.42)	0.219
Sample size estimation	2,749	0.32 (0.13–0.80)	NR	
Female authorship (per 10% increase)				
Reporting sex of animals	3,396	1.04 (0.98–1.09)	1.02 (0.97–1.09)	0.435
Inclusion of female animals‡	2,718	1.20 (1.14–1.26)	1.20 (1.13–1.26)	<0.001
Inclusion of animals of both sexes‡	2,718	1.13 (1.07–1.21)	1.12 (1.05–1.20)	<0.001
Sex-specific reporting of results‡	2,718	1.13 (1.08–1.19)	1.11 (1.05–1.17)	<0.001
Randomization	3,396	0.95 (0.90–1.00)	1.00 (0.94–1.06)	0.949
Blinding	3,396	0.99 (0.94–1.03)	1.04 (0.99–1.09)	0.173
Sample size estimation	3,396	1.08 (0.94–1.24)	NR	

*Refers to the total number of studies included in analyses. †Adjusted for disease studied, animal model(s) used, journal of publication, date of publication, and number of co-authors. ‡Analysis restricted to studies in which the sex of animals used was reported. Bonferroni corrected α level of 0.007 used to define statistical significance ($\alpha = 0.05$ divided by 7).

CI = confidence interval; NR = not reported due to small number of events per predictor variable; OR = odds ratio.

and valued (6)—our analysis highlights a persistent predominance of same-sex mentorships. Because of the relative paucity of available female mentors, this practice has the potential to perpetuate women's underrepresentation in the field and to hinder efforts to improve the status quo (7).

STUDY LIMITATIONS. The journals examined were selected based on their prominence in cardiovascular research, their collective focus on a wide range of cardiovascular disorders, and their endorsement of NIH guidelines on rigor and reproducibility (10). However, they might not be representative of all preclinical cardiovascular journals. Author sex was determined using an arbitrary certainty factor, which might have resulted in misclassification in a minority of cases. However, our results were comparable in sensitivity analyses using a more stringent criterion. Our analysis did not capture instances of multiple first or corresponding authors (equally contributing authors) and used author position as a proxy for mentor–mentee relationships. Presumed author sex might not reflect author gender, which might be a relevant distinction in our analysis. Our analysis also focused on experimental and reporting standards proposed by the NIH, which were not exhaustive.

CONCLUSIONS

Women's involvement in preclinical cardiovascular research is positively associated with considering sex as a biological variable, which is a practice that is expected to inform and promote advances in women's health. Researcher sex is not associated with other measures of experimental rigor or research impact. Limited mentorship opportunities may be contributing to women's underrepresentation in this field.

ADDRESS FOR CORRESPONDENCE: Dr. Benjamin Hibbert, University of Ottawa Heart Institute, 40 Ruskin Street, H-4238, Ottawa, Ontario K1Y 4W7, Canada. E-mail: bhibbert@ottawaheart.ca.

PERSPECTIVES

COMPETENCY IN MEDICAL KNOWLEDGE: In this analysis of 3,396 preclinical studies in 5 leading cardiovascular journals, female authorship was positively associated with considering sex as a biological variable, but not with other measures of methodological rigor or 60-month citation counts. Over a 10-year period, the proportion of studies with first and senior authors of differing sex was low and stable, suggesting that segregation by sex in mentorship relationships exists and persists. These data indicate that women's underrepresentation in preclinical cardiovascular research is not due to differences in research capacity or impact. Limited mentorship opportunities for women in preclinical cardiovascular research may be an important contributor.

TRANSLATIONAL OUTLOOK: Further study to identify and understand barriers to women's involvement in preclinical cardiovascular research is warranted. Enhancing mentorship opportunities for women should be explored as a potential strategy to improve the status quo.

REFERENCES

1. Ramirez FD, Motazedian P, Jung RG, et al. Sex bias is increasingly prevalent in preclinical cardiovascular research: implications for translational medicine and health equity for women: a systematic assessment of leading cardiovascular journals over a 10-year period. Circulation 2017;135:625–6.

2. Clayton JA, Collins FS. Policy: NIH to balance sex in cell and animal studies. Nature 2014;509:282–3.

3. Beery AK. Inclusion of females does not increase variability in rodent research studies. Curr Opin Behav Sci 2018;23:143–9.

4. Klein SL, Schiebinger L, Stefanick ML, et al. Opinion: sex inclusion in basic research drives discovery. Proc Natl Acad Sci U S A 2015;112:5257–8.

5. Rotenstein LS, Jena AB. Lost Taussigs - the consequences of gender discrimination in medicine. N Engl J Med 2018;378:2255–7.

6. Nielsen MW, Alegria S, Borjeson L, et al. Opinion: gender diversity leads to better science. Proc Natl Acad Sci U S A 2017;114:1740–2.

7. Asghar M, Usman MS, Aibani R, et al. Sex Differences in authorship of academic cardiology literature over the last 2 decades. J Am Coll Cardiol 2018;72:681–5.

8. Soklaridis S, Zahn C, Kuper A, Gillis D, Taylor VH, Whitehead C. Men's fear of mentoring in the #MeToo era - what's at stake for academic medicine? N Engl J Med 2018.

9. Valantine HA, Collins FS. National Institutes of Health addresses the science of diversity. Proc Natl Acad Sci U S A 2015;112:12240–2.

10. Ramirez FD, Motazedian P, Jung RG, et al. Methodological rigor in preclinical cardiovascular studies: targets to enhance reproducibility and promote research translation. Circ Res 2017;120:1916–26.

11. Wren JD, Kozak KZ, Johnson KR, Deakyne SJ, Schilling LM, Dellavalle RP. The write position. A survey of perceived contributions to papers based on byline position and number of authors. EMBO Rep 2007;8:988–91.

12. Lariviere V, Desrochers N, Macaluso B, Mongeon P, Paul-Hus A, Sugimoto CR. Contributorship and division of labor in knowledge production. Soc Stud Sci 2016;46:417–35.

13. Ceci SJ, Ginther DK, Kahn S, Williams WM. Women in academic science: a changing landscape. Psychol Sci Public Interest 2014;15:75–141.

KEY WORDS cardiology, mentorship, translational research, women

JACC: BASIC TO TRANSLATIONAL SCIENCE VOL. 4, NO. 4, 2019

EDITORIAL COMMENT

Sex Differences in Science

Do We Have a Problem?*

Eva van Rooij, PhD,[a,b] Nanette H. Bishopric, MD[c]

It is no secret that women have long been underrepresented in science. Although there is no clear biological explanation, this gap might have arisen through stereotypic perceptions that women are unsuited for science, either because of imagined intellectual incapacity, fear for their fecundity, or both. Similar beliefs, as well as widespread cultural, social, and economic factors, have limited the educational opportunities available to women, further discouraging their participation in scientific research. Although there are ample data to refute such premodern stereotypes, an unequal balance between male and female scientists remains. Despite the steadily increasing numbers of women entering science, the United Nations Educational, Scientific and Cultural Organization's Women in Science data show that <30% of the world's researchers at any level are women (1). Although men and women hold roughly the same numbers of bachelor's and master's degrees, at higher academic ranks, the balance tips in favor of male scientists. In the European Union, only 20% of full professors (and still fewer natural sciences professors) are women (2). Of all tenured, full professors in the United States, only 21% are women (3). In addition to being outnumbered, women are also under-rewarded. Women are still paid less for their science-related work (4), and their contracts are more precarious. But is this sex imbalance merely a problem of basic fairness, or does science itself pay a price for the lack of female voices? A study in this issue of *JACC: Basic to Translational Science* attempts to address this question.

SEE PAGE 471

In this study, Labinaz et al. (5) examined temporal trends in female authorship and mentorship and asked whether women or men are more likely to include animals of both sexes in research studies, a standard metric for experimental rigor. The investigators reviewed 3,396 articles published between 2006 and 2016 and classified them by sex of the first and last authors and by use of female animals in experiments. A mentorship relationship was assumed to exist between the first and last authors. Their analysis revealed that between 2006 and 2016, female authorship increased in both first and last positions between 2006 and 2016. They also identified a disproportionately high number of same-sex mentorships, the predominance of which persisted over time. Finally, although men and women were equally likely to report the sex of the animals used, studies led by female first and senior authors were more likely to include female animals in their experiments. This result suggests that women are more inclined to consider sex as a biological variable in preclinical experiments. At the same time, no association was found between the sex of the researcher and other measures of scientific rigor. The observed better sex-awareness in women could point to other unmeasured issues that are differentially noticed by men and women scientists. In this way, at least, underrepresentation of women in science may have ramifications not only for workforce diversity but also for critical aspects of the scientific enterprise.

*Editorials published in the *JACC: Basic to Translational Science* reflect the views of the authors and do not necessarily represent the views of *JACC: Basic to Translational Science* or the American College of Cardiology.

From the [a]Hubrecht Institute, Royal Netherlands Academy of Arts and Sciences (KNAW) and University Medical Center, Utrecht, the Netherlands; [b]Department of Cardiology, University Medical Center Utrecht, the Netherlands; and the [c]Department of Oncology, Georgetown Lombardi Comprehensive Cancer Center, Georgetown University, Washington, DC. Both authors have reported that they have no relationships relevant to the contents of this paper to disclose.

The authors attest they are in compliance with human studies committees and animal welfare regulations of the authors' institutions and Food and Drug Administration guidelines, including patient consent where appropriate. For more information, visit the *JACC: Basic to Translational Science* author instructions page.

ISSN 2452-302X https://doi.org/10.1016/j.jacbts.2019.07.007

Several potential confounding factors should be considered when analyzing these data. First, the investigators selected articles from a subset of cardiovascular journals that might not be fully representative of preclinical cardiovascular journals. In addition, adjudication criteria might have been biased because author sex was determined by using an arbitrary certainty factor assigned to the first name, potentially inducing a misclassification. This was even more problematic when considering that in American English, girls' first names became less sex-obvious for the trainee cohorts publishing during the decade under study. For example, Ashley, a classic male name, rose from the 140th to the third most common girl's name between 1970 and 1980. Thus, this paper should be viewed as hypothesis-generating rather than evidence of a systematic bias.

At the same time, the paper provides potentially several pieces of good news. Women were more likely to include both sexes in their preclinical studies, but equally likely to perform randomization of animals, blinding, and sample size and/or power estimations. At the very least, this result confirmed (if confirmation was needed) that there was no cost to scientific rigor for being more inclusive. That women in both first and senior authorships increased overall during the 10 years analyzed is more good news, suggesting that a lack of female mentors may be correcting itself as more women move into cardiovascular sciences. Increased awareness and future efforts to generate equal opportunities and rewards should continue to improve sex imbalances in science.

Another finding of the study was a preponderance of same-sex mentorships that remained constant throughout the 10-year study period. It was possible that the greater representation of men in both mentor and mentee populations simply makes male-sex pairings more likely. In contrast, if there truly is a preference for same-sex scientific pairings, does this reveal a problem of bias? If so, is there a remedy? It would be useful to know whether women were just as likely as men to choose a female mentor, and whether men were training young women and men in proportion to their representation in the trainee population. If male scientists prefer to work with other male scientists, further increasing the pool of female mentors will be critical to providing opportunities for women entering the field.

So, yes, there still is an imbalance between men and women in science, both in numbers and rewards. Although specific strategies are in place to promote women and girls in health and science, much more needs to be done to bring about the widespread social changes needed to ensure sex equality in science. Alleviating this imbalance would not only be the right and fair thing to do but would have objective advantages that have been shown elsewhere: sex diverse workplaces have increased productivity and innovation, and have better employee retention and satisfaction (6). The interesting new insight by Labinaz et al. (5) is that greater inclusiveness may improve the quality and depth of science, because men and women may contribute different beneficial skills and mindsets. A more diverse research team might develop more well-argued and relevant questions, resulting in research that is applicable (and beneficial) to a broader population. Increasing efforts to further reduce the sex gap in research will likely be highly cost effective on multiple fronts.

ADDRESS FOR CORRESPONDENCE: Dr. Nanette H. Bishopric, Department of Oncology, Georgetown Lombardi Comprehensive Cancer Center, Georgetown University, Washington, DC 20057. E-mail: nhb20@georgetown.edu.

REFERENCES

1. UNESCO Institute for Statistics. Women in Science. Available at: http://uis.unesco.org/sites/default/files/documents/fs51-women-in-science-2018-en.pdf. Accessed July 2019.

2. Kamerlin SC. Where are the female science professors? A personal perspective. F1000Res 2016;5:1224.

3. Shen H. Inequality quantified: mind the gender gap. Nature 2013;495:22–4.

4. Woolston C. Scientists' salary data highlight US$18,000 gender pay gap. Nature 2019;565:527.

5. Labinaz A, Marbach JA, Jung RG, et al. Female authorship in preclinical cardiovascular research: temporal trends and influence on experimental design. J Am Coll Cardiol Basic Trans Science 2019;4:471–7.

6. Shannon G, Jansen M, Williams K, et al. Gender equality in science, medicine, and global health: where are we at and why does it matter? Lancet 2019;393:560–9.

KEY WORDS cardiology, mentorship, translational research, women

JACC: BASIC TO TRANSLATIONAL SCIENCE VOL. 4, NO. 4, 2019

PRECLINICAL RESEARCH

Malondialdehyde Conjugated With Albumin Induces Pro-Inflammatory Activation of T Cells Isolated From Human Atherosclerotic Plaques Both Directly and Via Dendritic Cell–Mediated Mechanism

Mizanur Rahman, PhD,[a] Johnny Steuer, MD, PhD,[b] Peter Gillgren, MD, PhD,[b] Ákos Végvári, PhD,[c] Anquan Liu, MD, PhD,[a] Johan Frostegård, MD, PhD[a]

VISUAL ABSTRACT

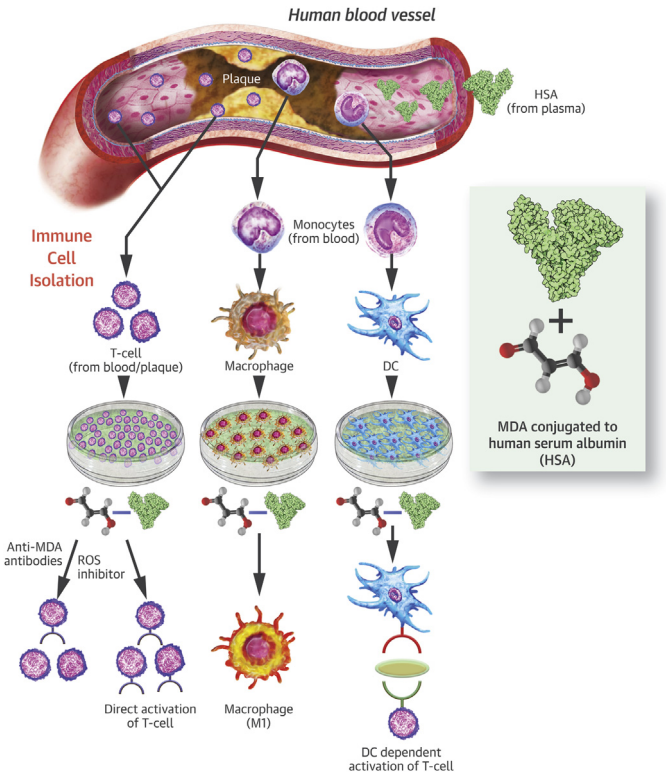

Rahman, M. et al. J Am Coll Cardiol Basic Trans Science. 2019;4(4):480–94.

HIGHLIGHTS

- MDA conjugated with HSA activates T cells from human atherosclerotic plaques through a direct mechanism.
- MDA-HSA also induces maturation and activation of human dendritic cells, which in turn promote activation of autologous T cells from the same donor's plaques, although this effect appears somewhat weaker than the direct activation.
- M1 polarization of macrophages, potentially an atherogenic effect, were also induced by MDA-HSA.
- Heat shock protein 60 was induced in T cells by MDA-HSA, is atherogenic, and could promote dendritic cell/T cell activation.
- Two peptide modifications of serum albumin in atherosclerotic patients' HSA were similar to those generated by treatment of HSA with MDA in vitro.

ISSN 2452-302X https://doi.org/10.1016/j.jacbts.2019.03.009

SUMMARY

Human dendritic cells were differentiated from blood monocytes and treated with malondialdehyde (MDA) conjugated with human serum albumin (HSA). Autologous T cells from human plaques or blood were co-cultured with the pre-treated dendritic cells or treated directly. MDA modifications were studied by mass spectrometry. MDA-HSA induced a pro-inflammatory DC-mediated T-cell activation and also a strong direct effect on T cells, inhibited by an inhibitor of oxidative stress and antibodies against MDA. Atherogenic heat shock protein-60 was strongly induced in T cells activated by MDA-HSA. Two peptide modifications in atherosclerotic patients' HSA were similar to those present in in vitro MDA-modified HSA.

ABBREVIATIONS AND ACRONYMS

ATP = adenosine triphosphate
CVD = cardiovascular disease
DC = dendritic cell
GM-CSF = granulocyte-macrophage colony-stimulating factor
HLA = human leukocyte antigen
HSA = human serum albumin
HSP = heat shock protein
IFN = interferon
IgM = immunoglobulin M
IL = interleukin
LDL = low-density lipoprotein
MDA = malondialdehyde
MS = mass spectrometry
OxLDL = oxidized low-density lipoprotein
PCR = polymerase chain reaction
TCR = T-cell receptor
TGF = transforming growth factor
TLR = Toll-like receptor
TNF = tumor necrosis factor

Typical of atherosclerosis, the major cause of cardiovascular disease (CVD) is the presence in atherosclerotic plaques of activated immune competent cells including T cells, dendritic cells (DCs) and monocytes/macrophages, dead cells (in a necrotic core), and oxidized low-density lipoprotein (OxLDL), commonly present in inert mainly macrophage-derived foam cells (1,2). In previous studies, findings have indicated that OxLDL can activate T cells (3-6), including those from human atherosclerotic plaques (3,6,7). Moreover, we have shown that the oxidized phospholipid moiety of OxLDL promotes immune activation, including production of interferon (IFN)-γ (8,9), but the underlying mechanisms and possible activation of T cells by other components of OxLDL remain unclear. In contrast to the situation in mice (10), we observed no low-density lipoprotein (LDL)-mediated activation of human T cells, including any that might be found isolated in plaques (6).

Both murine models of atherosclerosis and human ex vivo investigation indicate that T cells play major roles in atherosclerosis and ensuing CVD.

Transfer of $CD4^+$ T cells to atherosclerotic mice exacerbates atherosclerosis, possibly by abrogation of T-cell transforming growth factor-beta (TGF-β) signaling (11,12).

In humans, an association between the $CD8^+$ subset of T cells and CVD has been reported (13). The DCs and T cells co-localized in plaques may play a role in local immune reactions within lesions (14). DCs may be of major importance during different stages of the development of atherosclerosis in humans (15–17).

Oxidation of LDL generates a variety of compounds from both protein (apolipoprotein B [apoB]) and lipids. Two of the products from lipid malondialdehyde (MDA) and phosphorylcholine (PC) appear to be of particular interest and elicit a pronounced antibody response in humans that may have atheroprotective properties (2).

We reported recently that production of antibodies against both PC and MDA conjugated with an albumin is dependent on T cells in humans. Moreover, these antibodies together strongly and negatively correlated with atherosclerosis and vulnerable plaques in systemic lupus erythematosus (where the risk of CVD is exceedingly high) and also with the risk of CVD in a general population (18,19).

Heat shock protein (HSP) 60 may be involved in activation of T cells by OxLDL, as well as the atherosclerotic immunity in general (20), and more specifically in T-cell activation (6,21).

From the [a]Institute of Environmental Medicine, Karolinska Institutet, Stockholm, Sweden; [b]Section of Vascular Surgery, Department of Surgery, Södersjukhuset, Institution of Clinical Science and Education, Karolinska Institutet, Stockholm, Sweden; and the [c]Division of Chemistry I, Department of Medical Biochemistry and Biophysics, Biomedicum, Karolinska Institutet, Stockholm, Sweden. This research was financed by the Swedish Heart-Lung Foundation, the Swedish Research Council, the King Gustav V 80th Birthday Fund, the Swedish Association Against Rheumatism, Vinnova, and Torsten Söderberg's Foundation. These funders played no role in study design, data collection, and analysis; the decision to publish; or preparation of the manuscript. Dr. Frostegård is named as inventor on patents and patent applications related to phosphorylcholine, but also for malondialdehyde, which is a topic in this paper. All other authors have reported that they have no relationships relevant to the contents of this paper to disclose.

All authors attest they are in compliance with human studies committees and animal welfare regulations of the author's institutions and Food and Drug Administration guidelines, including patient consent where appropriate. For more information, visit the *JACC: Basic to Translational Science* author instructions page.

Manuscript received July 18, 2018; revised manuscript received March 11, 2019, accepted March 13, 2019.

JACC: BASIC TO TRANSLATIONAL SCIENCE VOL. 4, NO. 4, 2019
AUGUST 2019:480–94

We report that MDA-human serum albumin (HSA) activates DCs and T cells, the latter even directly, and that this effect is inhibited by anti-MDA antibodies. The implications of these findings are discussed.

METHODS

DC DIFFERENTIATION. Monocytes were isolated using human enrichment cocktail (STEMCELL Technologies, Grenoble, France) and thereafter were cultured in Roswell Park Memorial Institute (RPMI) medium containing 50 ng/ml each of recombinant human granulocyte-macrophage colony-stimulating factor (GM-CSF) and interleukin (IL)-4 (ImmunoTools, Friesoythe, Germany). After 72 h of incubation, half of the medium was replaced with fresh medium. After 6 days of culture, cells were collected and 2×10^6/ml were cultured in the presence or absence of 10 μg/ml MDA-HSA prepared as described previously (18). Endotoxin was not detected in MDA and HSA by the Limulus Amebocyte Lysate test.

The cells collected after 24 h were ≥90% viable. DCs were stained with antibodies against CD11C-PE/BV421, CD86-Percp-Cy5.5, CD80-FITC, and CD40-FITC (BD Bioscience, San Jose, California).

CO-CULTURE OF DCs AND T CELLS. CD3 T cells were isolated from the buffy coat of healthy donors with the human T-cell enrichment cocktail (STEMCELL Technologies) in accordance with the manufacturer's instructions. Differentiated DCs were cultured as described earlier in the presence or absence of MDA-HSA for overnight or for 12 h, then washed and resuspended in complete RPMI medium; thereafter, they were co-cultured with 4×10^5 CD3 T cells for 48 h. To block human leukocyte antigen II (HLA-II), 8 μg/ml of low-endotoxin, azide-free purified anti-HLA-II antibodies (Biolegend, Dedham, Massachusetts) were added to DCs before co-culturing with T cells. Cells collected after 48 h of co-culture were stained with anti-CD3-Percp Cy5.5, anti-CD 25-PE/FITC, anti-CD69-APC/FITC, and anti-CD71-BV421/FITC (BD Bioscience) antibodies.

ISOLATION AND CULTURE OF PLAQUE CELLS. Atherosclerotic plaques were obtained from patients who were undergoing carotid endarterectomy at the Department of Surgery, Vascular Surgery, Södersjukhuset, Stockholm, Sweden. This study was pre-approved by the research ethics committee of Karolinska Institutet and in accordance with the Declaration of Helsinki. All subjects gave their written informed consent before entering the study.

Cells were isolated from atherosclerotic plaques as described earlier (22). In brief, the plaques were first dissected into small pieces, which were then incubated with 1.25 mg/ml collagenase IV (Life Technologies Europe BV, Stockholm, Sweden), 25 μg/ml Liberase DL (Roche Applied Science, Stockholm, Sweden), and 0.2 mg/ml DNase I (Roche Applied Science, Stockholm, Sweden) for 1 h at 37°C. The dissociated plaque cells were then passed through a 100-μm Celltrics filter (Millipore AB, Stockholm, Sweden) to remove unwanted fat and debris, and T cells were purified with the EasySep T-cell enrichment kit (STEMCELL Technologies). DCs obtained from the peripheral blood of the plaque donors were treated with or without MDA-HSA as described above and thereafter co-cultured with plaque T cells for 48 h. In addition, plaque T cells were cultured in the presence or absence of MDA-HSA for 24 h.

T CELL CULTURES. Isolated CD3 T cells were cultured in the presence or absence of MDA-HSA and/or of 2 μg/ml anti-MDA antibodies (Academy Biomedical, Houston, Texas) for 24 h. Furthermore, CD3 T cells were incubated with 20 μmol/l/ml MitoTEMPO (Sigma Aldrich, St. Louis, Missouri) for 30 min to inhibit mitochondrial reactive oxygen species (ROS) production and subsequently cultured with or without MDA-HSA for a maximum of 20 h.

MACROPHAGE CULTURE. Isolated monocytes were cultured with 50 ng/ml recombinant human GM-CSF in RPMI medium, which was replaced on day 3 with fresh medium. On day 5, these cells were treated with MDA-HSA for 48 h to investigate M1 (pro-inflammatory) macrophage differentiation. Further, macrophages were co-cultured with T cells (pre-treated with MDA-HSA for 6 h, and then for 48 h).

CELL PROLIFERATION. Cell proliferation was determined using the colorimetric BrdU kit in accordance with the manufacturer's protocol (Sigma Aldrich). In brief, DCs cultured with or without 10 μg/ml MDA-HSA were cultured for 12 h, washed, and resuspended in the complete RPMI medium, and then 0.5×10^5 DCs were co-cultured with 2×10^5 autologous T cells in a 96-well round-bottom plate (Becton Dickinson, Franklin Lakes, New Jersey). In addition, T cells were also cultured alone with or without MDA-HSA. After 72 h of incubation, the cells were labeled with BrdU, incubated for 20 more hours, centrifuged, and dried at 60 °C for 1 h. The dried cells were fixed with a FixDenat (Roche) solution before incubation with anti-BrdU peroxidase antibodies. After 2 h of incubation, the cells were washed and substrate solution added for development of color. To stop the reaction, 1 mol/l H_2SO_4 was added and absorption at 450-nm wavelength (with 690 nm as reference) determined.

STAINING OF INTRACELLULAR CYTOKINES. CD3 T cells with or without MDA-HSA were incubated for 24 h; lysed with 0.1% saponin; stained for IFN-γ, IL-4, and IL-17A; and analyzed by flow cytometry.

CYTOKINE QUANTIFICATION. The levels of INF-γ, IL-6, IL-4, tumor necrosis factor (TNF)-α, IL-10, and TGF-β collected after 18 h were assessed by enzyme-linked immunosorbent assay (R&D systems, United Kingdom). In the same manner, HSP60 was determined in supernatant from CD3 T cells or DCs after 12 h of stimulation with MDA-HSA. In the case of CD3 T cells, the same was found from patients after 24 h of such stimulation.

GENE SILENCING. The gene encoding Toll-like receptor 4 (TLR4) or T-cell receptor (TCR) was silenced in T cells with a specific short hairpin RNA (shRNA) plasmid (Santa Cruz Biotechnology, Heidelberg, Germany). After 72 h of shRNA transfection, gene silencing was investigated at the protein level using flow cytometry. Nonspecific shRNA was used as a control.

ADENOSINE TRIPHOSPHATE ASSAY. T cells were stimulated with MDA-HSA for 2 h, then with cellular adenosine triphosphate (ATP), after which they were quantified with the ATP measurement kit (Promega, Madison, Wisconsin) in accordance with the manufacturer's instructions.

APOPTOSIS. After culturing DCs or CD3 T cells with 10 μg/ml MDA-HSA for 2, 4, 6, 18, and 24 h, apoptosis was assessed by flow cytometry using Annexin AV-FITC.

MDA-HSA BINDING. CD3 T cells were cultured in the presence or absence of MDA-HSA and/or anti-MDA (antibodies without fluorochrome conjugation) antibodies for 1 h and then centrifuged, washed, and resuspended in 100 μl phosphate-buffered saline. Fluorescein isothiocyanate-conjugated anti-MDA antibody (5 μg/ml) was added to both control and MDA-HSA–treated cells; after 30 min of incubation, the cells were washed and analyzed by flow cytometry.

QUANTITATIVE REAL-TIME POLYMERASE CHAIN REACTION. Total RNA was extracted with Qiagen mini (Qiagen, Hilden, Germany), and cDNA was synthesized from total RNA using the cDNA synthesis high capacity kit (Applied Biosystem, Foster City, California). One microliter of cDNA was used in each reaction of quantitative real-time polymerase chain reaction (PCR). Transcription factors TBET (Th1), GATA3 (Th2), RORC (Th17), and FOXP3 (T-reg) genes were analyzed. Housekeeping gene glyceraldehyde 3-phosphate dehydrogenase was used as a reference gene or to normalize the difference. Taq-man PCR master mix was used to run the reaction (Applied Biosystems) in 7500 Real-Time PCR system (Applied Biosystems). The ΔΔCT method was used to calculate the relative difference in gene expression.

MASS SPECTROMETRY SAMPLE PREPARATION AND ANALYSIS. In vitro, MDA-modified HSA was analyzed for peptide modification. HSA was first alkylated with dithiothreitol (Sigma) and iodoacetamide (Sigma), precipitated, and thereafter digested by sequencing grade trypsin in ammonium bicarbonate and dimethyl sulfoxide. The peptides thus obtained were desalted on a C18 column and analyzed by liquid chromatography–mass spectrometry (MS).

Plasma proteins (10 μg) from each of 10 patients' samples were dissolved in 50 mmol/l ammonium bicarbonate; reduced with 20 mmol/l DTT (Sigma) for 30 min at 56°C. Iodoacetamide (66 mmol/l) in 50 mmol/l ammonium bicarbonate was added for alkylation at room temperature for 30 min. Sequencing-grade trypsin (1:3, trypsin: protein; Promega) was incubated with each sample (1:33 trypsin: protein) at 37°C, and formic (final concentration of 5%) added to stop this digestion. After 20 min, the samples were placed on a C18 Hypersep plate (Thermo Scientific), dried using a Speedvac, and re-suspended in 25 μl 2% Acetonitrile/0.1% formic acid.

LIQUID CHROMATOGRAPHY–MS/MS ANALYSIS. Peptides were separated on a 50-cm Easy C18 chromatography column connected to an nLC1000 system (Thermo Fisher Scientific). The peptides were loaded onto this column at a flow rate of 1000 nl/min, and then eluted at 300 nl/min flow rate for 120 min with linear gradient from 4% to 26% AcN in 0.1% formic acid. After ionization by electrospray, the peptides eluted were analyzed in an orbitrap Q Exactive Plus mass spectrometer (Thermo Fisher Scientific). The MS spectrum was acquired at a resolution of 60,000 in the range of m/z 200 to 2,000. MS/MS data were obtained with a higher-energy collisional dissociation for ions with charge $z > 1$ at a resolution of 15,000.

MS DATA ANALYSIS. The raw data obtained were converted into the Mascot Generic Format (mgf) using a written Raw2mgf program written in-house. Proteins were identified by searching the SwissProt database (Porcine) with the Mascot v 2.4 (Matrix Science) database search engine.

STATISTICAL ANALYSIS. Statistical analysis was performed by Student's t-test; $p \leq 0.05$ was considered as statistically significant. $p \leq 0.05$, $p \leq 0.01$, and $p \leq 0.001$ were expressed as *, **, and ***, respectively. The bar diagrams are expressed as mean ± SD.

FIGURE 1 MDA-HSA Mediated Activation of DCs From CVD Patients or Healthy Blood Donors of DC Activation and Ensuing Activation of T Cells Exposed to the DCs

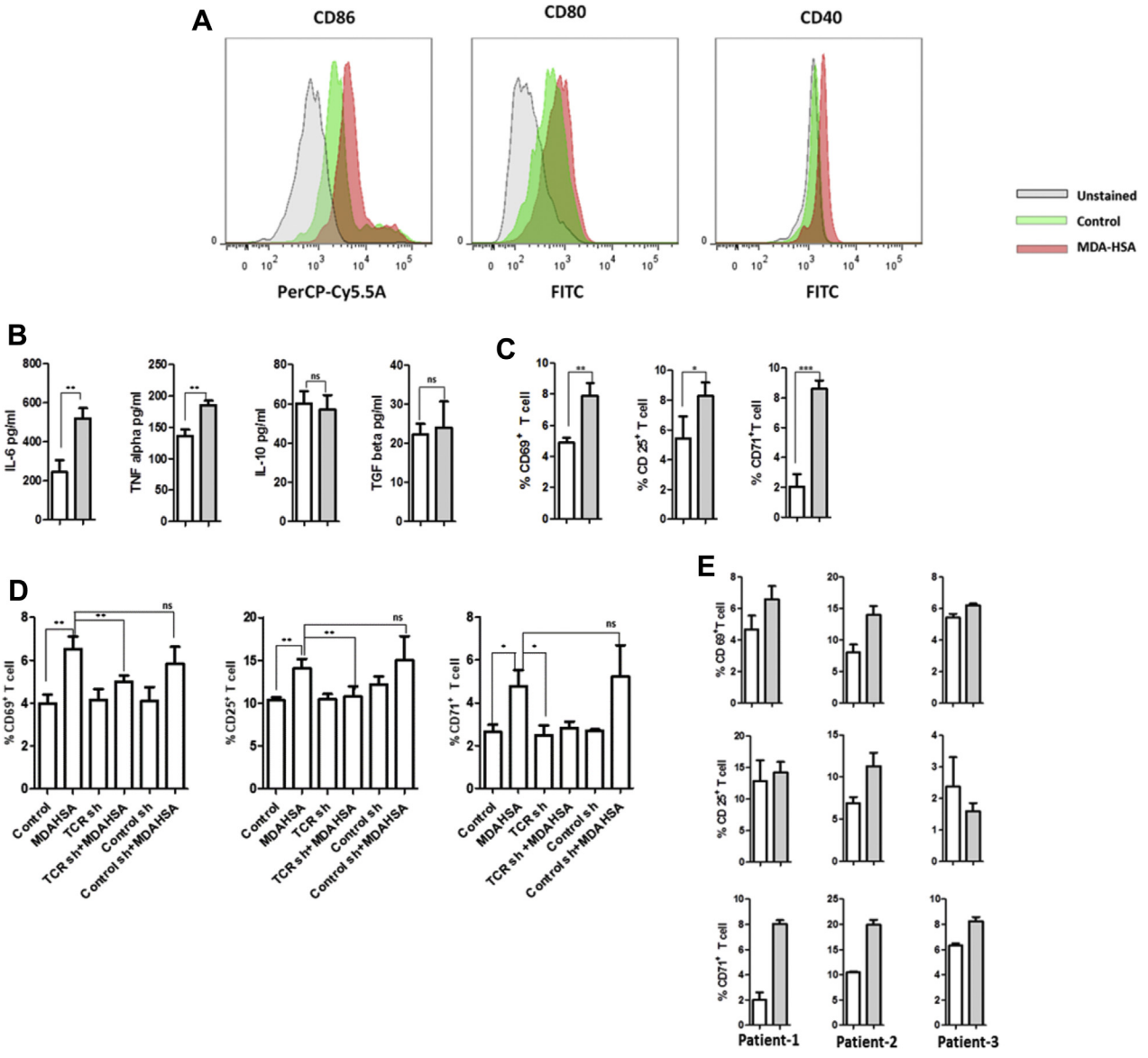

(A) DCs were stimulated with 10 μg/ml MDA-HSA for 24 h. Expression of the surface markers CD86, CD80, and CD40 was induced, as shown by 1 of 3 independent experiments. **(B)** MDA-HSA–stimulated DCs promoted production of pro-inflammatory but not anti-inflammatory cytokines, with no change in the level of TGF-β (mean value of 3 independent experiments). **(C)** MDA-HSA–induced DCs promoted T-cell activation (mean value of 3 independent experiments). **(D)** MDA-HSA–induced DC–mediated T-cell activation was inhibited when TCR (α and β) had been silenced (mean of 3 independent experiments). **(E)** MDA-HSA–treated peripheral blood DCs from atherosclerotic patients activated plaque T cells from same patients. DC = dendritic cell; FITC = fluorescein isothiocyanate; HSA = human serum albumin; IL = interleukin; MDA = malondialdehyde; sh = short hairpin; TCR = T cell receptor; TGF = transforming growth factor; TNF = tumor necrosis factor.

RESULTS

INDUCTION OF DC-MEDIATED T-CELL ACTIVATION BY MDA. After testing 1, 5, and 10 μg/ml MDA-HSA, we chose the highest dose for use. MDA-HSA enhanced the expression of markers of DC activation and several co-stimulatory proteins (Figure 1A) (median fluorescence intensity from 3 individual experiments are presented in Supplemental Figure 1A), as well as the levels of IL-6 and TNF-α. In contrast,

FIGURE 2 **MDA-HSA Induces Pro-Inflammatory Activation on T Cells From Both Plaques and Healthy Blood Donors**

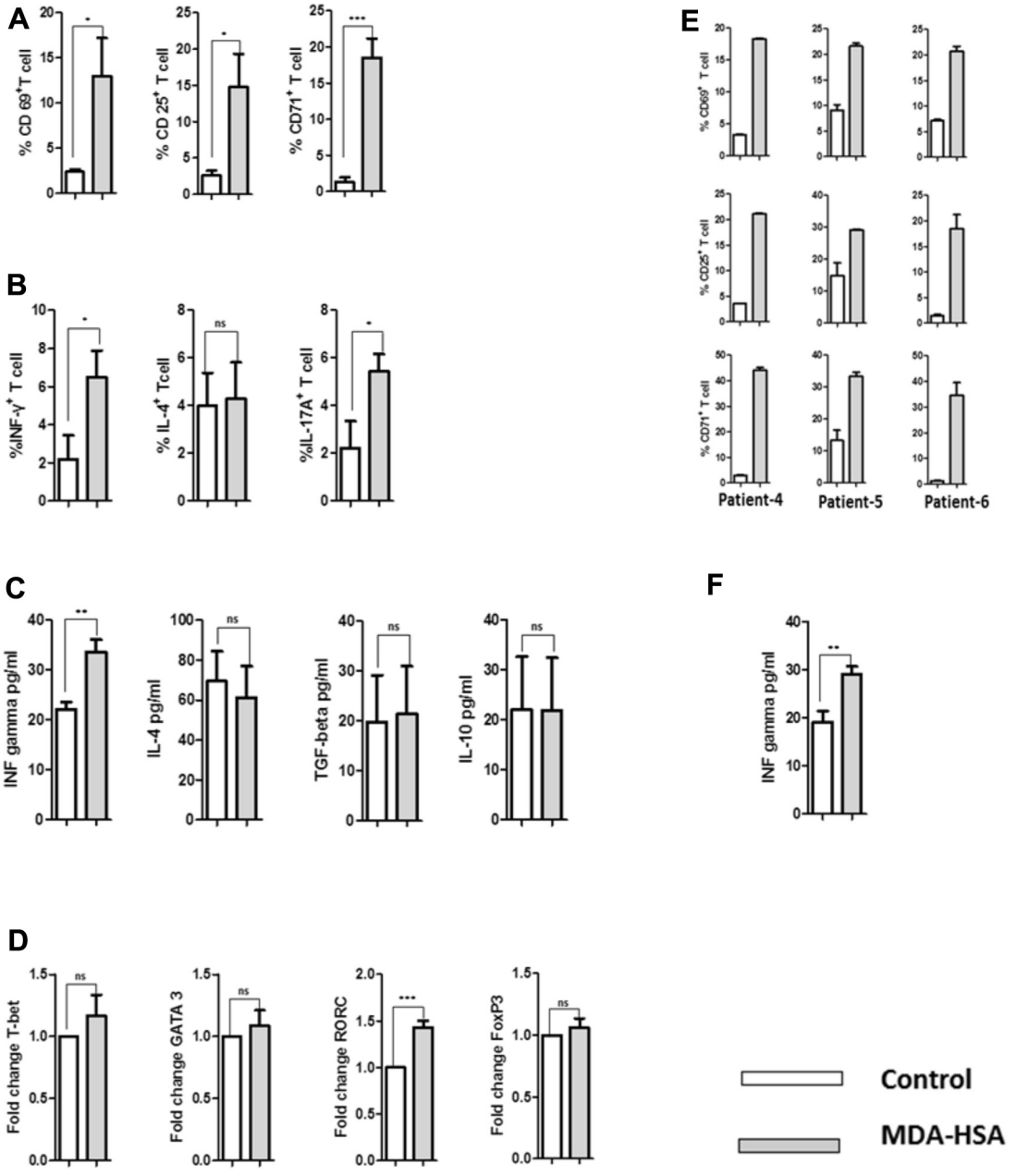

(A) CD3 T cells were activated by incubation with 10 μg/ml MDA-HSA and the treatment-induced T-cell activation. **(B)** MDA-HSA induced differentiation of INF-gamma- and IL-17A-positive cells but no significant change in IL-4-positive T cells. **(C)** MDA-HSA induced pro-inflammatory but not anti-inflammatory cytokines in plaque T cells. **(D)** MDA-HSA induced the transcription factors RORC, but not T-bet, GATA3, or FoxP3. Mean of 3 independent experiments **(A-D).** **(E)** T cells from atherosclerotic plaques duplicates were activated by MDA-HSA. **(F)** The level of IFN-gamma in the supernatant of plaque T cells from patients was elevated by MDA-HSA. (Mean of 3 patients.) FoxP3 = forkhead box P3; IFN = interferon; other abbreviations as in Figure 1.

FIGURE 3 Effects of MDA-HSA on HSP60 Production and Activation in DCs and T Cells

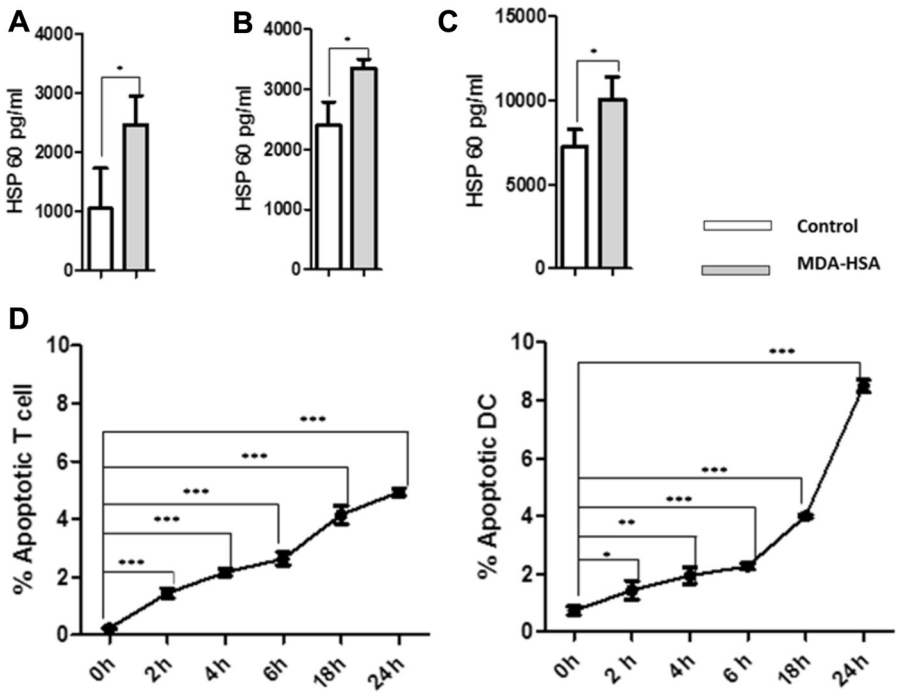

CD3 T cells or DCs were stimulated with MDA-HSA for 12 h, leading to much higher production of HSP60 in the former **(A)** than latter **(B)**. Three individual experiments are shown. **(C)** MDA-HSA elevated HSP60 production by plaque T cells. **(D)** Exposure of CD3 T cells or DCs to MDA-HSA for different periods promoted apoptosis among both. In both DCs and T cells, the percentage of apoptotic cells was increased by the time (mean of 3 individual samples). HSP = heat shock protein; other abbreviations as in Figure 1.

TGF-β levels were not significantly altered, and IL-10 levels declined (Figure 1B). HSA itself was without effect (Supplemental Figures 1B to 1D).

Furthermore, MDA-HSA promoted activation of T cells by DCs (Figure 1C). To investigate HLA-II-mediated T-cell activation, MDA-HSA-induced DCs were cultured with T-cell presence or absence of HLA-II blocking antibodies. Blockage of HLA-II with specific antibodies did not inhibit induction of CD25, a marker of activation, by MDA-HSA (not shown); whereas silencing of TCR-α and -β inhibited MDA-HSA-induced DC-mediated activation of T cells (Figure 1D).

Treatment of DCs derived from peripheral monocytes of patients with MDA-HSA and subsequent co-culture with T cells obtained from plaques of the same patients gave similar results (Figure 1E).

THE EFFECT OF MDA-HSA ON DC-INDEPENENT ACATIVATION OF T CELLS. MDA-HSA (Figure 2A) caused potent activation of T cells, whereas once again HSA alone had no effect (Supplemental Figure 2A). Silencing or inhibition of TLR2, TLR4, or TCR (α/β) did not alter this response to MDA-HSA (Supplemental Figure 2B). MDA-HSA was found to bind to the cell/cell membrane directly and/or penetrate into the cell (Supplemental Figure 2C), and intracellular staining showed activation of pro-inflammatory Th1 and Th17 but not Th2 T cells (Figure 2B). In the supernatants from cells treated with MDA-HSA, the levels of IFN-γ were increased; IL-4 and TGF-β showed no significant change (Figure 2C). IL-17 was undetectable in our enzyme-linked immunosorbent assay.

Transcription factors for Th17 cells (RORC) were induced by MDA-HSA with no alteration in the case of GATA3, Tbet-1, or Fox P3 (Figure 2D).

As with peripheral blood T cells, plaque T cells were also activated by MDA-HSA (Figure 2E), and the level of IFN-γ in the cells supernatant was elevated (Figure 2F).

CELL PROLIFERATION. MDA-HSA did not stimulate DCs and T cell proliferation (Supplemental Figure 2D).

INDUCTION OF HSP60. MDA-HSA induced HSP60 in both T-cells (Figure 3A) and DCs (Figure 3B) from healthy donors as well as plaque T cells (Figure 3C).

FIGURE 4 Macrophage Activation

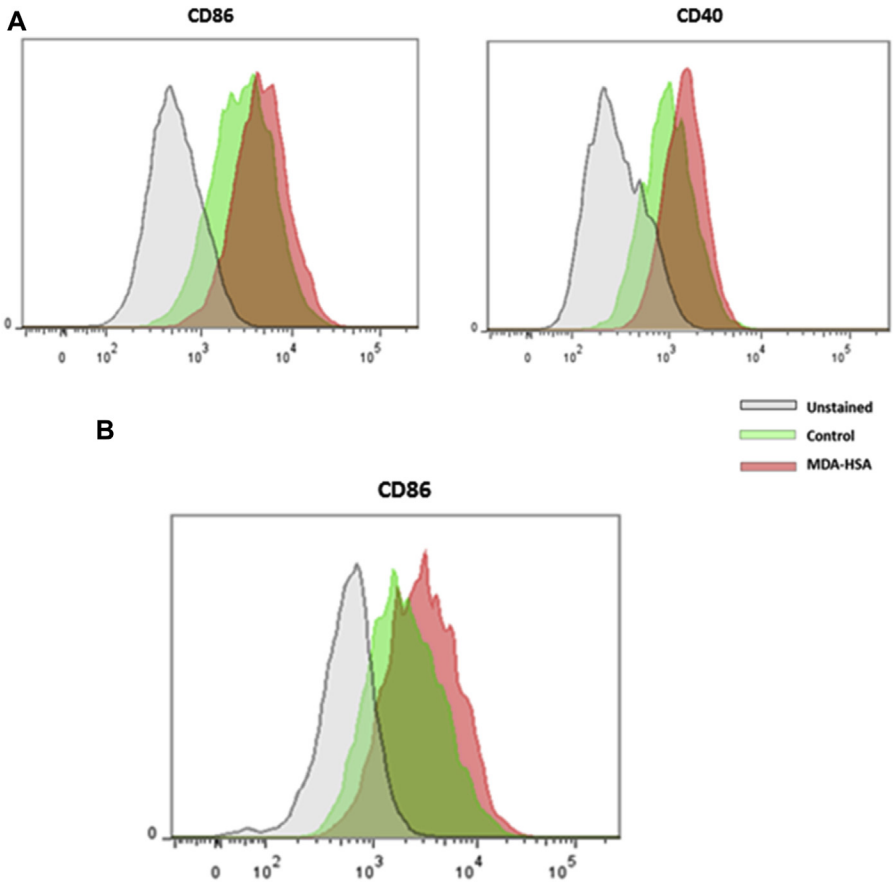

(A) One of 3 individual experiments. When monocytes were first cultured with GM-CSF for 5 days and then stimulated with MDA-HSA, expression of surface proteins CD86 and CD40 by macrophage was enhanced. **(B)** CD86 expression increased when MDA-HSA–stimulated T cells were co-cultured with monocytes derived macrophages for 48 h of incubation. GM-CSF = granulocyte-macrophage colony-stimulating factor; other abbreviations as in Figure 1.

ACTIVATION INDUCES APOPTOSIS IN DCs AND T CELLS. The concentration of MDA-HSA used, which is not highly toxic to the cells, induced apoptosis in both DCs and T cells that increased with time (Figure 3D).

M1 MACROPHAGE DIFFERENTIATION BY MDA-HSA. When macrophages (identified by CD11b) were treated with MDA-HSA, the percentage expressing M1-specific marker CD86 was increased (Figure 4A).

CD40 ligation plays an important role in the inflammation associated with CVDs; this protein was also induced by MDA-HSA (Figure 4A), and mean fluorescence intensity of 3 individual experiments is shown (Supplemental Figure 3A).

Our hypothesis that MDA-HSA-induced T cells influence M1 development in atherosclerotic lesions was supported by the finding that MDA-HSA-treated T cells induced expression of CD86 in macrophages (Figure 4B); MFI from 3 individual experiments are shown (Supplemental Figure 3B). Only mild apoptosis occurred in the macrophages treated with MDA-HSA (Supplemental Figure 3C).

INHIBITION OF T-CELL ACTIVATION. Direct activation of T cells by MDA-HSA was inhibited by anti-MDA antibodies (Figure 5A), as was the binding of MDA-HSA to T cells (Supplemental Figure 3D). Mito-TEMPO inhibited mitochondrial ROS as expected (Supplemental Figure 3E), and partially reduced the activation of T cells in response to MDA-HSA (Figure 5B).

MDA-HSA INDUCES P38 MITOGEN-ACTIVATED PROTEIN KINASE, TLR2, AND TLR4. MDA-HSA increased the activation of p38 mitogen-activated protein kinase (MAPKp38), as well as expression

FIGURE 5 Means of 3 Independent Experiments

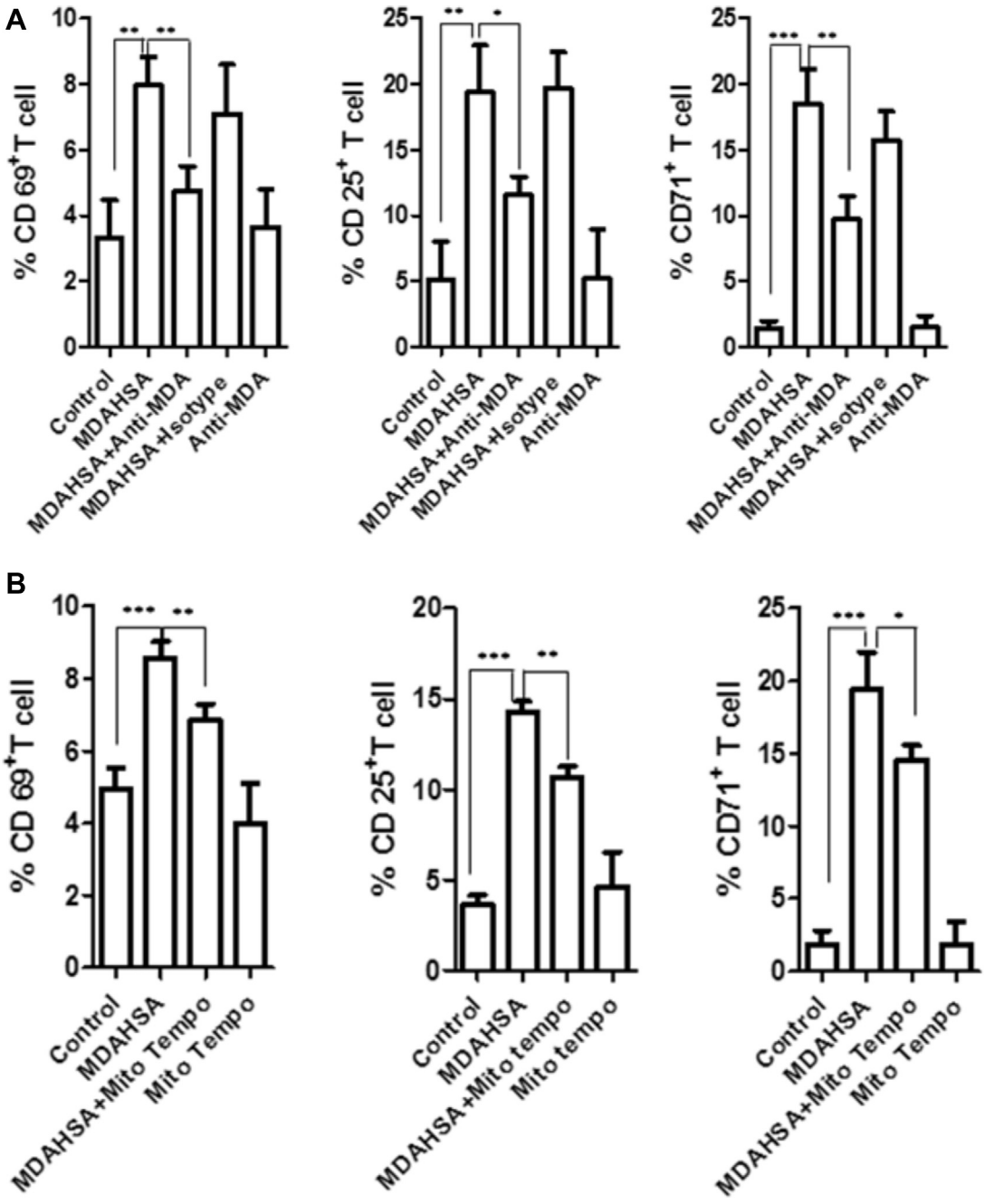

(A) The activation of T cells in response to MDA-HSA was inhibited by anti-MDA antibodies. **(B)** Pre-incubation of CD3 T cells Mito-TEMPO (Sigma Aldrich, St. Louis, Missouri), an inhibitor of mitochondrial ROS production, inhibited their subsequent activation by MDA-HSA slightly. ROS = reactive oxygen species; other abbreviations as in Figure 1.

levels of TLR2 and TLR4 in cells from each individual (Figure 6); MFI are shown from 3 individuals' experiments (Supplemental Figure 4), but not of the P65 subunit of nuclear factor kappa-light-chain-enhancer of activated B cells (NF-kB) (not shown).

MS ANALYSIS. After treating HSA in vitro, 31 peptides could be identified (Table 1) (see Supplemental

FIGURE 6 MAPK p38 Was Elevated in Response to MDA-HSA in Both DCs and T cells

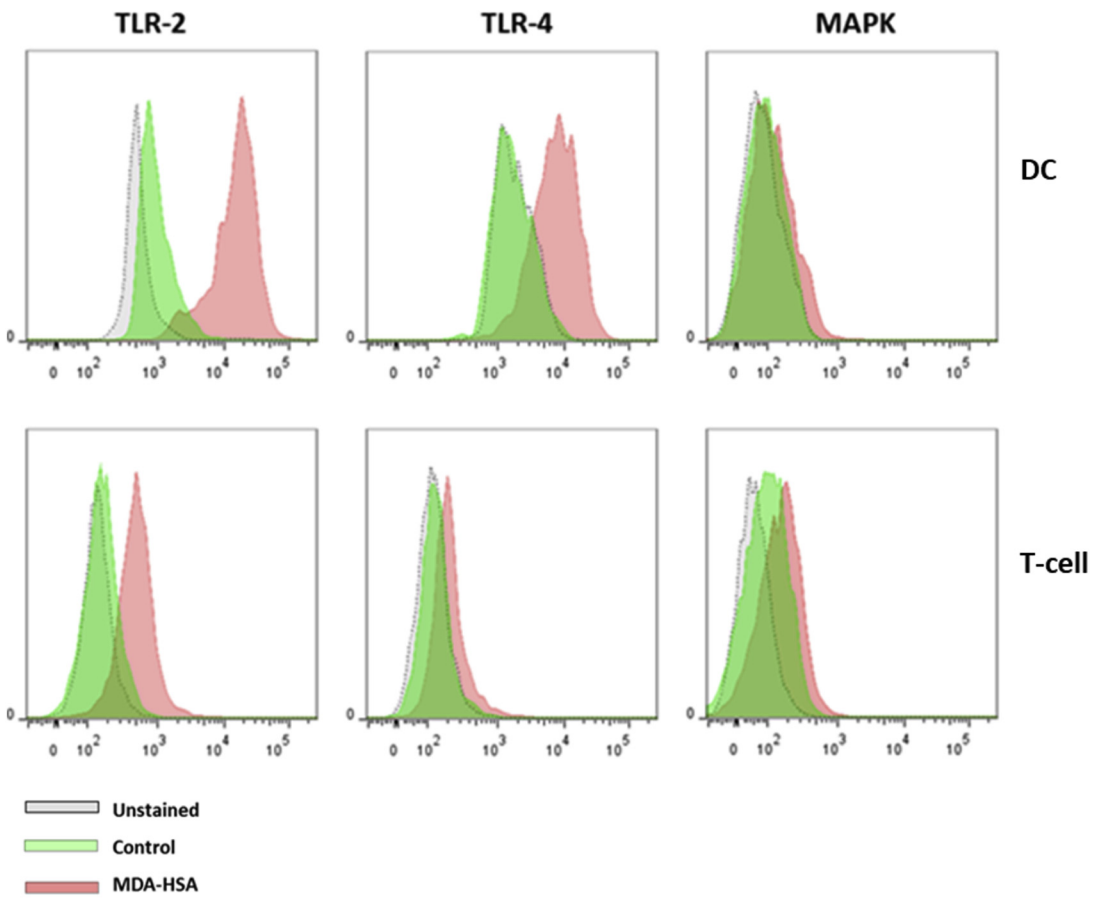

TLR2 expression was potently induced in both DCs and T cells, and TLR4 also increased. (One of 3 individuals' experiments is shown.)
MAPK = mitogen-activated protein kinase; TLR = Toll-like receptor; other abbreviations as in Figure 1.

Figure 5 for a representation of MS tracings). In the HSA of atherosclerotic patients, there were 9 MDA-modified peptides (Table 2), 2 of which were similar to those obtained in in vitro modification (set in boldface in Tables 1 and 2).

DISCUSSION

OxLDL has a complex structure, the different parts of which might play varying roles in immune activation. Apparently, mice and humans differ in this respect; LDL in a murine model activates T cells.

We have shown that OxLDL activates T cells in humans (4,5), which is a finding confirmed by others (7) that has recently been further developed (6,21).

Therefore, we chose here to study T cells isolated directly from human atherosclerotic plaques in relation to DCs from the same individuals, that is, an ex vivo human model similar to that described previously (6,21).

We report for the first time that MDA, conjugated with autologous human albumin, activates T cells, including those isolated from plaques, by both direct and, to some extent, indirect mechanisms via DCs. As expected, albumin itself has no effect.

MDA-HSA induced a pro-inflammatory activation of DCs, indicated by increased expression of CD86, CD80, and CD40 markers and production of cytokines. The direct effect on T cells from plaques (and peripheral blood) was strong, whereas DC-mediated MDA-HSA-induced T-cell activation was weaker. MDA-HSA induced secretion of pro-inflammatory cytokine secretion as IFN-γ, but not IL-17. At the same time, cell proliferation was unaltered, which is not the case with DC-mediated activation of T cells in response to OxLDL (6,21).

JACC: BASIC TO TRANSLATIONAL SCIENCE VOL. 4, NO. 4, 2019
AUGUST 2019:480–94

TABLE 1 Mass Spectrometric Analysis of MDA-Modified-HSA In Vitro

MDA Modified Peptide		
Sequence (HSA)	Peptide Position in Protein/MDA Site in Peptide	Mascot Scores
LVnEVTEFAK	66–75/N3	29.88
SLhTLFGDK	89–97/H3	23.33
LVnEVTEFAKTcVADESAENcDK	66–88/N3	71.82
SLhTLFGDKLcTVATLR	89–105/Q1	56.61
qEPERNEcFLQHK	118–130/Q1	28.78
qEPERNEcFLQHKDDNPNLPR	118–138/Q1	15.34
nEcFLQHK	123–130/N1	39.93
nEcFLQHKDDNPNLPR	123–138/N1	43.00
DDnPNLPR	131–138/N3	11.11
RhPYFYAPELLFFAKR	169–184/H2	35.63
AEFAEVSKLVTDLTKVhTEccHGDLLEcADDR	250–281/H17	31.06
LVTDLTKVHTEcchGDLLEcADDR	**258–281/H14**	**1.25**
VhTEccHGDLLEcADDR	265–281/H2	120.50
VhTEccHGDLLEcADDRADLAK	265–286/H2	68.46
LKEccEKPLLEKSHcIAEVEnDEMPADLPSLAADFVESK	299–337/N21	14.62
EccEKPLLEKShcIAEVENDEMPADLPSLAADFVESKDVcK	301–341/H12	4.20
nYAEAK	342–347/N1	23.17
RhPDYSVVLLLR	361–37/H2	77.98
hPDYSVVLLLR	362–372/H1	37.38
ccAAADPhEcYAKVFDEFKPLVEEPQNLIK	384–413/H8	7.40
QncELFEQLGEYK	414–426/N2	69.33
FqNALLVR	427–434/Q2	38.27
YTKKVPqVSTPTLVEVSR	435–452/Q7	39.37
KVPqVSTPTLVEVSR	438–452/Q4	38.21
VPqVSTPTLVEVSR	439–452/Q3	20.88
nLGKVGSK	453–460/N1	34.56
nLGKVGSKccK	453–463/N1	17.75
EFnAETFTFHADIcTLSEK	525–543/N3	114.90
EFnAETFTFHADIcTLSEKER	525–545/N3	41.65
qIKKQTALVELVK	546–558/Q1	69.53
QIKKqTALVELVK	546–558/Q5	38.42
KqTALVELVK	449–458/Q2	39.75
KqTALVELVKHKPK	449–462/Q2	25.23
qTALVELVK	550–558/Q1	51.03
LVAASqAALGL	599–609/Q6	24.37
TcVADESAEncDKSLHTLFGDK	**76–97/N10**	**3.92**

Two peptides from patients' plasma had similar modification as in vitro modification **(bold)**.
MDA = malondialdehyde; HSA = human serum albumin.

Because MDA is exposed extensively in atherosclerotic lesions (not only on proteins and OxLDL but also on the dead cells present) (23), this finding could have important implications for plaque rupture and thus CVD. Activation of pro-inflammatory T cells and DCs is a typical phenomenon in vulnerable plaques (1,14–17), and MDA has a danger-associated molecule pattern to promote inflammation (23). The presence of MDA-modified proteins in atherosclerotic plaques of animal models (Watanabe rabbits) (24), apoE knockout mice (25), and in the human atherosclerosis (23,26) has long been known. Furthermore, circulating levels of MDA are elevated in many conditions with increased oxidative stress and chronic inflammation, not only atherosclerosis and CVD but also diabetes, Alzheimer's disease, and systemic lupus erythematosus (23,27–29).

Previously, immunization with MDA-modified LDL (which is also produced during oxidation of LDL by copper ions among different methods) was found to inhibit the development of atherosclerosis in animal models (30,31). The MDA in OxLDL may play an important role in connection with pro-inflammatory effects and sterile inflammation (23,32). Little is known about the direct effects of MDA conjugates on T-cell activation (33), although in an earlier investigation, Jurkat cells developed a more pronounced pro-inflammatory phenotype in response to MDA (34).

DCs activated by MDA-HSA could promote T-cell activation induced by other antigens, presented to T cells by DCs. In addition, to some extent, T cells could be activated indirectly by MDA-HSA, although the underlying mechanism remains to be elucidated. However, 2 h of MDA-HSA stimulation caused a mild reduction in the level of ATP in T cells (Supplemental Figure 6), indicating an energy-dependent mechanism, possibly involving active diffusion. It is thus possible that MDA-HSA enters cells through diffusion and activates cells by mitochondrial ROS. This change in the ATP level was not due to cell death. Direct activation of T cells in plaques by pro-inflammatory MDA-modified proteins could thus, in principle, promote plaque rupture and ensuing CVD, stroke, and myocardial infarction because both activated DCs and T cells are localized in vulnerable plaques, that is, plaque especially close to areas prone to rupture or where rupture has already occurred.

Peptides of serum albumin from atherosclerotic patients' plasma are modified by MDA.

Circulating levels of antibodies against OxLDL (anti-OxLDL) have been reported to be both negatively and positively associated with atherosclerosis and CVD (2,18).

Different components of OxLDL could be involved here. For example, OxLDL cross-reacts with cardiolipin, and antibodies against cardiolipin are well known to be associated with an increased risk of CVD, most likely through oxidized phospholipids (35). Antibodies against apoB or peptides thereof have also produced varying results, sometimes as a protection, and in other cases they have provided to be risk markers (2,19).

We focused on the phospholipid portion of OxLDL, where compounds such as PC and MDA are typically

generated and exposed, the latter binding especially readily to proteins.

Both anti-PC and anti-MDA immunoglobulin M (IgM) antibodies are markers of protection, even when exposed on compounds other than those related to oxLDL such as albumin (2,18). Surprisingly, IgM anti-MDAs are T-cell dependent (18); therefore, we have focused on the effects of MDA conjugated with albumin on activation of T cells in human blood and plaques.

We hypothesized that OxLDLs promote immune activation and inflammation indirectly by inducing HSP60 in monocytes/macrophages (36) and recently confirmed and extended this notion by showing that OxLDL-induced activation of T cells (also from plaques) depends on HSP60 because silencing of HSP60 inhibited OxLDL-induced T-cell activation through DCs. Moreover, we recently reported that HSP60 is a classic T-cell antigen, presented by DCs to plaque T cells through major histocompatibility complex class II (22).

Our findings do not support the proposal that OxLDL induction of HSP in DCs is caused largely by MDA epitopes because this compound itself did not induce HSP60 strongly in DCs.

However, the direct induction of HSP60 in both plaque and blood T cells by MDA-HSA was pronounced.

This could contribute to activation of plaque T cells through DC-mediated activation as well as other mechanisms because HSP60 also elicits a more nonspecific pro-inflammatory state, such as activation of monocytes/macrophages.

We reported that HSP60 is essential for oxLDL-induced DC-mediated activation of T cells (6); however, it is also implicated in statin-induced inhibition of this effect (21) and could in principle be a target for atherogenic anti-HSP60 antibodies (37,38).

Moreover, we have recently shown that a classic T-cell antigen HSP60 elicits a pro-inflammatory response from atherosclerotic plaque cells (22). Induction of HSP60 in T cells by MDA-HSA could thus contribute to atherogenesis, as well as immune activation and inflammation in plaques.

We have recently shown that MDA-HSA induces oxidative stress in peripheral blood mononuclear cells/monocytes, and, furthermore, that anti-MDA IgM antibodies inhibit this effect (18). Such anti-MDA IgM (directed against MDA conjugated with HSA) are markers of protection in patients with SLE (especially in relation to atherosclerosis) and also for risk of CVD among 60-year-old patients (18,19). The underlying mechanisms proposed include enhanced clearance of dead or dying cells and inhibition of the uptake of OxLDL by macrophages/foam cells (2,18).

TABLE 2 Identification of MDA-Modified-HSA Peptides in Atherosclerotic Patients

MDA Modified Peptide		
Sequence (HSA)	Peptide Position in Protein/MDA Site in Peptide	Mascot Scores
AAFTECCQAADk	187–198/K12	4.29
VTkCCTESLVNR	497–508/K3	7.36
EQLkAVMDDFAAFVEK	566–581/K4	20.79
TCVADESAEnCDkSLhTLFGDK	**76–97/N10 K13 H16**	**17.42**
LVRPEVDVMCTAFhDNEETFLkk	139–16/1H14 K22 K23	17.01
LVTDLTkVhTECChGDLLECADDR	**258–281/K7 H9 H14**	**5.01**
QNCELFEQLGEYkFQnALLVrYTK	414–437/K13 N16 R21	1.17
TCVADESAEnCDkSLhTLFGDKLCTVATLR	76–105/N10 K13 H16	14.46
VHTECCHGDLLECADDrADLAkYICEnQDSISSK	265–298/R17 K22 N27	17.40

Two peptides from patients' plasma had similar modification as in vitro modification **(bold)**.
Abbreviations as in Table 1.

We show here that specific anti-MDA IgGs inhibited direct activation of T cells by MDA-HSA, indicating a potential protective property of these antibodies and providing support for elevation of anti-MDA levels through active or passive immunization as a therapeutic intervention.

In addition, direct activation of T cells by MDA-HSA was attenuated by an inhibitor of oxidative stress, MitoTEMPO. In general, ROS are chemically very active, small, and short-lived oxygen-containing molecules in which a common denominator is that their unpaired electrons (i.e., free radicals) may play various roles in both health and disease, for example, by damaging proteins, DNA, and lipid bilayers. ROS play a direct role in innate immune responses to pathogens and may also be common signaling molecules in cells, tissues, and organs.

Mitochondria are a source of ROS. Although the relationship between ROS and immunity in general has been studied extensively, the role of ROS in the activation of T cells is less well described. In general, ROS may participate and modulate various processes, including hyporesponsiveness and apoptosis in a complex and situation-dependent manner (39,40).

Our finding that MDA-HSA-induced apoptosis in both DCs and T cells after directly, indicates that MDA-HSA might contribute to cell death in plaques, in which accumulating dead cells is a typical characteristic.

TLR2 and TLR4 were induced in both T cells and DCs by MDA-HSA. Neither is involved T-cell activation, but they play a role in the inflammatory response to MDA-HSA.

Moreover, MDA-HSA promoted polarization of macrophages toward the M1 phenotype. Much attention has been paid to the macrophage subtypes M1 and M2, where M1 is involved in pro-inflammatory kill responses and M2 in repair.

M1 is associated with Th1 and M2 more with Th2 responses, whereas M1 may both be induced by and promote the Th1 phenotype (41).

Macrophages play major roles in all stages of atherogenesis, from the initiation with fatty streak formation and foam cells derived from macrophages, to later complex lesions with a necrotic core and inflammation with macrophages and other immune-competent cells producing primarily pro-inflammatory cytokines (1). However, apoptosis among macrophages' response to MDA-HSA was much less pronounced than that among T cells and DCs. Thus, macrophages may reprogram in response to MDA-HSA to adapt.

MDA-HSA induced activation of MAPKp38 but not NF-Kb in both DCs and T cells. MAPKp38 are signaling molecules of major importance, regulating cellular response to stressors. Because they regulate pro-inflammatory cytokines, these may be underlying factors in chronic inflammatory conditions, including rheumatic and autoimmune diseases, as well as atherosclerosis. Accordingly, inhibition of MAPKp38 is being tested in various clinical settings. Induction of MAPKp38 could thus represent yet another pro-inflammatory property of MDA-HSA (42).

TLRs, especially TLR2 and TLR4, are implicated in innate immune responses, and inhibition of these to ameliorate atherosclerosis, CVD, and other chronic inflammatory conditions is being discussed as a therapeutic possibility.

Although not directly involved here in MDA-HSA-mediated T-cell activation, TLR2 and TLR4 were induced by MDA-HSA and may thereby promote atherosclerosis and CVD through innate immune responses and inflammation in plaque (43). Furthermore, TLR2 may be involved in in plaque erosion, a potentially important underlying factor in CVD (44).

In addition, macrophages of the M1 and M2 phenotypes have been divided into further subtypes, and several stimuli have been described that could promote such processes. In general, the M1 subtype is believed to be atherogenic, and in light of its pro-inflammatory features, it may also promote CVD. Whereas the M1 phenotype is known to be induced by OxLDL and cholesterol crystals, little is known about the effect of MDA in this context. MDA coupled with carriers such as HSA might promote atherosclerosis and other complications by promoting the M1 phenotype.

The present investigation reveals that MDA modified HSA peptides in vitro and, moreover, that the serum of albumin of atherosclerotic patients contains MDA-modified HSA peptides.

Importantly, 2 of the modifications in atherosclerotic patients were similar to those in vitro. This is an indication that the in vitro MDA-modified HSA is of biological relevance and might cause T-cell activation in human atherosclerotic plaques.

Taken together, the novel properties of MDA-HSA observed here may play a role in inflammation and immune activation in atherosclerotic plaques. Both DCs and, directly, T cells were activated, in the latter case with the apparent involvement of ROS.

However, DC-mediated T-cell activation was modest. HSP60 was induced potently in T cells by MDA-HSA, which is interesting because HSP60 is a much-discussed possible contributing cause to atherosclerosis at different stages of disease development. IgG anti-MDA antibodies inhibited the effects of MDA-HSA on T cells, a finding with therapeutic implications. Amelioration of MDA-mediated immune activation in connection with atherosclerosis by immunization or by other means could be a valuable therapeutic option.

ADDRESS FOR CORRESPONDENCE: Dr. Johan Frostegård, Unit of Immunology and Chronic Disease, Institute of Environmental Medicine, Karolinska Institutet, Nobels väg 13, 171 65 Stockholm, Sweden. E-mail: Johan.frostegard@ki.se.

PERSPECTIVES

COMPETENCY IN MEDICAL KNOWLEDGE: In this paper, we delineate a possible new pathway and mechanism by which T cells could be activated in human atherosclerotic plaques. It is possible that immune modulation could be implemented in the future in this field, but there are also consequences of our study for current clinical practice.

TRANSITIONAL OUTLOOK: From a translational point of view, our findings provide information for further development aimed at ameliorating and modulating immune responses related to MDA in atherosclerotic plaques, where immunization is one interesting possibility we think deserves more attention.

REFERENCES

1. Frostegard J, Ulfgren AK, Nyberg P, et al. Cytokine expression in advanced human atherosclerotic plaques: dominance of pro-inflammatory (Th1) and macrophage-stimulating cytokines. Atherosclerosis 1999;145:33–43.

2. Frostegard J. Immunity, atherosclerosis and cardiovascular disease. BMC Med 2013;11:117.

3. Fei GZ, Huang YH, Swedenborg J, Frostegard J. Oxidised LDL modulates immune-activation by an IL-12 dependent mechanism. Atherosclerosis 2003;169:77–85.

4. Huang YH, Ronnelid J, Frostegard J. Oxidized LDL induces enhanced antibody formation and MHC class II-dependent IFN-gamma production in lymphocytes from healthy individuals. Arterioscler Thromb Vasc Biol 1995;15:1577–83.

5. Frostegard J, Wu R, Giscombe R, Holm G, Lefvert AK, Nilsson J. Induction of T-cell activation by oxidized low density lipoprotein. Arterioscler Thromb 1992;12:461–7.

6. Liu A, Ming JY, Fiskesund R, et al. Induction of dendritic cell-mediated T-cell activation by modified but not native low-density lipoprotein in humans and inhibition by annexin a5: involvement of heat shock proteins. Arterioscler Thromb Vasc Biol 2015;35:197–205.

7. Stemme S, Faber B, Holm J, Wiklund O, Witztum JL, Hansson GK. T lymphocytes from human atherosclerotic plaques recognize oxidized low density lipoprotein. Proc Natl Acad Sci U S A 1995;92:3893–7.

8. Huang YH, Schafer-Elinder L, Wu R, Claesson HE, Frostegard J. Lysophosphatidylcholine (LPC) induces proinflammatory cytokines by a platelet-activating factor (PAF) receptor-dependent mechanism. Clin Exp Immunol 1999;116:326–31.

9. Frostegard J, Huang YH, Ronnelid J, Schafer-Elinder L. Platelet-activating factor and oxidized LDL induce immune activation by a common mechanism. Arterioscler Thromb Vasc Biol 1997;17:963–8.

10. Hermansson A, Ketelhuth DF, Strodthoff D, et al. Inhibition of T cell response to native low-density lipoprotein reduces atherosclerosis. J Exp Med 2010;207:1081–93.

11. Zhou X, Nicoletti A, Elhage R, Hansson GK. Transfer of CD4(+) T cells aggravates atherosclerosis in immunodeficient apolipoprotein E knockout mice. Circulation 2000;102:2919–22.

12. Gojova A, Brun V, Esposito B, et al. Specific abrogation of transforming growth factor-beta signaling in T cells alters atherosclerotic lesion size and composition in mice. Blood 2003;102:4052–8.

13. Kolbus D, Ljungcrantz I, Andersson L, et al. Association between CD8+ T-cell subsets and cardiovascular disease. J Intern Med 2013;274:41–51.

14. Bobryshev YV, Watanabe T. Ultrastructural evidence for association of vascular dendritic cells with T-lymphocytes and with B-cells in human atherosclerosis. J Submicrosc Cytol Pathol 1997;29:209–21.

15. Millonig G, Niederegger H, Rabl W, et al. Network of vascular-associated dendritic cells in intima of healthy young individuals. Arterioscler Thromb Vasc Biol 2001;21:503–8.

16. Yilmaz A, Lochno M, Traeg F, et al. Emergence of dendritic cells in rupture-prone regions of vulnerable carotid plaques. Atherosclerosis 2004;176:101–10.

17. Liu P, Yu YR, Spencer JA, et al. CX3CR1 deficiency impairs dendritic cell accumulation in arterial intima and reduces atherosclerotic burden. Arterioscler Thromb Vasc Biol 2008;28:243–50.

18. Rahman M, Sing S, Golabkesh Z, et al. IgM antibodies against malondialdehyde and phosphorylcholine are together strong protection markers for atherosclerosis in systemic lupus erythematosus: regulation and underlying mechanisms. Clin Immunol 2016;166–167:27–37.

19. Thiagarajan D, Frostegard AG, Singh S, et al. Human IgM antibodies to malondialdehyde conjugated with albumin are negatively associated with cardiovascular disease among 60-year-olds. J Am Heart Assoc 2016;5:e004415.

20. Wick G, Jakic B, Buszko M, Wick MC, Grundtman C. The role of heat shock proteins in atherosclerosis. Nat Rev Cardiol 2014;11:516–29.

21. Frostegard J, Zhang Y, Sun J, Yan K, Liu A. Oxidized low-density lipoprotein (OxLDL)-treated dendritic cells promote activation of T cells in human atherosclerotic plaque and blood, which is repressed by statins: microRNA let-7c is integral to the effect. J Am Heart Assoc 2016;5:pii:e003976.

22. Rahman M, Steuer J, Gillgren P, Hayderi A, Liu A, Frostegard J. Induction of dendritic cell-mediated activation of T cells from atherosclerotic plaques by human heat shock protein 60. J Am Heart Assoc 2017;6:pii:e006778.

23. Papac-Milicevic N, Busch CJ, Binder CJ. Malondialdehyde epitopes as targets of immunity and the implications for atherosclerosis. Adv Immunol 2016;131:1–59.

24. Haberland ME, Fong D, Cheng L. Malondialdehyde-altered protein occurs in atheroma of Watanabe heritable hyperlipidemic rabbits. Science 1988;241:215–8.

25. Palinski W, Ord VA, Plump AS, Breslow JL, Steinberg D, Witztum JL. ApoE-deficient mice are a model of lipoprotein oxidation in atherogenesis. Demonstration of oxidation-specific epitopes in lesions and high titers of autoantibodies to malondialdehyde-lysine in serum. Arterioscler Thromb 1994;14:605–16.

26. Yla-Herttuala S, Palinski W, Rosenfeld ME, et al. Evidence for the presence of oxidatively modified low density lipoprotein in atherosclerotic lesions of rabbit and man. J Clin Invest 1989;84:1086–95.

27. Ayala A, Munoz MF, Arguelles S. Lipid peroxidation: production, metabolism, and signaling mechanisms of malondialdehyde and 4-hydroxy-2-nonenal. Oxid Med Cell Longev 2014;2014:360438.

28. Frostegard J, Svenungsson E, Wu R, et al. Lipid peroxidation is enhanced in patients with systemic lupus erythematosus and is associated with arterial and renal disease manifestations. Arthritis Rheum 2005;52:192–200.

29. Perl A. Oxidative stress in the pathology and treatment of systemic lupus erythematosus. Nat Rev Rheumatol 2013;9:674–86.

30. Freigang S, Horkko S, Miller E, Witztum JL, Palinski W. Immunization of LDL receptor-deficient mice with homologous malondialdehyde-modified and native LDL reduces progression of atherosclerosis by mechanisms other than induction of high titers of antibodies to oxidative neoepitopes. Arterioscler Thromb Vasc Biol 1998;18:1972–82.

31. Palinski W, Miller E, Witztum JL. Immunization of low density lipoprotein (LDL) receptor-deficient rabbits with homologous malondialdehyde-modified LDL reduces atherogenesis. Proc Natl Acad Sci U S A 1995;92:821–5.

32. Busch CJ, Binder CJ. Malondialdehyde epitopes as mediators of sterile inflammation. Biochim Biophys Acta Mol Cell Biol Lipids 2017;1862:398–406.

33. Raghavan S, Subramaniyam G, Shanmugam N. Proinflammatory effects of malondialdehyde in lymphocytes. J Leukoc Biol 2012;92:1055–67.

34. Natarajan K, Mathialagan GD, Raghavan S, Shanmugam N. The advanced lipoxidation end product precursor malondialdehyde induces IL-17E expression and skews lymphocytes to the th17 subset. Cell Mol Biol Lett 2015;20:647–62.

35. Vaarala O, Alfthan G, Jauhiainen M, Leirisalo-Repo M, Aho K, Palosuo T. Crossreaction between antibodies to oxidised low-density lipoprotein and to cardiolipin in systemic lupus erythematosus. Lancet 1993;341:923–5.

36. Frostegard J, Kjellman B, Gidlund M, Andersson B, Jindal S, Kiessling R. Induction of heat shock protein in monocytic cells by oxidized low density lipoprotein. Atherosclerosis 1996;121:93–103.

37. Xu Q, Willeit J, Marosi M, et al. Association of serum antibodies to heat-shock protein 65 with carotid atherosclerosis. Lancet 1993;341:255–9.

38. Frostegard J, Lemne C, Andersson B, van der Zee R, Kiessling R, de Faire U. Association of serum antibodies to heat-shock protein 65 with borderline hypertension. Hypertension 1997;29:40–4.

39. Belikov AV, Schraven B, Simeoni L. T cells and reactive oxygen species. J Biomed Sci 2015;22:85.

40. Murphy MP, Siegel RM. Mitochondrial ROS fire up T cell activation. Immunity 2013;38:201–2.

41. Mills CD. Anatomy of a discovery: m1 and m2 macrophages. Front Immunol 2015;6:212.

42. Fisk M, Gajendragadkar PR, Maki-Petaja KM, Wilkinson IB, Cheriyan J. Therapeutic potential of p38 MAP kinase inhibition in the management of cardiovascular disease. Am J Cardiovasc Drugs 2014;14:155–65.

43. Moghimpour Bijani F, Vallejo JG, Rezaei N. Toll-like receptor signaling pathways in cardiovascular diseases: challenges and opportunities. Int Rev Immunol 2012;31:379–95.

44. Quillard T, Franck G, Mawson T, Folco E, Libby P. Mechanisms of erosion of atherosclerotic plaques. Curr Opin Lipidol 2017;28:434–41.

KEY WORDS atherosclerosis, dendritic cells, T cells, malondialdehyde, oxidized low-density lipoprotein

APPENDIX For supplemental figures, see the online version of this paper.

JACC: BASIC TO TRANSLATIONAL SCIENCE VOL. 4, NO. 4, 2019

PRECLINICAL RESEARCH

Extracellular Matrix From Hypertrophic Myocardium Provokes Impaired Twitch Dynamics in Healthy Cardiomyocytes

Lorenzo R. Sewanan, MS,[a,*] Jonas Schwan, PhD,[a,*] Jonathan Kluger, BSE,[a] Jinkyu Park, PhD,[b,e] Daniel L. Jacoby, MD,[b] Yibing Qyang, PhD,[b,c,d,e] Stuart G. Campbell, PhD[a,f]

VISUAL ABSTRACT

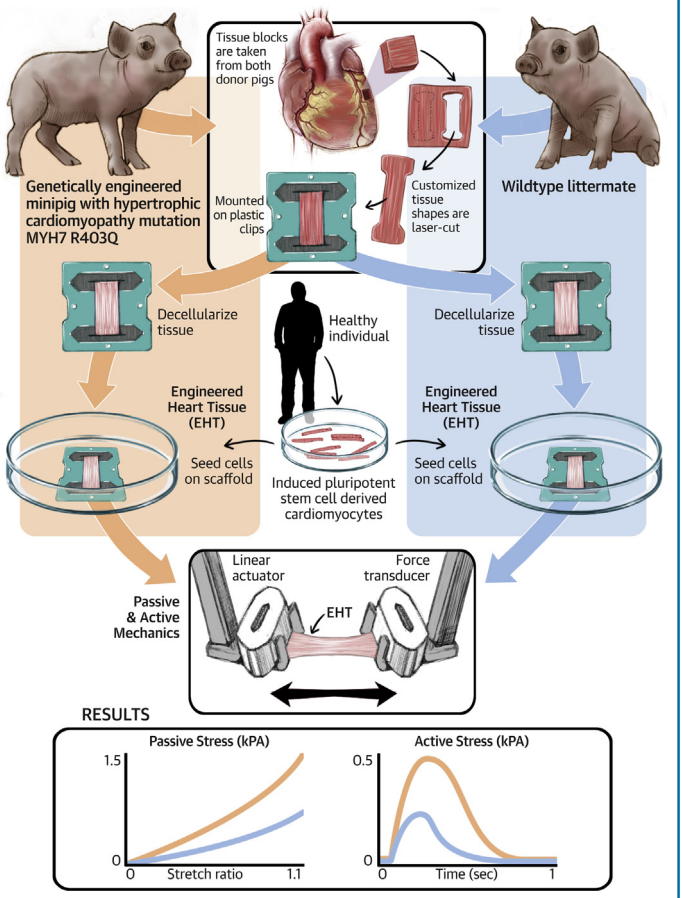

Sewanan, L.R. et al. J Am Coll Cardiol Basic Trans Science. 2019;4(4):495-505.

HIGHLIGHTS

- The goal of this study was to examine the effects of diseased extracellular matrix on the behavior of healthy heart cells.
- Myocardium was harvested from a genetically engineered miniature pig carrying the hypertrophic cardiomyopathy mutation MYH7 R403Q and from a wild-type littermate.
- Engineered heart tissues were created by seeding healthy human induced pluripotent stem cell-derived cardiomyocytes onto thin strips of decellularized porcine myocardium.
- Engineered heart tissues made from the extracellular matrix of hypertrophic cardiomyopathy hearts exhibit increased stiffness, impaired relaxation, and increased force development.
- This suggests that diseased extracellular matrix can provoke abnormal contractile behavior in otherwise healthy cardiomyocytes.

From the [a]Department of Biomedical Engineering, Yale University, New Haven, Connecticut; [b]Yale Cardiovascular Research Center, Section of Cardiovascular Medicine, Department of Internal Medicine, Yale School of Medicine, New Haven, Connecticut; [c]Yale Stem Cell Center, Yale University, New Haven, Connecticut; [d]Department of Pathology, Yale University, New Haven, Connecticut; [e]Vascular Biology and Therapeutics Program, Yale School of Medicine, New Haven, Connecticut; and the [f]Department of Cellular and Molecular Physiology, Yale School of Medicine, New Haven, Connecticut. *Mr. Sewanan and Dr. Schwan contributed equally to this work and are joint first authors. This research was supported by National Institutes of Health grants

ISSN 2452-302X https://doi.org/10.1016/j.jacbts.2019.03.004

JACC: BASIC TO TRANSLATIONAL SCIENCE VOL. 4, NO. 4, 2019
AUGUST 2019:495–505

ABBREVIATIONS AND ACRONYMS

cDNA = complementary deoxyribonucleic acid

CM = cardiomyocyte

ECM = extracellular matrix

EHT = engineered heart tissue

HCM = hypertrophic cardiomyopathy

H&E = hematoxylin and eosin

iPSC = induced pluripotent stem cell

SR = Sirius red

MTR = Masson trichrome

MUT = minipig carrying MYH7 R403Q mutation

RT50 = time from peak tension to 50% relaxation

TTP = time to peak tension

WT = wild-type

SUMMARY

Hypertrophic cardiomyopathy (HCM) is often caused by single sarcomeric gene mutations that affect muscle contraction. Pharmacological correction of mutation effects prevents but does not reverse disease in mouse models. Suspecting that diseased extracellular matrix is to blame, we obtained myocardium from a miniature swine model of HCM, decellularized thin slices of the tissue, and re-seeded them with healthy human induced pluripotent stem cell–derived cardiomyocytes. Compared with cardiomyocytes grown on healthy extracellular matrix, those grown on the diseased matrix exhibited prolonged contractions and poor relaxation. This outcome suggests that extracellular matrix abnormalities must be addressed in therapies targeting established HCM. (J Am Coll Cardiol Basic Trans Science 2019;4:495–505) © 2019 The Authors. Published by Elsevier on behalf of the American College of Cardiology Foundation. This is an open access article under the CC BY-NC-ND license (http://creativecommons.org/licenses/by-nc-nd/4.0/).

Hypertrophic cardiomyopathy (HCM) is an inherited disorder whose main clinical feature is severe left ventricular hypertrophy in the absence of elevated afterload, often leading to consequences such as diastolic heart failure, arrhythmia, and left ventricular outflow obstruction. Pathologically, HCM hearts display interstitial fibrosis and myocardial disarray (1). Decades of research into the genetic origins of HCM have identified sarcomeric gene mutations as the most common etiology (2). Such mutations have been clearly shown to alter the contractile characteristics of cardiomyocytes (CMs) (3-7), but exactly how simple contractile abnormalities lead to the diverse clinico-pathologic findings seen in HCM remains incompletely understood.

SEE PAGE 506

With the recent advent of targeted small molecule myosin modulators such as mavacamten, the possibility of preventing or even reversing HCM has emerged. Mavacamten acutely counteracts hypercontractility caused by gain-of-function HCM mutations. Studies in murine models of HCM explored the effect of myosin inhibition using mavacamten on disease development (8). As anticipated, mavacamten completely prevented hypertrophy and fibrosis in a mouse model of HCM, when administered chronically before the onset of hypertrophy. However, when the drug was introduced after the onset of measurable disease, its ability to reverse left ventricular wall thickening was limited. These findings suggest that key aspects of established HCM, including myocardial hypertrophy and perhaps even diastolic dysfunction, persist independent of the activity of the mutant protein. In other words, the pathophysiology of HCM may be self-sustaining in its more advanced stages.

One possible source of self-sustaining hypertrophic stimulus in HCM hearts is their extracellular matrix (ECM). Although the severity may vary, myocardial fibrosis is universally observed in established HCM. Evidence of abnormal ECM turnover is also seen in preclinical individuals who carry an HCM mutation (9), suggesting that ECM changes appear early and therefore could be involved in progression of the disease.

In pursuit of this hypothesis, we undertook a study of myocardial ECM obtained from a large animal model of genetic HCM (10). After histological and biomechanical characterization of myocardial samples from HCM hearts and healthy controls, we decellularized thin slices of myocardium and re-seeded them with healthy human CMs derived from an induced pluripotent stem cell (iPSC) line. By measuring the contractile behavior of these

R01 HL136590 (to Dr. Campbell) and R01 HL131940 (to Dr. Qyang), DOD 11959515 (to Dr. Qyang), an American Heart Association Predoctoral Fellowship (to Dr. Schwan), and a P.D. Soros Fellowship for New Americans (to Mr. Sewanan). Mr. Sewanan was also supported by a National Institutes of Health/National Institute of General Medical Sciences Medical Scientist Training Program Grant (T32GM007205). Drs. Schwan and Campbell have equity ownership in Propria LLC, which has licensed technology used in the research reported in this publication. This arrangement has been reviewed and approved by the Yale University Conflict of Interest Office. All other authors have reported that they have no relationships relevant to the contents of this paper to disclose. All authors attest they are in compliance with human studies committees and animal welfare regulations of the authors' institutions and Food and Drug Administration guidelines, including patient consent where appropriate. For more information, visit the *JACC: Basic to Translational Science* author instructions page.

Manuscript received December 6, 2018; revised manuscript received March 11, 2019, accepted March 13, 2019.

engineered myocardial constructs, it was possible to directly observe the effects of diseased ECM on cardiomyocyte performance and gain insights into how this factor may contribute to HCM pathophysiology.

METHODS

TISSUE HARVESTING. Flash-frozen left ventricular wall blocks from 3-month-old wild-type (WT) and mutant (R403Q) Yucatan miniature pigs (10) were provided by MyoKardia (South San Francisco, California). Breeding and tissue harvest were performed by a commercial vendor (Exemplar Genetics, Sioux Center, Iowa) and the samples shipped on dry ice. Tissues were kept frozen at -80°C until the beginning of experimental work.

HISTOLOGY. Wild-type and mutant native cardiac tissue were fixed for 24 h in 10% neutral buffered formalin (Shandon Formal-Fixx, Thermo Fisher Scientific, Waltham, Massachusetts), embedded in paraffin, sectioned at 5 μm thickness, and stained with either hematoxylin and eosin H&E. Masson trichrome (MTR), or Sirius Red (SR). Images were acquired by using 20× brightfield microscopy from multiple samples and image fields; image backgrounds were then corrected by using a 50 pixel rolling ball filter. To segment out specific features of the image, we performed color deconvolution using the ImageJ (version 1.51j8) toolbox (version 3.0.2) (11). Segmented fiber fields from MTR-stained sections and segmented nuclear fields from H&E stained sections were binarized, skeletonized, and processed by a custom MATLAB (R2017B) script (available from authors upon request), which implemented two-dimensional Fast Fourier Transform on binned and centered pixels to calculate the power distribution (12,13).

We quantified alignment as the anisotropy alignment index alpha such that $\alpha = 1 - \frac{\lambda_2}{\lambda_1}$, where the lambdas are the eigenvalues of the Cartesian fiber orientation tensor (12). To quantify the fibrosis fraction, both collagen content and total tissue content were segmented from either the MTR- or SR-stained tissue. The tissue and collagen segmentations were binarized by using the maximum entropy method in ImageJ, and the positive pixels were counted by using a custom MATLAB script; the fibrosis/tissue fraction was determined as the fraction of collagen pixels over total tissue pixels similar to published methods (14).

MAINTENANCE AND CARDIAC DIFFERENTIATION OF HUMAN iPSCs. The iPSCs used in this study were derived from T cells from a healthy adult man, previously described and extensively characterized (15). Human iPSC colonies were maintained on growth factor–reduced Matrigel (Corning, Corning, New York) at a 1:60 dilution and fed with mTESR medium every 24 h (STEMCELL Technologies, Vancouver, BC, Canada). When iPSCs reached 70% confluence, they were passaged as small colonies onto a new plate by using enzyme-free ReLeSR reagent (STEMCELL Technologies). All experiments were performed with human iPSCs between passages 35 and 45. The iPSCs were differentiated into CMs using a protocol modulating Wnt signaling as previously described (16). Briefly, after reaching ~90% confluence, iPSC colonies were treated with 17.5 μM CHIR99021 (STEMCELL Technologies) in a solution of 75% RPMI/B27-insulin and 25% mTeSR by volume. After 24 h, this culture medium was replaced with RPMI/B27-insulin. Seventy-two hours after CHIR99021 treatment, the differentiating cultures were exposed to the Wnt inhibitor IWP-4 (Tocris Bioscience, Minneapolis, Minnesota) at a concentration of 5 μM in RPMI/B27-insulin media. Media changes with RPMI/B27 (-) insulin were performed every 2 days until spontaneous beating was observed (usually between days 7 and 11 of differentiation), after which the medium was changed to RPMI/B27 (+) insulin. iPSC-CMs were used to create engineered heart tissues (EHTs) on day 14 after the start of differentiation.

EHT MANUFACTURING AND FUNCTIONAL TESTING. EHTs made out of decellularized myocardium were created similar to our previously published protocol (15). Briefly, we cut 150 μm slices from age-matched WT and mutant MYH7 R403Q porcine left ventricular blocks (MUT), which were frozen as discussed (**Figure 1A**). We omitted the sterilization process using peracetic acid and instead cultured the tissues in Dulbecco's modified Eagle medium with 10% fetal bovine serum and 2% penicillin-streptomycin overnight before seeding them the next day. For this study, we seeded both groups with exactly the same cell suspension at the same time. Active contraction mechanics were assessed as previously described (15) using a World Precision Instruments (WPI KG7) force transducer (**Figure 1B**) in Tyrode's solution at 35°C. The normalized tension-time integral was calculated as the area under the curve of the normalized twitch using numerical integration in MATLAB. To characterize intracellular calcium dynamics, some EHTs were loaded with the ratiometric fluorescent indicator Fura-2 AM (MilliporeSigma, Burlington, Massachusetts) by incubation at room temperature for 20 min in loading solution (Tyrode's solution with 17 μg/ml Fura 2-AM, 0.2% Pluronic F127, and 0.5%

FIGURE 1 Methods Used to Prepare and Test EHTs

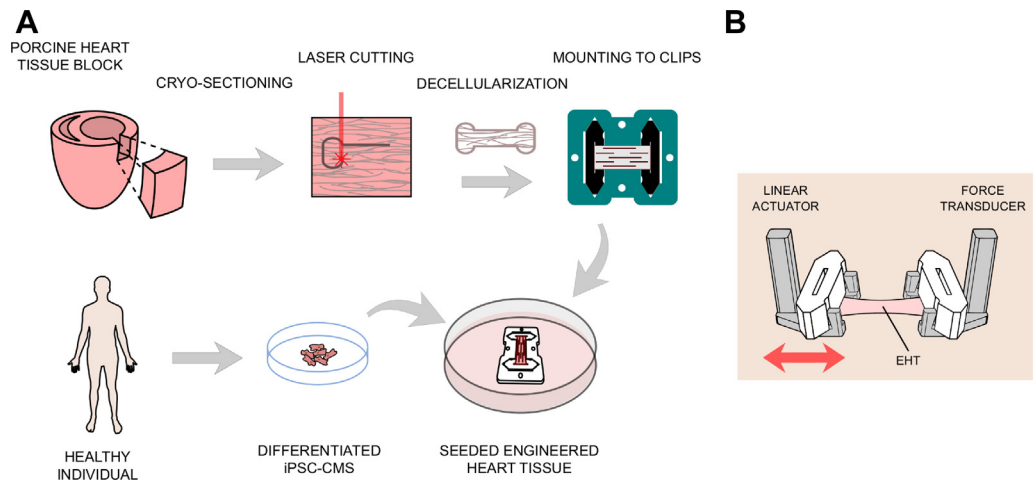

(A) Preparation of engineered heart tissues (EHTs). Tissue blocks were harvested from the left ventricular free wall and flash-frozen. Frozen blocks were sectioned into 150 μm thick slices, laser-cut into customized shapes, anchored into customized polytetrafluoroethylene (PTFE) tissue clips, and decellularized. Induced pluripotent stem cell–derived cardiomyocytes (iPSC-CMs) were seeded onto the scaffolds to create beating EHTs. **(B)** Clips were ejected out of the culturing frame and mounted on a testing setup consisting of a linear actuator and a force transducer. Force measurements were taken at different muscle lengths by moving the linear actuator.

Cremophor EL) and subsequently imaged at 35°C using a photometric system as previously described. EHTs were paced at 1 Hz during both contractile and calcium testing.

UNIAXIAL DIASTOLIC/PASSIVE MECHANICS. EHTs and tissue samples were brought to culture length (6.0 mm) on our apparatus at physiological pH (7.3) and temperature (36°C) and preconditioned for 3 cycles of 10% stretch (0.6 mm) at a rate of 0.015 mm/s (0.25% muscle length/s). After preconditioning, native and decellularized tissue from WT and MUT pig hearts were loaded and unloaded 3 times in Tyrode's solution supplemented with 20 mg/ml 2,3-butanedione monoxime (MilliporeSigma) under continuous linear stretch at a rate of 0.015 mm/s to 10% stretch. The diastolic force produced was extracted by a custom MATLAB script and normalized by cross-sectional area at culture length to calculate uniaxial tensile stress. For EHTs, a similar protocol was conducted without 2,3-butanedione monoxime.

QUANTITATIVE POLYMERASE CHAIN REACTION ANALYSIS. To analyze the gene expression patterns of EHTs generated from human iPSC-CMs, total ribonucleic acid from individual samples was extracted by using TRIzol reagent (Thermo Fisher Scientific) according to the manufacturer's instructions. Complementary deoxyribonucleic acid (cDNA) was synthesized by using an iScript cDNA synthesis Kit (Bio-Rad, Hercules, California) according to the manufacturer's instructions. Quantitative polymerase chain reaction amplifications were performed by using an IQ TM SYBR green supermix (Bio-Rad) with a total reaction volume of 15 μl, containing 1 μl of cDNA, 1.5 μl of primers, and 5 μl of distilled water, on a CFX96TM Real-Time System (Bio-Rad) using conditions of 95°C for 3 min followed by 46 amplification cycles (95°C for 10 s, 58°C for 10 s, and 72°C for 30 s). GAPDH was used as the reference gene in accordance with previous research (15). Three biological replicates were carried out for expression analysis of each gene. Primers used are listed in Supplemental Table 1.

STATISTICAL ANALYSIS. Results are given as the mean with its standard error. Statistical significance was determined by using the Student's t-test or Mann-Whitney *U* test where applicable with a confidence level of $p < 0.05$, unless stated otherwise. Calculations were conducted by using Prism 7 (GraphPad Software, La Jolla, California).

RESULTS

HISTOLOGICAL EVALUATION. Before generating EHTs from left ventricular myocardial tissue blocks from 3-month-old WT and mutant Yucatan miniature pigs, we investigated native tissue section characteristics utilizing standard histochemical stains, including H&E, MTR, and SR (**Figure 2**, Supplemental

FIGURE 2 Histological Findings in WT and MUT Porcine Extracellular Matrix

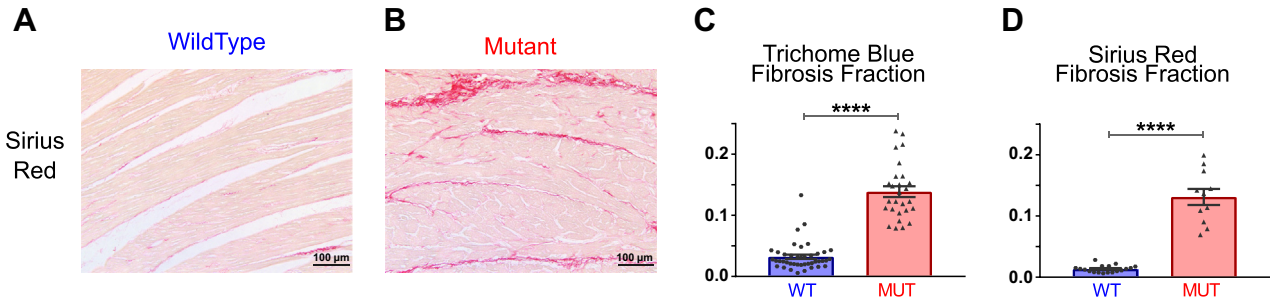

(A and B) Representative micrographs of wild-type (WT) and mutant (MUT) tissue sections stained with Sirius Red. **(C)** Masson trichrome-stained tissue showed statistically significant increase in fibrosis fraction in MUT samples (n = 27) compared with WT samples (n = 41). **(D)** Quantification of Sirius red-labeled tissue also exhibited a statistically significant increase in fibrosis fraction in MUT samples (n = 11) compared with WT samples (n = 18). ****p < 0.0001.

Figure 1). Consistent with previous microscopic findings in this large animal model (10), we observed myocyte disarray in the H&E and MTR stains and interstitial fibrosis in the MTR and SR stains, which are histopathological hallmarks of HCM (17). We further quantified the degree of disarray by image analysis of the H&E nuclear orientation and MTR fiber orientation. Significantly different alignment indexes were observed between the mutant and WT native tissue for both the nuclear alignment ($p = 0.0001$) and the fiber alignment ($p < 0.0001$); furthermore, the effect was similar for both (0.32 and 0.50, respectively), indicating a tight coupling between nuclear and fiber alignment in native cardiac tissue (18).

We quantified the degree of interstitial fibrosis and found significantly different fibrosis fraction between mutant and WT native tissues in both the MTR ($p < 0.0001$) and SR ($p < 0.0001$) stains (**Figure 2**) with a very similar average fibrosis fraction (13%) via both staining methods, indicative of moderate fibrosis (19). No overt cardiac hypertrophy was observed in these tissues; however, the occurrence of tissue remodeling and concomitant cardiac dysfunction before the development of myocardial hypertrophy and increased left ventricular wall thickness is consistent with both a previous study in this large animal model (10) and in human studies (9,20-25). We hypothesized that the moderate interstitial fibrosis and modest fiber disarray discerned through histological analysis of the mutant tissues would result in alterations of the passive properties of the mutant myocardium.

PASSIVE MECHANICS OF NATIVE TISSUE. Our EHTs allow us to perform uniaxial mechanical experiments. To determine whether the R403Q mutation leads to adverse remodeling ultimately changing uniaxial stiffness in native cardiac ECM, we used our cassette system to perform simple uniaxial characterization (**Figure 3**). In the native porcine samples (**Figure 3D**), R403Q mutant tissue exhibited an overall 3.4-fold increase in stiffness at 9% stretch (MUT [n = 3] vs. WT [n = 6], 19.6 ± 3.7 kPa vs. 5.8 ± 2 kPa; p = 0.0092) (**Figure 3E**).

PASSIVE MECHANICS OF CULTURED EHTs. Having found that native tissue of the R403Q mutant appears to be stiffer, we investigated whether decellularized tissue reseeded with iPSC-CMs maintained this property. **Figures 3A to 3C** shows typical experimental traces for 10% stretch administered to an isometrically contracting EHT (**Figure 3F**). The passive (diastolic) component of the mechanical response to stretch was obtained by examining the measured force that occurred immediately before the electrical stimulus, when the tissue was maximally relaxed. The stiffness of R403Q mutant ECM EHTs remained higher than the WT even after being seeded with healthy cells and cultured for 9 days. R403Q mutant ECM EHTs showed a 2.7-fold increased stiffness at 9% stretch (MUT EHT [n = 6] vs. WT EHT [n = 6], 21.74 ± 4.5 kPa vs. 8.05 ± 2 kPa; p = 0.0203) (**Figure 3G**). Interestingly, in 9-day-old cultured EHTs, the respective stiffness findings were similar to our native non-decellularized cardiac tissue strips; for example, non-decellularized R403Q mutant tissue had a stiffness of 19.6 kPa compared with 21.7 kPa in decellularized R403Q mutant tissue.

ACTIVE MECHANICS OF EHTs. To determine whether differences in the ECM might also alter the intrinsic contractile behavior of iPSC-CMs, we seeded tissue scaffolds of both ECM types (n = 6 each) on the same day with a homogeneous population of healthy 14-day-old iPSC-CMs. After 10 days in culture, EHTs were placed on a mechanical test apparatus and

FIGURE 3 Uniaxial Passive Mechanics of Native and Re-Cellularized Myocardial Strips

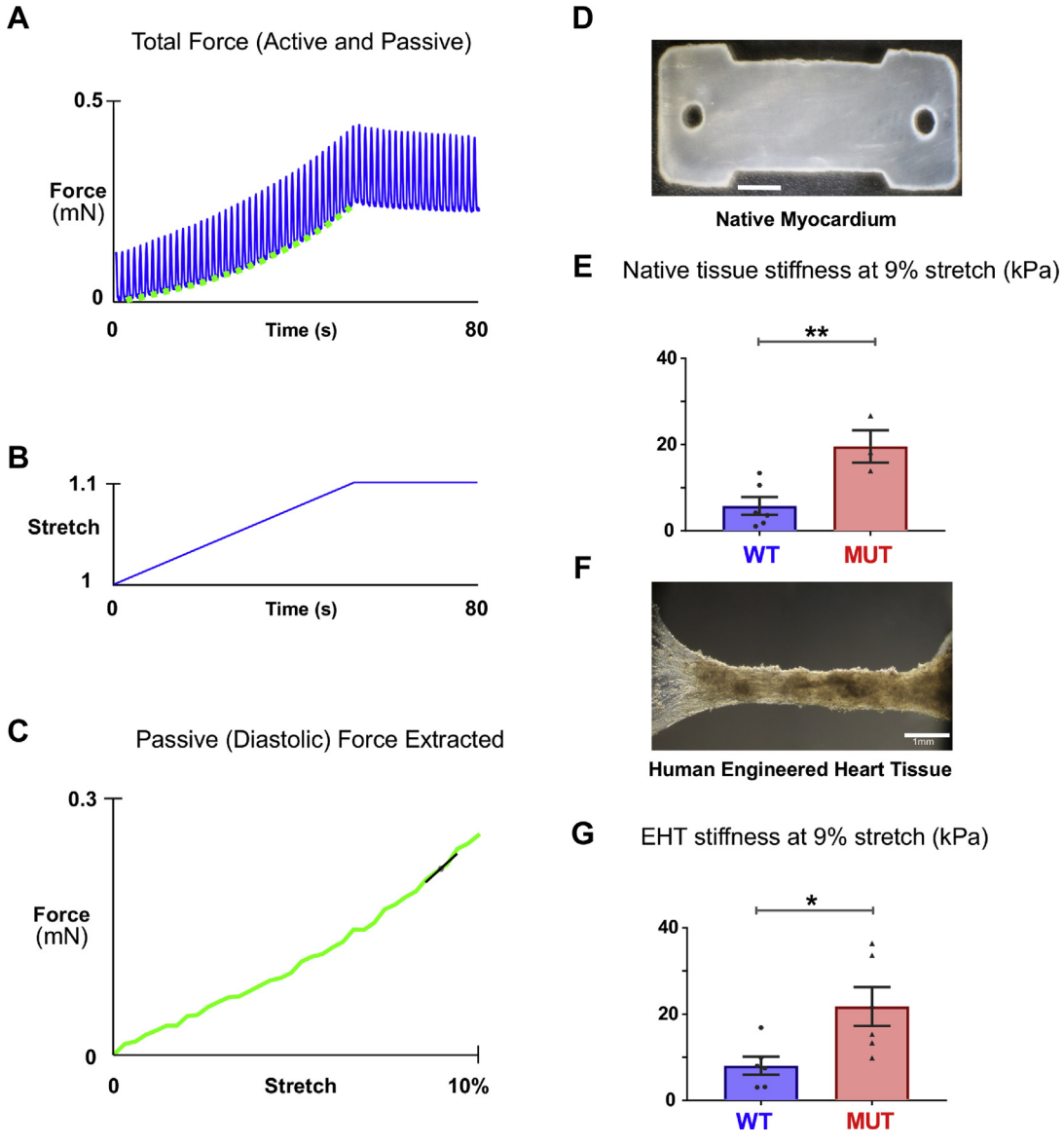

(A) Force response resulting from slow stretch of an EHT under physiological conditions paced at 1 Hz. **(B)** Tissue was uniaxially stretched at a rate of 0.25% muscle lengths per second to a final stretch of 10%. **(C)** Extracted diastolic force curve from native tissue and EHTs show the force-stretch relationship, with stiffness at 9% stretch extracted using finite difference calculation for comparison. **(D)** Typical image of a porcine myocardium laser-cut native tissue sample. **(E)** Native non-decellularized tissue stiffness of MUT samples ($n = 3$) were significantly higher than that of the WT samples ($n = 6$) ($p = 0.0092$). **(F)** Typical image of an EHT formed by re-seeding decellularized porcine myocardium with healthy iPSC-CMs. **(G)** Passive stiffness of EHTs created from MUT tissue ($n = 6$) were significantly higher than those created from WT tissue ($n = 6$) ($p = 0.0203$). *$p < 0.05$, **$p < 0.01$. Abbreviations as in Figures 1 and 2.

electrically paced at 1 Hz to capture isometric twitch force characteristics. Compared with EHTs made from healthy control ECM, R403Q mutant ECM EHTs showed prolonged early relaxation time (time from peak tension to 50% relaxation [RT50]) that was significant (190 ± 7 ms vs. 143 ± 2 ms, MUT vs. WT, respectively; $p = 0.0022$) (Figures 4A and 4B). In addition, time to peak force (TTP) was slowed significantly (262 ± 10 ms vs. 211 ± 4 ms, MUT vs. WT; $p = 0.0014$) (Figure 4C). Following on these previous observations, the normalized time tension integral was elevated in the R403Q mutant ECM EHTs

FIGURE 4 **Active Mechanics of EHTs Created From Healthy and Diseased Tissue Scaffolds**

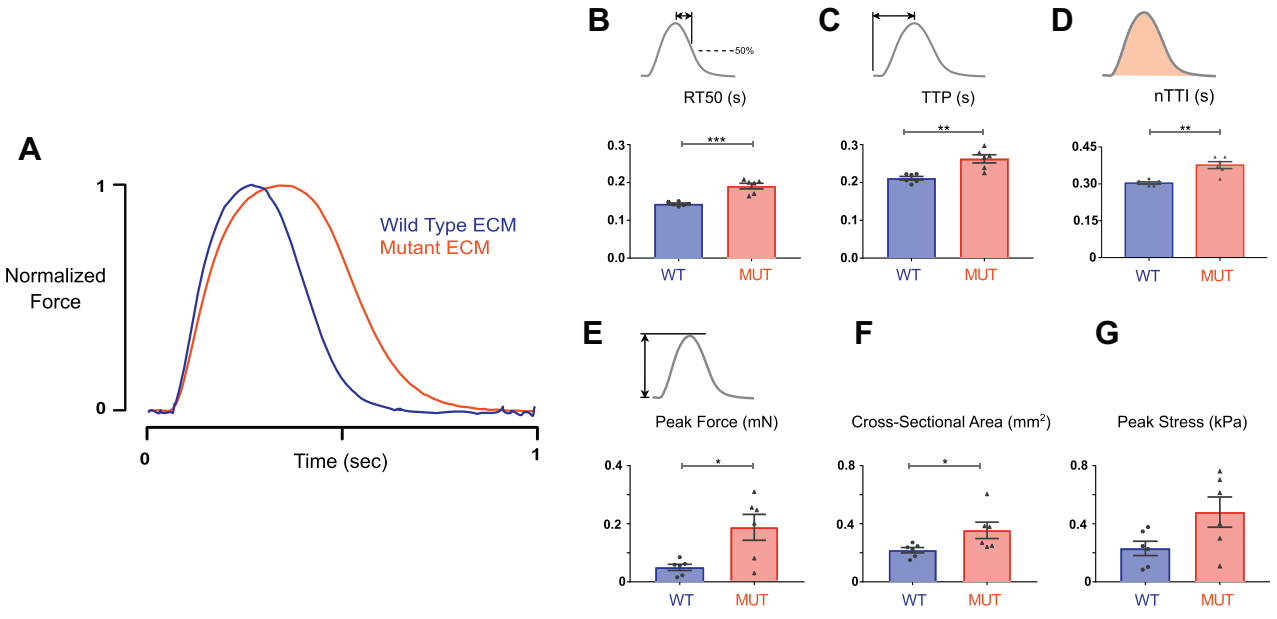

(A) Representative twitch force traces measured in EHTs created out of WT and MUT extracellular matrix (ECM). **(B)** R403Q mutant ECM EHTs showed a 33% increase in early relaxation (time from peak tension to 50% relaxation [RT50]; $p = 0.0022$). **(C)** Time to peak tension (TTP) in MUT ECM EHTs was 24% slower ($p = 0.0014$). **(D)** MUT ECM EHTs showed a 24% increase in the normalized time tension integral (nTTI; $p = 0.0043$). **(E)** Peak force was significantly increased in MUT EHTs ($p = 0.0411$). **(F)** Cross-sectional area was significantly increased in MUT EHTs ($p = 0.0411$). **(G)** Peak stress was not significantly different ($p = 0.054$). *$p < 0.05$; **$p < 0.01$; ***$p < 0.001$. Abbreviations as in Figures 1 and 2.

(0.376 ± 0.014 s vs. 0.303 ± 0.005 s, MUT vs. WT; p = 0.0043) (Figure 4D). Peak twitch force in R403Q mutant ECM EHTs was significantly higher than that of WT EHTs (0.18 ± 0.04 mN vs. 0.05 ± 0.01 mN, MUT vs. WT; p = 0.0411) (Figure 4E). Cross-sectional area differed significantly between mutant ECM EHTs and WT EHTs (0.37 ± 0.06 mm^2 vs. 0.23 ± 0.02 mm^2, MUT vs. WT; p = 0.0411) (Figure 4F). Peak twitch stress, calculated as the peak force of an EHT divided by its cross-sectional area, was not different between mutant ECM EHTs and WT EHTs (Figure 4G).

To determine whether these changes persisted beyond 10 days, we repeated EHT experiments, culturing tissues for an additional week. Differences in TTP and RT50 remained significant at this 16-day time point (Supplemental Figure 2). Furthermore, the increased contractile force in R403Q mutant ECM EHTs at 10 days remained significant at 16 days in culture.

To determine whether changes in calcium handling might account for these alterations in EHT twitch behavior, calcium transients were measured under 1 Hz electrical pacing in an independent batch of EHTs created from R403Q mutant ECM (n = 5) and WT ECM (n = 4) (Figure 5). EHTs made with mutant ECM showed a significant increase in time to peak in their calcium transients compared with EHTs made with WT ECM (0.174 ± 0.007 s vs. 0.135 ± 0.009 s, MUT vs. WT respectively; p = 0.0087). No differences were noted in other calcium transient properties, including the relaxation time constant, magnitude of calcium release, and time from peak to 80% of calcium magnitude. We further examined expression of a select panel of genes involved in HCM pathophysiology and Ca^{2+} handling, including ATP2A2, CACNA1C, TGFB2, PLN, and NPPB, using quantitative polymerase chain reaction (Supplemental Table 1). No significant differences were observed in expression of these genes between WT and MUT EHTs (Supplemental Figure 3).

DISCUSSION

To the best of our knowledge, the data presented here are the first to show the ability of diseased myocardial ECM to provoke abnormal contractile behavior in

FIGURE 5 Calcium Dynamics of EHTs Created From WT and Mutant Tissue Scaffolds

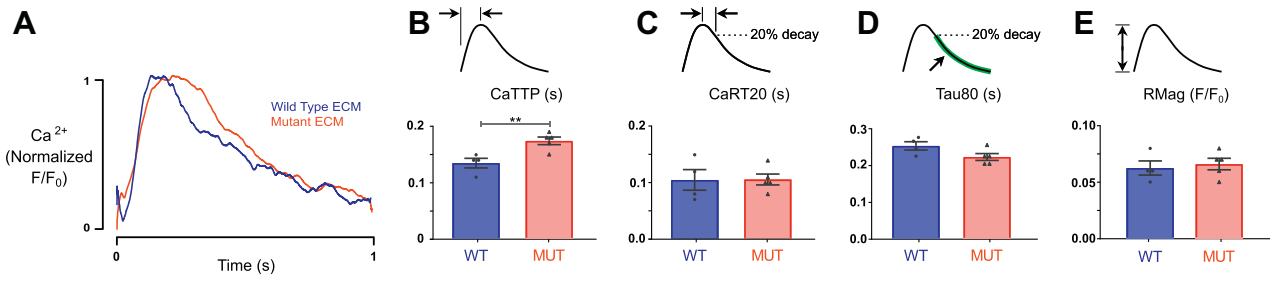

(A) Representative calcium transient traces measured in EHTs created from WT and MUT ECMs. **(B)** R403Q mutant ECM EHTs showed a 29% increase in time to peak calcium (CaTTP; $p = 0.0087$). **(C)** Time from peak to 80% calcium transient magnitude did not differ (CaRT20; $p = 0.70$). **(D)** Decay time constant from 80% peak calcium showed a trend toward being faster in the R403Q mutant ECM EHTs but did not significantly differ (Tau80; $p = 0.07$). **(E)** Peak change of calcium transient was not different (RMag; $p = 0.70$). **$p < 0.01$. Abbreviations as in Figures 1, 2, and 4.

otherwise healthy CMs, implying that ECM can store a memory of previous disease. Our findings have significant implications for understanding HCM pathogenesis and potential treatment paradigms.

It is striking that HCM ECM triggers excessive contractility and poor relaxation in CMs, because these are similar to characteristics observed in CMs expressing HCM-linked myosin mutations (26). In particular, diastolic dysfunction potentially arising from intrinsic cellular dysfunction has been increasingly recognized as a feature of HCM independent of systolic alteration and often preceding clinically significant fibrosis (27,28). Diseased ECM may have the ability to incite genetically normal cells to behave as though they harbored a sarcomeric HCM mutation. This discovery supports an intriguing hypothesis, namely that the progression of HCM is caused by a continuous cycle of mutually reinforcing phenomena: Initially, the presence of a mutant sarcomeric protein causes acute cardiomyocyte hypercontractility. This presumably triggers mechanosensitive pathways in the myocardium responsible for cellular hypertrophy and increased collagen production. As suggested by our experiments, the stiffened ECM exerts effects of its own on CMs, causing poor diastolic function and an increase in the tension-time integral. An increased tension-time integral leads to concentric hypertrophic remodeling (26,29), and the cycle repeats.

According to this paradigm, the sarcomeric mutation initiates disease but is only 1 of the factors driving disease progression in the long run. Once the secondary driver (pathological ECM remodeling) is established, removal of the sarcomeric mutation or its effects would merely diminish the disease stimulus without completely eliminating it. This viewpoint seems plausible when considering results obtained from treating mouse models of HCM with mavacamten. Green et al. (8) found that mavacamten eliminated the development of HCM pathologies in myh7 R403Q and R453C mice only when treatment began before the onset of substantial hypertrophy and fibrosis. When treatment was given after the emergence of detectable pathology, it failed to completely reverse the mechanical effects of disease, although signaling pathways leading to fibrosis were attenuated. This failure to reverse phenotype has also been shown in mouse models of HCM that feature mutations to *MYBPC3* (30). In that study, treatment with the calcium-channel blocker diltiazem was performed on 2-month-old mice with a preexisting cardiac disease phenotype. Although it had beneficial acute effects on isolated CMs, chronic treatment could not improve the tissue phenotype. The same was true for treatments with ranolazine and metoprolol (31,32).

Those studies, together with the observations presented here, offer collective insight into potential clinical treatment strategies for HCM. First, they point toward early intervention as the simplest means of preventing HCM, most easily through using targeted myosin modulators or other compounds that reduce contractility. However, in advanced HCM with significant ECM remodeling, contractile inhibition would only form part of the treatment paradigm; a secondary agent modifying the fibrotic environment described in our experiments will likely be required as well. Given the difficulty and complexity of multimodal therapy for advanced HCM, preventative therapy in patients with subclinical HCM and carriers would likely be a more fruitful approach.

The importance of fibrosis in the development of HCM is supported by numerous studies. Patients with HCM can exhibit diastolic dysfunction along with myocardial collagen deposition at early stages of the disease even when overt hypertrophy has not yet been observed (33), suggesting that subclinical fibrosis may not be merely a secondary effect but an important contributor to disease development. Indeed, one study reported an elevation of myocardial collagen content by 72% in patients with HCM compared with other hearts that had hypertrophied due to other reasons (34). A second study found that young patients with HCM and sudden death had an 8-fold increase in myocardial collagen fraction compared with control subjects and a 3-fold increase compared with patients with systemic hypertension (35). These findings are supported by the fact that systemic collagen I synthesis seems to be elevated in patients with both early and established HCM (9,36). The present study adds a new dimension of importance to fibrosis in HCM by showing a clear link between systolic contractile behavior of CMs and the supposedly "passive" mechanical characteristics of diseased ECM. Further study of the mechanisms that constitute the ECM–contractility axis is likely to yield novel therapeutic targets for disrupting and reversing established HCM.

Given the stark difference in matrix stiffness between HCM and control hearts, the observed contractility differences are not entirely surprising (37,38). The prolonged calcium transients that we observed in EHTs made from mutant ECM could easily account for the accompanying prolongation of twitch contractions. Aside from affecting contractile dynamics, ECM-mediated prolongation of the calcium transient could be a substrate for arrhythmias in HCM. Prolonged calcium transients have been linked to arrhythmogenic behavior in models of long QT syndrome (39) and sarcomeric HCM (40–42).

Changes in cardiomyocyte calcium handling have been reported before in studies in which substrate stiffness is altered in simplified biomaterial matrices and then seeded with neonatal rat CMs (38,43–45). These studies found either an increase in calcium transient duration or magnitude in response to increased substrate stiffness, at least up to a point. Extreme stiffness leads to decreased calcium transient duration and magnitude (38,44,46). Importantly, changes in calcium transient and altered contractility have also been observed in adult rat CMs grown on substrates of different stiffness (47), indicating that neonatal and adult CMs have a significant adaptive response to different mechanical environments.

Despite multiple reports linking substrate stiffness and cardiomyocyte phenotypes, the underlying mechanisms responsible remain incompletely understood. Nevertheless, stiffness-mediated changes in calcium transients have been correlated with SERCA2a expression, L-type calcium current, and action potential morphology in other studies (38,46). In the present study, we assessed expression of key calcium handling genes (ATP2A2, CACNA1C, and PLN), but these levels were unaltered in cells grown on the R403Q mutant ECM. This outcome suggests that mutant ECM provokes a response in CMs which differs from responses triggered by changes in substrate stiffness alone.

Even as these simple experiments have established an interesting relationship between myocyte contractility and diseased myocardial ECM, much remains to be determined. For instance, it is unclear whether ECM stiffness alone is sufficient to account for the observed effects. Healthy and mutation-produced matrices may also show differences in composition that go beyond ECM collagen fraction, orientation, and stiffness. Future research will explore experimental approaches for investigating matrix composition, cellular responses, and cellular mechanotransduction pathways in the context of HCM-derived ECM.

STUDY LIMITATIONS. Limitations of the artificial tissue system used to perform these initial studies should also be recognized. Our approach necessarily includes differences with native tissue; whereas native tissue consists of CMs and fibroblasts supplied by a dense capillary bed, our model system is avascular and lacks endothelial cells. Our experimental system has the advantage of allowing the introduction of CMs directly into mature matrix from any source, although this approach differs from the developmental process of native tissue, which produces and remodels ECM gradually over time. In terms of contractile behavior, EHTs created from WT myocardial ECM display twitch time-course characteristics that match those measured in isolated adult human trabeculae to well within the bounds of experimental uncertainty. Specifically, the WT EHTs exhibited mean TTP and RT50 values of 211 ms and 143 ms, compared with values of 219.3 $\pm$ 15.0 ms and 142.4 $\pm$ 11.4 ms, respectively, in isolated adult human trabeculae (48,49). We see this finding as confirming the relevance of kinetic changes observed in MUT EHTs. However, the peak active contractile stress

produced by EHTs in this study (0.23 kPa) is only a fraction of that measured in native human myocardium (~20 kPa). Differences between native and engineered myocardium suggest that complementary in vivo approaches should be developed to further probe the role of ECM remodeling in the progression and maintenance of HCM disease phenotypes.

CONCLUSIONS

Our research provides evidence that altered ECM might be a major player in the pathology and pathogenicity of HCM. The diseased ECM seems to push healthy CMs toward contractile characteristics reminiscent of those caused by HCM-linked sarcomeric mutations. Hence, contractile abnormalities in HCM may originate in sarcomeric proteins and worsen in advanced disease through the indirect influence of pathologically remodeled ECM. From a clinical standpoint, this finding suggests the importance of addressing ECM changes in any strategy for treating established HCM.

ACKNOWLEDGMENTS The authors thank Viet Dau for his assistance with imaging histological slides. Tissue samples were generously donated by MyoKardia (Dr. Sarah MacInnes).

ADDRESS FOR CORRESPONDENCE: Dr. Stuart G. Campbell, Department of Biomedical Engineering, Yale University, 55 Prospect Street, MEC 211, New Haven, Connecticut 06511. E-mail: stuart.campbell@yale.edu.

PERSPECTIVES

COMPETENCY IN MEDICAL KNOWLEDGE: Sarcomeric mutations leading to HCM alter contractile behavior and have recently become a target for treatment. Often when HCM has manifested clinically, significant remodeling of the ECM such as interstitial fibrosis has occurred. ECM remodeling likely serves to sustain and exacerbate disease phenotypes such as diastolic dysfunction.

TRANSLATIONAL OUTLOOK: Myosin modulator-dependent reversal of HCM disease expression is attenuated by ECM abnormalities once development of clinically significant hypertrophy has occurred. Future research should investigate modalities to reverse ECM remodeling to treat established HCM.

REFERENCES

1. Marian AJ, Braunwald E. Hypertrophic cardiomyopathy: genetics, pathogenesis, clinical manifestations, diagnosis, and therapy. Circ Res 2017;121:749–70.

2. Alfares AA, Kelly MA, McDermott G, et al. Results of clinical genetic testing of 2,912 probands with hypertrophic cardiomyopathy: expanded panels offer limited additional sensitivity. Genet Med 2015;17:319.

3. Ferrantini C, Coppini R, Pioner JM, et al. Pathogenesis of hypertrophic cardiomyopathy is mutation rather than disease specific: a comparison of the cardiac troponin T E163R and R92Q mouse models. J Am Heart Assoc 2017;6. pii.e005407.

4. Chuan P, Sivaramakrishnan S, Ashley EA, Spudich JA. Cell-intrinsic functional effects of the α-cardiac myosin Arg-403-Gln mutation in familial hypertrophic cardiomyopathy. Biophys J 2012;102:2782–90.

5. Viswanathan MC, Schmidt W, Rynkiewicz MJ, et al. Distortion of the actin A-triad results in contractile disinhibition and cardiomyopathy. Cell Rep 2017;20:2612–25.

6. Michele DE, Coutu P, Metzger JM. Divergent abnormal muscle relaxation by hypertrophic cardiomyopathy and nemaline myopathy mutant tropomyosins. Physiol Genomics 2002;9:103–11.

7. Fraysse B, Weinberger F, Bardswell SC, et al. Increased myofilament Ca2+ sensitivity and diastolic dysfunction as early consequences of Mybpc3 mutation in heterozygous knock-in mice. J Mol Cell Cardiol 2012;52:1299–307.

8. Green EM, Wakimoto H, Anderson RL, et al. A small-molecule inhibitor of sarcomere contractility suppresses hypertrophic cardiomyopathy in mice. Science 2016;351:617–21.

9. Ho CY, López B, Coelho-Filho OR, et al. Myocardial fibrosis as an early manifestation of hypertrophic cardiomyopathy. N Engl J Med 2010;363:552–63.

10. del Rio CL, Henze MP, Wong FL, et al. A novel mini-pig genetic model of hypertrophic cardiomyopathy: altered myofilament dynamics, hyper-contractility, and impaired systolic/diastolic functional reserve in vivo. Circulation 2018;136. Abstract 20770.

11. Schneider CA, Rasband WS, Eliceiri KW. NIH image to ImageJ: 25 years of image analysis. Nat Methods 2012;9:671–5.

12. Ayres C, Bowlin GL, Henderson SC, et al. Modulation of anisotropy in electrospun tissue-engineering scaffolds: analysis of fiber alignment by the fast Fourier transform. Biomaterials 2006;27:5524–34.

13. Sander EA, Barocas VH. Comparison of 2D fiber network orientation measurement methods. J Biomed Mater Res A 2009;88:322–31.

14. Hadi AM, Mouchaers KTB, Schalij I, et al. Rapid quantification of myocardial fibrosis: a new macro-based automated analysis. Cell Oncol 2011;34:343–54.

15. Schwan J, Kwaczala AT, Ryan TJ, et al. Anisotropic engineered heart tissue made from laser-cut decellularized myocardium. Sci Rep 2016;6:32068.

16. Lian X, Zhang J, Azarin SM, et al. Directed cardiomyocyte differentiation from human pluripotent stem cells by modulating Wnt/β-catenin signaling under fully defined conditions. Nat Protoc 2013;8:162–75.

17. Hughes SE. The pathology of hypertrophic cardiomyopathy. Histopathology 2004;44:412–27.

18. Zach B, Hofer E, Asslaber M, Ahammer H. Automated texture analysis and determination of fibre orientation of heart tissue: a morphometric study. PLoS One 2016;11:e0160735.

19. White SK, Sado DM, Fontana M, et al. T1 mapping for myocardial extracellular volume measurement by CMR. J Am Coll Cardiol Img 2013;6:955–62.

20. Germans T, Wilde AAM, Dijkmans PA, et al. Structural abnormalities of the inferoseptal left ventricular wall detected by cardiac magnetic resonance imaging in carriers of hypertrophic cardiomyopathy mutations. J Am Coll Cardiol 2006;48:2518–23.

21. Ho CY, Day SM, Colan SD, et al. The burden of early phenotypes and the influence of wall

thickness in hypertrophic cardiomyopathy mutation carriers: findings from the HCMNet study. JAMA Cardiol 2017;2:419–28.

22. Yiu KH, Atsma DE, Delgado V, et al. Myocardial structural alteration and systolic dysfunction in preclinical hypertrophic cardiomyopathy mutation carriers. PLoS One 2012;7:e36115.

23. Germans T, Rüssel IK, Götte MJW, et al. How do hypertrophic cardiomyopathy mutations affect myocardial function in carriers with normal wall thickness? Assessment with cardiovascular magnetic resonance. J Cardiovasc Magn Reson 2010; 12:13.

24. Noureldin RA, Liu S, Nacif MS, et al. The diagnosis of hypertrophic cardiomyopathy by cardiovascular magnetic resonance. J Cardiovasc Magn Reson 2012;14:17.

25. Rüssel IK, Brouwer WP, Germans T, et al. Increased left ventricular torsion in hypertrophic cardiomyopathy mutation carriers with normal wall thickness. J Cardiovasc Magn Reson 2011;13: 3.

26. Davis J, Davis LC, Correll RN, et al. A tension-based model distinguishes hypertrophic versus dilated cardiomyopathy. Cell 2016;165:1147–59.

27. Coppini R, Ho CY, Ashley E, et al. Clinical phenotype and outcome of hypertrophic cardiomyopathy associated with thin-filament gene mutations. J Am Coll Cardiol 2014;64:2589–600.

28. Tardiff JC, Hewett TE, Palmer BM, et al. Cardiac troponin T mutations result in allele-specific phenotypes in a mouse model for hypertrophic cardiomyopathy. J Clin Invest 1999;104:469–81.

29. Dorn GW. Tension-time integrals and genetic cardiomyopathy: the force is with you. Cell 2016; 165:1049–50.

30. Flenner F, Geertz B, Reischmann-Düsener S, et al. Diltiazem prevents stress-induced contractile deficits in cardiomyocytes, but does not reverse the cardiomyopathy phenotype in Mybpc3-knock-in mice. J Physiol 2017;595: 3987–99.

31. Flenner F, Friedrich FW, Ungeheuer N, et al. Ranolazine antagonizes catecholamine-induced dysfunction in isolated cardiomyocytes, but lacks long-term therapeutic effects in vivo in a mouse model of hypertrophic cardiomyopathy. Cardiovasc Res 2016;109:90–102.

32. Friedrich FW, Sotoud H, Geertz B, et al. I-1-deficiency negatively impacts survival in a cardiomyopathy mouse model. Int J Cardiol Hear Vasc 2015;8:87–94.

33. Brower GL, Gardner JD, Forman MF, et al. The relationship between myocardial extracellular matrix remodeling and ventricular function. Eur J Cardio-Thoracic Surg 2006;30:604–10.

34. Factor SM, Butany J, Sole MJ, Wigle ED, Williams WC, Rojkind M. Pathologic fibrosis and matrix connective tissue in the subaortic myocardium of patients with hypertrophic cardiomyopathy. J Am Coll Cardiol 1991;17:1343–51.

35. Shirani J, Pick R, Roberts WC, Maron BJ. Morphology and significance of the left ventricular collagen network in young patients with hypertrophic cardiomyopathy and sudden cardiac death. J Am Coll Cardiol 2000;35:36–44.

36. Lombardi R, Betocchi S, Losi MA, et al. myocardial collagen turnover in hypertrophic cardiomyopathy. Circulation 2003;108:1455–60.

37. Gershlak JR, Resnikoff JIN, Sullivan KE, Williams C, Wang RM, Black LD. Mesenchymal stem cells ability to generate traction stress in response to substrate stiffness is modulated by the changing extracellular matrix composition of the heart during development. Biochem Biophys Res Commun 2013;439:161–6.

38. Jacot JG, McCulloch AD, Omens JH. Substrate stiffness affects the functional maturation of neonatal rat ventricular myocytes. Biophys J 2008;95:3479–87.

39. Spencer CI, Baba S, Nakamura K, et al. Calcium transients closely reflect prolonged action potentials in iPSC models of inherited cardiac arrhythmia. Stem Cell Reports 2014;3:269–81.

40. Wang L, Kim K, Parikh S, et al. Hypertrophic cardiomyopathy-linked mutation in troponin T causes myofibrillar disarray and pro-arrhythmic action potential changes in human iPSC cardiomyocytes. J Mol Cell Cardiol 2018;114:320–7.

41. Wang L, Kryshtal DO, Kim K, et al. Myofilament calcium-buffering dependent action potential triangulation in human-induced pluripotent stem cell model of hypertrophic cardiomyopathy. J Am Coll Cardiol 2017;70:2600–2.

42. Landstrom AP, Dobrev D, Wehrens XHT. Calcium signaling and cardiac arrhythmias. Circ Res 2017;120:1969–93.

43. Hazeltine LB, Simmons CS, Salick MR, et al. Effects of substrate mechanics on contractility of cardiomyocytes generated from human pluripotent stem cells. Int J Cell Biol 2012;2012:1–13.

44. Rodriguez AG, Han SJ, Regnier M, Sniadecki NJ. Substrate stiffness increases twitch power of neonatal cardiomyocytes in correlation with changes in myofibril structure and intracellular calcium. Biophys J 2011;101:2455–64.

45. Ribeiro AJS, Ang YS, Fu JD, et al. Contractility of single cardiomyocytes differentiated from pluripotent stem cells depends on physiological shape and substrate stiffness. Proc Natl Acad Sci 2015;112:12705–10.

46. Boothe SD, Myers JD, Pok S, et al. The effect of substrate stiffness on cardiomyocyte action potentials. Cell Biochem Biophys 2016;74:527–35.

47. van Deel ED, Najafi A, Fontoura D, et al. In vitro model to study the effects of matrix stiffening on Ca2+ handling and myofilament function in isolated adult rat cardiomyocytes. J Physiol 2017;595:4597–610.

48. Milani-Nejad N, Canan BD, Elnakish MT, et al. The Frank-Starling mechanism involves deceleration of cross-bridge kinetics and is preserved in failing human right ventricular myocardium. Am J Physiol Heart Circ Physiol 2015;309:H2077–86.

49. Chung JH, Martin BL, Canan BD, et al. Etiology-dependent impairment of relaxation kinetics in right ventricular end-stage failing human myocardium. J Mol Cell Cardiol 2018;121:81–93.

KEY WORDS diastolic dysfunction, engineered heart tissue, fibrosis, hypertrophic cardiomyopathy, iPSC-derived cardiomyocyte, MYH7 mutation

APPENDIX For a supplemental table and figures, please see the online version of this paper.

JACC: BASIC TO TRANSLATIONAL SCIENCE VOL. 4, NO. 4, 2019

EDITORIAL COMMENT

Role of the Extracellular Matrix in the Pathogenesis of Hypertrophic Cardiomyopathy*

Ali J. Marian, MD

The prevailing hypothesis in the pathogenesis of human hypertrophic cardiomyopathy (HCM) places the primary abnormality in cardiac myocytes (1). The hypothesis is in accord with the genetic evidence defining HCM mostly as a disease of mutations in genes encoding sarcomere proteins (reviewed in Marian and Braunwald [2]). Sarcomere proteins are predominantly, if not exclusively, expressed in the straited muscles and not other cell types, such as fibroblasts or endothelial cells. Thus, the primary abnormality in HCM has to reside in cardiac myocytes. The pathological and clinical manifestations of HCM, however, are the consequences of intertwined and complex interactions among cellular constituents of the myocardium, including myocytes and fibroblasts. Accordingly, the impetus for the pathogenesis of the histological, functional, and clinical phenotypes originates from cardiac myocytes, the site of expression of mutant sarcomere proteins. The causal mutations by impairing interactions among the protein constituents of sarcomeres, such as myosin heavy chain (MYH) and actin, alter biochemical and mechanical properties of myofibrils, including calcium sensitivity of myofibrillar adenosine triphosphatase (ATPase) activity, force generation, and relaxation (2). These biochemical and functional perturbations result in activation of stress-sensitive pathways and expression of trophic and mitotic autocrine and paracrine factors that target the cells in the myocardium and induce secondary changes, such as myocyte hypertrophy and interstitial fibrosis, followed by the ensuing clinical phenotypes of cardiac hypertrophy, cardiac arrhythmias, and systolic and diastolic dysfunction (2).

Interstitial fibrosis is a well-recognized and common histological feature of HCM (3). Classically, it is recognized in post-mortem histological examination of HCM hearts and on occasion by measuring circulating cleaved products of collagens (4–6). In recent years, however, cardiac magnetic resonance (CMR) imaging has enabled in vivo assessment of interstitial fibrosis in patients with HCM. The modality enables detecting and quantifying extracellular volume, which is tagged by late gadolinium enhancement (LGE), as a surrogate for myocardial fibrosis. Increased myocardial fibrosis, although secondary to the effects of paracrine factors emanating from cardiac myocytes carrying the pathogenic variants in genes coding for sarcomere proteins, is recognized as a risk factor for cardiac arrhythmias and sudden cardiac death (3,7–13). Myocardial fibrosis is also considered a determinant of diastolic and to a lesser degree systolic dysfunction in HCM and other myocardial diseases (12,13). However, it has not been implicated in the enhancement of myocardial or myocyte contraction, as observed in HCM.

In this issue of *JACC: Basic to Translational Science*, Sewanan et al. (14) provide evidence implicating

*Editorials published in *JACC: Basic to Translational Science* reflect the views of the authors and do not necessarily represent the views of *JACC: Basic to Translational Science* or the American College of Cardiology.

From the Center for Cardiovascular Genetics, Institute of Molecular Medicine and Department of Medicine, University of Texas Health Sciences Center at Houston, Houston, Texas. Dr. Marian's research programs are supported in part by grants from the National Institutes of Health (NIH), the National Heart, Lung and Blood Institute (NHLBI) R01 HL088498 and 1R01HL132401), the Leducq Foundation (14 CVD 03), The Ewing Halsell Foundation, the George and Mary Josephine Hamman Foundation, and the TexGen Fund from the Greater Houston Community Foundation.

The author attests he is in compliance with human studies committees and animal welfare regulations of the authors' institutions and Food and Drug Administration guidelines, including patient consent where appropriate. For more information, visit the *JACC: Basic to Translational Science* author instructions page.

ISSN 2452-302X https://doi.org/10.1016/j.jacbts.2019.03.011

extracellular matrix (ECM) in the pathogenesis of myocardial mechanical dysfunction in HCM. Using a clever approach, the authors decellularize myocardial strips collected from the hearts of a Yucatan minipig model of HCM, caused by the classic HCM mutation, namely, the p.Arg403Gln, in the gene encoding MYH7 sarcomere protein. They then seed the decellularized myocardial strips with human induced pluripotent stem cell-derived cardiac myocytes (iPSC-CMs) originated from a healthy individual. They culture the seeded cells to generate an engineered heart tissue (EHT) and then characterize effects of ECM originated from HCM hearts on mechanical properties of EHT generated from a normal individual. The authors report that ECM originating from the mini swine hearts with HCM enhanced contraction and impaired relaxation of the healthy EHT. The authors suggest that the ECM from the HCM myocardium stores the memory of the diseased heart and, upon exposure to wild type myocytes, incites phenotypic changes that resemble those of the ECM host (i.e., HCM). The authors conclude that their findings highlight the significant role of the ECM in the pathogenesis of HCM phenotypes.

SEE PAGE 495

The findings of the study by Sewanan et al. (14) are provocative because they indicate that altered ECM in HCM, which is not expected to express the causal mutation, not only impairs relaxation but also enhances contractility of the normal EHT. The extent of these changes is similar to those observed for cardiac myocytes carrying the causal mutation. The findings, therefore, suggest that ECM is a major determinant of the classic functional phenotypes of HCM, including enhanced contraction. Whereas the findings are conceptually in accord with the existence of extensive cross-talks among the heterogenous group of cells in the myocardium, including cross-talks between myocytes and the ECM, they are observational in nature and require further validation. In addition, they lack mechanistic evidence to support validity of the findings. A notable deficiency is the missing cellular composition of the decellularized tissue prior to seeding of the normal iPSC-CMs. Likewise, there is no information on cellular composition of the EHT prior to functional characterization. Data on cellular composition prior to seeding with iPSC-CMs as well as after extended culture but before functional characterization of EHT would have enabled assessing purity of the preparations in excluding cellular admixture with the residual native myocytes harboring the *MYH7* mutation and the seeded wild type iPSC-CMs. Equally unclear is the composition of the altered ECM in the HCM samples, besides increased fibrosis. Thus, it remains to be determined which component of ECM is involved and how it affects EHT functions. The authors provide some evidence of altered calcium transient, namely, a 29% increase in time to reach peak calcium transient, which occurs in the absence of significant changes in other characteristics of the calcium transients. Likewise, there were no changes in the transcript levels of selected genes involved in calcium handling. Thus, the mechanism by which ECM from HCM hearts affects function of wild type EHT remains unclear. It also merits noting that the authors did not provide data on the characteristics of the iPSC-CMs and EHT used in these studies. Such data would have been valuable in determining whether these cells and tissues properly represented molecular and functional signatures of adult cardiac myocytes. By and large, myocytes and tissues derived from iPSCs are immature, resembling early fetal cardiac myocytes, and significantly differ from adult cardiac myocytes in epigenetics, gene expression, signal sensing, calcium handling, and excitation-contraction (EC) coupling (15). The latter is particularly pertinent to findings of the present study because iPSC-CMs do not form proper t tubules and sarcoplasmic reticulum, which are necessary for proper calcium handling and EC coupling. Finally, iPSC-CM and EHT lines exhibit significant line-to-line variability and characterization of a single line is insufficient to make firm conclusions. Therefore, as in most if not all initial observations, the intriguing findings of the present study should be considered provisional, pending replication in independent studies and further characterization in multiple lines to reduce and preferably eliminate compounding as well as confounding effects of line-to-line variability, cellular admixture, and effects of decellularization and reseeding processes. Equally important is to delineate the molecular mechanisms by which altered ECM in HCM affects myocyte functions, enhancing its contractile performance while impairing its relaxation. These initial observations could heighten the interest in the role of ECM in the pathogenesis of HCM.

ADDRESS FOR CORRESPONDENCE: Dr. Ali J. Marian, Brown Foundation Institute of Molecular Medicine, The University of Texas Health Sciences Center, 6770 Bertner Street, Suite C900A, Houston, Texas 77030. E-mail: Ali.J.Marian@uth.tmc.edu.

JACC: BASIC TO TRANSLATIONAL SCIENCE VOL. 4, NO. 4, 2019
AUGUST 2019:506–8

REFERENCES

1. Marian AJ. Pathogenesis of diverse clinical and pathological phenotypes in hypertrophic cardiomyopathy. Lancet 2000;355:58–60.

2. Marian AJ, Braunwald E. Hypertrophic cardiomyopathy: genetics, pathogenesis, clinical manifestations, diagnosis, and therapy. Circ Res 2017; 121:749–70.

3. Briasoulis A, Mallikethi-Reddy S, Palla M, Alesh I, Afonso L. Myocardial fibrosis on cardiac magnetic resonance and cardiac outcomes in hypertrophic cardiomyopathy: a meta-analysis. Heart 2015;101:1406–11.

4. Lombardi R, Betocchi S, Losi MA, Tocchetti CG, Aversa M, Miranda M, et al. Myocardial collagen turnover in hypertrophic cardiomyopathy. Circulation 2003;108:1455–60.

5. Ho CY, Lopez B, Coelho-Filho OR, Lakdawala NK, Cirino AL, Jarolim P, et al. Myocardial fibrosis as an early manifestation of hypertrophic cardiomyopathy. N Engl J Med 2010; 363:552–63.

6. Ellims AH, Taylor AJ, Mariani JA, Ling LH, Iles LM, Maeder MT, et al. Evaluating the utility of circulating biomarkers of collagen synthesis in hypertrophic cardiomyopathy. Circulation. Heart Failure 2014;7:271–8.

7. Almaas VM, Haugaa KH, Strom EH, Scott H, Dahl CP, Leren TP, et al. Increased amount of interstitial fibrosis predicts ventricular arrhythmias, and is associated with reduced myocardial septal function in patients with obstructive hypertrophic cardiomyopathy. Europace 2013;15: 1319–27.

8. Chan RH, Maron BJ, Olivotto I, Pencina MJ, Assenza GE, Haas T, et al. Prognostic value of quantitative contrast-enhanced cardiovascular magnetic resonance for the evaluation of sudden death risk in patients with hypertrophic cardiomyopathy. Circulation 2014;130:484–95.

9. O'Hanlon R, Grasso A, Roughton M, Moon JC, Clark S, Wage R, et al. Prognostic significance of myocardial fibrosis in hypertrophic cardiomyopathy. J Am Coll Cardiol 2010;56:867–74.

10. McLellan AJ, Ellims AH, Prabhu S, Voskoboinik A, Iles LM, Hare JL, et al. Diffuse ventricular fibrosis on cardiac cardiac magnetic resonance associates with ventricular tachycardia in patients with hypertrophic cardiomyopathy. J Cardiovasc Electrophysiol 2016;27:571–80.

11. Schelbert EB, Piehler KM, Zareba KM, Moon JC, Ugander M, Messroghli DR, et al. Myocardial fibrosis quantified by extracellular volume is associated with subsequent hospitalization for heart failure, death, or both across the spectrum of ejection fraction and heart failure stage. J Am Heart Assoc 2015;4(12). pii:e002613.

12. Rommel KP, von Roeder M, Latuscynski K, Oberueck C, Blazek S, Fengler K, et al. Extracellular volume fraction for characterization of patients with heart failure and preserved ejection fraction. J Am Coll Cardiol 2016;67:1815–25.

13. Maragiannis D, Alvarez PA, Ghosn MG, Chin K, Hinojosa JJ, Buergler JM, et al. Left ventricular function in patients with hypertrophic cardiomyopathy and its relation to myocardial fibrosis and exercise tolerance. Int J Cardiovasc Imaging 2018; 34:121–9.

14. Sewanan LR, Schwan J, Kluger J, et al. Extracellular matrix from hypertrophic myocardium provokes impaired twitch dynamics in healthy cardiomyocytes. J Am Coll Cardiol Basic Trans Science 2019;4:495–505.

15. Yang X, Pabon L, Murry CE. Engineering adolescence: maturation of human pluripotent stem cell-derived cardiomyocytes. Circ Res 2014;114:511–23.

KEY WORDS engineered heart tissue, fibrosis, hypertrophic cardiomyopathy, induced pluripotent stem cell–cardiomyocytes

JACC: BASIC TO TRANSLATIONAL SCIENCE VOL. 4, NO. 4, 2019

PRECLINICAL RESEARCH

A Mechanism for Statin-Induced Susceptibility to Myopathy

Sabine Lotteau, PhD,[a] Niklas Ivarsson, PhD,[b,†] Zhaokang Yang, PhD,[a] Damien Restagno, PhD,[c] John Colyer, PhD,[a] Philip Hopkins, MD,[d] Andrew Weightman, PhD,[e] Koichi Himori, MSc,[f] Takashi Yamada, PhD,[f] Joseph Bruton, PhD,[b] Derek Steele, PhD,[a] Håkan Westerblad, MD, PhD,[b,*] Sarah Calaghan, PhD[a,*]

VISUAL ABSTRACT

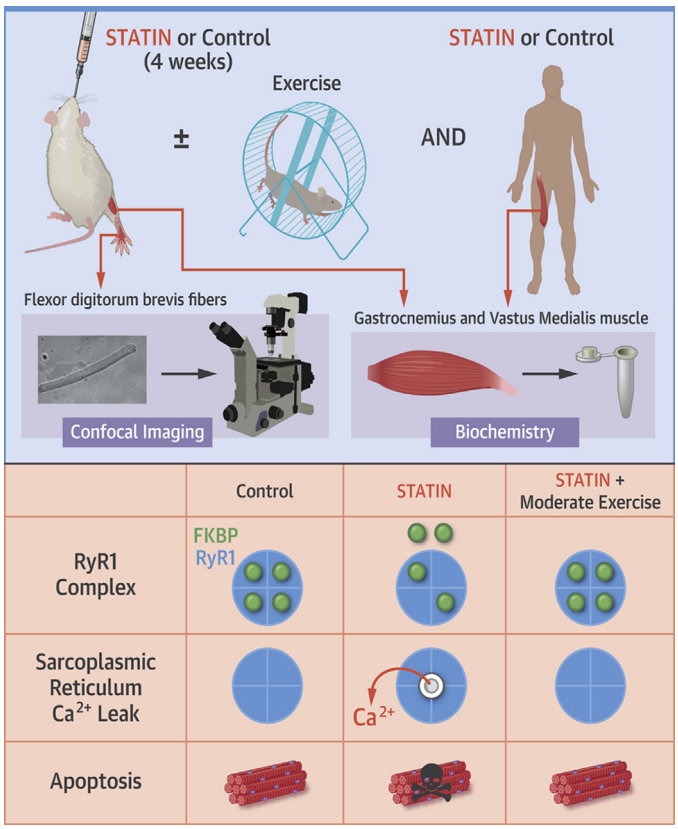

Lotteau, S. et al. J Am Coll Cardiol Basic Trans Science. 2019;4(4):509-23.

HIGHLIGHTS

- The authors used human and rat muscle to study the mechanism of statin myopathy and its interaction with exercise.
- Statin treatment triggered loss of the modulator protein FKBP from the sarcoplasmic reticulum (SR) calcium (Ca^{2+}) release channel, ryanodine receptor 1 (RyR1).
- Loss of FKBP was associated with reactive nitrogen species/reactive oxygen species-dependent SR Ca^{2+} leak and pro-apoptotic signaling, but had no overt impact on muscle function.
- Moderate running wheel exercise prevented the effects of statin treatment on the FKBP/RyR complex, SR Ca^{2+} leak, and pro-apoptotic signaling.
- Our data show that statin treatment induces a potentially harmful SR Ca^{2+} leak that might trigger statin myopathy in susceptible individuals, but could be prevented by moderate exercise.

From the [a]School of Biomedical Sciences, Faculty of Biological Sciences, University of Leeds, Leeds, United Kingdom; [b]Department of Physiology and Pharmacology, Karolinska Institutet, Stockholm, Sweden; [c]VetAgro Sup, APCSe, Université de Lyon, Marcy l'Etoile, France; [d]Leeds Institute of Medical Research at St James's, University of Leeds, Leeds, United Kingdom; [e]School of Mechanical, Aerospace and Civil Engineering, University of Manchester, Manchester, United Kingdom; and the [f]Graduate School of Health Sciences, Sapporo Medical University, Chuo-ku, Sapporo, Japan. *Prof. Westerblad and Dr. Calaghan contributed equally to this work and are joint senior authors. This work was supported by a British Heart Foundation project grant (PG/12/88/29951; 80%) and a Swedish Research Council project grant (Medicine and Health, K2014-52X-10842-21-5; 20%). Prof. Colyer is the founder and CEO of Badrilla, a life science company. All other authors have reported that they have no relationships relevant to the contents of this paper to disclose. †Dr. Ivarsson is deceased.

All authors attest they are in compliance with human studies committees and animal welfare regulations of the authors' institutions and Food and Drug Administration guidelines, including patient consent where appropriate. For more information, visit the *JACC: Basic to Translational Science* author instructions page.

Manuscript received January 24, 2019; revised manuscript received March 27, 2019, accepted March 27, 2019.

ISSN 2452-302X https://doi.org/10.1016/j.jacbts.2019.03.012

ABBREVIATIONS AND ACRONYMS

Ca^{2+} = calcium

FDB = flexor digitorum brevis

FKBP12 = FK506 binding protein (calstabin)

GAS = gastrocnemius

HADHA = hydroxyacyl-CoA dehydrogenase/3-ketoacyl-CoA thiolase/enoyl-CoA hydratase

HMG CoA = 3-hydroxy-3-methylglutaryl coenzyme A

L-NAME = N(ω)-nitro-L-arginine methyl ester

NOS = nitric oxide synthase

PGC1α = peroxisome proliferator-activated receptor γ co-activator 1α

RNS = reactive nitrogen species

ROS = reactive oxygen species

RyR = ryanodine receptor

SOD = superoxide dismutase

SR = sarcoplasmic reticulum

TUNEL = terminal deoxynucleotidyl transferase dUTP nick end labeling

SUMMARY

This study aimed to identify a mechanism for statin-induced myopathy that explains its prevalence and selectivity for skeletal muscle, and to understand its interaction with moderate exercise. Statin-associated adverse muscle symptoms reduce adherence to statin therapy; this limits the effectiveness of statins in reducing cardiovascular risk. The issue is further compounded by perceived interactions between statin treatment and exercise. This study examined muscles from individuals taking statins and rats treated with statins for 4 weeks. In skeletal muscle, statin treatment caused dissociation of the stabilizing protein FK506 binding protein (FKBP12) from the sarcoplasmic reticulum (SR) calcium (Ca^{2+}) release channel, the ryanodine receptor 1, which was associated with pro-apoptotic signaling and reactive nitrogen species/reactive oxygen species (RNS/ROS)–dependent spontaneous SR Ca^{2+} release events (Ca^{2+} sparks). Statin treatment had no effect on Ca^{2+} spark frequency in cardiac myocytes. Despite potentially deleterious effects of statins on skeletal muscle, there was no impact on force production or SR Ca^{2+} release in electrically stimulated muscle fibers. Statin-treated rats with access to a running wheel ran further than control rats; this exercise normalized FKBP12 binding to ryanodine receptor 1, preventing the increase in Ca^{2+} sparks and pro-apoptotic signaling. Statin-mediated RNS/ROS–dependent destabilization of SR Ca^{2+} handling has the potential to initiate skeletal (but not cardiac) myopathy in susceptible individuals. Importantly, although exercise increases RNS/ROS, it did not trigger deleterious statin effects on skeletal muscle. Indeed, our results indicate that moderate exercise might benefit individuals who take statins. (J Am Coll Cardiol Basic Trans Science 2019;4:509–23)

Statins are the most widely prescribed drug in the Western world. Their use is predicted to rise further due to recent reductions in the cardiovascular risk threshold for statin prescription across the globe (1,2). However, cardiovascular benefits of statins are restricted by adverse effects that limit adherence (3,4) and, in turn, increase cardiovascular events (5) and mortality (6). The most common side effects and main reason for discontinuation of therapy emerge from skeletal muscle (statin myopathy or statin-associated adverse muscle symptoms). Although no strict definition of statin myopathy has been universally adopted (7–10), we use this term to encompass the full spectrum of the effects of statins on skeletal muscle.

SEE PAGE 524

This includes mild to moderate muscle symptoms and/or signs (myalgia: muscle pain with stiffness and weakness), as well as more severe potentially life-threatening outcomes (myositis and/or rhabdomyolysis) that are associated with raised creatine kinase (8,11). Although physical activity counteracts metabolic and cardiovascular diseases that are prevalent in subjects prescribed statins, exercise has been reported to exacerbate statin myopathy (12–19), which may further limit the benefits of statins in those at risk of cardiovascular disease.

Statins are inhibitors of 3-hydroxy-3-methylglutaryl coenzyme A (HMG CoA) reductase that limit the production of cholesterol, isoprenoids, and coenzyme Q. Despite extensive research, which has focused on calcium (Ca^{2+}) homeostasis and mitochondrial function (20–25), a cohesive mechanism for statin-induced myopathy is lacking. Furthermore, an understanding of why myopathy is not experienced by everyone who takes statins and the reason for its selectivity for skeletal muscle has not been fully addressed.

Using human and rodent muscle, we investigated the mechanism for statin-induced myopathy and described its interaction with voluntary moderate exercise. We revealed a mechanism by which statin treatment can make skeletal muscles susceptible to myopathy–dissociation of the FK506 binding protein (FKBP12) from the sarcoplasmic reticulum (SR) Ca^{2+} release channel, the ryanodine receptor 1 (RyR1), which is accompanied by numerous spontaneous Ca^{2+} release events (i.e., Ca^{2+} sparks) (26). Statin treatment had no effect on Ca^{2+} sparks in cardiac muscle. Aberrant SR Ca^{2+} handling was associated with pro-apoptotic signaling in skeletal muscle. However, despite this myopathy-promoting signaling, statin treatment had no obvious detrimental effect on the contractile function of skeletal muscle, which suggests that additional factors are required to produce myopathic symptoms. Furthermore, in rats that underwent voluntary exercise, no overt muscle dysfunction was evident. Our data demonstrate that individuals taking statins might benefit from moderate exercise.

TABLE 1 Patient Data

			Statin				Matched Control Subjects			
Statin	Dose (mg)	Sex	Age (yrs)	Histology	CK (IU/l)	Disease	Age (yrs)	Histology	CK (IU/l)	Disease
SIMV	40	F	48	Type 2b fiber atrophy		HC, H	47	Normal		Treated hypothyroidism
SIMV	40	M	72	Type 2b fiber atrophy		RM	73	Type 2b fiber atrophy	110	H, DM, minor CVA
SIMV	20	M	65	Fiber size, variation, increase in mitochondria	76	H, RM	65	Type 2b fiber atrophy	200	
SIMV	40	F	60	Normal		Type 2 DM, CVA, obese	60	Normal	110	
SIMV	40	M	70	Normal		H, AA	70	Normal	142	H
SIMV	10	M	71		122	H	71	Fiber size variation		H, CVA
SIMV	40	M	48	Normal	157	H	48			
PRAV	30	M	58	Atrophy in scattered fibers		H	58	Normal	102	
SIMV	20	M	72	Atrophy and angulation in many fibers	116	H	71	Normal	138	MV
SIMV	40	M	59			Type 2 DM, CVA, obese	59	Normal	97	
ATOR	20	M	56			IHD	56	Normal		H
ROSU	10	F	54	Normal	114	H	54			
SIMV	20	F	52	Normal	57	H	51	Normal		

All samples from patients taking statins were paired with sex- and age-matched control subjects. Details of histology, serum creatine kinase (CK), and disease are given where available. AA = aortic aneurysm; CVA = cerebrovascular accident; DM = diabetes mellitus; H = hypertension; HC = high cholesterol; IHD = ischemic heart disease; MV = mitral valve disease; RM = risk modification.

METHODS

STUDY APPROVAL. Anonymized vastus medialis samples were obtained from patients who were screened (and tested negative) for malignant hyperthermia. Individuals taking statins were age- and sex-matched with control subjects (Table 1). All patients gave informed consent. This study complied with the principles of the Declaration of Helsinki and was approved by the Leeds East Local Research Ethics Committee. Work with rodents was performed in strict accordance with the recommendations of the Directive 2010/63/EU of the European Parliament and was approved by animal welfare committees at the University of Leeds and the Karolinska Institutet.

RODENT MODELS. Male Wistar rats (130 to 160 g) received simvastatin (40 mg/kg/day) or saline by oral gavage at the beginning of the dark cycle for 28 days (see Supplemental Methods for justification of dose). For exercise studies, rats were given free access to an in-cage running wheel. Custom-built hardware and software allowed detailed characteristics of running activity to be recorded for each animal (see Supplemental Methods). All animals were killed by stunning and cervical dislocation.

RODENT MUSCLE PREPARATIONS. For protein chemistry, rat gastrocnemius (GAS) muscle (a predominantly type II muscle) was dissected to remove slow oxidative type I fibers (dark red in color). For confocal microscopy, rat flexor digitorum brevis (FDB) fibers were isolated by collagenase digestion (27). FDB is predominantly type IIa; the choice of this muscle was informed by the short length of the fibers that allows the isolation and study of intact cells. In some cases, fibers were permeabilized by 2-min exposure to 0.005% (w/v) saponin (28). Rat cardiac myocytes were isolated from Langendorff-perfused hearts by collagenase and protease digestion (29).

MUSCLE FUNCTION IN VITRO. Rat single FDB fibers were dissected, mounted, and electrically stimulated via platinum plates. The isolated muscle preparations were stimulated for 350 ms at 10 to 150 Hz at 1-min intervals, and the resultant force was measured. The fluorescent Ca^{2+} indicator indo-1 was pressure injected into fibers, and the fluorescence signals of indo-1 were recorded at rest and during contractions as described previously (30).

CONFOCAL MICROSCOPY. Confocal images were acquired with a Eclipse TE300 inverted microscope (Nikon, Minato, Tokyo, Japan) equipped with a confocal scanhead, MicroRadiance 2000 (Bio-Rad, Hercules, California), and a ×60 water-immersion objective. FDB fibers were loaded with fluo 4-AM (5 μM, for intact cells), fluo 3 (50 μM, for permeabilized cells), or DAF-2 (5 μM). Cardiac myocytes were loaded with fluo 4-AM (6 μM). Dyes were excited with the 488-nm line of a 20-mW coherent sapphire laser (attenuated ≈90%), and emitted fluorescence

was measured at >515 nm. Images were acquired in x-y (every 5 s) or line scan mode (every 6 ms). Ca^{2+} sparks were identified and analyzed with ImageJ software version 1.51j8, National Institutes of Health, Bethesda, Maryland) using the Sparkmaster plugin (see Supplemental Methods).

PROTEIN CHEMISTRY AND ASSAYS. Sodium dodecyl sulfate-polyacrylamide gel electrophoresis and Western blotting were carried out as described in Calaghan et al. (29). Data were normalized to glyceraldehyde-3-phosphate dehydrogenase (GAPDH) expression. Because it was not possible to load all samples on the same gel, a standard calibration sample (mixed from 4 human vastus medialis samples or 3 rat GAS samples) was loaded in duplicate on gels to allow between-gel comparisons. For RyR post-translational modifications and protein associations, RyR1 was immunoprecipitated from GAS as described previously (31) (see Supplemental Methods). The terminal deoxynucleotidyl transferase dUTP nick end labeling (TUNEL) assay was performed on cryostat sections (10 μm; Leica CM 1900), visualized using the detection kit TACS 2TdT-DAB for In situ Apoptosis (4810-30-K, Trevigen) (32). Calpain activity was assessed using the assay kit QIA120 (Merck Millipore).

ANTIBODIES. Antibodies were as follows: calmodulin Abcam Cat# ab45689 RRID:AB_725815, 1:1,000; FKBP12 Abcam Cat# ab58072 RRID:AB_941602, 1:200; hydroxyacyl-CoA dehydrogenase/3-ketoacyl-CoA thiolase/enoyl-CoA hydratase (HADHA) Abcam Cat# RRID:AB_2263836 1:1,000; peroxisome proliferator-activated receptor γ co-activator 1α (PGC1α) Abcam Cat# ab54481 RRID:AB_881987, 1:1,000; RyR clone 34C Abcam Cat# ab2868 RRID:AB_2183051, 1:5,000; Cav 3 BD Biosciences Cat# 610420 RRID:AB_397800, 1:5000; endothelial nitric oxygen synthase eNOS BD Biosciences Cat# 610297 RRID:AB_397691, 1:2,500; Cav 1 Boster Biological Technology Cat# PA1514, RRID: AB_2651038, 1:1,000; caspase-3 Cell Signaling Technology Cat# 9665 also 9665S RRID:AB_2069872, 1:1000; nNOS Cell Signaling Technology Cat# 4231S RRID:AB_2152485, 1:1,000; and glyceraldehyde-3-phosphate dehydrogenase (GAPDH) Sigma-Aldrich Cat# G9545 RRID:AB_796208, 1:100,000.

STATISTICAL ANALYSIS. Results are expressed as mean ± SEM of number of observations, with $p < 0.05$ used to denote statistical significance. The Shapiro-Wilk test was used to test for normality. For the human study, we had access to 13 samples from statin-treated individuals and 13 age- and sex-matched control subjects. The paired Student's *t*-test (normally distributed data) or the Wilcoxon signed-rank test (non-normally distributed data) were used to compare groups. This sample size gave power >0.8 to detect a 100% change in parameter (SD: 100% of mean; paired Student's *t*-test). For rodent samples, comparison of 2 groups was performed using the Student's *t*-test (normal distribution) and the Mann-Whitney rank test (non-normal distribution). For tetanic and force Ca^{2+} measurements at different frequencies of stimulation, a 2-way repeated measures analysis of variance was used (with the Holm-Sidak post hoc test). Two-way analysis of variance (with the Tukey post hoc test) was used to analyze daily running distance with time in the control and statin groups, and the effect of exercise and statin treatment on markers of mitochondrial biogenesis. For rodent studies, we used 10/11 and 5/6 animals in the sedentary control/statin groups in the United Kingdom and Sweden (tetanic force and Ca^{2+} measurements), respectively. For the exercise study, we used 6/6 control/statin-treated animals. Group sizes were based on power calculations for protein chemistry data from the rat, which showed power >0.8 to detect a 50% difference in means when $n = 6$ (SD: 25% of mean; *t*-test). Presented data might have different numbers of animals for some endpoints due to sample limitations. GraphPad Prism (version 7.05, Graphpad, San Diego, California) was used for all statistical analysis, with the exception of tetanic force and Ca^{2+} measurements (Sigmaplot for Windows, version 13.0, Systat Software Inc., San Jose, California).

RESULTS

SUMMARY OF EXPERIMENTAL PLAN AND KEY FINDINGS. Supplemental Table 1 provides a summary of all experiments performed, with key findings for both human and rodent preparations.

DISSOCIATION OF FKBP12 FROM RyR1 AND PRO-APOPTOTIC SIGNALING IN SKELETAL MUSCLE OF STATIN-TREATED HUMANS AND RATS. Post-translational modifications of RyR1 and changes in the molecular composition of the RyR1 protein complex are present in several conditions with dysfunctional skeletal muscle (33–35). To test whether similar alterations occurred with statin treatment, we immunoprecipitated RyR1 in homogenates prepared from biopsies of human vastus medialis muscles and from isolated rat GAS muscles, and measured the expression of the RyR1 binding partners FK506 binding protein 12 (FKBP12) and calmodulin. Statin treatment caused a marked decrease in FKBP12 bound to RyR1 in both human and rat muscle, whereas the calmodulin binding remained intact (**Figures 1A and 1B**). It was

FIGURE 1 Dissociation of FKBP12 From RyR1 and Pro-Apoptotic Signaling in Skeletal Muscle From Statin-Treated Humans and Rats

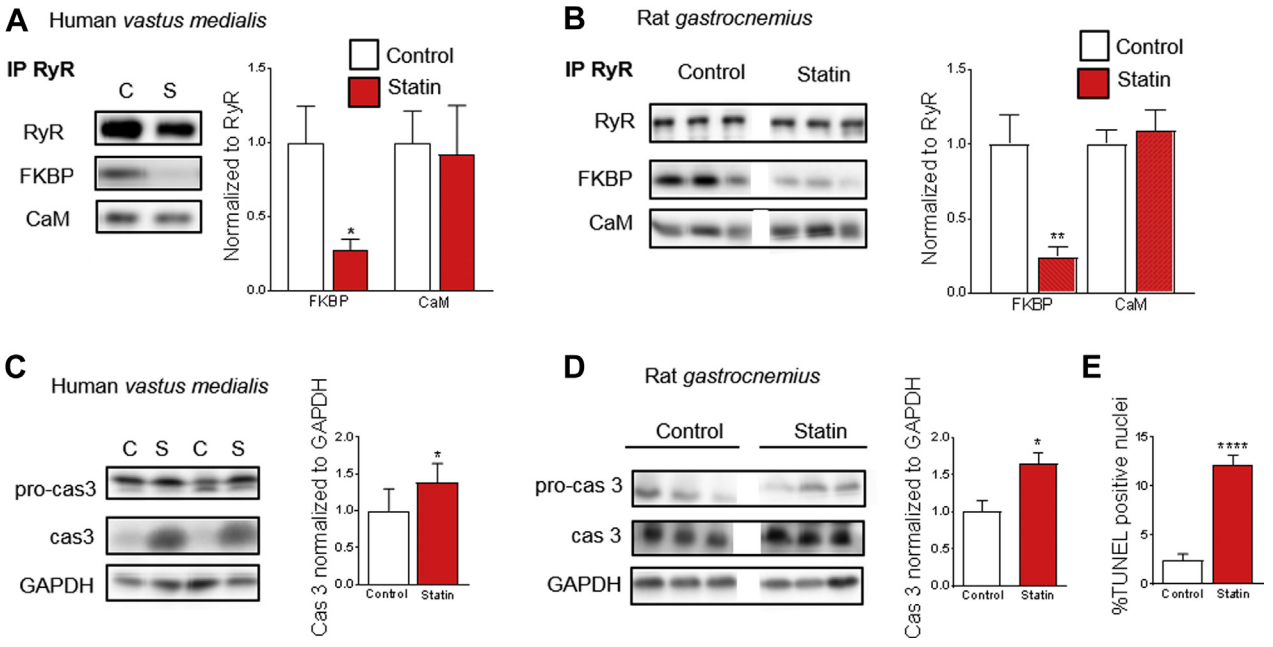

Representative blots from the same gel and mean data showing FK506 binding protein (FKBP12) and calmodulin (CaM) in ryanodine receptor (RyR) immunoprecipitates from **(A)** human and **(B)** rat muscle. All values are standardized to the mean of the control group. There was no difference ($p > 0.05$) in total RyR1 or FKBP12 expression between groups. Data from 11/11 (FKBP) and 13/13 (CaM) patients taking statins (S) and age- and sex-matched controls (C); n = 10 to 11 rats. **(C)** Representative blots from the same gel and mean data from human muscle showing pro-caspase 3 (pro-cas3; 35 kDa) and cleaved caspase 3 (cas3; 17 kDa). Data from 13/13 patients. **(D)** Expression of pro-cas3, cleaved cas3 and **(E)** proportion of terminal deoxynucleotidyl transferase dUTP nick end labeling (TUNEL) positive nuclei (%) in rat muscle. Cas3 expression is standardized to the mean of the control group. Data from 5 to 7 animals. All data are mean + SEM. **(A)** *p = 0.0127 (paired Student's *t*-test). **(B)** **p = 0.0023 (Student's *t*-test). **(C)** *p = 0.0425 (Wilcoxon signed-rank test). **(D)** *p = 0.0158 (Student's *t*-test); ****$p < 0.0001$ (Student's *t*-test). GADPH = glyceraldehyde-3-phosphate dehydrogenase.

noteworthy that a robust dissociation of FKBP12 from RyR1 could be detected, although muscle biopsies were obtained from a diverse patient group (Table 1).

FKBP12 dissociation from RyR1 has been shown to increase spontaneous SR Ca^{2+} leak, which, in turn, promotes protein degradation and programmed cell death (33). Therefore, we next studied whether the change in the RyR complex in muscles of statin-treated subjects was accompanied by indexes of pro-apoptotic signaling. For this purpose, we measured the protein expression of the inactive pro-caspase-3 and its cleaved active product, the pro-apoptotic enzyme caspase-3. Statin treatment increased caspase-3 expression in both human and rat muscles (Figures 1C and 1D). In rat muscle, we also measured the proportion of TUNEL positive nuclei, which is another marker for pro-apoptotic signaling, and observed a marked increase with statin treatment (Figure 1E). Thus, muscles from both humans and rats treated with statins showed major alterations that were potentially deleterious and might underlie statin-induced myopathy. In subsequent experiments, we delved deeper into mechanisms of the statin-induced effects; these experiments were only performed on rat muscles due to limitations in what can be performed on human muscle biopsy material.

STATIN TREATMENT INCREASES SR Ca^{2+} LEAK IN INTACT SKELETAL MUSCLE. SR Ca^{2+} leak in the form of Ca^{2+} sparks (elementary Ca^{2+} release events from clusters of RyR1) is a myopathic mechanism common to many skeletal muscle diseases, including muscular dystrophy and malignant hyperthermia (33,36). Although spark-mediated SR Ca^{2+} leak is an attractive culprit for statin-induced myopathy, no overt changes in Ca^{2+} spark characteristics with (in vivo) statin treatment have been documented to date (20,21,23). However, all previous work has been performed on permeabilized muscle fibers, in which the constitutive inhibition of RyR1 by magnesium (37) and the dihydropyridine receptor (38) is reduced, which may mask the effects of statins. Therefore, we evaluated the effect of statin treatment on the SR

FIGURE 2 Statin Treatment Provokes SR Ca^{2+} Leak in Skeletal, But Not Cardiac, Myocytes

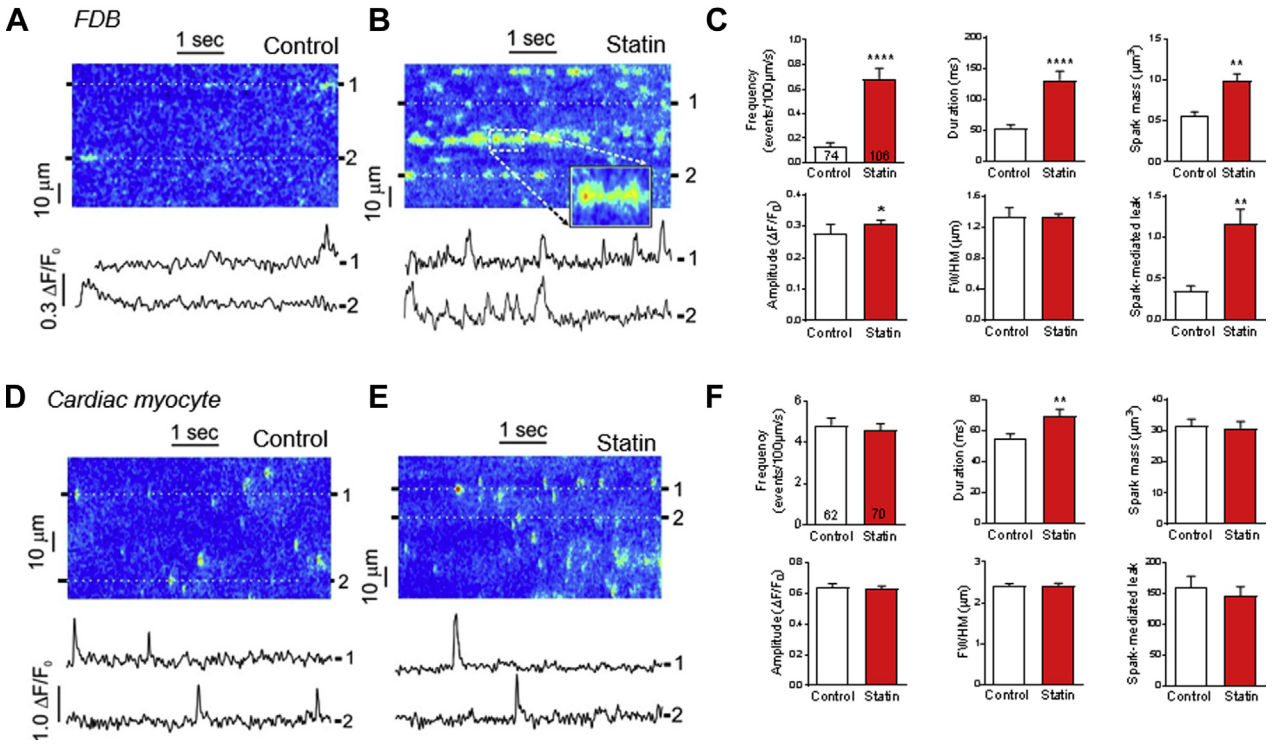

Representative confocal line scans (F/F_0) with associated line profiles and mean data from **(A to C)** intact flexor digitorum brevis (FDB) fibers and **(D to F)** cardiac myocytes; n = 11/10 (FDB) and 5/5 (cardiac myocytes) rats for control/statin-treated groups, number of cells shown on graphs. Data are mean + SEM and compared using the Mann-Whitney rank test. **(C)** ****$p < 0.0001$; *$p = 0.0307$; **$p = 0.0029$ (mass); **$p = 0.0091$ (leak). **(F)** **$p = 0.0024$. Ca^{2+} = calcium; FWHM = full width at half maximum; SR = sarcoplasmic reticulum.

Ca^{2+} leak in intact muscle fibers. Ca^{2+} sparks were recorded in nonpermeabilized fluo 4-loaded FDB fibers from the rat (Figures 2A to 2C). As predicted (39), spark frequency was low in intact fibers from control animals. In marked contrast, in fibers from statin-treated rats, sparks were much more frequent, of longer duration, and larger in amplitude, which resulted in an increased spark mass and spark-mediated Ca^{2+} leak. Interestingly, this robust effect of statins on spark characteristics was lost following fiber permeabilization (Supplemental Figure S1), which explains discrepancies with previous work (20,21,23) and suggests that statin effects in intact cells depend on the normal regulation of the RyR1 and/or effects of a soluble mediator.

An important question is whether statin-induced SR Ca^{2+} leak is also seen in cardiac muscle because this could have additional detrimental consequences by promoting triggered arrhythmias (40). Reassuringly, there was minimal impact of statin treatment on Ca^{2+} sparks in intact cardiac myocytes from statin-treated rats (Figures 2D to 2F). Thus, statin treatment induces SR Ca^{2+} leak in skeletal muscle, whereas cardiac muscle is protected from this potentially deleterious effect.

NOS AND REACTIVE OXYGEN SPECIES PROMOTE SR Ca^{2+} LEAK WITH STATIN TREATMENT. Reactive nitrogen species and reactive oxygen species (RNS/ROS) could account for the statin-induced SR Ca^{2+} leak; both can be increased by statin treatment (25,41,42), target the RyR and its associated proteins directly (43,44) and indirectly (45), and affect RyR activity (46). Inhibition of NOS isoforms with N(ω)-nitro-L-arginine methyl ester (L-NAME) had a greater impact on NO (indexed with DAF-2) in FDB fibers from statin-treated rats than in control rats, which was consistent with higher NOS activity in the statin group (Figure 3A). This could be explained by increased expression of endothelial NOS and reduced expression of the NOS-inhibitory caveolin isoform Cav1 (Figure 3B). These observations were consistent with statins acting as inhibitors of HMG CoA reductase and established pathways in which

FIGURE 3 Nitric Oxide Synthase and Reactive Oxygen Species Promote SR Ca^{2+} Leak With Statin Treatment

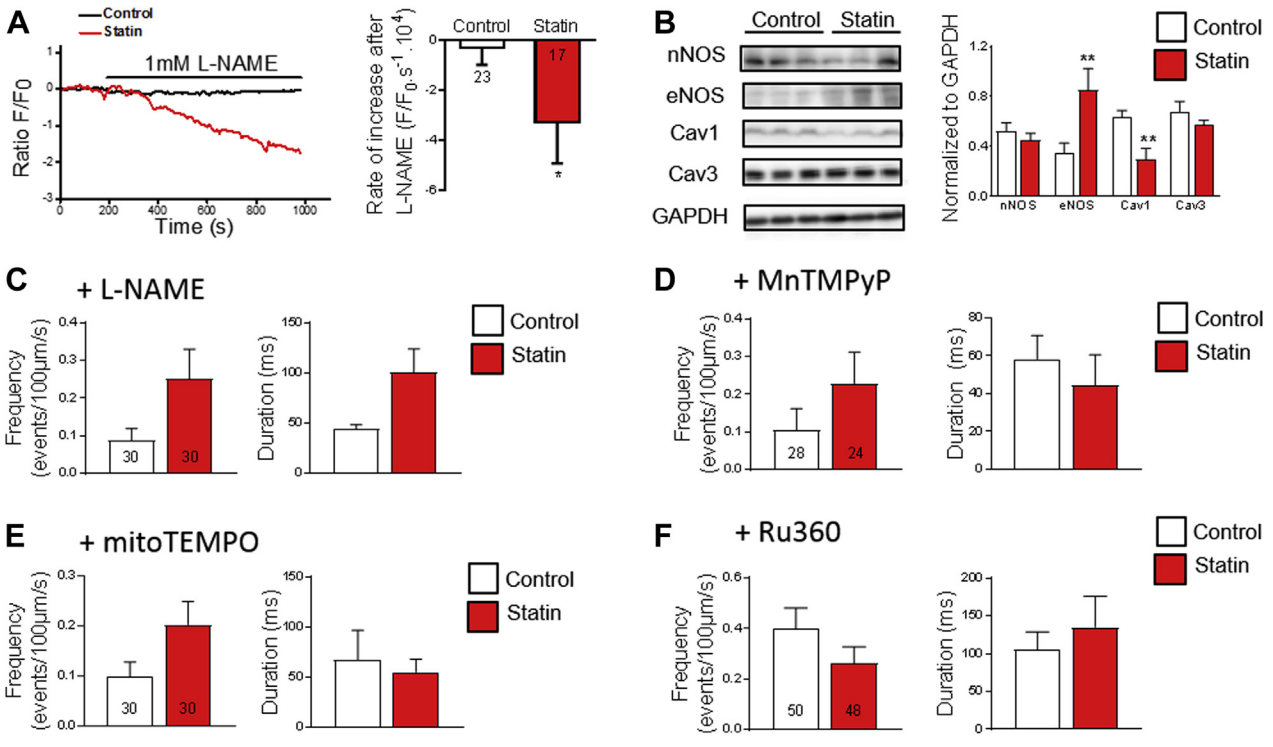

(A) Representative traces and mean data showing the impact of N(ω)-nitro-L-arginine methyl ester (L-NAME) (1 mM) on DAF-2 fluorescence in FDB fibers. Within each cell, the rate of increase in DAF-2 fluorescence recorded before L-NAME was subtracted from the entire trace; n = 7/8 animals for control/statin-treated rats, number of cells shown on graph. **(B)** Representative blots from the same gel and mean data from rat gastrocnemius (n = 9 to 11 animals). Ca^{2+} spark frequency and duration in intact FDB fibers in the presence of **(C)** L-NAME (1 mM), **(D)** Mn (III)tetrakis(1-methyl-4-pyridyl)porphyrin (MnTMPyP) (0.1 mM), and **(E)** (2-(2,2,6,6-Tetramethylpiperidin-1-oxyl-4-ylamino)-2-oxoethyl)triphenylphosphonium chloride (mitoTEMPO) (25 µM); n = 3 animals, number of cells shown on graphs. **(F)** The impact of the mitochondrial Ca^{2+} uniporter inhibitor Ru360 (20 µM, 15 min) in intact FDB fibers on increased Ca^{2+} spark frequency and duration. Data from 7 animals (number of cells shown on graph). All data are mean + SEM and compared using Mann-Whitney rank test. **(A)** * p = 0.034. **(B)** ** p = 0.0042 (endothelial nitric oxygen synthase [eNOS]), **p = 0.0073 (caveolin 1 [Cav1]); other abbreviations as in Figures 1 and 2.

products of the HMG CoA reductase cascade regulate NOS (isoprenoids) and caveolin (cholesterol) expression (47). Enhanced NOS activity was directly linked with Ca^{2+} leak because, in the presence of L-NAME, there was no longer any difference ($p > 0.05$) in Ca^{2+} spark frequency or duration between fibers from control and statin-treated rats (**Figure 3C**). L-NAME inhibits NO and superoxide production from NOS (48), which indicates a role for NO, superoxide, and/or peroxynitrite in the spark-mediated leak.

Statin treatment has been shown to increase ROS production in skeletal muscle (25). We showed that these ROS played a role in the SR Ca^{2+} leak, because the superoxide dismutase (SOD) and peroxynitrite scavenger Mn(III)tetrakis(1-methyl-4-pyridyl) porphyrin (MnTMPyP) and the mitochondrial-targeted SOD mimetic (2-(2,2,6,6-Tetramethylpiperidin-1-oxyl-4-ylamino)-2-oxoethyl)triphenylphosphonium chloride (mitoTEMPO) eliminated the difference ($p > 0.05$) in Ca^{2+} spark frequency and duration between fibers from control and statin-treated rats (**Figures 3D and 3E**).

Bidirectional Ca^{2+} fluxes between SR and mitochondria affect both SR and mitochondrial function. Mitochondria accumulate close to SR Ca^{2+} release sites during postnatal skeletal muscle maturation, which facilitates mitochondrial Ca^{2+} uptake and is associated with reduced susceptibility to Ca^{2+} spark activation (49). Conversely, excessive mitochondrial Ca^{2+} uptake may promote Ca^{2+} sparks by enhancing ROS production from complexes I and III (50,51). In support of this latter mechanism, the difference in Ca^{2+} spark frequency and duration between fibers from control and statin-treated rats was no longer present after inhibiting Ca^{2+} entry

FIGURE 4 Impact of Statin Treatment on Basal and Tetanic $[Ca^{2+}]_i$ and Force Production

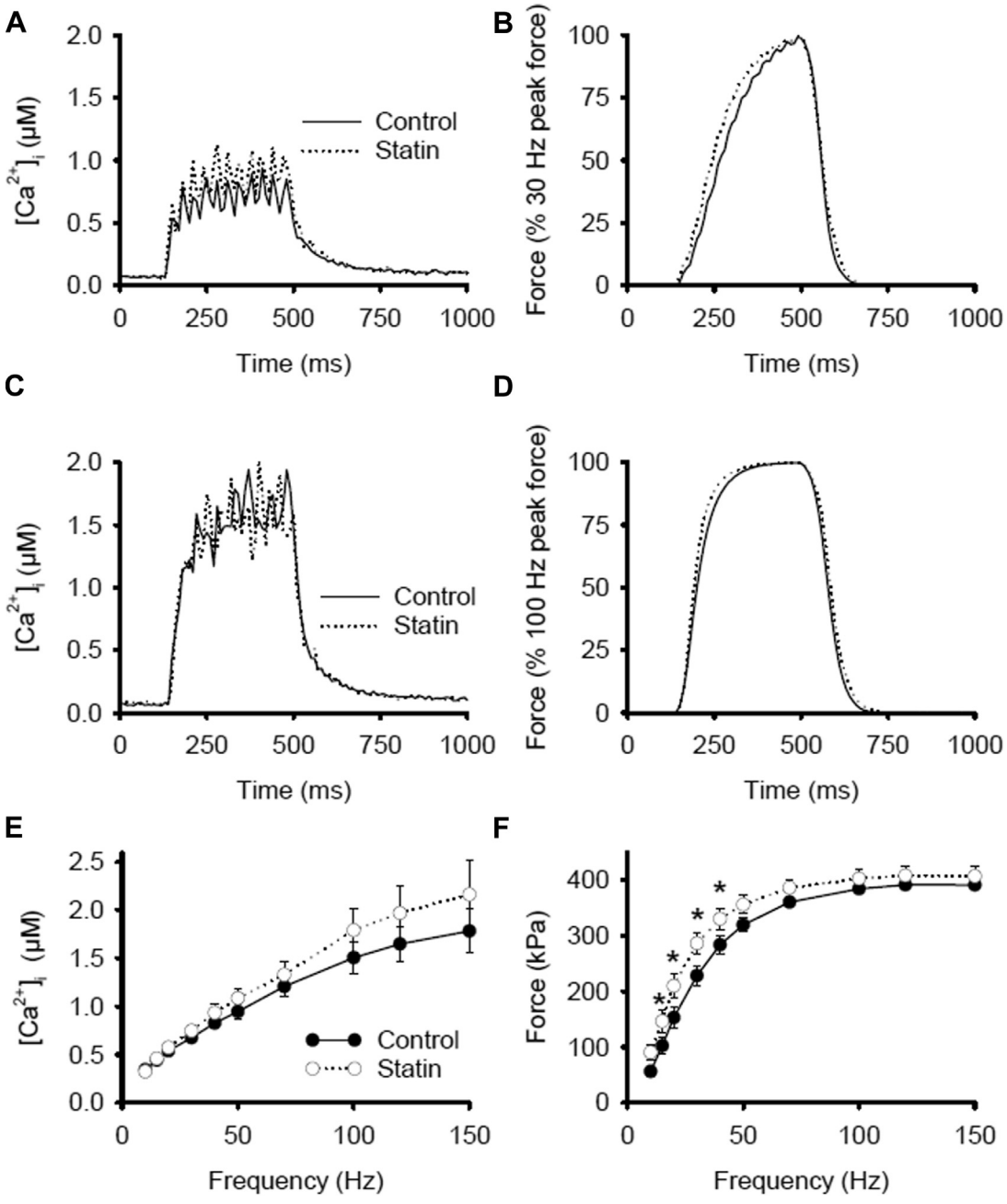

Representative $[Ca^{2+}]_i$ transients at **(A)** 30 Hz and **(C)** 100 Hz, and **(E)** mean data for 10 to 150 Hz in FDB fibers stimulated with 350 ms trains of pulses at 1-min intervals. Corresponding representative force records at **(B)** 30 Hz and **(D)** 100 Hz, and **(F)** mean data for 10 to 150 Hz. From n = 13/11 fibers from 5/6 animals for control/statin-treated animals. Data are mean ± SEM and compared with 2-way repeated-measures analysis of variance. **(F)** *p = 0.020 (15 Hz); p = 0.003 (20 Hz); p = 0.005 (30 Hz); p = 0.042 (40 Hz) versus control subjects. Abbreviations as in Figure 2.

into the mitochondria via the mitochondrial Ca^{2+} uniporter with Ru360 (52) (Figure 3F). Taken together, the impact of NOS inhibition with L-NAME, ROS scavengers, and mitochondrial Ca^{2+} uniporter inhibition suggests that mitochondrial Ca^{2+} uptake stimulates RNS/ROS production, which, in turn, acts on RyR1 to maintain and/or exacerbate the SR Ca^{2+} leak.

FIGURE 5 **Statin Treatment Increases Physical Activity**

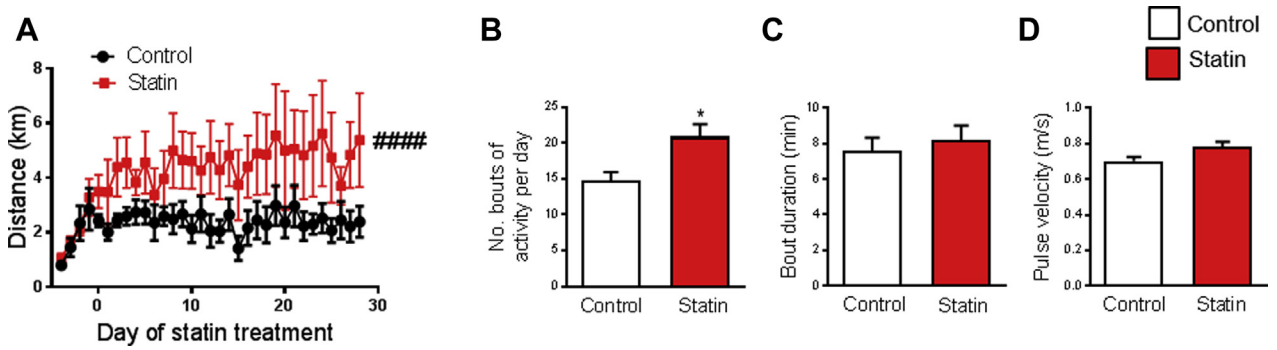

Running wheel data from the dark cycle (active period). Rats were acclimatized to the wheel for 4 days before statin treatment commenced (day 0). **(A)** Daily running distance over the duration of the study. **(B to D)** Detailed analysis of activity for the 28-day treatment period. Bouts (continuous periods of activity) were defined as activity seen in ≥2 consecutive minutes. Pulse velocity represents the mean velocity of each one-quarter revolution (pulse) of the wheel. Data are mean ± SEM (n = 6 animals per group). **(A)** ####$p < 0.0001$ for statin effect (2-way analysis of variance). **(B)** *$p = 0.0148$ versus control (*t*-test).

CONSEQUENCES OF STATIN-INDUCED SR Ca^{2+} LEAK FOR MUSCLE FUNCTION. Next, we determined whether the observed effects of statins had a net impact on muscle function by measuring the free cytosolic $[Ca^{2+}]$ ($[Ca^{2+}]_i$) and force production in electrically stimulated single FDB fibers (30). There was no significant difference in basal $[Ca^{2+}]_i$ (69 ± 5 nM vs. 72 ± 3 nM; n = 13/11) or tetanic $[Ca^{2+}]_i$ (**Figures 4A, 4C, and 4E**) between FDB fibers from control and statin-treated animals. Furthermore, statin treatment did not reduce force production at any frequency; at low-frequency stimulation (≤40 Hz) there was a small increase in tetanic force in the statin group (**Figures 4B and 4F**). Calpains belong to a family of Ca^{2+}-dependent proteolytic enzymes with pro-apoptotic activity (53). Calpain activity did not differ between control and statin-treated muscle (9.3 ± 0.4 vs. 9.3 ± 0.2 AU; n = 10), which was consistent with the unaltered basal $[Ca^{2+}]_i$. Thus, in resting muscle, the statin-induced SR Ca^{2+} leak was effectively counteracted by alterations in SR Ca^{2+} uptake and/or Ca^{2+} fluxes across the cell membrane (54). This concept of compensated leak was proposed to explain normal basal $[Ca^{2+}]_i$ in conjunction with Ca^{2+} leak from RyR1 due to a mutation found in malignant hyperthermia (Y522S) (36). During contractions, the amount of Ca^{2+} released in response to action potential stimulation remains constant over a wide range of SR Ca^{2+} content in fast-twitch muscle fibers (55), and depletion of SR Ca^{2+} promotes refilling via store-operated Ca^{2+} entry (56). Thus, the unaffected tetanic $[Ca^{2+}]_i$ in muscle fibers from statin-treated rats was also compatible with the observed spark-mediated SR Ca^{2+} leak in these fibers.

MODERATE EXERCISE REVERSES THE IMPACT OF STATINS ON SKELETAL MUSCLE. Exercise is recommended for those at risk of cardiovascular disease (i.e., those who take statins). However, there are reports that exercise reveals or exacerbates statin myalgia (13,14) and myositis (12,15,16), and that statins limit training adaptations in skeletal muscle (57,58). Therefore, we gave statin-treated and control rats access to an in-cage running wheel, which resulted in a type of voluntary exercise similar to that recommended for human subjects prescribed statins. Rats were acclimatized to the wheel for 4 days before statin treatment commenced. Unexpectedly, the daily running distance was greater for statin-treated rats than for control rats across the 4 weeks of the study (**Figure 5A**). The larger daily running distance in the statin group was due to an increase in the number of bouts of activity (**Figure 5B**), whereas the running bout duration (**Figure 5C**) and running velocity (**Figure 5D**) were similar in the 2 groups.

In sharp contrast to the situation in muscles of sedentary subjects (see **Figure 1**), binding of FKBP12 to RyR1 showed no significant difference between muscles of statin-treated and control rats after 4 weeks of exercise (**Figures 6A and 6B**). Moreover, in the exercised state, statin treatment no longer caused a significant increase in caspase 3 expression (**Figures 6C and 6D**). Intriguingly, in the exercised state, the frequency of SR Ca^{2+} sparks was lower in muscle fibers of statin-treated rats than in control rats, which contributed to a smaller spark-mediated Ca^{2+} leak in this group (**Figures 6E to 6G**).

A number of studies have linked statin-induced myopathy with impaired mitochondrial biogenesis.

FIGURE 6 Exercise Reverses the Effect of Statin Treatment on the RyR Complex, Apoptosis, and SR Ca^{2+} Leak

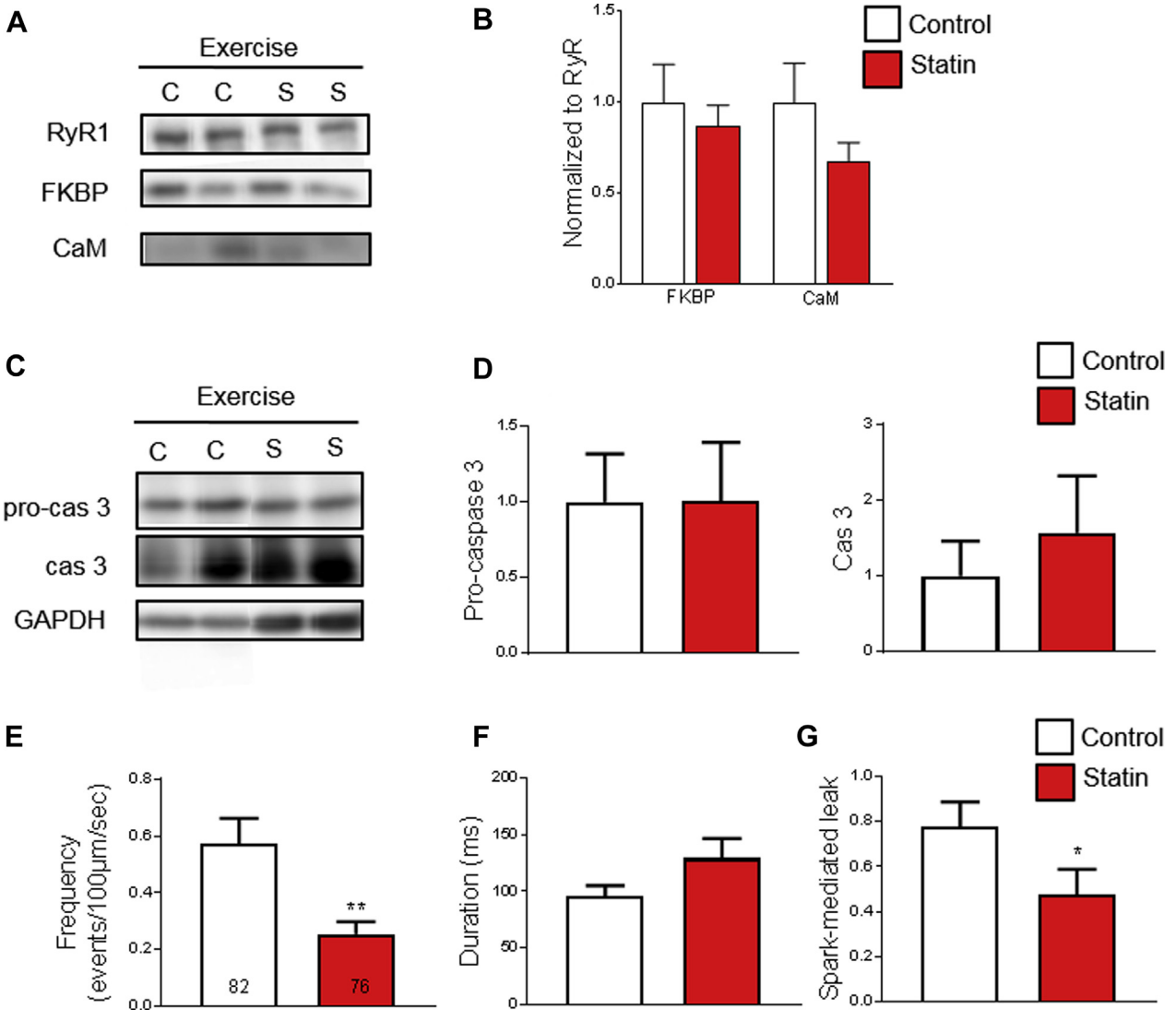

(A) Representative blots and **(B)** mean data of FKBP12 and CaM in RyR immunoprecipitates from gastrocnemius muscle of exercised animals. Data are normalized to RyR and standardized to the mean of the control exercise group (n = 6 animals). C = control, S = statin. **(C)** Representative blots and **(D)** mean data of pro-cas 3 and cleaved cas 3 expression in gastrocnemius homogenates of exercised animals. Data are normalized to GAPDH and standardized to the mean of the control exercise group (n = 6 animals). **(E)** Mean data for spark frequency, duration, and spark-mediated leak in intact FDB fibers from n = 6 exercised animals per group, number of cells shown on graph. Data are mean + SEM and compared using the **(B)** Student's *t*-test and **(D to G)** Mann-Whitney. *p = 0.0197; **p = 0.0061. Abbreviations as in Figures 1 to 3.

The transcriptional co-activator PGC1 is a key mediator of mitochondrial biogenesis in response to endurance exercise (59-61). Statin treatment has been shown to decrease PGC1α mRNA expression in human and rodent fast skeletal muscle (24); however, no change in PGC1α protein was detected in rodent muscle (62). We saw no impact of statin treatment on protein expression of PGC1α or HADHA (which is used as an index of mitochondrial biogenesis) either in sedentary or exercised animals (Figures 7A to 7C). Together, these data show that statin treatment did not limit moderate physical activity or markers of training adaptation in skeletal muscle. Exercise reversed the statin-dependent SR Ca^{2+} leak, which suggests a potentially beneficial effect.

DISCUSSION

The prevalence of statin-induced muscle symptoms varies between 7% and 29% in registries and

FIGURE 7 **Statins Do Not Limit Mitochondrial Biogenesis in Sedentary or Exercised Rats**

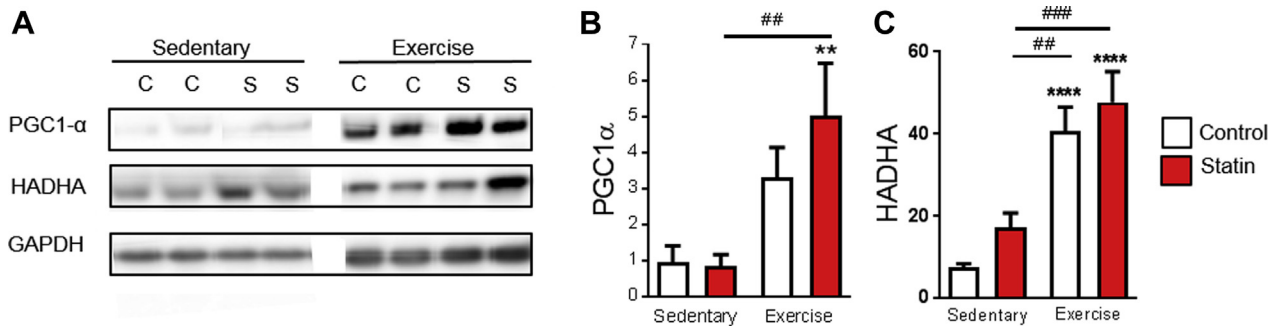

(A) Representative blots and **(B and C)** mean data from rat gastrocnemius homogenates showing peroxisome proliferator-activated receptor γ co-activator 1α (PGC1α) and hydroxyacyl-CoA dehydrogenase/3-ketoacyl-CoA thiolase/enoyl-CoA hydratase (HADHA) expression. Mean data are normalized to GAPDH. Data are mean + SEM from 6 to 11 animals. **(B)** **p = 0.0034 versus sedentary control animals; ##p = 0.0034 between groups as indicated. **(C)** ****p < 0.0001 versus sedentary control animals; ##p = 0.0025; ###p = 0.0001 between groups as indicated (2-way analysis of variance with Tukey test for post hoc analysis). Abbreviation as in Figure 1.

observational studies (63). Thus, most patients taking statins do not experience skeletal muscle problems. In skeletal muscle of statin-treated humans and rats, we showed FKBP12 dissociation from RyR1, which resulted in a ROS/RNS–dependent Ca^{2+} spark-mediated SR Ca^{2+} leak. Such destabilization of RyR1 has been associated with muscle dysfunction in a variety of conditions, including heart failure, aging, and muscular dystrophy (33-35). Accordingly, we observed indexes of pro-apoptotic signaling in statin-treated subjects. Nevertheless, in the rodent model, statin-induced FKBP12 dissociation from RyR1 and Ca^{2+} sparks were not accompanied by any obvious defects in the overall control of $[Ca^{2+}]_i$ at rest or during tetanic stimulation, and force production was not decreased. Unaltered muscle function, despite potentially deleterious changes in cellular Ca^{2+} handling, fits with the clinical picture that although statin treatment increases the risk of myopathy, most patients do not experience statin-associated adverse muscle symptoms. Indeed, analysis of mitochondrial DNA and muscle gene expression profiles in a small group of patients taking simvastatin for 8 weeks revealed evidence of mitochondrial damage, pro-apoptotic signaling, and altered Ca^{2+} flux despite an absence of muscle symptoms (64). Thus, we argue that statin treatment initiates potentially detrimental changes in skeletal muscle as a result of Ca^{2+} dysregulation, but that this does not usually translate into myalgia or more serious muscle derangement.

CARDIAC MUSCLE IS PROTECTED FROM STATIN-INDUCED MYOPATHY. In contrast to skeletal muscle, we observed no increase in spark-mediated SR Ca^{2+} leak in cardiac myocytes from statin-treated rats. Our results showed a central role of increased ROS/RNS in the statin-induced destabilization of SR Ca^{2+} control. This offers a simple explanation for the selectivity of statins for skeletal muscle: cardiac muscle has superior enzymatic (e.g., SOD) and nonenzymatic (e.g., glutathione) ROS/RNS defense systems to fast skeletal muscle (24,25). Furthermore, statin treatment has been shown to enhance the antioxidant defense in cardiac muscle while limiting the defense in skeletal muscle (24). In addition, direct effects of the statin molecule on RyR might also contribute to selective skeletal myopathy. In planar lipid bilayers, simvastatin increases the open probability of RyR1 but not RyR2 (28). Similarly, acute application of simvastatin to permeabilized cells shifts the distribution of Ca^{2+} spark frequency toward higher values in skeletal fibers (which express predominantly RyR1) but lower values in cardiac myocytes (which express RyR2) (28). Thus, a central role for RyR in statin myopathy fully explains the selectivity of this effect for skeletal over cardiac muscle.

MODERATE EXERCISE MAY LIMIT DETERIMENTAL EFFECTS OF STATINS ON SKELETAL MUSCLE. The prevalence of statin-induced myopathy has been reported to increase with physical activity in rodent models (16) and in humans (12,15). RNS/ROS increase during exercise and strenuous skeletal muscle activity can result in severe FKBP12 dissociation from RyR1 and impaired contractile function (65,66), thus providing a mechanism by which exercise could exaggerate the negative effects of statin treatment. In contrast, increased RNS/ROS and altered SR Ca^{2+}

handling play an important role in the adaptation to endurance training (67-70), and a moderate SR Ca^{2+} leak has been linked to increased fatigue resistance (71,72). We showed beneficial effects of voluntary running exercise in muscle of statin-treated rats. Statin treatment no longer reduced FKBP12 binding to RyR1, increased caspase 3 expression, or increased Ca^{2+} spark frequency. Measures of mitochondrial biogenesis (PGC1α and HADHA expression) were enhanced, at least to the same extent, as in muscle of trained control rats. Thus, our results imply that combining moderate voluntary exercise with statin treatment is not detrimental and might limit potentially harmful muscle effects of statins. Of note, most reports of exacerbation of statin myopathy are with intense, prolonged, or enforced exercise regimens (12,15,16). Data from the PRIMO study (73) hinted at the relationship between exercise intensity and the incidence of statin-associated muscle symptoms, and it was recently suggested that reducing the intensity of exercise could mitigate the myopathy risk (18). The opposing intensity-dependent effects of exercise likely reflect a narrow span between limited FKBP12 dissociation from RyR1 accompanied by improved muscle endurance (71,72) and severe FKBP12 dissociation resembling 'overtraining' with marked muscle weakness (65,66).

Unexpectedly, statin-treated rats performed more bouts of activity per day, which translated into longer distances run, compared with control rats. This finding seemingly excluded statin-induced muscle pain or other sensory-related symptoms, because such symptoms were unlikely to result in an increased willingness to perform voluntary exercise. The increased voluntary running of statin-treated rats might relate to their increased muscular NO production, because mice given dietary nitrate supplementation run more than control mice (74).

STUDY LIMITATIONS AND SIGNIFICANCE. A limitation of the present study is that although we identified a potentially harmful effect of statin treatment, we did not provide direct evidence of conditions in which the increased SR Ca^{2+} leak resulted in myopathic symptoms. The likely scenario is that the statin-induced RyR1 destabilization has to be combined with other factor(s) for myopathic symptoms to occur. The concept that individuals might be genetically predisposed to myopathy as a result of altered statin metabolism and/or muscle susceptibility is gaining acceptance (75-77). There is strong support for dysregulation of Ca^{2+} handling contributing to muscle susceptibility. For example, disease-causing mutations or rare variants in *RyR1* have been found in those who experienced statin-associated muscle symptoms (78). Nearly one-fifth of a cohort of subjects who had severe statin myositis had rare variants within genes for RyR1 and the pore-forming subunit of the L-type Ca^{2+} channel (76). Gene expression analysis of muscle from patients with a history of statin myalgia who were re-challenged with statins revealed a number of pathways and networks linked with RyR regulatory proteins, including calmodulin and autocrine motility factor (which plays a role in endoplasmic reticulum (ER)/SR-mitochondrial communication) (79), and regulatory Ca^{2+}-binding proteins (calpain, calcineurin) (75). Accordingly, in a study on patients with statin-induced myositis, most (7 of 9) of the in vitro muscle tests showed halothane- and caffeine-induced contractures suggestive of impaired SR Ca^{2+} control and, in 1 patient, the abnormality was consistent with malignant hyperthermia, a disorder linked to variants in *RYR1* (80). Moreover, lifestyle habits, such as excessive exercise regimens that induce SR Ca^{2+} leak via RyR1 FKBP12 dissociation, might also reveal overt myopathy with statin treatment as discussed above.

We only studied rats treated with statins for 4 weeks, and it is possible that a more prolonged treatment could result in functional abnormalities in muscle. However, because statin myopathy can occur at any time during long-term statin treatment (81) and most people taking statins over many years do not experience overt muscle symptoms, this suggests that this is generally not the case. Thus, it is an additional susceptibility (e.g., genetic or exercise-induced SR Ca2+ leak) that reveals myopathy in a small proportion of the cohort.

CONCLUSIONS

Conditions in which increased SR Ca^{2+} leak can be expected should be considered a risk factor when statins are prescribed. Identifying risk factors underlying statin-induced myopathy is important because recent modeling experiments have indicated that improving statin adherence by 50% (e.g., by preventing statin-induced myopathy) would prevent twice as many deaths as a 5% reduction in the cardiovascular risk threshold for statin prescription (82).

ADDRESS FOR CORRESPONDENCE: Dr. Sarah Calaghan, School of Biomedical Sciences, Garstang Building, University of Leeds, Leeds LS2 9JT, United Kingdom. E-mail: s.c.calaghan@leeds.ac.uk.

PERSPECTIVES

COMPETENCY IN MEDICAL KNOWLEDGE: Up to one-third of patients report statin-associated muscle symptoms in observational studies. The incidence in randomized controlled trials is much less. In part, this difference may arise because those susceptible to myopathy or with indications of myopathy in the run-in phase are excluded from trials. However, the experience of muscle pain is subjective, and many patients are primed to expect this because of patient information leaflets and widespread reporting of side effects of statins in the press. Therefore, an understanding of the mechanism of statin myopathy and factors that make users more susceptible to overt muscle pain and weakness (even potentially fatal rhabdomyolysis) are essential. In this study, we demonstrated leaky RyRs in skeletal muscle following statin treatment. Although this by itself did not cause overt myopathy, it did provide a strong indicator of the populations who are at real risk of myopathy—those whose lifestyle or genotype predispose them to SR Ca^{2+} leak. This includes patients who undertake regular high-intensity exercise or have mutations in the RyR1 associated with malignant hyperthermia. In these individuals, statins should be used cautiously with consideration of dose, alternative cholesterol-lowering strategies, and monitoring of serum creatine kinase levels. However, our data do support the view that moderate exercise should be actively encouraged in those who take statins. As well as the positive effects of exercise on cardiovascular health, this type of activity appears to limit potentially harmful effects of statins on skeletal muscle.

TRANSLATIONAL OUTLOOK: There are several barriers to clinical translation of this work. The first is the sheer scale of the problem, because of the number of people who are (and should be) prescribed statins. Second, we have not yet identified directly the conditions that precipitate overt myopathy, although our data provided a strong indication of what these factors may be. Third, there are currently no cost-effective alternative antilipidemic agents that match the efficacy of statins for those at high risk of myopathy. Statins confer additional therapeutic benefits independent of their ability to lower serum cholesterol (pleiotropic actions), which are not evident with other drugs. For example, the recently licensed PCSK9 inhibitors cost 50 to 100 times more than generic statins and lack the pleiotropic actions effects of statins.

REFERENCES

1. NICE. Cardiovascular disease: risk assessment and reduction, including lipid modification. Available at: https://www.nice.org.uk/guidance/cg181/chapter/1-recommendations 2014. Accessed May 21, 2019.

2. Stone NJ, Robinson JG, Lichtenstein AH, et al. 2013 ACC/AHA guideline on the treatment of blood cholesterol to reduce atherosclerotic cardiovascular risk in adults: a report of the American College of Cardiology/American Heart Association Task Force on Practice Guidelines. J Am Coll Cardiol 2014;63:2889–934.

3. Chowdhury R, Khan H, Heydon E, et al. Adherence to cardiovascular therapy: a meta-analysis of prevalence and clinical consequences. Eur Heart J 2013;34:2940–8.

4. Mefford MT, Tajeu GS, Tanner RM, et al. Willingness to be reinitiated on a statin (from the REasons for Geographic and Racial Differences in Stroke Study). Am J Cardiol 2018;122:768–74.

5. Serban MC, Muntner P, Rosenson RS. Reply: statin intolerance and risk for recurrent myocardial infarction, coronary heart disease events, and all-cause mortality. J Am Coll Cardiol 2017;70:685–6.

6. Zhang H, Plutzky J, Shubina M, Turchin A. Continued statin prescriptions after adverse reactions and patient outcomes: a cohort study. Ann Intern Med 2017;167:221–7.

7. Vrablik M, Zlatohlavek L, Stulc T, Adamkova V, et al. Statin-associated myopathy: from genetic predisposition to clinical management. Physiol Res 2014;63 Suppl 3:S327–34.

8. Pasternak RC, Smith SC Jr., Bairey-Merz CN, Grundy SM, Cleeman JI, Lenfant C. ACC/AHA/NHLBI clinical advisory on the use and safety of statins. Circulation 2002;106:1024–8.

9. Rosenson RS. Current overview of statin-induced myopathy. Am J Med 2004;116:408–16.

10. Rosenson RS, Baker SK, Jacobson TA, Kopecky SL, Parker BA. The National Lipid Association. An assessment by the Statin Muscle Safety Task Force: 2014 update. J Clin Lipidol 2014;8:S58–71.

11. Joy TR, Hegele RA. Narrative review: statin-related myopathy. Ann Intern Med 2009;150:858–68.

12. Thompson PD, Zmuda JM, Domalik LJ, Zimet RJ, Staggers J, Guyton JR. Lovastatin increases exercise-induced skeletal muscle injury. Metabolism 1997;46:1206–10.

13. Sinzinger H, O'Grady J. Professional athletes suffering from familial hypercholesterolaemia rarely tolerate statin treatment because of muscular problems. Br J Clin Pharmacol 2004;57:525–8.

14. Sinzinger H, Schmid P, O'Grady J. Two different types of exercise-induced muscle pain without myopathy and CK-elevation during HMG-Co-enzyme-A-reductase inhibitor treatment. Atherosclerosis 1999;143:459–60.

15. Parker BA, Augeri AL, Capizzi JA, et al. Effect of statins on creatine kinase levels before and after a marathon run. Am J Cardiol 2012;109:282–7.

16. Seachrist JL, Loi CM, Evans MG, Criswell KA, Rothwell CE. Roles of exercise and pharmacokinetics in cerivastatin-induced skeletal muscle toxicity. Toxicol Sci 2005;88:551–61.

17. Parker BA, Thompson PD. Effect of statins on skeletal muscle: exercise, myopathy, and muscle outcomes. Exerc Sport Sci Rev 2012;40:188–94.

18. Deichmann RE, Lavie CJ, Asher T, DiNicolantonio JJ, O'Keefe JH, Thompson PD. The interaction between statins and exercise: mechanisms and strategies to counter the

musculoskeletal side effects of this combination therapy. Ochsner J 2015;15:429–37.

19. Meador BM, Huey KA. Statin-associated myopathy and its exacerbation with exercise. Muscle Nerve 2010;42:469–79.

20. Vincze J, Jenes A, Fuzi M, et al. Effects of fluvastatin and coenzyme Q on skeletal muscle in normo- and hypercholesterolaemic rats. J Muscle Res Cell Motil 2015;36:263–74.

21. Galtier F, Mura T, Raynaud De ME, Chevassus H, et al. Effect of a high dose of simvastatin on muscle mitochondrial metabolism and calcium signaling in healthy volunteers. Toxicol Appl Pharmacol 2012;263:281–6.

22. Sirvent P, Mercier J, Vassort G, Lacampagne A. Simvastatin triggers mitochondria-induced Ca^{2+} signaling alteration in skeletal muscle. Biochem Biophys Res Commun 2005;329:1067–75.

23. Sirvent P, Fabre O, Bordenave S, et al. Muscle mitochondrial metabolism and calcium signaling impairment in patients treated with statins. Toxicol Appl Pharmacol 2012;259:263–8.

24. Bouitbir J, Charles AL, Echaniz-Laguna A, et al. Opposite effects of statins on mitochondria of cardiac and skeletal muscles: a 'mitohormesis' mechanism involving reactive oxygen species and PGC-1. Eur Heart J 2011;33:1397–407.

25. Bouitbir J, Singh F, Charles AL, et al. Statins trigger mitochondrial reactive oxygen species-induced apoptosis in glycolytic skeletal muscle. Antioxid Redox Signal 2016;24:84–98.

26. Brillantes AB, Ondrias K, Scott A, et al. Stabilization of calcium release channel (ryanodine receptor) function by FK506-binding protein. Cell 1994;77:513–23.

27. Pickering JD, White E, Duke AM, Steele DS. DHPR activation underlies SR Ca2+ release induced by osmotic stress in isolated rat skeletal muscle fibers. J Gen Physiol 2009;133:511–24.

28. Venturi E, Lindsay C, Lotteau S, et al. Simvastatin activates single skeletal RyR1 channels but exerts more complex regulation of the cardiac RyR2 isoform. Br J Pharmacol 2018;175:938–52.

29. Calaghan SC, White E, Colyer J. Co-ordinated changes in cAMP, phosphorylated phospholamban, Ca^{2+} and contraction following β-adrenergic stimulation of rat heart. Pflugers Arch 1998;436:948–56.

30. Cheng AJ, Westerblad H. Mechanical isolation, and measurement of force and myoplasmic free $[Ca^{2+}]$ in fully intact single skeletal muscle fibers. Nat Protoc 2017;12:1763–76.

31. Yamada T, Fedotovskaya O, Cheng AJ, et al. Nitrosative modifications of the Ca^{2+} release complex and actin underlie arthritis-induced muscle weakness. Ann Rheum Dis 2014;74:1907–14.

32. Egginton S. In vivo models of muscle angiogenesis. Methods Mol Biol 2016;1430:355–73.

33. Bellinger AM, Reiken S, Carlson C, et al. Hypernitrosylated ryanodine receptor calcium release channels are leaky in dystrophic muscle. Nat Med 2009;15:325–30.

34. Andersson DC, Betzenhauser MJ, Reiken S, et al. Ryanodine receptor oxidation causes intracellular calcium leak and muscle weakness in aging. Cell Metab 2011;14:196–207.

35. Reiken S, Lacampagne A, Zhou H, et al. PKA phosphorylation activates the calcium release channel (ryanodine receptor) in skeletal muscle: defective regulation in heart failure. J Cell Biol 2003;160:919–28.

36. Durham WJ, Racena-Parks P, et al. RyR1 S-nitrosylation underlies environmental heat stroke and sudden death in Y522S RyR1 knockin mice. Cell 2008;133:53–65.

37. Lamb GD, Stephenson DG. Effects of intracellular pH and $[Mg^{2+}]$ on excitation-contraction coupling in skeletal muscle fibres of the rat. J Physiol 1994;478 Pt 2:331–9.

38. Shirokova N, Shirokov R, Rossi D, et al. Spatially segregated control of Ca^{2+} release in developing skeletal muscle of mice. J Physiol 1999;521:483–95.

39. Conklin MW, Barone V, Sorrentino V, Coronado R. Contribution of ryanodine receptor type 3 to Ca^{2+} sparks in embryonic mouse skeletal muscle. Biophys J 1999;77:1394–403.

40. Li N, Wehrens XH. Extinguishing intracellular calcium leak: a promising antiarrhythmic approach. Heart Rhythm 2013;10:108–9.

41. Pugh SD, Macdougall DA, Agarwal SR, Harvey RD, Porter KE, Calaghan S. Caveolin contributes to the modulation of basal and β-adrenoceptor stimulated function of the adult rat ventricular myocyte by simvastatin: a novel pleiotropic effect. PLoS One 2014;9:e106905.

42. Tousoulis D, Charakida M, Stefanadi E, Siasos G, Latsios G, Stefanadis C. Statins in heart failure. Beyond the lipid lowering effect. Int J Cardiol 2007;115:144–50.

43. Xu L, Eu JP, Meissner G, Stamler JS. Activation of the cardiac calcium release channel (ryanodine receptor) by poly-S-nitrosylation. Science 1998;279:234–7.

44. Kanski J, Hong SJ, Schoneich C. Proteomic analysis of protein nitration in aging skeletal muscle and identification of nitrotyrosine-containing sequences in vivo by nanoelectrospray ionization tandem mass spectrometry. J Biol Chem 2005;280:24261–6.

45. Luczak ED, Anderson ME. CaMKII oxidative activation and the pathogenesis of cardiac disease. J Mol Cell Cardiol 2014;73:112–6.

46. Hidalgo C, Aracena P, Sanchez G, Donoso P. Redox regulation of calcium release in skeletal and cardiac muscle. Biol Res 2002;35:183–93.

47. Bist A, Fielding PE, Fielding CJ. Two sterol regulatory element-like sequences mediate up-regulation of caveolin gene transcription in response to low-density lipoprotein free cholesterol. Proc Natl Acad Sci U S A 1997;94:10693–8.

48. Xia Y, Tsai AL, Berka V, Zweier JL. Superoxide generation from endothelial nitric-oxide synthase. A Ca^{2+}/calmodulin-dependent and tetrahydrobiopterin regulatory process. J Biol Chem 1998;273:25804–8.

49. Rossi AE, Boncompagni S, Wei L, Protasi F, Dirksen RT. Differential impact of mitochondrial positioning on mitochondrial Ca^{2+} uptake and Ca^{2+} spark suppression in skeletal muscle. Am J Physiol Cell Physiol 2011;301:C1128–39.

50. Brookes PS, Yoon Y, Robotham JL, Anders MW, Sheu SS. Calcium, ATP, and ROS: a mitochondrial love-hate triangle. Am J Physiol Cell Physiol 2004;287:C817–33.

51. Rossi AE, Boncompagni S, Dirksen RT. Sarcoplasmic reticulum-mitochondrial symbiosis: bidirectional signaling in skeletal muscle. Exerc Sport Sci Rev 2009;37:29–35.

52. Matlib MA, Zhou Z, Knight S, et al. Oxygen-bridged dinuclear ruthenium amine complex specifically inhibits Ca^{2+} uptake into mitochondria in vitro and in situ in single cardiac myocytes. J Biol Chem 1998;273:10223–31.

53. Murphy RM. Calpains, skeletal muscle function and exercise. Clin Exp Pharmacol Physiol 2010;37:385–91.

54. Rios E. The cell boundary theorem: a simple law of the control of cytosolic calcium concentration. J Physiol Sci 2010;60:81–4.

55. Posterino GS, Lamb GD. Effect of sarcoplasmic reticulum Ca^{2+} content on action potential-induced Ca^{2+} release in rat skeletal muscle fibres. J Physiol 2003;551:219–37.

56. Launikonis BS, Murphy RM, Edwards JN. Toward the roles of store-operated Ca^{2+} entry in skeletal muscle. Pflugers Arch 2010;460:813–23.

57. Mikus CR, Boyle LJ, Borengasser SJ, et al. Simvastatin impairs exercise training adaptations. J Am Coll Cardiol 2013;62:709–14.

58. Chung HR, Vakil M, Munroe M, et al. The impact of exercise on statin-associated skeletal muscle myopathy. PLoS One 2016;11:e0168065.

59. Jornayvaz FR, Shulman GI. Regulation of mitochondrial biogenesis. Essays Biochem 2010;47:69–84.

60. Hood DA, Uguccioni G, Vainshtein A, D'souza D. Mechanisms of exercise-induced mitochondrial biogenesis in skeletal muscle: implications for health and disease. Compr Physiol 2011;1:1119–34.

61. Lin J, Handschin C, Spiegelman BM. Metabolic control through the PGC-1 family of transcription coactivators. Cell Metab 2005;1:361–70.

62. Goodman CA, Pol D, Zacharewicz E, Lee-Young RS, Snow RJ, Russell AP, McConell GK. Statin-induced increases in atrophy gene expression occur independently of changes in PGC1α protein and mitochondrial content. PLoS One 2015;10:e0128398.

63. Stroes ES, Thompson PD, Corsini A, et al. Statin-associated muscle symptoms: impact on statin therapy-European Atherosclerosis Society Consensus Panel Statement on Assessment, Aetiology and Management. Eur Heart J 2015;36:1012–22.

64. Laaksonen R, Katajamaa M, Paiva H, et al. A systems biology strategy reveals biological pathways and plasma biomarker candidates for potentially toxic statin-induced changes in muscle. PLoS One 2006;1:e97.

65. Bellinger AM, Reiken S, Dura M, et al. Remodeling of ryanodine receptor complex causes "leaky" channels: a molecular mechanism for

decreased exercise capacity. Proc Natl Acad Sci U S A 2008;105:2198–202.

66. Aydin J, Shabalina IG, Place N, et al. Non-shivering thermogenesis protects against defective calcium handling in muscle. FASEB J 2008;22:3919–24.

67. Hoppeler H. Molecular networks in skeletal muscle plasticity. J Exp Biol 2016;219:205–13.

68. Powers SK, Talbert EE, Adhihetty PJ. Reactive oxygen and nitrogen species as intracellular signals in skeletal muscle. J Physiol 2011;589:2129–38.

69. Camera DM, Smiles WJ, Hawley JA. Exercise-induced skeletal muscle signaling pathways and human athletic performance. Free Radic Biol Med 2016;98:131–43.

70. Ferraro E, Giammarioli AM, Chiandotto S, Spoletini I, Rosano G. Exercise-induced skeletal muscle remodeling and metabolic adaptation: redox signaling and role of autophagy. Antioxid Redox Signal 2014;21:154–76.

71. Bruton JD, Aydin J, Yamada T, et al. Increased fatigue resistance linked to Ca^{2+}-stimulated mitochondrial biogenesis in muscle fibres of cold-acclimated mice. J Physiol 2010;588:4275–88.

72. Ivarsson N, Mattsson CM, Cheng AJ, et al. SR Ca^{2+} leak in skeletal muscle fibers acts as an intracellular signal to increase fatigue resistance. J Gen Physiol 2019;151:567–77.

73. Bruckert E, Hayem G, Dejager S, Yau C, Begaud B. Mild to moderate muscular symptoms with high-dosage statin therapy in hyperlipidemic patients–the PRIMO study. Cardiovasc Drugs Ther 2005;19:403–14.

74. Ivarsson N, Schiffer TA, Hernandez A, et al. Dietary nitrate markedly improves voluntary running in mice. Physiol Behav 2017;168:55–61.

75. Elam MB, Majumdar G, Mozhui K, et al. Patients experiencing statin-induced myalgia exhibit a unique program of skeletal muscle gene expression following statin re-challenge. PLoS One 2017;12:e0181308.

76. Isackson PJ, Wang J, Zia M, et al. RYR1 and CACNA1S genetic variants identified with statin-associated muscle symptoms. Pharmacogenomics 2018;19:1235–49.

77. Brunham LR, Baker S, Mammen A, Mancini GBJ, Rosenson RS. Role of genetics in the prediction of statin-associated muscle symptoms and optimization of statin use and adherence. Cardiovasc Res 2018;114:1073–81.

78. Vladutiu GD, Isackson PJ, Kaufman K, et al. Genetic risk for malignant hyperthermia in non-anesthesia-induced myopathies. Mol Genet Metab 2011;104:167–73.

79. Csordas G, Hajnoczky G. SR/ER-mitochondrial local communication: calcium and ROS. Biochim Biophys Acta 2009;1787:1352–62.

80. Guis S, Figarella-Branger D, Mattei JP, et al. In vivo and in vitro characterization of skeletal muscle metabolism in patients with statin-induced adverse effects. Arthritis Rheum 2006;55:551–7.

81. Hansen KE, Hildebrand JP, Ferguson EE, Stein JH. Outcomes in 45 patients with statin-associated myopathy. Arch Intern Med 2005;165:2671–6.

82. Shroufi A, Powles JW. Adherence and chemoprevention in major cardiovascular disease: a simulation study of the benefits of additional use of statins. J Epidemiol Community Health 2010;64:109–13.

KEY WORDS calcium leak, exercise, myopathy, ryanodine receptor, statin

APPENDIX For an expanded Methods section and supplemental table and figure, please see the online version of this paper.

JACC: BASIC TO TRANSLATIONAL SCIENCE VOL. 4, NO. 4, 2019

EDITORIAL COMMENT

A Novel Mechanism to Explain Statin-Associated Skeletal Muscle Symptoms*

Paul D. Thompson, MD,[a] Beth Taylor, PhD[a,b]

The first commercially available statin, lovastatin, was approved by the US Food and Drug Administration in 1987. The first cases of lovastatin-associated rhabdomyolysis were reported in cardiac transplant patients in 1988 (1,2). Reports of increased creatine kinase (CK) levels associated with exercise were reported in 1990 (3). Thus, one would think that by 2019 we would definitively know what physiological mechanisms cause statin-associated muscle symptoms (SAMS), how exercise affects SAMS and vice versa, and why statins affect skeletal, but not cardiac, muscle. But we do not. There is not even consensus that statins cause SAMS in the absence of overt muscle damage as evidenced by increased CK levels (4,5).

In this issue of *JACC: Basic to Translational Science*, Lotteau et al. (6) present a series of elegant studies examining the mechanisms producing SAMS, an explanation of why skeletal and not cardiac muscles are affected, and new evidence on the interaction of exercise and statin treatment. A full description of the protocols used to develop and support this hypothesis is beyond the scope of this editorial but we present here the salient points.

SEE PAGE 509

It is well known that statins inhibit the rate-limiting enzyme in the mevalonate-cholesterol pathway, but inhibition of this pathway has other effects such as reducing the production of various isoprenoids. Some of these isoprenoids increase nitric oxide synthase activity, thereby increasing nitric oxide production. Reducing nitric oxide by inhibiting the mevalonate-cholesterol pathway can increase both reactive nitrogen species (RNS) and reactive oxygen species (ROS), and atorvastatin is known to increase the generation of ROS (7). RNS and ROS can cause the ryanodine receptor 1 (RyR1) to dissociate from its stabilizing protein, FKB12 (FK506 binding protein [calstabin]). RyR1 releases calcium (Ca^{2+}) from the sarcoplasmic reticulum into the cytosol, thus initiating muscle contraction. Dissociating FKPB12 from RyR1 increases Ca^{2+} leakage from the sarcoplasmic reticulum, producing spontaneous Ca^{2+} release events called Ca^{2+} sparks. Ca^{2+} sparks are observed in other human muscle diseases, including muscular dystrophy and malignant hyperthermia. Bidirectional Ca^{2+} fluxes occur between the sarcoplasmic reticulum and mitochondria and thus increased cytosolic Ca^{2+} increases mitochondrial Ca^{2+}, which increases mitochondrial ROS production. Consequently, Lotteau et al. (6) propose that this dissociation of RyR1 from FKPB12 causes SAMS by initiating a cascade of deleterious effects related to increased cytosolic and mitochondrial Ca^{2+}. Stains can initiate the process in skeletal but not cardiac muscle because cardiac muscle has better antioxidant

*Editorials published in *JACC: Basic to Translational Science* reflect the views of the authors and do not necessarily represent the views of *JACC: Basic to Translational Science* or the American College of Cardiology.

From the [a]Division of Cardiology, Hartford Hospital, Hartford, Connecticut; and the [b]Department of Kinesiology, University of Connecticut, Hartford, Connecticut. Dr. Thompson serves as a consultant to Amgen, Regeneron, Sanofi, and Esperion; has received grants from Sanofi, Regeneron, Esperion, Amarin, and Amgen; payment for lectures from Amarin, Regeneron, Sanofi, Amgen, Kowa, and Boehringer Ingelheim; and owns stock in AbbVie, Abbott Laboratories, CVS, General Electric, Johnson & Johnson, Medtronic, Sarenta, Boston Scientific, and MyoKardia. Dr. Taylor has received financial support from Regeneron and Amgen for research and consulting.

The authors attest they are in compliance with human studies committees and animal welfare regulations of the authors' institutions and Food and Drug Administration guidelines, including patient consent where appropriate. For more information, visit the *JACC: Basic to Translational Science* author instructions page.

ISSN 2452-302X https://doi.org/10.1016/j.jacbts.2019.07.001

protection against RNS and ROS activity and because RyR2 is the dominant cardiac RyR and may be less susceptible to dissociation from FKBP12.

What evidence do Lotteau et al. (6) provide to support this hypothetical chain of events? They show that Ca^{2+} sparks in muscle fibers from statin-treated rats are more frequent, last longer, and are of greater amplitude, indicating a greater Ca^{2+} leak. They note that sparking has not been observed previously with in vivo statin treatment but also note that previous statin studies used permeabilized muscle fibers, a process requiring magnesium, which could inhibit RyR1 function. Indeed, the present investigators did not observe Ca^{2+} sparking when they repeated their studies using permeabilized, instead of intact, muscle fibers. They also did not observe any Ca^{2+} sparks in cardiac muscle from statin-treated animals.

They further showed that statin treatment decreases FKBP12 binding to RyR1 in both biopsy-obtained, human vastus lateralis and rat type II muscle fibers (6). Type II muscle fibers are mitochondrial poor and primarily glycolytic, and some (8), but not all (9), rodent research suggests that this fiber type is most vulnerable to statin muscle injury. There was robust dissociation of FKBP12 from RyR1 in the 13 statin-treated patients compared with control subjects matched with their number, age, and sex, which is noteworthy given the variability in the statin-treated subjects' ages (range 48 to 71 years). Dissociation of FKBP12 from RyR1 not only increases spontaneous Ca^{2+} leaking but also promotes protein degradation and programmed cell death. Evidence for programmed cell death was provided by increases in the proapoptotic enzyme caspase-3, as well as a marked increase in terminal deoxynucleotidyl transferase dUTP nick end labeling (TUNEL) nuclei, in skeletal muscle from both humans and rats treated with statins. Evidence that nitric oxide and superoxide production play a role in this process was provided by the observation that administration of a nitric oxide synthase inhibitor, N(ω)-nitro-L-arginine methyl ester (L-NAME), eliminated the differences in Ca^{2+} spark frequency and duration between the rat control and statin-treated muscle fibers. Differences in Ca^{2+} spark frequency and duration between statin-treated and control rat muscle fibers were also eliminated when the statin-treated fibers were treated with the superoxide dismutase/peroxynitrite scavenger Mn(III)tetrakis(1-methyl-4-pyridyl)porphyrin (MnTMPyP) and the mitochondrial-targeted superoxide dismutase mimetic (2-(2,2,6,6-tetramethylpiperidin-1-oxyl-4-ylamino)-2-oxoethyl)triphenylphosphonium chloride (mitoTEMPO). A role for increased cytosolic Ca^{2+} leading to increased mitochondrial Ca^{2+} was shown by the observation that Ca^{2+} spark frequency and duration were no longer different between muscle fibers from statin-treated and untreated rats when Ca^{2+} mitochondrial entry was inhibited by Ru360, an inhibitor of the mitochondrial Ca^{2+} uniporter. Consequently, this series of experiments provides strong support for the authors' proposed mechanism for SAMS.

Physical activity and exercise are generally believed to increase SAMS (10). We have documented increased CK levels after 45 min of downhill treadmill walking in a double-blind study of men randomly assigned to receive lovastatin 40 mg daily or placebo (11). We have also documented increased CK levels in runners taking statins completing the Boston Marathon versus nonstatin-treated control subjects (12). Both studies show that statins increase the muscle injury from exercise. Statins also seem to affect exercise-related mitochondrial adaptations to exercise training. Maximal oxygen uptake increased only 1.5% after 12 weeks of aerobic exercise training in subjects treated with simvastatin 40 mg daily but increased 10% in exercise-trained subjects not taking statins (13). Citrate synthase activity, a marker of muscle mitochondrial content, increased only 4.5% in the statin-treated subjects but 13% in the subjects not taking statins. A comparison of exercise performance and mitochondrial function in symptomatic ($n = 10$) and asymptomatic ($n = 10$) statin-treated subjects and untreated control subjects ($n = 10$) showed comparable exercise performance among the groups but a lower onset of exercise lactate accumulation, a crude measure of mitochondrial function, in both statin-treated groups (14). Muscle fatigue was measured by the rate of maximal force rise during electrical stimulation of the quadriceps muscle. Muscle contractile function was similar among groups after a single stimulus, but with repetitive stimuli, maximal force rise declined more rapidly in both statin-treated groups, consistent with a more rapid onset of muscle fatigue. Mitochondrial complexes II and IV were also reduced in the symptomatic statin-treated subjects compared with control subjects. Such results support the possibility that statins negatively affect exercise performance; documentation of this hypothesis is limited in part, however, because of the weak design of many exercise training studies (15).

In contrast to a possible negative effect of statins on exercise performance, Lotteau et al. (6) suggest a potential beneficial interaction between statins and exercise. These authors found no effect of statins on single-muscle fiber tetanic force production, and even a small increase in the statin-treated rats.

JACC: BASIC TO TRANSLATIONAL SCIENCE VOL. 4, NO. 4, 2019
AUGUST 2019:524–6

Surprisingly, statin-treated rats with access to a running wheel ran farther than the control rats. Wheel running also prevented the statin-mediated dissociation of FKBP12 to RyR1, which reduced Ca2+ sparks and proapoptotic signaling. Rather than a deleterious interaction of statins and exercise, these results suggest 2 beneficial effects: statin-treated rats exercised more, and exercise reduced statin-associated deleterious muscle effects.

Neither concept would be an easy sell to clinicians who prescribe, or patients who use, statins. Statins are life-saving medications, but many patients who would benefit from statin treatment discontinue statin therapy because of real or perceived SAMS. Lotteau et al. (6) present an elegant series of studies suggesting how statins could affect skeletal muscle. Much more work is required to better define the relation of statins, muscle, and exercise performance, and how insights into the mediating mechanisms for SAMS can be used in clinical practice.

ADDRESS FOR CORRESPONDENCE: Dr. Paul D. Thompson, Cardiology, Hartford Hospital, 80 Seymour Street, Hartford, Connecticut 06102. E-mail: paul.thompson@hhchealth.org.

REFERENCES

1. East C, Alivizatos PA, Grundy SM, Jones PH, Farmer JA. Rhabdomyolysis in patients receiving lovastatin after cardiac transplantation. N Engl J Med 1988;318:47–8.

2. Norman DJ, Illingworth DR, Munson J, Hosenpud J. Myolysis and acute renal failure in a heart-transplant recipient receiving lovastatin. N Engl J Med 1988;318:46–7.

3. Thompson PD, Nugent AM, Herbert PN. Increases in creatine kinase after exercise in patients treated with HMG Co-A reductase inhibitors. JAMA 1990;264:2992.

4. Thompson PD, Taylor B. Safety and efficacy of statins. Lancet 2017;389:1098–9.

5. Collins R, Reith C, Emberson J, et al. Interpretation of the evidence for the efficacy and safety of statin therapy. Lancet 2016;388:2532–61.

6. Lotteau S, Ivarsson N, Yang Z, et al. A mechanism for statin-Induced susceptibility to myopathy. J Am Coll Cardiol Basic Trans Science 2019;4:509–23.

7. Bouitbir J, Singh F, Charles AL, et al. Statins trigger mitochondrial reactive oxygen species-induced apoptosis in glycolytic skeletal muscle. Antioxid Redox Signal 2016;24:84–98.

8. Westwood FR, Bigley A, Randall K, Marsden AM, Scott RC. Statin-induced muscle necrosis in the rat: distribution, development, and fibre selectivity. Toxicol Pathol 2005;33:246–57.

9. Obayashi H, Nezu Y, Yokota H, et al. Cerivastatin induces type-I fiber-, not type-II fiber-, predominant muscular toxicity in the young male F344 rats. J Toxicol Sci 2011;36:445–52.

10. Bruckert E, Hayem G, Dejager S, Yau C, Begaud B. Mild to moderate muscular symptoms with high-dosage statin therapy in hyperlipidemic patients—the PRIMO study. Cardiovasc Drugs Ther 2005;19:403–14.

11. Thompson PD, Gadaleta PA, Yurgalevitch S, Cullinane E, Herbert PN. Effects of exercise and lovastatin on serum creatine kinase activity. Metabolism 1991;40:1333–6.

12. Parker BA, Augeri AL, Capizzi JA, et al. Effect of statins on creatine kinase levels before and after a marathon run. Am J Cardiol 2012;109:282–7.

13. Mikus CR, Boyle LJ, Borengasser SJ, et al. Simvastatin impairs exercise training adaptations. J Am Coll Cardiol 2013;62:709–14.

14. Allard NAE, Schirris TJJ, Verheggen RJ, et al. Statins affect skeletal muscle performance: evidence for disturbances in energy metabolism. J Clin Endocrinol Metab 2018;103:75–84.

15. Noyes AM, Thompson PD. The effects of statins on exercise and physical activity. J Clin Lipidol 2017;11:1134–44.

KEY WORDS exercise, skeletal muscle, statin, statin myopathy, statin side effects

JACC: BASIC TO TRANSLATIONAL SCIENCE VOL. 4, NO. 4, 2019

PRECLINICAL RESEARCH

Adaptive Reductions in Left Ventricular Diastolic Compliance Protect the Heart From Stretch-Induced Stunning

Brian R. Weil, PhD,[a,b] George Techiryan, BS,[b,c] Gen Suzuki, MD, PhD,[b,c] Filip Konecny, DVM, PhD,[d] John M. Canty, Jr, MD[a,b,c,e,f]

VISUAL ABSTRACT

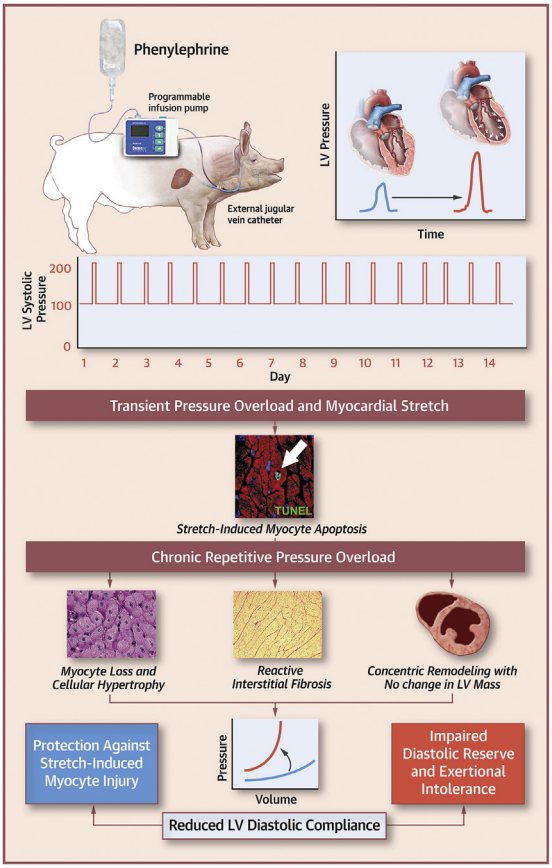

Weil, B.R. et al. J Am Coll Cardiol Basic Trans Science. 2019;4(4):527–41.

HIGHLIGHTS

- **A transient elevation in preload produces mechanical stretch-induced myocyte injury and measurable cardiac troponin I release that is associated with reversible contractile dysfunction and myocyte apoptosis.**
- **Using a porcine model of intermittent pressure overload, this study demonstrates that repetitive exposure to cyclical elevations in preload elicits significant myocyte loss, yet left ventricular systolic function is preserved and chamber dilatation is absent.**
- **Instead, myocardial remodeling characterized by myocyte hypertrophy and interstitial fibrosis produces a reduction in left ventricular diastolic compliance that protects the heart from subsequent stretch-induced myocyte injury.**
- **These results support a novel paradigm that links cardiac adaptations to repetitive stretch-induced injury with the pathogenesis of myocardial stiffening and may explain how reductions in left ventricular diastolic compliance can occur in the absence of sustained hypertension or anatomic hypertrophy.**

From the [a]Department of Physiology and Biophysics, University at Buffalo, Buffalo, New York; [b]The Clinical and Translational Research Center, University at Buffalo, Buffalo, New York; [c]Department of Medicine, University at Buffalo, Buffalo, New York; [d]Department of Surgery, McMaster University, Hamilton, Ontario, Canada; [e]VA WNY Health Care System, Buffalo, New York; and the [f]Department of Biomedical Engineering, University at Buffalo, Buffalo, New York. This study was supported by the National Heart Lung and Blood Institute (HL-055324, HL-061610, and F32HL-114335), the American Heart Association (17SDG33660200), the National Center for Advancing Translational Sciences (UL1TR001412), the Department of Veterans Affairs (1IO1BX002659), the

ISSN 2452-302X https://doi.org/10.1016/j.jacbts.2019.04.002

JACC: BASIC TO TRANSLATIONAL SCIENCE VOL. 4, NO. 4, 2019
AUGUST 2019:527–41

ABBREVIATIONS AND ACRONYMS

BP = blood pressure

cTnI = cardiac troponin I

EDPVR = end-diastolic pressure–volume relationship

ΔEDP/ΔEDV = changes in end-diastolic pressure/end-diastolic volume

HFpEF = heart failure with preserved ejection fraction

LV = left ventricular

LVEDP = left ventricular end-diastolic pressure

LVEDV = left ventricular end-diastolic volume

RPO = repetitive pressure overload

PE = phenylephrine

PV = pressure–volume

TUNEL = terminal deoxynucleotidyl transferase-mediated dUTP nick end labeling

SUMMARY

Swine subjected to 2 weeks of repetitive pressure overload (RPO) exhibited significant myocyte loss, but left ventricular (LV) systolic function was preserved, and chamber dilatation did not occur. Instead, myocardial remodeling characterized by myocyte hypertrophy and interstitial fibrosis led to a marked reduction in LV diastolic compliance, which protected the heart from stretch-induced myocyte injury and preserved LV ejection fraction without anatomic LV hypertrophy. These results support a novel paradigm that links cardiac adaptations to RPO with the pathogenesis of reduced LV diastolic compliance and may explain how LV stiffening can occur in the absence of sustained hypertension or anatomic hypertrophy.

Cardiomyocyte loss is a central component of the adverse left ventricular (LV) remodeling that often underlies deterioration of cardiac performance and the development of chronic heart failure (1,2). Although myocyte loss is typically believed to arise as the result of myocardial ischemia, it is increasingly clear that other types of pathophysiological stress can contribute to irreversible myocyte injury (3). Excessive mechanical stretch caused by hemodynamic overload has been implicated as an important mechanism from among the potential nonischemic causes of myocyte death based on clinical data that demonstrated elevated serum cardiac troponin (cTn) concentrations in patients with high filling pressures

SEE PAGE 542

in the setting of heart failure and other fluid overload states (4). In support of this notion, we recently demonstrated that acutely raising arterial blood pressure to transiently elevate LV preload without ischemia in swine elicited reversible systolic dysfunction ("stretch-induced stunning") and measurable transcoronary release of cTnI, which indicates myocyte injury (5). Although this response occurred without pathological evidence of necrosis or infarction, post-mortem histopathological analysis revealed an increased number of cardiomyocytes undergoing apoptosis. This indicated that even in the absence of ischemia, transient pressure overload elicits stretch-induced myocyte injury.

It is therefore possible that long-term repetitive exposure to brief episodes of pressure overload could lead to cumulative myocyte loss that results in LV systolic dysfunction in the absence of infarction. This notion was supported by our laboratory's previous work in swine that involved single and repetitive episodes of "reversible" regional ischemia. In these studies, a single 10-min transient coronary occlusion resulted in stunned myocardium and regionally increased myocyte apoptosis without necrosis in the area at risk of ischemia (6). Although the rate of myocyte apoptosis was low, repeated bouts of demand-induced ischemia distal to a chronic coronary stenosis were shown to lead to chronic myocardial stunning that progressed to hibernating myocardium (7). This progression was accompanied by chronic regional systolic dysfunction, myocyte apoptosis, and substantial regional myocyte loss (8). Thus, it is plausible that repetitive brief episodes of preload elevation, each eliciting stretch-induced injury throughout the entire LV, could lead to cumulative myocyte loss that results in global systolic dysfunction. Clinically, a similar process may occur in older adults who experience repetitive episodes of increased afterload due to aortic stenosis, labile hypertension (9), or age-related aortic stiffening (10) that intermittently impose high levels of mechanical stress on the heart,

New York State Department of Health (NYSTEM CO24351), and the Albert and Elizabeth Rekate Fund in Cardiovascular Medicine. Dr. Canty has been a consultant for Lantheus Medical Imaging, Inc. All other authors have reported that they have no relationships relevant to the contents of this paper to disclose.

All authors attest they are in compliance with human studies committees and animal welfare regulations of the authors' institutions and Food and Drug Administration guidelines, including patient consent where appropriate. For more information, visit the *JACC: Basic to Translational Science* author instructions page.

Manuscript received January 23, 2019; revised manuscript received April 19, 2019, accepted April 20, 2019.

potentially contributing to adverse LV remodeling and heart failure.

Accordingly, we developed a large animal model of repetitive pressure overload (RPO) to test the hypothesis that repeated short-term elevations in hemodynamic load that stretch the myocardium would elicit chronic stretch-induced stunning with significant cardiomyocyte loss and the development of heart failure with reduced ejection fraction. Our results showed that swine subjected to 2 weeks of RPO exhibited rapid and substantial myocyte loss, yet, in contrast to our hypothesis, LV systolic function was preserved and LV dilatation was absent. Instead, myocardial remodeling characterized by myocyte cellular hypertrophy and interstitial fibrosis produced a marked reduction in LV diastolic compliance. This functions as an adaptive mechanism to protect the heart from subsequent stretch-induced stunning and preserves LV ejection fraction in the absence of overt anatomic LV hypertrophy.

METHODS

All procedures and protocols conformed to institutional guidelines for the care and use of animals in research and were approved by the University at Buffalo Institutional Animal Care and Use Committee. Long-term RPO studies were conducted in Yorkshire cross-bred pigs (n = 9; 34 ± 2 kg; 7 males/2 females) that were 3 to 4 months of age (WBB Farm, Alden, New York). Seven additional Yorkshire cross-bred pigs were used as control animals for post-mortem histological measurements (n = 4) and/or admittance catheter-derived LV pressure–volume (PV) relations (n = 5). A flowchart summarizing the sample sizes used for each comparison is included in the Supplemental Figure.

PORCINE MODEL OF RPO. Animals were initially instrumented with an indwelling jugular vein catheter for blood sampling and phenylephrine (PE) infusion. Following sedation with a telazol/xylazine mixture (0.037 ml/kg intramuscularly), anesthesia was maintained by an infusion of propofol (5 to 10 mg/kg/h). After infiltrating the skin and subcutaneous tissues with marcaine (0.5%), a small incision was made, followed by blunt dissection to isolate the jugular vein. A catheter (18-gauge) was advanced into the vessel over a guidewire and secured to the vessel by fixation ligatures with the proximal end connected to polyethylene tubing. This was tunneled subcutaneously and led out through a small incision between the shoulder blades. Animals subsequently underwent multidetector computed tomography (MDCT) and physiological studies as described in the following sections.

PHYSIOLOGICAL STUDY PROTOCOL. Hemodynamics and echocardiographic indexes of LV function were assessed before, during, and 1 h after PE-induced pressure overload in the closed-chest anesthetized state. On return to the laboratory following MDCT imaging, a micromanometer (5-F, SPR-450, AD Instruments, Inc., Colorado Springs, Colorado) was advanced through the introducer and into the LV under fluoroscopic guidance for assessment of LV pressure, whereas arterial blood pressure (BP) was continuously monitored via the side port. LV volumes and wall thickening were assessed with transthoracic echocardiography (GE Vivid 7, Milwaukee, Wisconsin) (5,6). Briefly, the LV was imaged in the short- and long-axes projections from a right parasternal approach. Short-axis images were used to assess regional wall thickening, end-systolic and end-diastolic volumes, and LV ejection fraction using American Society of Echocardiography criteria (11). We subsequently infused PE (2 mg/ml infused at 9 ml/h) for 1 h to transiently raise LV systolic and LV end-diastolic pressure (LVEDP). Hemodynamic parameters were continuously recorded, and echocardiography was performed every 15 min throughout the infusion period and for 1 h after PE was stopped. Hemodynamic measurements at selected time points reported in the results section were obtained from 5-s digital averages before and after echocardiographic data collection that were averaged to obtain each value. During the time period of each reported measurement, there was little change in hemodynamic variables due to the stable nature of the experimental preparation. Following data collection at the 1-h post-PE timepoint, catheters were removed, anesthesia was discontinued, and the animal was returned to the animal housing facility. Blood samples for serum troponin I (5) were collected at baseline, as well as 1 and 24 h after PE infusion.

After completing the initial study, the jugular vein catheter was connected to an external programmable infusion pump (OrchesTA Model 500, Instech Laboratories, Plymouth Meeting, Pennsylvania) housed in a standard laboratory animal jacket. The infusion pump was manually programmed to infuse PE to produce RPO for 2 h daily (2 mg/ml infused at 9 ml/h for 2 h/day) for 2 weeks. Thus, the duration of each daily PE infusion was 2 h in conscious animals during the RPO period, whereas an infusion period of 1 h was used in anesthetized animals during physiological studies before and after RPO. On day 14, animals were re-anesthetized for repeat MDCT imaging and a

final physiological study. Animals were recovered and a repeat blood sample was obtained 24 h later (day 15). A subset of animals were anaesthetized to obtain LV PV relations as previously described (12) and detailed in the following section. After all measurements and blood sampling was completed, animals were deeply anesthetized with isoflurane (5%) and killed via administration of potassium chloride directly into the LV chamber. The heart was rapidly removed and sectioned for post-mortem tissue sampling.

LV DIASTOLIC COMPLIANCE VIA ADMITTANCE CATHETER. LV PV loops were obtained from a subset of animals (n = 5) for assessment of diastolic compliance via placement of an admittance catheter (ADV500, Transonic Scisense, Inc., London, Ontario, Canada) following collection of the 24-h post-PE blood sample after 2 weeks of RPO as previously described (12). These were compared to values in normal swine (n = 4). Recent data from our laboratory that compared admittance catheter-derived ventricular volumes to simultaneously acquired contrast-enhanced, MDCT-derived ventricular volumes demonstrated the accuracy of this approach (13). The LV end-diastolic PV relationship (EDPVR) and end-systolic PV relationship (ESPVR) were measured by collecting PV loops during transient preload reductions induced by rapid inferior vena cava occlusion using a 12-F, 20-mm balloon catheter (Z-Med, B. Braun Interventional Systems, Inc., Bethlehem, Pennsylvania) placed via the femoral vein. In each case, LV pressure and volume at end-systole (for the ESPVR) and end-diastole (for the EDPVR) were identified during each cardiac cycle throughout the transient preload reduction period. Nonlinear regression was applied to characterize the slope (i.e., end-systolic elastance) and volume-axis intercept (V_o) of the ESPVR using a quadratic fit, in which $P_{es} = a \bullet V_{es}^2 + b \bullet V_{es} + c$, with P_{es} representing end-systolic LV pressure, V_{es} representing end-systolic volume, and constants a, b, and c determined by nonlinear least-squares regression (14). For characterization of the EDVPR, an exponential curve fit was applied to calculate the LV diastolic stiffness constant (β) using the equation $P_{es} = Ae^{\beta Ves}$, where P_{es} is end-systolic LV pressure, V_{es} is end-systolic volume, and A and β are empirically determined constants (15). Additional PV loops were obtained during a brief (15 min) infusion of PE to corroborate measurements of changes in end-diastolic pressure/end-diastolic volume (ΔEDP/ΔEDV) during PE made via echocardiographic assessment of LV EDV (n = 3/group). Acquisition and analysis of all LV PV parameters were performed with an IX-228S data acquisition system and PV module data analysis LabScribe2 software (iWorx Systems, Inc., Dover, New Hampshire).

CARDIAC MDCT IMAGING. MDCT imaging was performed before initiating PE infusion at the initial study and 2 weeks after RPO to assess LV remodeling. Under anesthesia (as described previously), the femoral artery and vein were catheterized with introducers (6-F) and the animals were transported to the scanner. Animals were placed in the supine position and scanned on a 64-slice GE Discovery 690 positron-emission tomographic/CT scanner during suspended respiration to minimize movement-related artifact. After scout acquisition to localize the heart, iohexol (Omnipaque, GE Healthcare; 350 mg iodine/ml; 2 ml/kg) was injected via the femoral vein, followed by a 30-ml saline chaser (both infusions at 4 ml/s). First-pass imaging with retrospective electrocardiographic gating was performed to assess LV mass and LV volumes in 8-mm-thick short-axis slices reconstructed at end-diastole (i.e., 95% of the RR interval) and analyzed using ImageJ software (National Institutes of Health, Bethesda, Maryland). The following parameters were used for each scan: gantry rotation time 400 ms, temporal resolution 175 ms, slice thickness 0.625 mm, spatial resolution 0.97 × 0.97 mm (voxel size 0.97 × 0.97 × 0.625 mm), helical pitch variable depending on heart rate (range: 0.20 to 0.26), tube voltage 120 kV, and tube current 600 mA. Upon completion of MDCT imaging, the animals were transported back to the laboratory for physiological studies.

POST-MORTEM MYOCARDIAL HISTOPATHOLOGY. Histopathological data derived from animals subjected to 2 weeks of RPO (n = 8) were compared with values obtained from normal control swine (n = 4; 3 males/1 female) matched for age, sex, and body mass.

Myocyte nuclear density and morphometry. Paraffin-embedded myocardial tissue samples were fixed for morphometry as previously described (16). PAS-stained sections were used to quantify myocyte diameter by counting at least 100 cells from the inner and outer halves of each tissue section. Myocytes were included regardless of size as long as myofilaments could be identified surrounding the nucleus. Myocyte nuclear density was also assessed in periodic acid-Schiff–stained sections as previously described (16).

Interstitial fibrosis. Cardiac fibrosis was assessed via light microscopy of picrosirius red–stained myocardial tissue sections and quantification of collagen volume fraction, as previously described (17).

Myocyte apoptosis. Cardiomyocyte apoptosis was assessed using the In-Situ Cell Death Detection Kit (Roche Diagnostics, Mannheim, Germany) according to manufacturer's guidelines (5,6). Briefly, apoptotic cells were detected by terminal deoxynucleotidyl transferase-mediated dUTP nick-end labeling (TUNEL) and epiflourescence with a fluorescein isothiocyanate filter. Samples were co-stained with an F-Actin antibody conjugated to fluorescent Alexa Fluor 555 dye (Alexa Fluor 555 Phalloidin, Life Technologies, Burlington, Ontario, Canada), and co-localization with TUNEL was used to quantify apoptotic cardiomyocytes. At least 100 microscopic fields (132 ± 5 fields; 200×) were examined per sample, and the number of apoptotic myocytes was expressed as $TUNEL^+$ myocytes per square centimeters. Only $TUNEL^+$ nuclei that could be confirmed to be from myocytes via F-Actin co-staining were included.

Capillary density. Myocardial tissue sections were incubated with anti–von Willebrand factor antibodies with appropriate fluorescent-labeled secondary antibodies to identify coronary capillaries, as previously described (16). Vessels were counted in at least 20 random fields from each tissue sample and expressed per tissue area (millimeters squared).

ASSESSMENT OF SERUM cTnI. Blood samples were allowed to clot at room temperature for 40 min, centrifuged at 1,500*g* for 15 min, aliquoted, and frozen for storage at −80°C. Serum was thawed once, and cTnI quantified in duplicate with a porcine specific cTnI enzyme-linked immunosorbent assay kit for serum (Life Diagnostics) according to manufacturer's instructions. We previously demonstrated that the 99th percentile for normal values of cTnI in swine was 38 ng/l with this assay (5,6).

STATISTICAL ANALYSIS. Data are expressed as mean ± SE. Histopathological, MDCT, and LV PV loop-derived data analysis was performed simultaneously in RPO and control animals in a blinded fashion to ensure scientific rigor. To control for animal growth during the 2-week study period (8 ± 1 kg), LV volumes were expressed relative to body surface area, which was calculated by multiplying body mass (in kilograms) by 0.0734 (18). Differences between time points in physiological studies (e.g., baseline vs. post-PE) were assessed by repeated measures analysis of variance and the post hoc Holm-Sidak test. Although surgical placement of an indwelling jugular vein catheter was successful in all animals, the catheter was displaced in 1 animal 2 days after the initial study. As a result, a total of 8 animals completed the 2-week RPO protocol, and temporal physiological changes between the initial study (n = 9) and after 2 weeks RPO (n = 8) were assessed by unpaired *t*-tests. Unpaired *t*-tests were also used to assess differences in PV loop endpoints and post-mortem histopathology between animals subjected to RPO and normal control animals. Statistical analysis was performed with SPSS Statistics 23 (IBM, Armonk, New York), and the acceptable type 1 error rate was prospectively set at 5%.

TABLE 1 Hemodynamic Response to Intravenous Phenylephrine Before and After 2 Weeks of RPO

	Baseline	60-Min	60-Min Post-PE
Heart rate, beats/min			
Initial	92 ± 7	84 ± 5	90 ± 7
2-week RPO	96 ± 4	87 ± 7	97 ± 8
Mean arterial pressure, mm Hg			
Initial	86 ± 5	167 ± 2*	80 ± 5†
2-week RPO	84 ± 6	176 ± 8*	91 ± 9†
LV peak systolic pressure, mm Hg			
Initial	102 ± 3	192 ± 4*	99 ± 4†
2-week RPO	104 ± 5	210 ± 10*	112 ± 9†
LV end-diastolic pressure, mm Hg			
Initial	11 ± 1	31 ± 2*	12 ± 1†
2-week RPO	12 ± 1	26 ± 1*	12 ± 2†
dP/dt_{max}, mm Hg/s			
Initial	2,243 ± 88	3,290 ± 579	1,605 ± 170*†
2-week RPO	2,465 ± 201	3,632 ± 436*	2,195 ± 278†
dP/dt_{min}, mm Hg/s			
Initial	−2,217 ± 162	−3,802 ± 675	−2,108 ± 233
2-week RPO	−2,016 ± 156	−4,413 ± 282*	−3,023 ± 300*†‡

Values are mean ± SEM. *p < 0.05 vs. baseline. †p < 0.05 vs. 60-min PE. ‡p < 0.05 vs. initial.
LV = left ventricular; PE = phenylephrine; RPO = repetitive pressure overload.

RESULTS

HEMODYNAMICS AND ECHOCARDIOGRAPHY AFTER RPO. Hemodynamics and echocardiography before, during, and 1 h after intravenous PE at the initial study and after 2 weeks of RPO are summarized in Tables 1 and 2. On day 1, PE increased peak LV systolic pressure from 102 ± 3 mm Hg to 192 ± 4 mm Hg (p < 0.0001) with a corresponding rise in LVEDP from 11 ± 1 mm Hg to 31 ± 2 mm Hg (p = 0.0002). These returned to baseline within 30 min after PE infusion (Figure 1). Despite normalization of hemodynamics after LV pressure overload, LVEDV remained elevated (from 20 ± 1 ml/m² to 29 ± 5 ml/m²; p = 0.0565) (Figure 1). As a result, LV ejection fraction declined from 69 ± 3% to 51 ± 7% (p = 0.0217) (Figure 2).

After 2 weeks of RPO, hemodynamics and echocardiographic parameters of LV function were normal at rest (Tables 1 and 2). Although PE infusion at this time point produced a comparable increase in

TABLE 2 Selected Echocardiographic Parameters Before, During, and After Intravenous Phenylephrine at the Initial Study and After 2-Weeks of RPO

	Baseline	60-Min PE	60-Min Post-PE
LV end-diastolic volume, ml/m^2			
Initial	20 ± 1	34 ± 4*	29 ± 5*
2-week RPO	20 ± 1	22 ± 2†	17 ± 1†‡
LV end-systolic volume, ml/m^2			
Initial	6 ± 1	21 ± 6*	16 ± 5*
2-week RPO	6 ± 1	7 ± 1†	5 ± 1†‡
Stroke volume, ml/m^2			
Initial	14 ± 1	13 ± 2	13 ± 1
2-week RPO	14 ± 1	14 ± 1	12 ± 1
LV ejection fraction, %			
Initial	69 ± 3	46 ± 9*	51 ± 7*
2-week RPO	71 ± 2	66 ± 2†	70 ± 2†
Septal wall thickening, mm			
Initial	5.8 ± 0.4	3.8 ± 0.6*	3.6 ± 0.5*
2-week RPO	6.0 ± 0.3	5.2 ± 0.4*	5.7 ± 0.3†
Posterior wall thickening			
Initial	5.9 ± 0.4	4.1 ± 0.8*	3.8 ± 0.4*
2-week RPO	6.7 ± 0.4	6.5 ± 0.4†	5.8 ± 0.2†

Values are mean ± SEM. *p < 0.05 vs. baseline. †p < 0.05 vs. initial. ‡p < 0.05 vs. 60-min PE. Abbreviations as in Table 1.

LV systolic pressure (from 104 ± 5 mm Hg to 210 ± 10 mm Hg; p < 0.0001) and LVEDP (from 12 ± 1 mm Hg to 26 ± 1 mm Hg; p < 0.0001), echocardiographic assessment of LV volumes revealed a markedly different effect on LV function. In contrast to the initial study, there was only a small, insignificant increase in LVEDV during PE infusion after 2 weeks of RPO (from 20 ± 1 ml/m^2 to 22 ± 2 ml/m^2; p = 0.4347). This reflected a substantial reduction in myocardial compliance (Figure 1). The absence of LV distension prevented stretch-induced stunning because the LV ejection fraction remained normal during (66 ± 2%) and after (70 ± 2%) PE infusion (Figure 2, left panel). Representative videos of short-axis echocardiograms that illustrated the LV response to PE at the initial study (Supplemental Videos 1A to 1C) and after 2 weeks of RPO (Supplemental Videos 2A to 2C) are included in the Supplemental Appendix.

SERUM TROPONIN I RELEASE BEFORE AND AFTER RPO. Figure 2 (right panel) summarizes the effects of pressure overload on cTnI release. One hour after the initial episode of pressure overload, the LV distension and reduction in systolic function were accompanied by a significant increase in serum cTnI (from 13 ± 9 ng/l to 186 ± 69 ng/l; p = 0.0075) that persisted 24 h later (260 ± 141 ng/l; p = 0.0419 vs. baseline). There was a positive correlation between the degree of LV distension during PE infusion (LVEDV) and serum cTnI concentrations at 1 h (r = 0.75; p = 0.0199) and 24 h (r = 0.77; p = 0.0152) post-PE infusion, which suggested that the extent of LV dilatation and stretch was a determinant of myocyte injury. After 14 days of RPO, transient pressure overload produced minimal LV distention and no increase in serum cTnI (from 5 ± 5 ng/l to 15 ± 10 ng/l; p = 0.2793) (Figure 2). Consistent with this, the number of apoptotic myocytes identified via post-mortem TUNEL staining was not different between animals subjected to 2 weeks of RPO (0.8 ± 0.5 myocytes/cm^2) and normal control animals (0.7 ± 0.5 myocytes/cm^2; p = 0.9085).

EFFECT OF RPO ON MDCT-DERIVED INDEXES OF LV REMODELING. Serial cardiac MDCT imaging was performed to assess LV mass and geometry before and after 2 weeks of RPO. RPO did not cause significant anatomic hypertrophy because the LV mass/body weight ratio was similar to that of normal control animals (2.3 ± 0.1 g/kg) at the initial study (2.3 ± 0.1 g/kg; p = 0.9324) and after 2 weeks of RPO (2.4 ± 0.1 g/kg; p = 0.3716). However, it did produce mild concentric remodeling, with an increase in the LV mass/LVEDV ratio from 1.13 ± 0.04 in normal animals to 1.32 ± 0.07 g/ml after RPO (p = 0.0231) (Figure 3).

CELLULAR HYPERTROPHY, MYOCYTE LOSS, AND INTERSTITIAL FIBROSIS AFTER RPO. Although anatomic hypertrophy was absent, post-mortem histopathological analysis of LV tissue revealed myocyte cellular hypertrophy (myocyte diameter 16.8 ± 0.4 vs. 13.5 ± 0.1 μm; p < 0.0001) in animals subjected to RPO compared with normal control animals (Figure 3). The increase in myocyte size in the face of comparable LV mass reflected substantial global myocyte loss arising from RPO. After only 2 weeks of RPO, myocyte nuclear density declined by nearly 20%, from 1,455 ± 23 nuclei/mm^2 in normal control animals to 1,184 ± 29 nuclei/mm^2 after RPO (p = 0.0001). This was accompanied by a marked increase in interstitial fibrosis (12.9 ± 1.8% area vs. 6.5 ± 1.5% area; p = 0.0431) (Figure 4). Immunostaining also demonstrated capillary rarefaction with reductions in capillary density in animals subjected to RPO (1,542 ± 26 capillaries/mm^2 vs. 1,745 ± 79 capillaries/mm^2 in normal control animals; p = 0.0301). Collectively, these data demonstrated that 2 weeks of RPO led to myocardial remodeling characterized by substantial myocyte loss, myocyte cellular hypertrophy, increased interstitial connective tissue, and capillary rarefaction.

REDUCED MYOCARDIAL COMPLIANCE AFTER RPO. The small changes in LVEDV, despite a large increase in LVEDP during PE infusion at the 2-week study, indicated that RPO elicited a significant reduction in

FIGURE 1 RPO Elicits a Reduction in LV Compliance That Prevents Chamber Distension During an Acute Elevation in Afterload

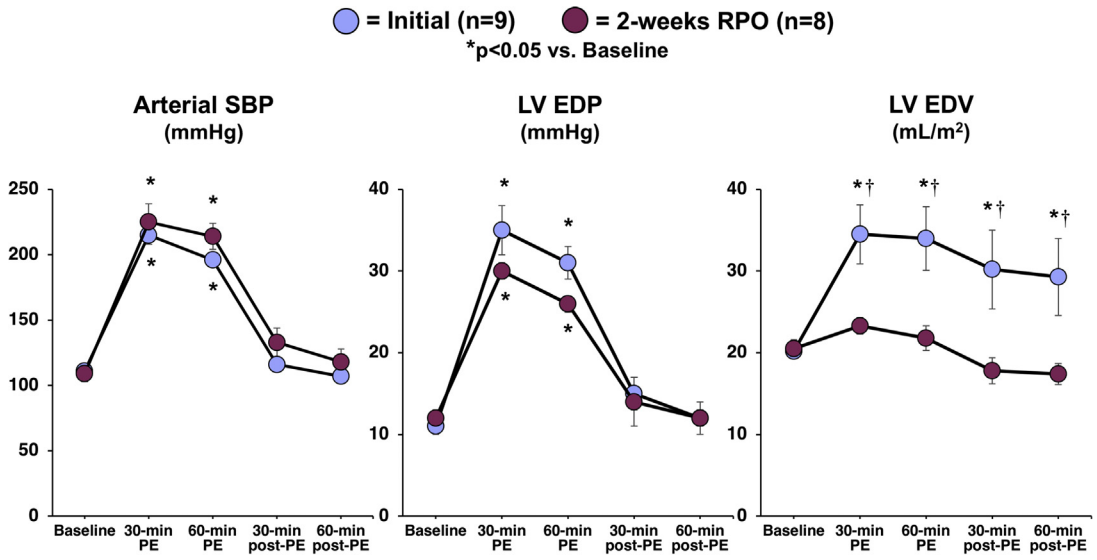

A 60-min intravenous infusion of phenylephrine (PE) elicited a similar increase in arterial systolic blood pressure (SBP) and left ventricular end-diastolic pressure (LVEDP) at the initial study **(blue)** and after 2 weeks of repetitive pressure overload (RPO) **(purple)**. At the initial study, this was associated with an increase in left ventricular end-diastolic volume (LVEDV) that persisted after cessation of PE despite normalization of SBP and LVEDP. However, transient PE infusion no longer produced a significant increase in LVEDV when the study was repeated after 2 weeks of RPO, which was indicative of reduced LV compliance after RPO. Values are mean ± SEM. *$p < 0.05$ versus baseline; †$p < 0.05$ versus initial.

LV compliance. This was further evaluated before and after PE infusion using admittance catheter-derived PV loops (Figure 5A) and 2-point diastolic PV curves to quantify the change in diastolic compliance (i.e., ΔEDV/ΔEDP ratio during PE infusion) (Figure 5B). This analysis revealed an approximate 65% reduction in the ΔEDV/ΔEDP ratio (from 1.7 ± 0.2 to 0.6 ± 0.2 ml/mm Hg; $p = 0.0025$), which demonstrated a marked reduction in LV diastolic compliance after RPO. We also assessed admittance catheter-derived LV PV loops during changes in preload elicited by rapid inferior vena cava occlusion in animals subjected to RPO ($n = 5$). These also revealed reduced diastolic compliance after RPO as assessed using the EDPVR (Figure 6A). Compared with normal control animals ($n = 5$), RPO animals exhibited a higher LV stiffness constant (β: 0.053 ± 0.005 vs. 0.035 ± 0.005; $p = 0.0258$), which reflected an upward and leftward shift of the EDPVR (Figure 6B). This was accompanied by a significant increase in the slope of the ESPVR (from 7.1 ± 0.5 mm Hg/ml to 10.7 ± 1.3 mm Hg/ml; $p = 0.0349$) without a significant change in the volume axis intercept (from 10.5 ± 3.6 ml to 18.1 ± 4.6 ml; $p = 0.2545$), which indicated an increase in end-systolic elastance after RPO.

DISCUSSION

The results of the present study offered novel insight regarding changes in LV diastolic compliance and the myocardial adaptations to intermittent hemodynamic overload. First, we reproduced our recent finding (5) that an acute elevation in LV preload elicited by a transient increase in arterial BP produced LV distension, reversible stretch-induced myocardial stunning, and a significant rise in circulating cTnI concentrations, which are indicative of myocyte injury in the normal heart. When the heart was exposed to long-term transient elevations in preload via RPO, a reduction in LV compliance developed. This was accompanied by an increase in interstitial connective tissue that ultimately prevented chronic stretch-induced stunning and myocyte injury. Although this adaptive decrease in compliance did not affect LV filling pressures at rest, it was associated with an upward and leftward shift of the EDPVR that resulted

FIGURE 2 Cardiac Adaptations to RPO Prevent Acute Stretch-Induced Stunning and Myocyte Injury During a Transient Elevation in Afterload

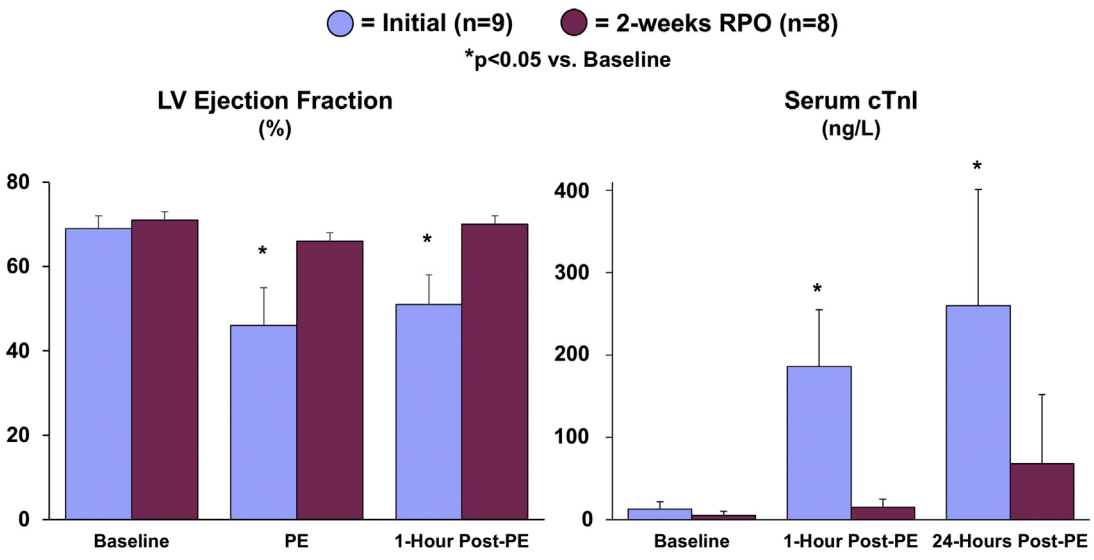

The attenuation of LV distension during PE infusion after RPO was associated with a preserved LV ejection fraction and the absence of a significant elevation in serum cardiac troponin I (cTnI) concentrations, indicating that RPO led to an adaptive reduction in LV compliance that protected the heart from stretch-induced stunning and myocyte injury during PE-mediated pressure overload. Values are mean ± SEM. *p < 0.05 versus baseline. Abbreviations as in Figure 1.

in marked elevations in LVEDP, with relatively minor increases in LVEDV when loading conditions were altered. Collectively, these results demonstrated that reductions in LV compliance that were independent of anatomic hypertrophy could occur relatively quickly following repetitive hemodynamic overload and could serve as an adaptive mechanism to protect the heart from subsequent stretch-induced stunning.

REDUCED LV DIASTOLIC COMPLIANCE PREVENTS STRETCH-INDUCED MYOCYTE INJURY. Among the potential nonischemic causes of myocyte injury, myocyte diastolic stretch from elevations in preload has been implicated as an important mechanism. This is based on preclinical studies that demonstrated apoptosis (19) and troponin I degradation (20), as well as clinical observations that demonstrated elevated cTn concentrations in patients with chronically elevated LV filling pressures in the setting of heart failure (3). Although elevations in circulating cTnI are commonly interpreted as evidence of ischemic myocyte necrosis and is the standard biomarker used to diagnose myocardial infarction, we recently demonstrated that cTnI rapidly rises above normal after brief ischemia (6) and nonischemic myocardial stress. Elevating LVEDP for 1 h elicited prolonged cTnI release with an approximate 6-fold increase in myocyte apoptosis (5). The latter changes occurred without subendocardial ischemia or histopathological evidence of myocyte necrosis. These results complemented earlier studies in isolated myocardium (21) and an intact LV during brief episodes of pressure overload (22), in which time-dependent alterations of the passive length–tension relationship following elevations in systolic and diastolic pressures were ascribed to the viscous properties of creep and stress relaxation (23). Our data demonstrated that creep was not simply a mechanical phenomenon, but was also associated with myocardial damage as assessed by circulating cTnI concentrations and post-mortem measurements of myocyte apoptosis.

The present findings built on this observation by demonstrating that the LV quickly adapts in a fashion that attenuates stretch-induced myocyte injury. Animals subjected to 2 weeks of RPO exhibited cumulative myocyte loss as reflected by a nearly 20% reduction in myocyte nuclear density compared with normal control animals. Nevertheless, after 2 weeks of RPO, they were protected from the development of stretch-induced myocardial injury, and the ejection fraction remained normal before, during, and after preload elevation. This largely reflected reduced diastolic strain arising from increases in interstitial connective tissue. The latter adaptation ultimately

FIGURE 3 **RPO Produces Significant Cardiomyocyte Loss and Compensatory Cellular Hypertrophy of Remaining Myocytes**

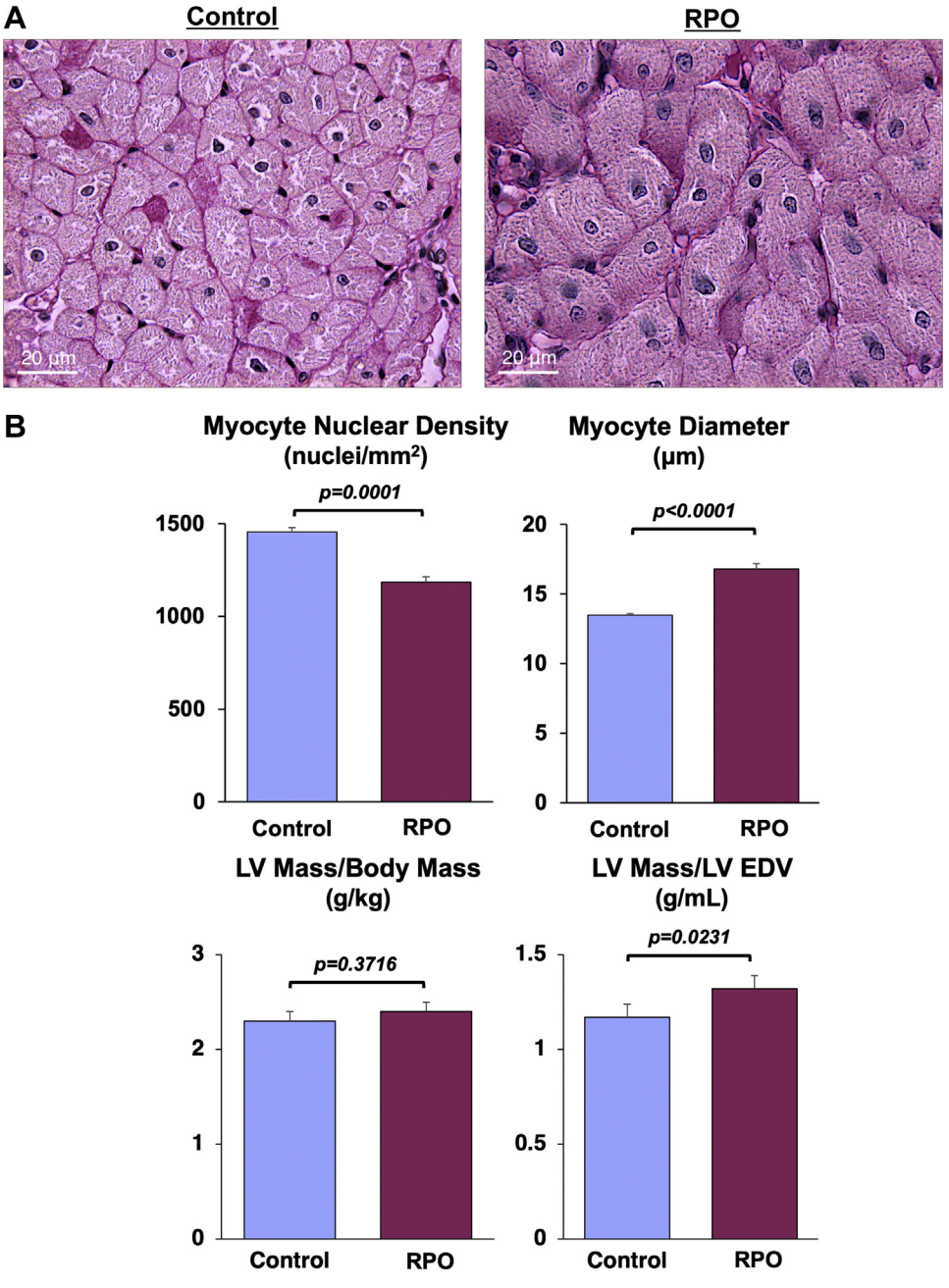

Examples of periodic acid-Schiff–stained myocardial tissue sections from a normal control animal **(left)** and an animal subjected to RPO **(right)** illustrate the reduction in myocyte nuclear density and increase in myocyte diameter elicited by RPO. Although RPO did not elicit a change in total LV mass, the LV mass/LVEDV was increased compared with normal control animals (n = 20), which was indicative of concentric LV remodeling in the absence of overt anatomic hypertrophy in swine subjected to RPO. Values are mean ± SEM. Abbreviations as in Figure 1.

FIGURE 4 Swine Subjected to RPO Exhibit Increased Interstitial Fibrosis

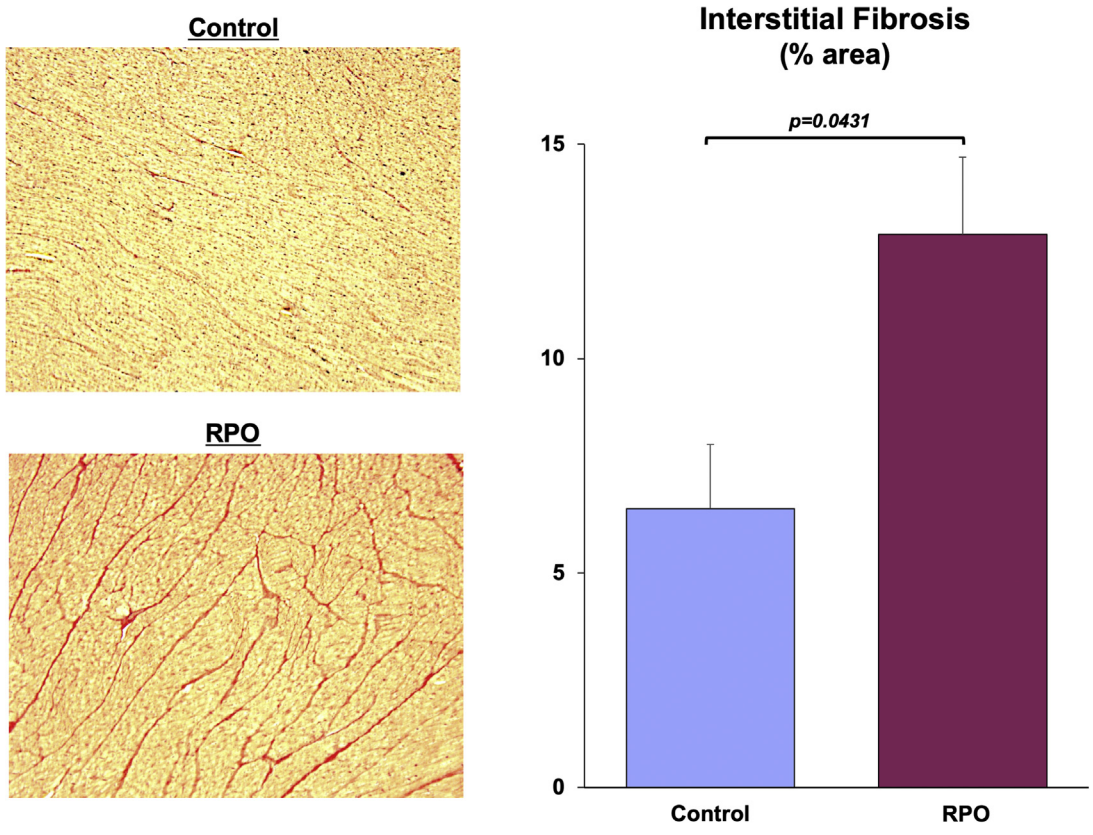

Picrosirius red–stained tissue sections demonstrate a marked increase in interstitial collagen deposition **(red areas)** in myocardial samples from animals subjected to RPO compared with normal control swine. Values are mean ± SEM. Abbreviations as in Figure 1.

prevented further stretch-induced myocyte injury, as indicated by the attenuation of cTnI release following 14 days of RPO. The adaptive reduction in LV compliance also prevented the development of progressive LV dilatation and chronic systolic dysfunction.

The cumulative myocyte loss that developed from RPO in concert with the proliferation of interstitial connective tissue was substantial and of a similar magnitude to that which we previously reported regionally in response to chronic repetitive ischemia (8). In the latter circumstance, the progressive loss of myocytes was accompanied by regional contractile dysfunction and the development of hibernating myocardium. Like chronic hibernating myocardium, the myocyte loss elicited by long-term RPO was accompanied by compensatory cellular hypertrophy of remaining myocytes, which allowed total LV mass to remain normal without the development of anatomic LV hypertrophy. Surprisingly, and in contrast to the deterioration in systolic function from chronic repetitive ischemia, LV ejection fraction was preserved in animals subjected to RPO in the present study. Instead of systolic dysfunction, RPO led to a marked reduction in LV diastolic compliance. This developed in concert with substantial remodeling of the extracellular matrix, because histopathological evaluation of picrosirius red–stained tissue sections revealed that interstitial collagen deposition was nearly doubled in swine subjected to RPO. Thus, the LV response to repetitive myocyte injury appears to be dependent on the nature of the physiological stimulus (i.e., ischemia stretch vs. mechanical stretch). In both circumstances, a constellation of phenotypic changes occurred that appeared to be adaptive in nature. In the case of hibernating myocardium and repetitive ischemia, these included a downregulation in oxidative metabolism that lowered myocardial oxygen demand to protect against further ischemia-induced injury, with only minor

FIGURE 5 RPO Reduces LV Diastolic Compliance

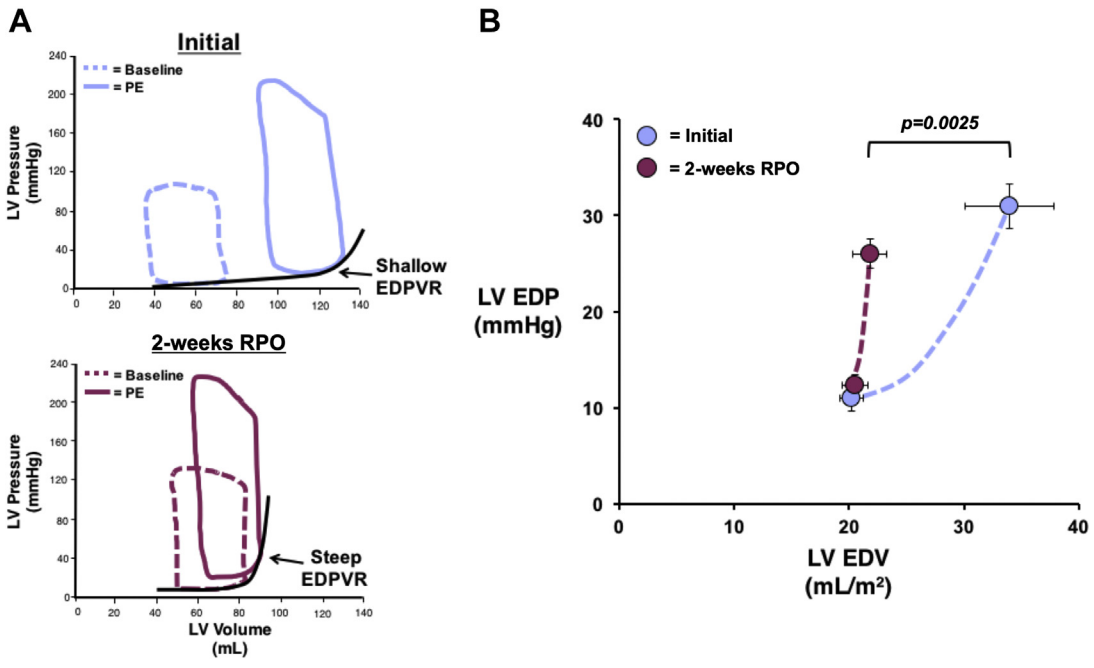

(A) Example admittance catheter-derived LV pressure–volume loops at rest and during PE infusion demonstrate that swine subjected to 2 weeks of RPO exhibited a steeper end-diastolic pressure-volume relationship during elevations in afterload. **(B)** This was visualized via construction of 2-point diastolic pressure–volume curves and quantified via calculation of the ΔLVEDV/ΔLVEDP ratio during acute episodes of PE-induced pressure overload, which was significantly lower after RPO. Values are mean ± SEM. EDPVR = end-diastolic pressure-volume relationship; other abbreviations as in Figure 1.

increases in interstitial connective tissue (24). In contrast, the myocardial adaptations to RPO led to a reduction in diastolic compliance with preserved systolic function.

The mechanisms responsible for reducing LV compliance might extend beyond the increased interstitial connective tissue demonstrated pathologically. For example, hypertrophied myocytes might also exhibit alterations in cellular proteins responsible for diastolic compliance. In this regard, isoform changes and/or post-translational modifications of the giant sarcomeric protein titin might have contributed to reductions in LV compliance by increasing myocyte-dependent stiffness (25). An adaptive increase in myocyte stiffness was recently shown to occur in remote, noninfarcted myocardium after myocardial infarction via relatively rapid alterations in titin phosphorylation (26). Furthermore, titin was shown to activate signaling pathways that regulate cellular hypertrophy in response to changes in mechanical stress elicited by alterations in hemodynamic load (27), which suggested a potentially important link among titin, myocyte stiffness, and cellular hypertrophy. Further studies will be required to identify myocyte structural alterations and to quantify the extent that these also contribute to myocardial diastolic properties in the present RPO model.

CONSEQUENCES OF MYOCARDIAL REMODELING ELICITED BY RPO. Our findings indicated that the reduction in diastolic LV compliance elicited by RPO might be a double-edged sword. Although these alterations provide protection against stretch-induced myocyte injury, the alterations in passive filling mechanics will elevate LV diastolic pressure at any LV volume and could conceivably limit the extent that cardiac output increases during exercise. This pattern of myocardial remodeling was similar to that observed in many patients with HFpEF. Although the etiology of this clinical syndrome is heterogeneous, and therefore, difficult to fully reproduce in a single experimental model, it is consistently characterized by reductions in LV chamber compliance that compromise the ability of the heart to increase cardiac output because of prominent increases in LV

FIGURE 6 RPO Elicits an Upward and Leftward Shift in the LV EDPVR

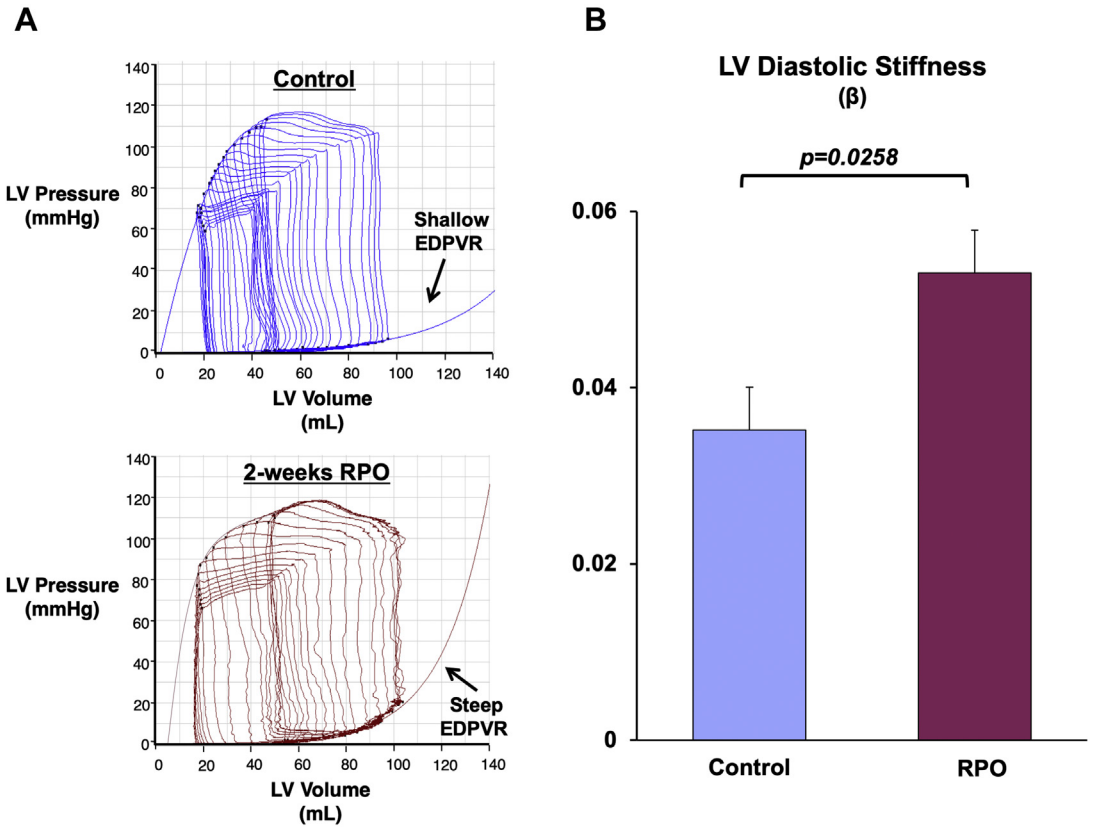

(A) Example admittance catheter-derived LV pressure–volume loops during transient inferior vena cava occlusion show a steeper EDPVR after 2 weeks of RPO compared with normal control animals. **(B)** The upward and leftward shift of the EDPVR led to a higher LV diastolic chamber stiffness constant (β) in animals subjected to RPO compared with normal control swine. Values are mean ± SEM; n = 5/group. Abbreviations as in Figures 1 and 5.

filling pressure during exercise. Several phenotypic characteristics exhibited by the animals subjected to RPO in the present study recapitulated aspects of cardiac remodeling that were reported in a large number of human patients with HFpEF. These included cellular myocyte hypertrophy, interstitial fibrosis, and capillary rarefaction demonstrated histologically, as well as concentric LV remodeling in the absence of anatomic hypertrophy frequently seen on cardiac imaging (28-31). Thus, it was intriguing to speculate that the myocardial adaptations to intermittent stretch-induced injury from transient pressure overload might lead to reductions in LV diastolic compliance in the absence of chronic hypertension and anatomic LV hypertrophy.

METHODOLOGICAL LIMITATIONS. Several experimental considerations merit discussion. First, we used intravenous PE to pharmacologically increase arterial BP and elevate LV preload to induce RPO. Although we were unable to completely rule out a direct effect of PE on myocardial remodeling in the present study, several lines of evidence argued against this notion. Although alpha-adrenergic receptors are expressed in the swine heart at similar levels to that observed in humans, this level of expression is markedly lower than that of rodents (particularly rats) from which isolated myocytes are often used to study PE-induced cellular hypertrophy (32). Coronary vascular expression of alpha-adrenergic receptors is minimal or absent in swine (33), and our own data demonstrated that subendocardial perfusion and coronary flow reserve were unaffected by PE infusion at this dose (5), which indicated that PE-mediated coronary vasoconstriction was unlikely to be involved. In addition, a

previous study in mice that used a mechanical approach to induce intermittent aortic constriction also observed myocyte cellular hypertrophy in the absence of anatomic hypertrophy (34). Although the LV response to acute pressure overload was not examined in that study, chronic intermittent aortic constriction was associated with a leftward and upward shift of the LV EDPVR and preserved ejection fraction. Although myocyte nuclear density, cTnI, or acute diastolic strain were not reported, the cellular hypertrophy in the absence of anatomic hypertrophy was consistent with stretch-induced myocyte loss. Thus, regardless of whether a mechanical or pharmacological approach is used to elicit RPO, it leads to myocyte loss with a compensatory increase in cardiomyocyte size. Second, it was important to acknowledge that age-, sex-, and body mass–matched swine were used for assessment of histopathology and LV PV analysis in normal control animals, instead of true sham-instrumented animals. Third, conclusions regarding myocyte loss based on changes in myocyte nuclear density assumed that a systematic change in the number of nuclei per myocyte did not occur. However, the observation of myocyte cellular hypertrophy (i.e., increase in myocyte cell diameter) in the absence of a change in LV mass was consistent with the notion that there were fewer myocytes per gram of tissue and net myocyte loss following RPO. Fourth, although microsphere perfusion measurements from our previous study that examined acute pressure overload were consistent with the absence of subendocardial ischemia during PE infusion (5), we did not assess myocardial blood flow in the present study, and therefore, could not completely rule out the presence of subendocardial ischemia during prolonged and/or repeated PE infusions. Finally, although swine subjected to RPO failed to demonstrate overt signs and symptoms of heart failure at rest, several clinical studies of exercise hemodynamics in patients with established HFpEF showed that a large number of patients only exhibited elevated LV filling pressures during exercise and displayed fairly normal resting hemodynamics (35–37). Data from the present study demonstrated a steeper LV EDPVR and an increased ΔEDP/ΔEDV ratio with increased afterload after RPO and supported the notion that these animals would exhibit impaired diastolic reserve and attenuated increases in cardiac output during exercise. Future studies that use invasive assessment of exercise hemodynamics, which are often neglected in preclinical animal studies (38), will be critical to evaluate HFpEF pathophysiology in this model.

CONCLUSIONS

In summary, our results demonstrated that repetitive episodes of transient preload elevation elicited by RPO produced profound changes in LV structure and function. These appeared to arise as an adaptive response to prevent the stretch-induced stunning and myocyte injury that initially develop following acute hemodynamic overload in the normal heart. This pattern of remodeling was characterized by reduced LV diastolic compliance, increased interstitial fibrosis, cardiomyocyte cellular hypertrophy, capillary rarefaction, and concentric LV remodeling, thereby recapitulating a phenotype commonly observed in human patients with HFpEF. These changes all developed in the absence of overt anatomic LV hypertrophy and collectively supported a novel paradigm that linked cardiac adaptations to RPO with the pathogenesis of reduced LV diastolic compliance. In contrast to the persistent hemodynamic overload commonly produced in preclinical models, patients might experience intermittent episodes of preload elevation during labile BP elevations associated with mental stress and activities of daily living (9). These transient periods of hemodynamic overload become exacerbated with age-related stiffening of the aorta (10) and could intermittently impose high levels of mechanical stress on the myocardium, leading to chronic myocyte loss via repetitive stretch-induced programmed cell death (19). Further studies will be required to identify the multiple cellular mechanisms involved in the response and to assess the impact of these changes on diastolic and systolic cardiac function during exercise.

ACKNOWLEDGMENTS These studies could not have been completed without the assistance of Elaine Granica, Rebeccah Young, Beth Palka, and Cheryl Knapp.

ADDRESS FOR CORRESPONDENCE: Dr. Brian R. Weil, Department of Physiology and Biophysics, Jacobs School of Medicine and Biomedical Sciences, University at Buffalo, Clinical Translational Research Center, Suite 7030, 875 Ellicott Street, Buffalo, New York 14203. E-mail: bweil@buffalo.edu.

PERSPECTIVES

COMPETENCY IN MEDICAL KNOWLEDGE: A transient elevation in preload produces mechanical stretch-induced myocyte injury and measurable cTnI release in the absence of ischemia that is associated with reversible contractile dysfunction and myocyte apoptosis. The findings of this study demonstrated that repetitive exposure to cyclical elevations in preload elicited significant myocyte loss, but LV systolic function was preserved and chamber dilatation was absent. Instead, myocardial remodeling characterized by myocyte hypertrophy and interstitial fibrosis produced a reduction in diastolic compliance that protected the heart from subsequent stretch-induced injury.

TRANSLATIONAL OUTLOOK: Long-term repetitive pressure overload–induced interstitial fibrosis and cellular hypertrophy appear to arise as an adaptive response to intermittent episodes of stretch-induced cardiomyocyte apoptosis. This pattern of remodeling produces a reduction in LV diastolic compliance that has the beneficial effect of protecting the heart from stretch-induced injury during subsequent periods of hemodynamic overload. Nevertheless, protection may come at the cost of a compromised ability to increase cardiac output because of prominent elevations in LV filling pressure and inadequate augmentation of stroke volume during exercise, a hallmark characteristic of HFpEF. Because these changes develop without a significant increase in LV mass, they may explain how reductions in myocardial diastolic compliance can occur when persistent hypertension and anatomic LV hypertrophy are absent.

REFERENCES

1. Whelan RS, Kaplinskiy V, Kitsis RN. Cell death in the pathogenesis of heart disease: mechanisms and significance. Ann Rev Physiol 2010;72:19–44.

2. Braunwald E. Heart failure. J Am Coll Cardiol HF 2013;1:1–20.

3. Thygesen K, Alpert JS, Jaffe AS, et al. Fourth universal definition of myocardial infarction (2018). J Am Coll Cardiol 2018;72:2231–64.

4. Giannitsis E, Katus HA. Cardiac troponin level elevations not related to acute coronary syndromes. Nat Rev Cardiol 2013;10:623–34.

5. Weil BR, Suzuki G, Young RF, Iyer V, Canty JM Jr. Troponin release and reversible left ventricular dysfunction after transient pressure overload. J Am Coll Cardiol 2018;71:2906–16.

6. Weil BR, Young RF, Shen X, et al. Brief myocardial ischemia produces cardiac troponin I release and focal myocyte apoptosis in the absence of pathological infarction in swine. J Am Coll Cardiol Basic Transl Sci 2017;2:105–14.

7. Fallavollita JA, Canty JM Jr. Differential 18F-2-deoxyglucose uptake in viable dysfunctional myocardium with normal resting perfusion: evidence for chronic stunning in pigs. Circulation 1999;99:2798–805.

8. Lim H, Fallavollita JA, Hard R, Kerr CW, Canty JM Jr. Profound apoptosis-mediated regional myocyte loss and compensatory hypertrophy in pigs with hibernating myocardium. Circulation 1999;100:2380–6.

9. Komajda M, Lam CS. Heart failure with preserved ejection fraction: a clinical dilemma. Eur Heart J 2014;35:1022–32.

10. Sun Z. Aging, arterial stiffness, and hypertension. Hypertension 2015;65:252–6.

11. Lang RM, Badano LP, Mor-Avi V, et al. Recommendations for cardiac chamber quantification by echocardiography in adults: an update from the American Society of Echocardiography and the European Association of Cardiovascular Imaging. Eur Heart J Cardiovasc Imaging 2015;16:233–70.

12. Weil BR, Konecny F, Suzuki G, Iyer V, Canty JM Jr. Comparative hemodynamic effects of contemporary percutaneous mechanical circulatory support devices in a porcine model of acute myocardial infarction. J Am Coll Cardiol Intv 2016;9:2292–303.

13. Konecny F, Smith C, Techiryan G, Canty JM Jr., Weil BR. Dual admittance catheter-derived biventricular pressure-volume analysis in swine: comparison with contrast-enhanced computed tomography during transient pressure overload. FASEB J 2019;33:531.12.

14. van der Velde ET, Burkhoff D, Steendijk P, Karsdon J, Sagawa K, Baan J. Nonlinearity and load sensitivity of end-systolic pressure-volume relation of canine left ventricle in vivo. Circulation 1991;83:315–27.

15. Burkhoff D, Mirsky I, Suga H. Assessment of systolic and diastolic ventricular properties via pressure-volume analysis: a guide for clinical, translational, and basic researchers. Am J Physiol Heart Circ Physiol 2005;289:H501–12.

16. Weil BR, Suzuki G, Leiker MM, Fallavollita JA, Canty JM Jr. Comparative efficacy of intracoronary allogeneic mesenchymal stem cells and cardiosphere-derived cells in swine with hibernating myocardium. Circ Res 2015;117:634–44.

17. Schipke J, Brandenberger C, Rajces A, et al. Assessment of cardiac fibrosis - a morphometric method comparison for collagen quantification. J Appl Physiol 2017;122:1019–30.

18. Swindle MM, Makin A, Herron AJ, Clubb FJ Jr., Frazier KS. Swine as models in biomedical research and toxicology testing. Vet Pathol 2012;49:344–56.

19. Cheng W, Li B, Kajstura J, et al. Stretch-induced programmed myocyte cell death. J Clin Invest 1995;96:2247–59.

20. Abdelmeguid AA, Feher JJ. Effect of low perfusate [Ca2+] and diltiazem on cardiac sarcoplasmic reticulum in myocardial stunning. Am J Physiol Heart Circ Physiol 1994;266:H406–14.

21. Sonnenblick EH, Ross J Jr., Covell JW, Braunwald E. Alterations in resting length-tension relations of cardiac muscle induced by changes in contractile force. Circ Res 1966;19:980–8.

22. LeWinter MM, Engler R, Pavelec RS. Time-dependent shifts of the left ventricular diastolic filling relationship in conscious dogs. Circ Res 1979;45:641–53.

23. Pinto JG, Patitucci PJ. Creep in cardiac muscle. Am J Physiol 1977;232:H553–63.

24. Page B, Young R, Iyer V, et al. Persistent regional downregulation in mitochondrial enzymes and upregulation of stress proteins in swine with chronic hibernating myocardium. Circ Res 2008;102:103–12.

25. LeWinter MM, Granzier H. Cardiac titin: a multifunctional giant. Circulation 2010;121:2137–45.

26. Kotter S, Kazmierowska M, Andresen C, et al. Titin-based cardiac myocyte stiffening contributes to early adaptive ventricular remodeling after myocardial infarction. Circ Res 2016;119:1017–29.

27. Kotter S, Andresen C, Kruger M. Titin: central player of hypertrophic signaling and sarcomeric protein quality control. Biol Chem 2014;395:1341–52.

28. van Heerebeek L, Borbely A, Niessen HW, et al. Myocardial structure and function differ in systolic and diastolic heart failure. Circulation 2006;113:1966–73.

29. Kasner M, Westermann D, Lopez B, et al. Diastolic tissue Doppler indexes correlate with the degree of collagen expression and cross-linking in heart failure and normal ejection fraction. J Am Coll Cardiol 2011;57:977–85.

30. Zile MR, Baicu CF, J SI, et al. Myocardial stiffness in patients with heart failure and a preserved ejection fraction: contributions of collagen and titin. Circulation 2015;131:1247–59.

31. Mohammed SF, Hussain S, Mirzoyev SA, Edwards WD, Maleszewski JJ, Redfield MM. Coronary microvascular rarefaction and myocardial fibrosis in heart failure with preserved ejection fraction. Circulation 2015;131:550–9.

32. Steinfath M, Chen YY, Lavicky J, et al. Cardiac alpha 1-adrenoceptor densities in different mammalian species. Br J Pharmacol 1992;107:185–8.

33. Schulz R, Oudiz RJ, Guth BD, Heusch G. Minimal alpha 1- and alpha 2-adrenoceptor-mediated coronary vasoconstriction in the anaesthetized swine. Naunyn Schmiedebergs Arch Pharmacol 1990;342:422–8.

34. Perrino C, Naga Prasad SV, Mao L, et al. Intermittent pressure overload triggers hypertrophy-independent cardiac dysfunction and vascular rarefaction. J Clin Invest 2006;116:1547–60.

35. Andersen MJ, Olson TP, Melenovsky V, Kane GC, Borlaug BA. Differential hemodynamic effects of exercise and volume expansion in people with and without heart failure. Circ Heart Fail 2015;8:41–8.

36. Borlaug BA, Nishimura RA, Sorajja P, Lam CS, Redfield MM. Exercise hemodynamics enhance diagnosis of early heart failure with preserved ejection fraction. Circ Heart Fail 2010;3:588–95.

37. Obokata M, Kane GC, Reddy YN, Olson TP, Melenovsky V, Borlaug BA. Role of diastolic stress testing in the evaluation for heart failure with preserved ejection fraction: a simultaneous invasive-echocardiographic study. Circulation 2017;135:825–38.

38. Roh J, Houstis N, Rosenzweig A. Why don't we have proven treatments for HFpEF? Circ Res 2017;120:1243–5.

KEY WORDS diastolic dysfunction, fibrosis, heart failure, myocardial stunning, stretch

APPENDIX For a supplemental figure and videos, please see the online version of this paper.

JACC: BASIC TO TRANSLATIONAL SCIENCE
PUBLISHED BY ELSEVIER ON BEHALF OF THE AMERICAN COLLEGE OF CARDIOLOGY FOUNDATION.

VOL. 4, NO. 4, 2019

EDITORIAL COMMENT

Repetitive Acute Hemodynamic Load

Progression From Systolic Decompensation to Cellular/Extracellular Compensation to Diastolic Decompensation*

Michael R. Zile, MD,[a,b] Catalin F. Baicu, PhD,[a] Ryan J. Tedford, MD[a]

The development of myocardial cellular and extracellular changes that result in abnormal left ventricular (LV) structure and diastolic dysfunction are fundamental to the development of heart failure with preserved ejection fraction (HFpEF) (1). These changes in LV structure and function result from abnormal hemodynamic and metabolic load that occur with comorbid diseases (e.g., hypertension, diabetes, ischemia, and obesity) that are antecedent to the development of HFpEF (2). However, as many as 40% of patients with HFpEF studied in randomized clinical trials do not have LV structural changes (e.g., frank LV chamber hypertrophy) (3). In addition, patients with HFpEF remain symptomatic, with significant abnormalities in diastolic function at rest and during exercise, even when hemodynamic and metabolic load have been normalized by appropriate medical management. These facts raise several questions. Do increased loads need to be persistent (or chronic) to cause HFpEF? What cellular and extracellular changes are present in HFpEF in the absence of chamber hypertrophy that explain the presence of diastolic dysfunction? Are load-induced cellular and extracellular changes compensatory or decompensatory?

The translational studies presented by Weil et al. (4) in this issue of *JACC: Basic to Translational Science* provide novel data and important insights that help to address these questions. In their study, Weil et al. performed 2-h infusions of phenylephrine (PE) daily for 2 weeks in adult pigs with doses sufficient to raise systolic blood pressure (SBP) to 190 to 200 mm Hg.

SEE PAGE 527

The hemodynamic, structural, and functional responses to the PE infusion changed significantly over time and essentially converted from systolic decompensation to diastolic decompensation (**Figure 1**). This change in response to PE infusion was caused by alterations in cellular and extracellular structures. At baseline, 60-min PE infusion caused increased SBP, LV end-diastolic pressure (EDP), end-diastolic volume (EDV), end-systolic volume (ESV), and decreased EF (**Figure 1C**). Sixty minutes after cessation of PE infusion, SBP and LVEDP returned to normal; however, LVEDV and LVESV remained higher, and EF was still decreased. These acute changes were accompanied by myocyte injury, manifest as significant cardiac troponin I (cTNI) release and cellular apoptosis. By contrast, after 2 weeks of repetitive 2-h PE infusions, while 60-min PE infusion led to similar increases in SBP and LVEDP, no significant changes in EDV, ESV, or EF were observed (**Figure 1D**). This differential change in response was associated with a marked reduction in LV diastolic ventricular compliance (steeper end-diastolic pressure–volume relationship), concentric LV remodeling without chamber hypertrophy, cardiomyocyte hypertrophy, and a marked interstitial fibrosis as evidenced by an

*Editorials published in the *JACC: Basic to Translational Science* reflect the views of the authors and do not necessarily represent the views of *JACC: Basic to Translational Science* or the American College of Cardiology.

From the [a]Division of Cardiology, Department of Medicine, Medical University of South Carolina, Charleston, South Carolina; and the [b]Division of Cardiology, Department of Medicine, Ralph H. Johnson Department of Veterans Affairs Medical Center, Charleston, South Carolina. Dr. Tedford has been a member of the Advisory Board for Abiomed; has been a member of the hemodynamic core laboratories for Merck and Actelion; and has been a consultant for United Therapeutics and Arena Pharmaceuticals. All other authors have reported that they have no relationships relevant to the contents of this paper to disclose.

The authors attest they are in compliance with human studies committees and animal welfare regulations of the authors' institutions and Food and Drug Administration guidelines, including patient consent where appropriate. For more information, visit the *JACC: Basic to Translational Science* author instructions page.

ISSN 2452-302X

https://doi.org/10.1016/j.jacbts.2019.07.006

increase in collagen volume fraction. The associated myocyte injury was also blunted, with significantly less cTNI release. The investigators proposed these structural and functional changes provided a protective effect against PE-induced myocardial injury. The resultant changes in cellular and extracellular structure and function in this porcine model of repetitive PE infusion have direct application to, and are comparable with, the changes seen in patients with hypertensive heart disease–induced HFpEF.

HEMODYNAMIC LOAD: DECOMPENSATION TO COMPENSATION TO DECOMPENSATION

Hemodynamic load is one of the fundamental determinants of myocardial structure and function. PE infusion causes changes in both preload and afterload. As defined by the Law of Laplace, LV chamber preload is calculated as: end-diastolic wall stress = LVEDP × LVEDV/LVED wall thickness; and afterload is calculated as: end-systolic wall stress = LVESP × LVESV/LVES wall thickness. Therefore, the PE resultant acute (within the first few minutes) changes in EDV and EDP (increased preload) and ESV and ESP (increased afterload) cause alterations in the LV pressure–volume relations (LVPVRs) as shown in **Figures 1A and 1B**, respectively.

However, 60 min of PE infusion alters the LVPVR beyond that expected from acute changes in preload and afterload (5). Both heterometric (length-dependent) and homeometric (length-independent) autoregulation are activated during 60 min of PE infusion and result in an increase in developed pressure, caused by an increase in length-dependent myofilament calcium sensitivity (Frank-Starling mechanism) and a length-independent increase in the calcium transient amplitude (Anrep effect). These forms of autoregulation represent the direct effects of 60 min of hemodynamic load on molecular and/or cellular signaling (1,2) and activation of the sympathetic nervous system (SNS) and the renin-angiotensin-aldosterone system (RAAS). In addition, PE infusion may result in "creep," a myocardial length increase that occurs at a constant load, and stunning (as proposed by the investigators). All of these effects of PE may be responsible for the change in the LVPVR (shown in **Figure 1C**) and based on the data presented in Weil et al. (4).

Sixty minutes of PE resulted in a reduced EF, cTNI release, and apoptosis; this represents decompensated systolic function. However, the repetitive application of PE infusion and the hemodynamic, neurohumoral, and signaling changes that occurred with each infusion served as a direct stimulus to produce cardiomyocyte hypertrophy and LV concentric remodeling. In part, these changes served to compensate systolic function. By contrast, chronic activation of SNS and RAAS also led to cardiomyocyte loss through apoptosis and necrosis. In addition, hemodynamic, neurohumoral, and signaling changed the constitutive material properties of the cardiomyocyte that reduced cellular distensibility and increased myocardial stiffness. Finally, hemodynamic, neurohumoral, and signaling resulted in interstitial fibrosis that further contributed to increased myocardial and LV diastolic chamber stiffness. These changes in diastolic stiffness prevented PE-induced increases in LVEDV and preserved EF but did so at the cost of decompensated abnormal diastolic function (**Figure 1D**). Therefore, although hemodynamic load played a central role, it was the resultant neurohumoral activation and molecular signaling that were responsible for the chronic structural changes that resulted from repetitive PE infusion. Thus, when increased preload, afterload, heterometric, and homeometric autoregulation were applied (through PE infusion) in the presence of these structural changes, systolic performance was compensated at the cost of diastolic decompensation (**Figure 1D**).

CLINICAL INSIGHTS

The antecedent and/or comorbid disease processes that lead to the development of HFpEF and its characteristic structural and functional remodeling are generally viewed as imposing a constant, steady-state increase on hemodynamic and/or metabolic load. However, they are not constant or in a steady state. Hypertension-induced increases in afterload vary from hour to hour and day to day based on sleep and/or wake cycles, activity and/or exercise, emotional stress, medication half-life, and patient compliance with pharmacological and non-pharmacological management. The same applies to glucose management in diabetes. The control of each of these hemodynamic and metabolic loads also affects neurohumoral activation and molecular signaling, which, in turn, will have intrinsic variability. Therefore, the effects of the repetitive PE infusion provide an increased understanding of the pathophysiological mechanisms that result in the clinical syndrome of HFpEF. In addition, these data provide an understanding of the progressive structural and functional changes at the cellular and

FIGURE 1 Effects of Changes in Hemodynamic Load on the LVPVR

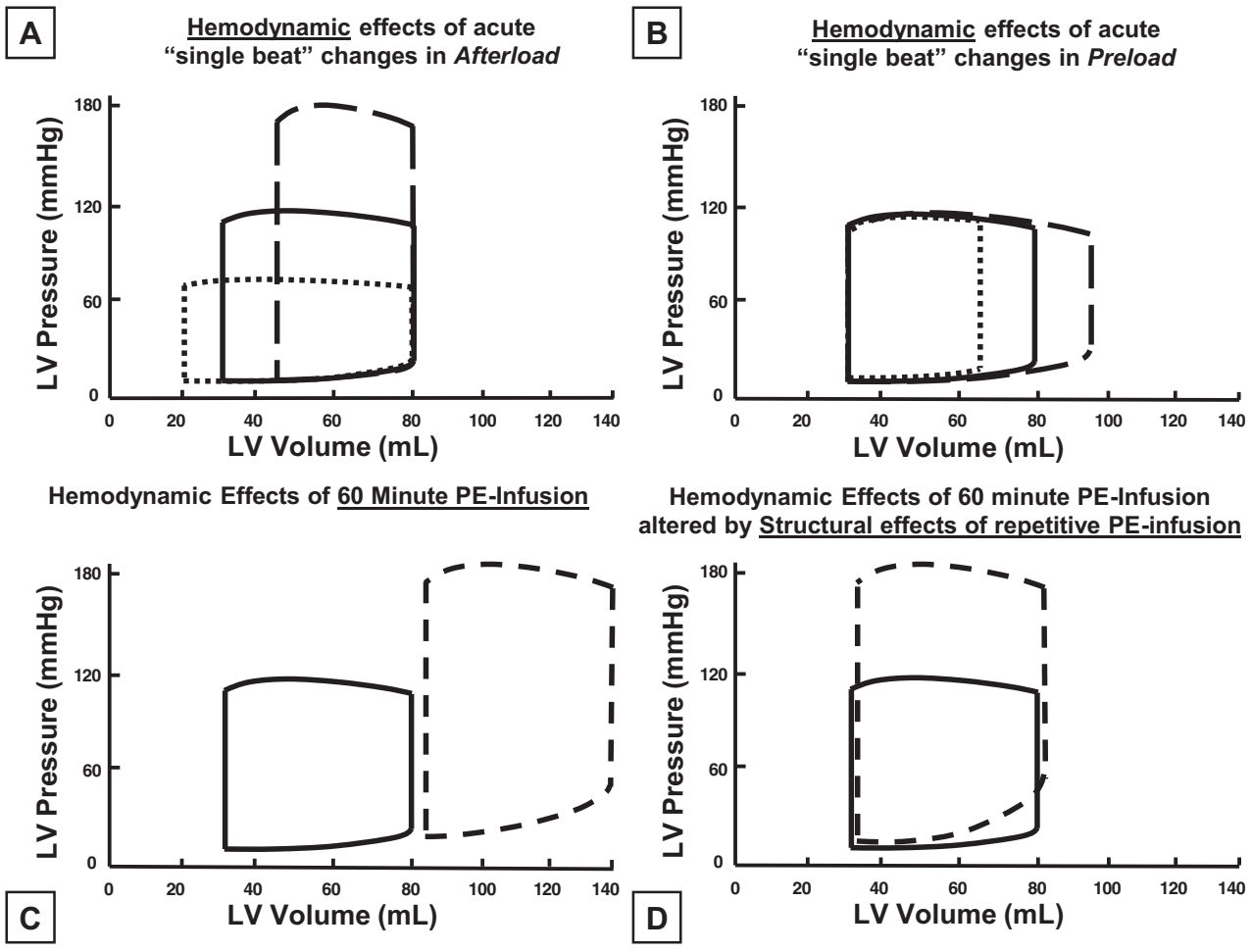

(A) Hemodynamic effects of acute, isolated, single-beat changes in afterload on the left ventricular pressure–volume relationship (LVPVR). Images represent idealized schematic drawings. **Solid line** = controls; **dashed line** = acute, isolated, single beat increase in afterload; **dotted line** = acute, isolated, single beat decrease in afterload. **(B)** Hemodynamic effects of acute isolated, single beat changes in preload on the LVPVR. Images represent idealized schematic drawings. **Solid line** = controls; **dashed line** = acute, isolated single beat increase in preload; **dotted line** = acute, isolated, single beat decrease in preload. **(C)** Hemodynamic effects of 60-min phenylephrine (PE) infusion induced changes in afterload and preload, as well as activation of both heterometric and homeometric autoregulation on LVPVR at baseline before repetitive daily PE infusions. Sixty minutes of PE infusion caused reversible increases in LV systolic and diastolic pressure, but sustained increases in LV end-diastolic and end-systolic volume and decreased ejection fraction (EF); there was evidence of decompensated systolic function. **Solid line** = controls; **dashed line** = effects on LVPVR of PE infusion. Images represent idealized schematic drawings derived from data from study by Weil et al (4). **(D)** Hemodynamic and structural effects of repetitive PE infusion on the LVPVR. After 2 weeks of repetitive PE infusions, the effects of a 60-min PE infusion–induced changes in hemodynamic load (increased afterload and preload, as well as activation of both heterometric and homeometric autoregulation) were superimposed on cellular and extracellular structural remodeling. The observed changes in LV diastolic stiffness prevented PE-induced increases in LVEDV and preserved EF but did so at the cost of increased LV diastolic PVR, decreased LV distensability, and decompensated diastolic function. **Solid line** = controls; **dashed line** = effects on LVPVR of PE infusion. Images represent idealized schematic drawings derived from data from the study of Weil et al. (4).

extracellular level that result in rest and exercise diastolic dysfunction, increased LV diastolic stiffness, and clinical presentation of heart failure in patients with HFpEF.

The data presented by Weil et al (4) present the 2-sided coin of compensatory and/or decompensatory changes in structure and function. In response to increased hemodynamic load, the cellular and/or extracellular changes in structure and/or function preserve systolic properties but degrade diastolic properties. The model presented in Weil et al. (4) results in many of the characteristics common in the

clinical syndrome of HFpEF; after the phenotype is established, these characteristics should be amenable to testing novel management schemes that reverse fibrosis and normalize cardiomyocyte structure and function.

CONCLUSIONS

The study by Weil et al. (4) provides important insights into the pathophysiological mechanisms underlying the development of clinical HFpEF and provides a porcine translational model that should be useful in further studies that examine novel therapeutic approaches to manage patients with HFpEF.

ADDRESS FOR CORRESPONDENCE: Dr. Michael R. Zile, Division of Cardiology, Department of Medicine, Medical University of South Carolina, Thurmond/Gazes, Room 323, 30 Courtenay Drive, Charleston, South Carolina 29425. E-mail: zilem@musc.edu.

REFERENCES

1. Zile MR, Baicu CF, Ikonomidis J, et al. Myocardial stiffness in patients with heart failure and a preserved ejection fraction: contributions of collagen and titin. Circulation 2015;131:1247–59.

2. Paulus WJ, Tschöpe C. A novel paradigm for heart failure with preserved ejection fraction: comorbidities drive myocardial dysfunction and remodeling through coronary microvascular endothelial inflammation. J Am Coll Cardiol 2013;62:263–71.

3. Zile MR, Gottdiener JS, Hetzel SJ, et al. Prevalence and significance of alterations in cardiac structure and function in patients with heart failure and a preserved ejection fraction. Circulation 2011;124:2491–201.

4. Weil BR, Techiryan G, Suzuki G, Konecny F, Canty JM Jr. Adaptive reductions in left ventricular diastolic compliance protect the heart from stretch-induced stunning. J Am Coll Cardiol Basic Transl Sci 2019;4:527–41.

5. Cingolani HE, Pérez NG, Cingolani OH, Ennis IL. The Anrep effect: 100 years later. Am J Physiol Heart Circ Physiol 2013;304:H175–82.

KEY WORDS diastolic dysfunction, fibrosis, heart failure

JACC: BASIC TO TRANSLATIONAL SCIENCE VOL. 4, NO. 4, 2019

STATE-OF-THE-ART REVIEW

Neuromodulation for the Treatment of Heart Rhythm Disorders

Nathan H. Waldron, MD, MHS,[a,b,*] Marat Fudim, MD,[b,c,*] Joseph P. Mathew, MD, MHS, MBA,[a,b] Jonathan P. Piccini, MD, MHS[b,c]

JACC: BASIC TO TRANSLATIONAL SCIENCE CME/MOC/ECME

This article has been selected as this month's *JACC: Basic to Translational Science* CME/MOC/ECME activity, available online at http://www.acc.org/jacc-journals-cme by selecting the *JACC* Journals CME/MOC/ECME tab.

Accreditation and Designation Statement

The American College of Cardiology Foundation (ACCF) is accredited by the Accreditation Council for Continuing Medical Education (ACCME) and the European Board for Accreditation in Cardiology (EBAC) to provide continuing medical education for physicians.

The ACCF designates this Journal-based CME/MOC/ECME activity for a maximum of 1 AMAPRA Category 1 Credit or 1 EBAC Credit. Physicians should only claim credit commensurate with the extent of their participation in the activity.

Successful completion of this CME activity, which includes participation in the evaluation component, enables the participant to earn up to 1 Medical Knowledge MOC point in the American Board of Internal Medicine's (ABIM) Maintenance of Certification (MOC) program. Participants will earn MOC points equivalent to the amount of CME credits claimed for the activity. It is the CME activity provider's responsibility to submit participant completion information to ACCME for the purpose of granting ABIM MOC credit.

Neuromodulation for the Treatment of Heart Rhythm Disorders will be accredited by the European Board for Accreditation in Cardiology (EBAC) for 1 hour of External CME credits. Each participant should claim only those hours of credit that have actually been spent in the educational activity. The Accreditation Council for Continuing Medical Education (ACCME) and the European Board for Accreditation in Cardiology (EBAC) have recognized each other's accreditation systems as substantially equivalent. Apply for credit through the post-course evaluation.

Method of Participation and Receipt of CME/MOC/ECME Certificate

To obtain credit for JACBTS: Basic to Translational Science CME/MOC/ECME, you must:

1. Be an ACC member or JACBTS subscriber.
2. Carefully read the CME/MOC/ECME-designated article available online and in this issue of the *journal*.
3. Answer the post-test questions. At least 2 questions provided must be answered correctly to obtain credit.
4. Complete a brief evaluation.
5. Claim your CME/MOC/ECME credit and receive your certificate electronically by following the instructions given at the conclusion of the activity.

CME/MOC/ECME Objective for This Article: Upon completion of this activity, the learner should be able to: 1) describe the neurohormonal pathways that affect cardiac arrhythmias; 2) identify therapeutic options for refractory ventricular tachycardia; and 3) discuss the potential mechanisms for neurohormonal modulation.

CME/MOC/ECME Editor Disclosure: CME/MOC/ECME Editor L. Kristin Newby, MD, is supported by research grants from Amylin, Bristol-Myers Squibb Company, GlaxoSmithKline, Sanofi, Verily Life Sciences (formerly Google Life Sciences), the MURDOCK Study, NIH, and PCORI; receives consultant fees/honoraria from BioKier, DemeRx, MedScape/TheHeart.org, Metanomics, Philips Healthcare, Roche Diagnostics, CMAC Health Education & Research Institute; serves as an Officer, Director, Trustee, or other fiduciary role for the AstraZeneca HealthCare Foundation and the Society of Chest Pain Centers (now part of ACC); and serves in another role for the American Heart Association and is the Deputy Editor of *JACC: Basic to Translational Science*.

Author Disclosures: Dr. Waldron has received personal fees and grants from Allergan, and AHA grant 16MCPRP30700010 and the NIGMS T32 postdoctoral training grant T32GM008600. Dr. Fudim has received grants from AHA grant 17MCPRP33460225 and NIH T32 grant 5T32HL007101; and has received personal fees from Galvani, Coridea, and Axon Therapies. Dr. Mathew is on the Board of Directors and owns equity in MedBlue Data; and has received grants from NIH R01 grant number HL130443. Dr. Piccini has received grants for clinical research from Abbott, the American Heart Association, Boston Scientific, Gilead, Janssen Pharmaceuticals, and the NHLBI; and serves as a consultant to Abbott, Allergan, ARCA Biopharma, Biotronik, Boston Scientific, Johnson & Johnson, LivaNova, Medtronic, Milestone, Oliver Wyman Health, Sanofi, Philips, and Up-to-Date.

Medium of Participation: Online (article and quiz).

CME/MOC/ECME Term of Approval

Issue Date: August 2019
Expiration Date: July 31, 2020

From the [a]Department of Anesthesia, Duke University Medical Center, Durham, North Carolina; [b]Duke Clinical Research Institute, Durham, North Carolina; and the [c]Electrophysiology Section, Duke University Medical Center, Durham, North Carolina. *Drs.Waldron and Fudim contributed equally to this work and are joint first authors. Dr. Waldron has received personal fees and grants from Allergan, and AHA grant 16MCPRP30700010 and the NIGMS T32 postdoctoral training grant T32GM008600. Dr. Fudim has received grants from AHA grant 17MCPRP33460225 and NIH T32 grant 5T32HL007101; and has received personal fees from

ISSN 2452-302X https://doi.org/10.1016/j.jacbts.2019.02.009

Neuromodulation for the Treatment of Heart Rhythm Disorders

Nathan H. Waldron, MD, MHS,[a,b,*] Marat Fudim, MD,[b,c,*] Joseph P. Mathew, MD, MHS, MBA,[a,b] Jonathan P. Piccini, MD, MHS[b,c]

HIGHLIGHTS

- **Derangement of autonomic nervous signaling is an important contributor to cardiac arrhythmogenesis.**
- **Modulation of autonomic nervous signaling holds significant promise for the prevention and treatment of cardiac arrhythmias.**
- **Further clinical investigation is necessary to establish the efficacy and safety of autonomic modulatory therapies in reducing cardiac arrhythmias.**

SUMMARY

There is an increasing recognition of the importance of interactions between the heart and the autonomic nervous system in the pathophysiology of arrhythmias. These interactions play a role in both the initiation and maintenance of arrhythmias and are important in both atrial and ventricular arrhythmia. Given the importance of the autonomic nervous system in the pathophysiology of arrhythmias, there has been notable effort in the field to improve existing therapies and pioneer additional interventions directed at cardiac-autonomic targets. The interventions are targeted to multiple and different anatomic targets across the neurocardiac axis. The purpose of this review is to provide an overview of the rationale for neuromodulation in the treatment of arrhythmias and to review the specific treatments under evaluation and development for the treatment of both atrial fibrillation and ventricular arrhythmias. (J Am Coll Cardiol Basic Trans Science 2019;4:546–62)

ANATOMY OF THE NEUROCARDIAC AXIS

The neurocardiac axis is composed of multiple intricate areas that provide an interface between the nervous system and the cardiovascular system (**Figure 1**). This neurocardiac anatomy has been elegantly detailed in a recent review (1). A number of diverse brain structures contribute to efferent cardiac autonomic signaling, including the amygdala, insula, thalamus, and cerebellum (2). In general, second-to-second control of autonomic tone occurs at the level of the brainstem, whereas forebrain structures including the hypothalamus effect more prolonged or gradual shifts in autonomic tone (3). From these various brain areas, sympathetic signals are first transmitted via the cervical and thoracic spinal cord to the stellate (cervicothoracic) ganglion before synapsing with nerves of the intrinsic cardiac nervous system (4). In contrast, parasympathetic fibers originate in the brainstem and travel primarily via the vagus nerve into the pericardial sack (1). There, sympathetic and parasympathetic efferent fibers form a branching neural network clustering in autonomic ganglionic plexi (AGP) contained in fat pads on the posterior surface of the atria and the superior aspect of the ventricles (**Figure 1**) (5). AGP contain large populations of colocalized sympathetic and parasympathetic neurons (1), and may serve as

Galvani, Coridea, and Axon Therapies. Dr. Mathew is on the Board of Directors and owns equity in MedBlue Data; and has received grants from NIH R01 grant number HL130443. Dr. Piccini has received grants for clinical research from Abbott, the American Heart Association, Boston Scientific, Gilead, Janssen Pharmaceuticals, and the NHLBI; and serves as a consultant to Abbott, Allergan, ARCA Biopharma, Biotronik, Boston Scientific, Johnson & Johnson, LivaNova, Medtronic, Milestone, Oliver Wyman Health, Sanofi, Philips, and Up-to-Date.

All authors attest they are in compliance with human studies committees and animal welfare regulations of the authors' institutions and Food and Drug Administration guidelines, including patient consent where appropriate. For more information, visit the *JACC: Basic to Translational Science* author instructions page.

Manuscript received December 31, 2018; revised manuscript received February 22, 2019, accepted February 22, 2019.

JACC: BASIC TO TRANSLATIONAL SCIENCE VOL. 4, NO. 4, 2019
AUGUST 2019:546–62

ABBREVIATIONS AND ACRONYMS

AERP = atrial effective refractory period

AF = atrial fibrillation

AGP = autonomic ganglionic plexus

ANS = autonomic nervous system

CABG = coronary artery bypass grafting

HRV = heart rate variability

ICD = implantable cardioverter-defibrillator

LLVNS = low-level vagal nerve stimulation

OSA = obstructive sleep apnea

POAF = post-operative atrial fibrillation

PVI = pulmonary vein isolation

RDN = renal denervation

SCS = spinal cord stimulation

SGB = stellate ganglion blockade

SNS = sympathetic nervous system

VF = ventricular fibrillation

VNS = vagal nerve stimulation

VT = ventricular tachycardia

"integration centers" modulating cardiac responses to autonomic input (6). Emerging evidence indicates that these AGP contain an amalgam of afferent neurons, motor neurons, interconnecting local circuit neurons, and that some proportion of these neurons expresses both cholinergic as well as adrenergic immunoreactivity (1). The extensive interconnections as well as the colocalization of cholinergic and adrenergic neurons set the stage for interplay between the parasympathetic and sympathetic nervous system at the level of the AGPs. Beyond the direct communication between the autonomic nervous system (ANS) and the heart, the neurocardiac axis is under modulatory control from additional autonomic reflexes, including afferent nervous input from the baroreflex and the renal nerves, which may modulate the global and regional (cardiac) sympathetic tone.

ATRIAL FIBRILLATION

RATIONALE FOR AUTONOMIC MODULATION FOR ATRIAL FIBRILLATION. Atrial fibrillation (AF) is a common and significant medical problem that affects approximately 3% of the population (7). As the population ages, the incidence and prevalence of AF are projected to increase even further (8). In addition to being a leading cause of stroke, AF is associated with increased risks of heart failure (HF), myocardial infarction (MI), cognitive impairment, and death (9). The severity or persistence of AF has been associated with worse outcomes, including a higher risk of stroke (10); however, the role of AF burden (proportion of time spent in AF) in adverse outcomes remains incompletely understood (11). Given both its prevalence and impact, AF is a significant public health concern, and reduction of AF and its attendant complications remains a priority for the cardiovascular community.

An increasing body of evidence suggests that activity of the ANS can contribute to the initiation and perpetuation of cardiac arrhythmias, including AF. In isolated atrial myocytes, parasympathetic input shortens the atrial effective refractory period (AERP) (12) and increases dispersion of refractoriness (13), whereas sympathetic input increases calcium transient currents and afterdepolarizations (4), synergistically promoting the onset of AF (14). Similar responses to sympathetic stimulation are observed in pulmonary veins, a common site of ectopy that triggers AF (15). Although both parasympathetic and sympathetic stimulation may individually promote AF (16,17), data suggest that combined parasympathetic and sympathetic (sympathovagal) discharges are especially potent initiators of AF (15,18) due to the combined effects of shortened AERP and increased calcium transient currents, respectively. Changes in heart rate variability (HRV) before onset of AF (19,20) are consistent with combined sympathovagal discharges. There are also data to suggest that AGP may influence focal sources or drivers of AF. For example, a study of 97 patients undergoing catheter ablation of AF has shown that the majority of patients had a focal source or rotor that overlapped with the anatomic location of an AGP (21). Because AGPs play a crucial role in AF, several strategies to prevent or reduce AF have centered around modulating AGP activity directly or indirectly through the extrinsic cardiac nervous system.

PAST AND PRESENT. Current strategies in autonomic modulation for atrial arrhythmias. A number of strategies to reduce AF partially exert their effects through modulation of the cardiac ANS (**Table 1**). Beta blockers antagonize the effects of catecholamines on a variety of target tissues, such as cardiac and vascular adrenergic receptors (22). AF ablation may also exert some benefit through autonomic modulation. In addition to creating electrical isolation of the pulmonary veins from the left atrium (23), pulmonary vein isolation (PVI) also reduces AGP-induced firing of pulmonary vein potentials that initiate AF. A positive response to AGP stimulation after extensive PVI independently predicts recurrence of AF (24), suggesting that AGP modulation may contribute to the efficacy of AF ablation.

Aggressive risk factor reduction also reduces the risk of AF. Part of the benefit of weight loss may be explained by alteration of autonomic tone as the metabolic syndrome has been associated with increased sympathetic tone (25). Similarly, obstructive sleep apnea (OSA) results in sympathetic activation (26) and increased focal sources of AF (27) both contributing to an increased risk of AF. Management of these risk factors reduces ANS hyperactivity and may impact the success of AF ablation (28). Treatment of sleep apnea with continuous positive airway pressure decreases risk of AF progression (29), and reduces risk of recurrent AF after catheter ablation (30). Adaptive servo-ventilation, which may be used to treat obstructive, central, or mixed sleep apnea, was recently shown to decrease AF burden in patients with HF and sleep apnea (31). Risk factor reduction such as weight loss and treatment of sleep apnea has the

FIGURE 1 Overview of the Neurocardiac Axis

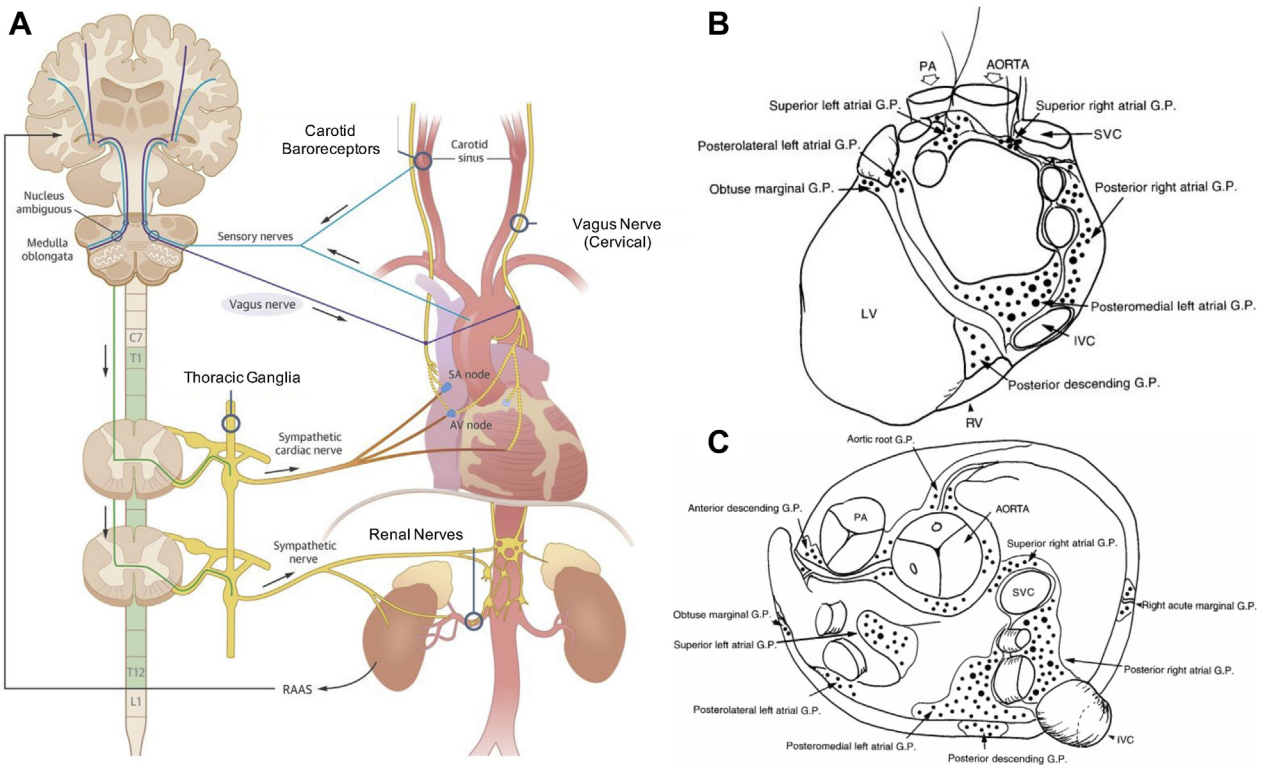

(A) Depiction of hierarchical organization of cardiovascular innervation as it proceeds from cerebral structures to individual nerves. Adapted with permission from Chatterjee et al. (133). **(B, C)** Locations of autonomic ganglionic plexi (represented as **small black dots**) as viewed from the posterior **(B)** and superior **(C)** aspect of the heart. Reprinted with permission from Armour et al. (5). RAAS = renin-angiotensin-aldosterone system.

potential to improve autonomic function and reduce AF through several different mechanisms.

DEVELOPING NEUROMODULATORY APPROACHES. **Ablation-based approaches.** ***AGP ablation.*** Ablation of AGP by either catheter-based or surgical approaches has shown some promise in improving the success of AF ablation (**Central Illustration**). Percutaneous anatomically guided AGP ablation as a stand-alone technique has limited efficacy (32) and is inferior to circumferential PVI (33). However, randomized data have shown that the addition of AGP ablation to PVI may increase freedom from AF compared to either technique in isolation (34). Additionally, AGP ablation combined with PVI may result in increased long-term freedom from AF and lower rates of atrial flutter than PVI + linear ablation (35). Not all studies have supported the efficacy of AGP ablation. A recent comparison of video-assisted thoracoscopic surgery for AF with or without AGP ablation showed no difference in freedom from AF; additionally, patients undergoing epicardial AGP ablation had higher rates of procedural complications and pacemaker implantation (36). Further studies are needed to clarify optimal methods of AGP localization and ablation, and the potential benefits of AGP ablation.

TABLE 1 Current Therapeutic Strategies for Rhythm Control of AF

Current Therapeutic Strategies for AF	Examples
Antiarrhythmic drug therapy	Class I: flecainide, propafenone Class III: amiodarone, dronedarone, sotalol, dofetilide
Catheter ablation	Pulmonary vein isolation Substrate modification Ablation of nonpulmonary vein triggers
Surgical ablation	Cox-Maze procedure Thoracoscopic ablation ("mini-maze")
Risk-factor modification	Positive airway pressure for obstructive sleep apnea Blood pressure reduction Weight Loss

AF = atrial fibrillation.

CENTRAL ILLUSTRATION **Neuromodulatory Approaches and Techniques**

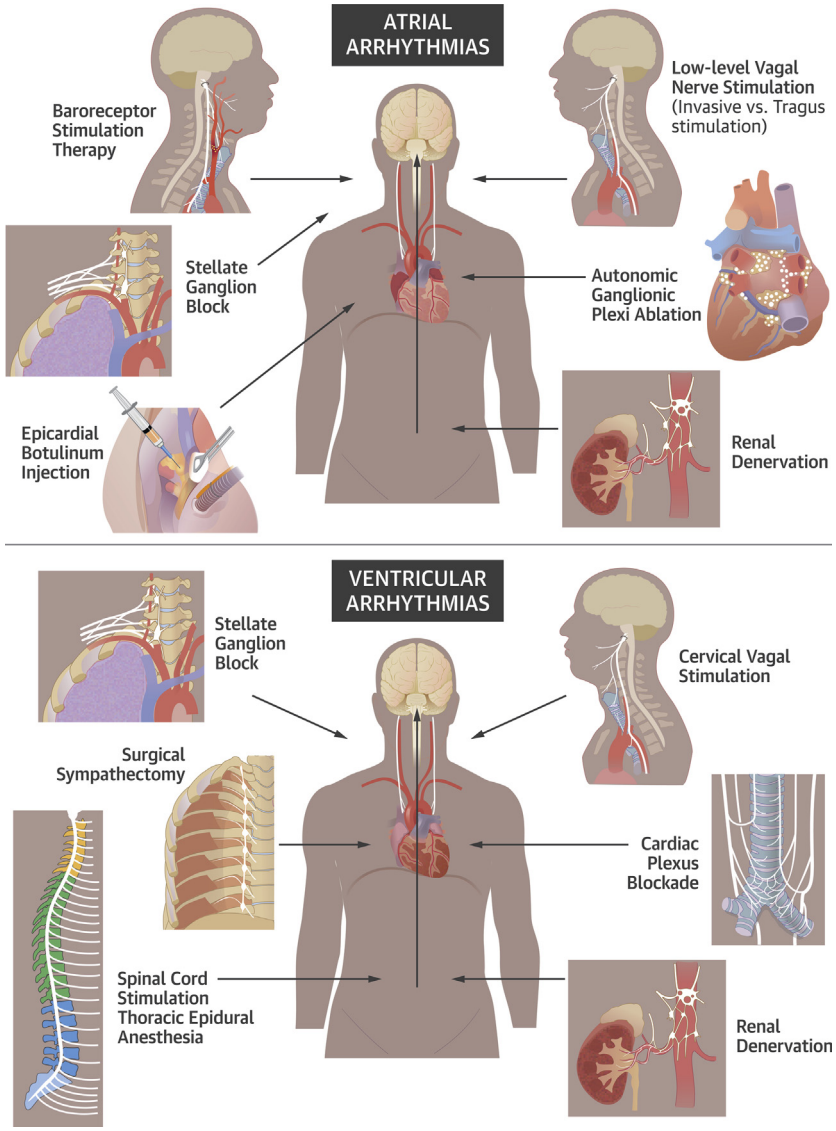

Waldron, N.H. et al. J Am Coll Cardiol Basic Trans Science. 2019;4(4):546–62.

Neuromodulatory approaches and techniques for atrial **(top)** and ventricular **(bottom)** arrhythmias.

Renal denervation. Renal denervation (RDN) is a method of modulating central afferent input. Renal afferent and efferent nerves function in a reflex loop where afferent input from the kidney to the central nervous system (CNS) regulates the efferent sympathetic nerve output to the heart and back to the kidney. Renal afferent nerves are diverse and represent a heterogeneous population of fibers including myelinated and nonmyelinated fibers (37,38). Two main types of renal afferents are responsible for relaying information to the CNS, mechanosensitive (hydrostatic pressure from renal vasculature), and chemosensitive receptors (sensitive to ischemia, osmolar changes, and ionic composition) (39). Functionally, the renal afferent fibers can be divided into: 1) pressor; 2) reno-renal; and 3) depressor types (40,41). In other words, some fibers when activated contribute to the elevation of the sympathetic tone (sympatho-stimulant), whereas others reduce the sympathetic tone (sympatholytic). This is supported

TABLE 2 Current Status of Developing Neuromodulatory Strategies for Arrhythmias

Intervention	Anatomical Target	Current Status	Diseases of Interest	Number of Patients	Ongoing Clinical Trials
AGP ablation	Autonomic Ganglionic Plexi	Clinical trials	AF	60	NCT03535818: Adjunctive Ganglionated Plexus Ablation in Redo-Pulmonary Vein Isolation (ADD-GP); Randomized trial testing the efficacy of AGP ablation in patients with ongoing paroxysmal arrhythmias after PVI
			AF	14	NCT03636100: Release of Acetylcholine From the Ganglionated Plexus During the Thaw Phase of Cryoballoon Pulmonary Vein Ablation (GP RESPONSE Study); Observational study designed to study the role of systemic acetylcholine release in response to cryoballoon ablation.
			POAF	62	NCT02035163: Atrial Fibrillation Prevention in Post Coronary Artery Bypass Graft Surgery with Cryoablation for Ganglionic Plexi; A randomized study to test the ability of AGP cryoablation during cardiac surgery to prevent POAF.
Epicardial botulinum toxin injection	Autonomic ganglionic plexi	Clinical trials	POAF	170	NCT02617069: Botulinum Toxin Injection Into Epicardial Fat Pads to Prevent Atrial Fibrillation in Patients Undergoing Cardiac Surgery; Randomized trial of epicardial botulinum toxin for the prevention of POAF after cardiac surgery in patients with paroxysmal AF.
			POAF	330	NCT03779841: A Phase II, Multi-Center, Randomized, Double-Blind, Placebo-Controlled, Dose-Ranging Study to Evaluate the Efficacy and Safety of Botulinum Toxin Type A (AGN-151607) Injections Into the Epicardial Fat Pads to Prevent Post-Operative Atrial Fibrillation in Patients Undergoing Open-Chest Cardiac Surgery; Randomized double-blind, placebo-controlled, dose-ranging trial evaluating the efficacy and safety of epicardial botulinum toxin type injections to prevent POAF in patients undergoing cardiac surgery.
BRS therapy	Carotid and aortic baroreceptors	Preclinical	POAF	95	NCT03243279: BRS and Outcomes in Cardiothoracic Surgery; Observational study to determine if perioperative baroreceptor sensitivity (BRS) correlates with POAF and outcomes after cardiothoracic surgery
TVNS	Auricular branch of the Vagus Nerve (Afferent)	Clinical trials	POAF	42	NCT03533140: Postoperative Atrial Fibrillation Suppression By Nerve Stimulation; Randomized trial testing TVNS to prevent POAF and reduce inflammation
			POAF	200	NCT02783157: Transcutaneous Autonomic Modulation In Thoracic Surgery (TON-POINTS); Trial evaluating TVNS to reduce POAF after cardiothoracic surgery.
			AF	52	NCT02548754: Transcutaneous Electrical Vagus Nerve Stimulation to Suppress Atrial Fibrillation (TREAT-AF); A small study to evaluate the ability of TVNS to reduce atrial fibrillation burden and inflammation in patients with paroxysmal AF.
RDN	Sympathetic nerves around the renal arteries (afferent)	Clinical trials	AF	300	NCT01635998: Adjunctive Renal Denervation in the Treatment of Atrial Fibrillation (H-FIB); Phase II trial to evaluate the ability of combined RND and PVI versus PVI only to reduce recurrent AF.
			AF	100	NCT01990911: Renal Sympathetic Denervation Prevents Atrial Fibrillation in Patients with Hypertensive Heart Disease: a Pilot Study (RDPAF); Phase II trial testing efficacy of RDN to reduce subclinical AF and restore autonomic imbalance.
			AF	138	NCT02115100: Treatment of Atrial Fibrillation in Patients by Pulmonary Vein Isolation in Combination With Renal Denervation or Pulmonary Vein Isolation Only (ASAF); Open-label trial testing the ability of combined RDN and PVI to reduce recurrent AF after PVI.
			AF	61	NCT01907828: A Feasibility Study to Evaluate the Effect of Concomitant Renal Denervation and Cardiac Ablation on AF Recurrence (RDN+AF); Phase II trial evaluating the feasibility of RDN combined with AF ablation in reducing recurrent AF in patients with AF and uncontrolled hypertension.
			AF	40	NCT03246568: Renal Nerve Denervation After Pulmonary Vein Isolation for Persistent Atrial Fibrillation; Phase II study to evaluate the efficacy of RDN added to PVI in reducing recurrent AF in patients with persistent AF.
			AF	100	NCT01686542: CPVI Plus Renal Sympathetic Modification Versus CPVI Alone for AF (Atrial Fibrillation) Ablation; Open-label trial evaluating the ability of RDN combined with PVI to reduce recurrent AF compared with PVI alone.
			AF	245	NCT02064764: Renal Nerve Denervation in Patients with Hypertension and Paroxysmal and Persistent Atrial Fibrillation (Symplicity AF); Phase II trial to assess the feasibility of concurrent RDN and PVI, and the rate of chronic treatment success in patients receiving RDN and PVI vs. PVI only
			AF	40	NCT01952925: Combined Afib Ablation and RA Denervation for the Maintenance of Sinus Rhythm and Management of Resistant Hypertension; Non-randomized prospective study to evaluate the ability of concurrent AF ablation and RDN to reduce ambulatory blood pressure.
			VT/VF	60	NCT02856373: Renal Nerve Stimulation and Renal Denervation in Patients With Sympathetic Ventricular Arrhythmias (Redress VT); Will assess impact of renal nerve stimulation before and after percutaneous transluminal RDN on cardiac excitable properties including induction of ventricular tachyarrhythmias before and after RDN
			VT/VF	38	NCT01858194: REnal Sympathetic dEnervaTion as an Adjunct to Catheter-based VT Ablation (RESET-VT); Prospective, multicenter, randomized control trial testing the impact of catheter-based renal sympathetic denervation (RSDN) as an adjunctive treatment for patients with cardiomyopathy undergoing catheter ablation of ventricular tachycardia (VT).

Continued on the next page

TABLE 2 Continued

Intervention	Anatomical Target	Current Status	Diseases of Interest	Number of Patients	Ongoing Clinical Trials
			VT/VF	462	NCT01747837: REnal SympathetiC Denervation to sUpprEss Tachyarrhythmias in ICD Recipients (RESCUE); Randomized, blinded trial to assess the efficacy of RDN in preventing ventricular arrhythmias and ICD shocks.
SCS	Efferent sympathetic fibers in the spinal cord	Clinical trials	POAF	60	NCT03539354: Temporary Spinal CoRd StiMulatIon to PreveNt Atrial FibrillaTION After Cardiac Surgery (TerminationAF); Phase II trial to assess the ability of temporary spinal cord stimulation in preventing POAF
TEA	Efferent sympathetic fibers in the spinal cord	Preclinical	AF or VT/VF		None, though TEA infrequently used in some centers to reduce pain and prevent POAF after cardiac surgery
SGB	Stellate ganglion (efferent fibers)	Clinical trials	POAF	707	NCT03269383: Study to Evaluate the Effectiveness of SGB in Preventing Post-Op Atrial Fibrillation; Phase II trial to evaluate the efficacy of safety of temporary SGB with bupivacaine to prevent POAF.
			VT/VF	20	NCT02646501: Prospective Randomized Clinical Trial for Effect of Stellate Ganglion Block in Medically Refractory Ventricular Tachycardia; Study evaluates the effect of SGB in patients with recurrent VT/VF despite optimal medical management
			VT/VF or AF	40	NCT03450226: Effects of Stellate Ganglion Block on Hemodynamics Instability During Beating Heart Surgery; A randomized controlled, blinded trial evaluating the effect of pre-operative SGB on perioperative arrhythmias and myocardial infarction after off-pump CABG.
Invasive VNS	Vagus nerve (efferent fibers)	Preclinical	VT/VF or AF		None, although animal studies have demonstrated the ability of low-level invasive VNS to reduce sympathetic outflow as well as AF inducibility
Surgical sympathectomy	Thoracic sympathetic ganglia (efferent fibers)	Clinical trials	Heart failure - VT/VF prevention	30	NCT03071653: Left Cardiac Sympathetic Denervation for Cardiomyopathy Feasibility Pilot Study (LCSD); A randomized controlled trial to test the potential safety and efficacy of LCSD in patients with heart failure due to non-ischemic and ischemic cardiomyopathy
Transtracheal cardiac plexus blockade	Cardiac plexus (efferent fibers)	Preclinical	VT/VF		None

AF= atrial fibrillation; AGP = autonomic ganglionic plexus; BRS = baroreceptor stimulation; ICD = implantable cardioverter-defibrillator; POAF= postoperative atrial fibrillation; PVI = pulmonary vein isolation; RDN = renal denervation; SCS = spinal cord stimulation; SGB = stellate ganglion block; TEA = thoracic epidural anesthesia; TVNS = transcutaneous vagal nerve stimulation; VF = ventricular fibrillation; VNS = vagal nerve stimulation; VT = ventricular tachycardia.

by increasing preclinical and clinical evidence suggesting that endovascular electrical mapping with stimulation of the renal arteries can result in a differential response including an elevation in blood pressure (42-46).

RDN has received a lot of interest for the treatment of hypertension but may also have utility in reducing arrhythmias through autonomic mechanisms. As mentioned above, the renal vasculature is richly innervated by both afferent and efferent sympathetic nerves which contribute to systemic autonomic signaling. Ablating these nerves may reduce both systemic and cardiac catecholamine levels, as well as reduce atrial fibrosis through modulation of the renin-angiotensin-aldosterone system (47). In a rabbit model of ischemic cardiomyopathy, RDN reduced deleterious atrial structural and electrical remodeling and AF inducibility (48). Additionally, percutaneous RDN reduces atrial nerve sprouting, catecholamine levels, atrial fibrosis, and complexity of AF in a goat model of pacing-induced AF (49). Finally, RDN has been shown to attenuate the electrical and structural remodeling of the left atrium induced by long-term intermittent atrial pacing in a canine model (50).

There are few clinical trials evaluating RDN as an adjunct to PVI for the treatment of recurrent AF. A pilot study of 69 patients with chronic kidney disease and paroxysmal AF showed improved freedom from AF and reduction of AF burden at 1 year in patients randomized to PVI and RDN compared with PVI and spironolactone (51). A study of 86 patients with moderate or severe treatment-resistant hypertension randomized to either PVI alone or PVI with RDN showed improved freedom from AF with the addition of RDN; however, the benefit was most apparent in patients with severe hypertension (52). A follow-up analysis from this cohort has shown a reduction in AF recurrences and burden of AF in patients receiving RDN and PVI (53).

As a stand-alone therapy, RDN may also promote reverse-remodeling and improve atrial substrate. A pilot trial of 20 patients with paroxysmal or persistent AF and hypertension showed that RDN reduced AF burden and improved quality of life (54). Moreover, RDN reduced atrial conduction time, complex fractionated atrial activity, and ventricular mass in 14 patients with treatment-resistant hypertension (55). Multiple upcoming trials will help elucidate the role of

FIGURE 2 Stellate Ganglion Block

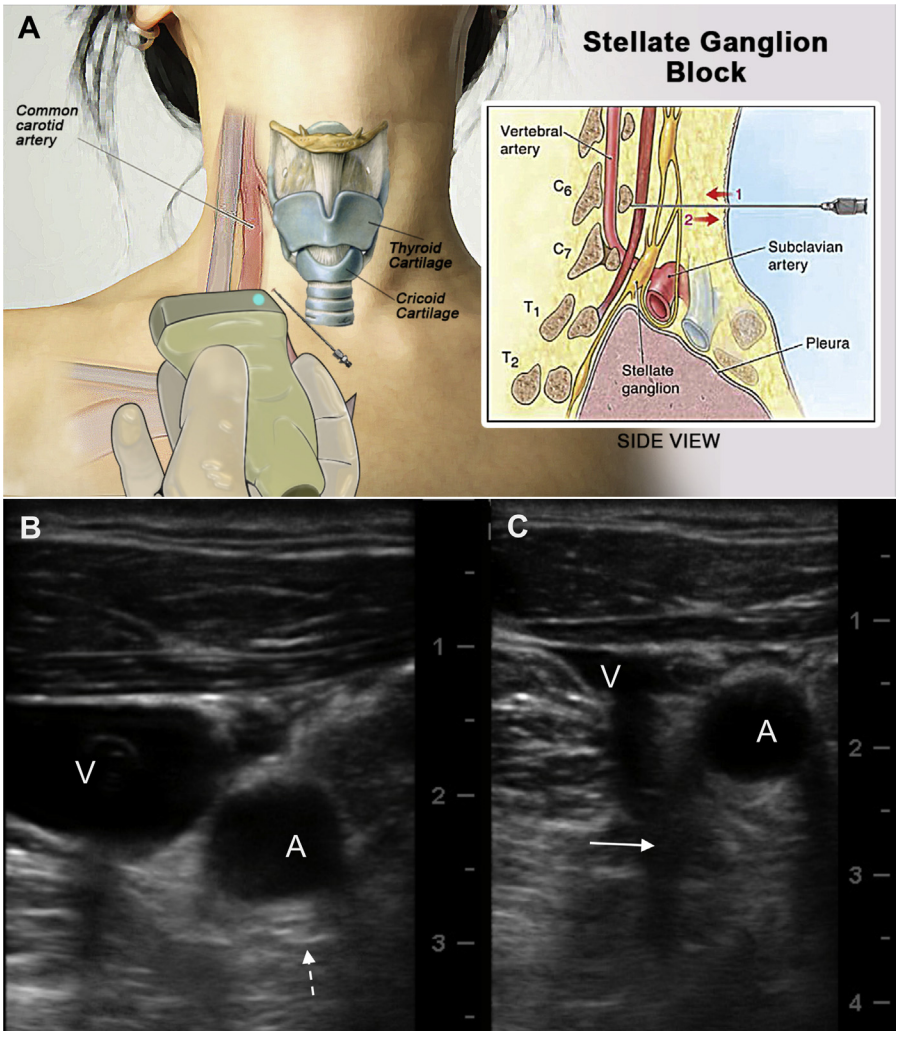

(A) Illustration of an ultrasound-guided percutaneous stellate ganglion block. **(B, C)** Ultrasound images of the percutaneous approach on the right side. **(B)** Image obtained before needle insertion. **Dashed arrow** indicates the sympathetic ganglion. **(C)** Image obtained during needle insertion (**arrow**) and anesthetic infusion. **A** marks the carotid artery. **V** marks the jugular vein. Adopted with permission from Armour et al. (104).

RDN as a stand-alone technique or in addition to PVI to reduce sympathetically mediated AF (Table 2).

Pharmacologic approaches. ***Epicardial botulinum toxin injection.*** Given the role of the AGP in the initiation and perpetuation of AF, additional nonablative strategies to modulate AGP signaling are currently under active investigation (Table 2). Injection of botulinum toxin into AGP reduces vagal influences on the AERP as well as vulnerability to AF in both canine (12,56) and ovine models (57). Given the temporary nature of this strategy, autonomic modulation using botulinum toxin injected into AGP has recently gained attention as a potential strategy to reduce post-operative AF (POAF), a common and impactful complication after cardiac surgery (58,59).

This approach has been studied in 2 small clinical trials. In the first study, 60 patients with paroxysmal AF undergoing coronary artery bypass grafting (CABG) received botulinum toxin or placebo injected into the 4 major left atrial fat pads. With this approach, patients receiving epicardial botulinum toxin had reduced incidence of POAF in the first month after surgery (60), as well as reduced recurrent AF and AF burden at 1 and 3 years after surgery,

FIGURE 3 Unifying Framework for the Mechanisms of Autonomic Regulation of Ventricular Arrhythmias

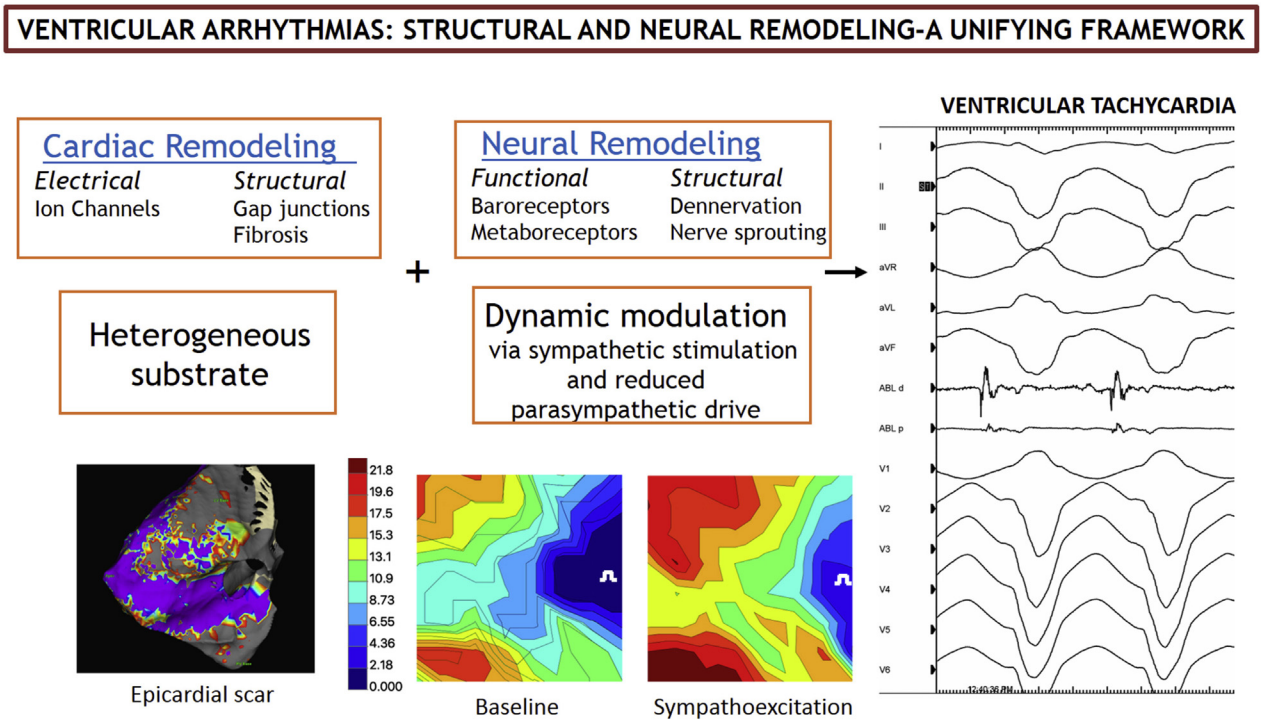

Adapted with permission from Bradfield et al. (132).

respectively (61,62). In the second study, 130 patients undergoing CABG and/or valve surgery were randomized to receive epicardial botulinum toxin or placebo injected into the 4 left atrial fat pads as well as the anterior fat pad. Using this technique, there was no difference between groups in the occurrence of in-hospital POAF; however, initial POAF episodes were shorter and there were no discernible adverse effects of botulinum toxin injections (63). Further large-scale clinical trials are necessary to determine the utility of this strategy in preventing POAF after cardiac surgery. Additionally, future work is necessary to determine whether botulinum toxin could be delivered to AGP in a less invasive fashion.

Stellate ganglion block. Percutaneous stellate ganglion block (SGB) is a minimally invasive interruption of autonomic innervation from the cervical sympathetic ganglia to the heart (**Figure 2**). As a key relay station for sympathetic nerve signaling, the stellate ganglion is a prime target for autonomic modulation to reduce AF. Ablation of bilateral stellate ganglia eliminates atrial tachycardia episodes in a canine model of pacing-induced HF (64). A promising minimally invasive strategy to temporarily modulate autonomic signaling is SGB with percutaneous injection of local anesthetic—a procedure frequently used to treat pain syndromes in ambulatory clinics. A pilot study of 36 patients undergoing PVI as well as short duration SGB (unilateral, left or right) has shown that

TABLE 3 Current Therapeutic and Adjunctive Strategies for VT/VF

Current Therapeutic Strategies for VT/VF	Examples
Pharmacotherapy	Beta-adrenergic blockade Nonselective (ß-1, ß-2): carvedilol, nadolol, propranolol Selective (ß-1): metoprolol, esmolol Membrane active antiarrhythmic drugs Class I: lidocaine, mexiletine, procainamide Class III: sotalol, amiodarone, dofetilide
Ablation	Catheter ablation of focal VT, triggers, and substrate modification (endocardial and epicardial)
Mechanical circulatory support	Temporary: Intra-aortic balloon pump, Impella (ABIOMED, Danvers, Massachusetts) extracorporeal membrane oxygenation, et cetera Permanent: Left ventricular assist device, et cetera
Surgery	Surgical ablation Ventricular aneurysm resection Transplantation

Abbreviations as in Table 2.

SGB lengthened the AERP while reducing inducibility and duration of AF (65). Similarly, a pilot study of 25 patients undergoing CABG and/or aortic valve surgery showed the feasibility and potential efficacy of left-sided SGB for the prevention of POAF (66). A larger study of SGB to prevent POAF is forthcoming and will provide important insight regarding the potential effectiveness of this technique (NCT03269383).

Bioelectronic approaches. ***Low-level vagal nerve stimulation.*** High-frequency vagal nerve stimulation (VNS) shortens the AERP (67) and action potential duration in the pulmonary veins (68), facilitating the initiation of AF. However, the intensity of VNS appears to modulate its arrhythmogenicity, with low-level VNS (LLVNS) (below the bradycardia threshold) generally showing a protective or antiarrhythmic effect. Left-sided LLVNS causes upregulation of inhibitory small-conductance calcium-activated potassium channels in the stellate ganglia (69). Similarly, intermittent left cervical VNS is able to slow the ventricular rate in a canine model of pacing-induced AF by damaging the ganglion (70) and increasing activity of the AGP (71). Together, these studies suggest that the antiarrhythmic effect of LLVNS may be mediated through decreased stellate ganglia activity as well as alteration of AGP signaling.

The vagus nerve can be stimulated directly with electrodes; however, given the risks of cervical VNS implantation, recent attention has focused on alternative and less-invasive methods of delivering VNS. Stavrakis et al. (72) recently explored the role of LLVNS in preventing POAF. In their study, 54 patients undergoing cardiac surgery who had a temporary bipolar pacing wire placed in vagal preganglionic fibers near the superior vena cava were randomized to LLVNS or sham stimulation for the duration of post-operative intensive care unit stay. They found that LLVNS reduced the occurrence of POAF. They also found that LLVNS ameliorated the post-operative cytokine elevation associated with cardiac surgery, raising the hypothesis that LLVNS has an anti-inflammatory effect (72).

Because vagal nerve projections exist in the ear, LLVNS may be delivered through stimulation of the tragus. In canine models of pacing-induced AF, LLVNS delivered by tragus stimulation reduced the electrical and structural remodeling induced by rapid atrial pacing (73). Transcutaneous LLVNS increases HRV and decreases muscle sympathetic nerve activity in healthy volunteers, reflecting an anti-adrenergic effect (74). In a pilot study of 40 patients undergoing AF ablation, 1 hour of transcutaneous LLVNS via tragus stimulation decreased pacing-induced AF duration as well as systemic cytokine levels (75). Two trials are currently underway to evaluate the effectiveness of transcutaneous LLVNS in reducing ambulatory (NCT02548754) as well as postoperative AF (NCT02783157).

Baroreceptor stimulation. Mechanoreceptors in the carotid sinus and aortic arch (baroreceptors) generate dynamic feedback to brainstem centers responsible for autonomic tone, thereby exerting beat-to-beat control of blood pressure and heart rate (76). Electric stimulation of carotid baroreceptors reduces sympathetic tone (77) while augmenting vagal tone (78). Thus, baroreceptor stimulation (BRS) has the capacity to generate both pro-arrhythmic and antiarrhythmic influences relative to AF. In a canine model of low-level BRS at a voltage below the threshold to lower systemic blood pressure, 2 h of BRS was associated with increased AERP, increased AF threshold, and decreased cardiac AGP activity (79). This effect was further confirmed in porcine model of high- versus low-level BRS in simulated OSA, where low-level BRS prolonged AERP and reduced AF inducibility, whereas high-level baroreceptor stimulation shortened AERP and did not meaningfully impact AF inducibility. Whether low-level BRS can reduce the occurrence of AF remains to be seen. However, investigation into this potential avenue of neuromodulation for treatment of AF continues.

FUTURE OUTLOOK. Given the increasing prevalence as well as the morbidity associated with AF, new strategies to prevent or reduce AF remain an important unmet need. There has been great progress with current therapeutic strategies to reduce the morbidity of AF, including ablation-based as well as pharmacologic techniques. However, current therapies incompletely use the developing mechanistic understanding of the pathogenesis of AF. Because the ANS is an important contributor in the development of AF, strategies to modulate autonomic signaling hold significant promise in reducing both the incidence and consequences of AF. As outlined above, a number of early-stage clinical trials are ongoing to directly translate promising basic science findings into safe, efficacious strategies to reduce AF (**Table 2**). As the evidence base surrounding autonomic modulation to reduce AF continues to develop, one can anticipate a growing number of effective strategies using autonomic modulation to reduce AF.

VENTRICULAR TACHYCARDIA

RATIONALE FOR AUTONOMIC MODULATION FOR VENTRICULAR TACHYCARDIA. Despite improvements in our therapies for cardiovascular disease,

ventricular tachycardia (VT) and ventricular fibrillation (VF) remain significant challenges in cardiovascular practice. These life-threatening dysrhythmias are particularly common in cardiac and surgical intensive care units, and are responsible for more than 450,000 deaths every year in the United States alone (80). The sympathetic nervous system (SNS) plays a significant role in the genesis of ventricular arrhythmias, and thus represents an important therapeutic target (**Central Illustration**).

The interaction between the SNS and the heart can be reduced to efferent signals to the heart and afferent signaling from the heart. Sympathetic efferent signaling induces maladaptive changes in ventricular electrophysiology. Sympathetic activation has been shown to be able to either activate or maintain ventricular arrhythmias via the following mechanisms: 1) shortened refractory periods (81,82); 2) abbreviated action potential duration (83,84); 3) increased dispersion of refractoriness (85); 4) increased heterogeneity of repolarization (86), and; 5) induced early afterdepolarizations (87). In sum, sympathetically mediated changes in electrophysiology decrease the ventricular threshold and can induce ventricular arrhythmias. Furthermore, the underlying cardiomyopathy often results in autonomic imbalance and dysregulation as a result of underlying structural changes (scar/fibrosis) or persistent/recurrent states of HF (**Figure 3**).

It is now increasingly well understood that the afferent inputs from the heart and peripheral organs (such as the kidney to the ANS) contribute to maladaptive remodeling of the ANS in the presence of myocardial injury. For example, investigations in a canine model of MI have shown that myocardial injury induces morphologic and neurochemical changes in the bilateral stellate ganglia approximately 5 weeks after the initial insult (88,89). Beyond an increase in neuronal size, MI results in a persistent increase in the synaptic density of bilateral stellate ganglia and is associated with increased stellate ganglion nerve activity for up to 8 weeks.

Furthermore, there is evidence of circadian variation in the stellate ganglion nerve activity. Changes in gene expression and neuronal structure are not restricted to the stellate ganglia but can also be found in the dorsal root ganglia of the spinal cord (90,91). Finally, even without an apparent neuroanatomical link between renal nerves and the cardiac sympathetic tone, direct or indirect (myocardial ischemia) renal nerve activation leads to central nervous remodeling (stellate ganglia) with direct impact on cardiac sympathetic tone (92). These results suggest a potential mechanistic link between neural remodeling and ventricular arrhythmias.

PAST AND PRESENT. Current strategies in autonomic modulation for ventricular arrhythmias. ***Clinical management.*** At present, clinical management of VT/VF is often restricted to pharmacological therapy and catheter ablation (**Table 3**). In the setting of VT/VF storm, the underlying sympathetic hyperactivation is further exacerbated by ventricular arrhythmias, internal or external defibrillations, pain, anxiety, and progressive HF (93). Initial medical management that targets the ANS includes beta blockade.

Use of beta blockade is commonly the first and most important pharmacologic intervention for preventing VT/VF given its effectiveness in reducing sympathetic tone. However, beta blockade in the acute setting of electrical storm (≥ 3 VT/VF episodes in 24 h) is often underused due to concerns for potential beta blockade–induced cardiac decompensation. The recently presented clinical study evaluating a non-selective beta blocker propranolol versus a selective beta blocker metoprolol in the setting of electrical storm has shown the safety and effectiveness of nonselective beta blockers in patients with high morbidity and mortality (94). In these patients, propranolol led to less ventricular arrhythmia compared with metoprolol. However, VT and VF are often refractory to medical management including beta blockade, antiarrhythmic drug therapy, and even mechanical hemodynamic support. Although monomorphic VT and premature ventricular contraction - triggered polymorphic VT may be amenable to successful radiofrequency ablation, this approach is not always immediately feasible, especially in critically ill or hemodynamically unstable patients.

Surgical approach. The concept of physically interrupting cardiac sympathetic innervation to treat ventricular arrhythmias was first introduced by Schwartz et al. (95), who studied the interaction of the ANS with ventricular arrhythmias and showed that surgical cardiac denervation increases the ventricular arrhythmia threshold in healthy dogs (n = 11), preventing induction of VT/VF with external stimulation. In the 1990s, unilateral (predominantly left-sided) surgical sympathectomy was applied in patients (n = 40) at high risk for ventricular arrhythmias after an MI and was found to reduce risk of sudden death significantly compared to controls without pharmacologic or surgical sympathetic inhibition (96). Given the success with SGB in patients with MI, surgical sympathectomy has been used to

treat patients with long-QT syndrome and catecholaminergic polymorphic VT (97).

Because unilateral sympathetic denervation may be insufficient in some cases, bilateral surgical sympathetic denervation has been proposed as an alternative and more effective therapy (98). Bilateral sympathetic denervation may be more effective due to bilateral stellate ganglion remodeling with cardiac injury (89) and anatomical variation in cardiac innervation (99). Ajijola et al. (98) have shown that bilateral surgical cardiac sympathetic denervation can be useful for the treatment of medically refractory electrical storm due to a number of causes and may result in improved outcomes compared to unilateral surgical denervation (100). With the exception of a single prospective study (96) that compared surgical sympathectomy to placebo, contemporary studies have been limited to retrospective observational studies. The largest published experience now encompasses 121 cases, and shows an association with decreased sustained VT and implantable cardioverter-defibrillator (ICD) shocks in patients with refractory VT (101).

Interventional approaches. Today, the modulation of the autonomic tone via operative sympathetic denervation (i.e., sympathectomy) is considered a useful intervention only when all other therapeutic options have been exhausted. However, not infrequently, patients presenting with electrical storm (≥3 VT/VF episodes in 24 h) have either failed traditional therapeutic approaches or are deemed too unstable to undergo surgical sympathectomy. These situations have led some investigators to use minimally invasive approaches to achieve temporary blockade cardiac sympathetic innervation. As a result, minimally invasive approaches to cardiac sympathetic blockade have emerged as therapeutic options and diagnostic tools to help gauge whether a given patient would benefit from the permanent surgical sympathectomy (**Figure 2**). Notably, interventional approaches to modulate the ANS in patients with VT are not widely adopted and often limited to select institutions across the world.

SGB. Similar to the limited evidence base for the use of SGB in the treatment of AF, the utility of SGB for the treatment of ventricular arrhythmias has been chronicled in individual case reports (102,103). Moreover, SGB has never been investigated in a prospective, controlled clinical study for the treatment of VT/VF. A systematic review of the literature yielded 35 published cases using mostly unilateral SGB (86% of cases) (104). SGB resulted in a significant reduction of ventricular arrhythmia episodes from 24-h pre- to 24-h post-SGB (mean, 16.5; 95% confidence interval [CI]: 9.7 to 23.1 events vs. mean, 1.4; 95% CI: 0.85 to 2.01 events; $p = 0.0002$) (104). The need for defibrillation decreased comparably (pre-SGB mean, 14.2; 95% CI: 6.8 to 21.6 events vs. post-SGB mean, 0.6; 95% CI: 0.3 to 0.9 events; $p = 0.0026$). Importantly, SGB was associated with a reduction of ventricular arrhythmia burden regardless of the etiology of cardiomyopathy (nonischemic vs. ischemic), type of ventricular arrhythmia (monomorphic vs. polymorphic), and degree of contractile dysfunction (preserved vs. reduced ejection fraction). In this series of uncontrolled observations, SGB was followed by surgical sympathectomy in 21% of cases.

An observational study of several different methods of autonomic blockade for the treatment of electrical storm has shown a substantial difference in mortality (~60% absolute risk reduction compared with standard care) in 49 patients (only 6 received unilateral percutaneous SGB) (105). Finally, the repeated observation that SGB is associated with a prolonged duration of arrhythmia suppression (3 to 4 days) well beyond what is expected from the duration of a pharmacological bock (~1 day) (102,103,106) suggests the presence of an afferent mechanism with potential effects on neural remodeling. The safety profile of this intervention appears to be favorable given the ability to deliver the nerve block under ultrasound guidance.

Thoracic epidural anesthesia. An alternative pathway to block the central sympathetic output and input to/from the heart is thoracic epidural anesthesia (TEA). Using an established anesthetic approach, TEA blocks afferent and efferent innervation between the heart and CNS. Anti-arrhythmic properties of TEA have been shown in several preclinical models (107,108). The safety and efficacy of thoracic epidural anesthesia was explored as part of several small case series (109,110). Successful reduction of ventricular arrhythmia burden was achieved in the majority of patients with refractory arrhythmias (6 of 11 patients, 55%). Notably, the use of thoracic epidural anesthesia is limited in the setting of antiplatelet or oral anticoagulation therapy due to concerns for high-risk bleeding.

Developing neuromodulatory approaches. ***Alternative approaches to cardiac sympathetic modulation.*** Beyond the direct surgical or minimally invasive approaches to modulate the autonomic innervation of the heart, there are series of novel interventional approaches to alter the sympathetic nervous tone. Spinal cord stimulation (SCS) at the level of T1 to T5 can modulate autonomic output, likely via inhibition of the stellate

ganglia, and possibly increased vagal activity (111,112). In animal models, SCS reduces HRV, decreases the incidence of ventricular arrhythmias, and reduces left stellate ganglion activity in acute MI (111). There are limited preliminary clinical data regarding the use of SCS. In 2 patients with ischemic and nonischemic cardiomyopathy, SCS reduced the VT and VF burden up to 75% to 100% (113). A prospective, multicenter randomized clinical study (N = 81 patients) that investigated the effects of SCS therapy for the treatment of systolic HF failed to show improved outcomes (114). Nevertheless, the exact mechanism of SCS on ventricular arrhythmias remains to be determined, and the clinical safety and efficacy of SCS for the prevention of recurrent ventricular arrhythmia remains unknown.

Transtracheal cardiac plexus blockade is a most recent novel attempt to interrupt cardiac sympathetic innervation. Sympathetic nerves converge from both stellate ganglia to form the cardiac plexus. Given the anatomical location of the cardiac plexus between pulmonary artery, aortic arch, and anterior wall of the trachea (115), the cardiac plexus is amendable to a transtracheal access. In a recent study, investigators provided initial evidence that temporary interruption of nerve traffic via lidocaine injection can counteract the effects of stellate ganglion stimulation and thus serve as a new avenue for temporary or permanent minimally invasive cardiac denervation (116).

RDN. As previously mentioned, RDN was initially developed for the treatment of hypertension and has been shown to reduce global and regional sympathetic nerve activity (117). In a porcine ischemia model, RDN reduced the number of spontaneous ventricular extrasystoles and VF in a similar manner to beta blocker therapy (118). The effects of RDN on ventricular electrophysiology appear to be independent of its effects on blood pressure as shown in initial preclinical and clinical studies. The early clinical experience with RDN and ventricular arrhythmias has also been encouraging (119). The largest multicenter case series has shown that bilateral RDN in 13 patients with refractory VT was associated with an 85% freedom from VT at 3 months and no periprocedural complications (120). In a second study including 10 patients, RDN led to a significant decrease in VT/VF burden and ICD shocks at 6 months (121). Despite recent advances for RDN as an antihypertensive strategy (122) and our improved understanding of the best procedural approach (46), definitive evidence to support its use as supplementary strategy for ventricular arrhythmias is needed.

VNS. VNS to augment cardiac parasympathetic tone and oppose sympathetic hyperactivation is also being evaluated for the prevention of ventricular arrhythmias. Preclinical studies support a favorable sympatholytic effect of direct efferent via the cervical vagus nerve or indirect afferent VNS via its auricular branches (123). Post-MI models provide additional evidence for the protective myocardial effects of VNS that are heart rate independent. In canine model of MI, high-intensity vagal stimulation led to a 71% VF-free survival versus 40% with low intensity and 10% in the control group (124). In parallel, prophylactic VNS in the setting of MI minimized the risk of VF onset (125).

FUTURE OUTLOOK.

The growing burden of ventricular arrhythmias and their significant morbidity and mortality demands new effective therapeutic approaches. While there are several effective pharmacologic and catheter-based therapies for ventricular arrhythmias, these therapies frequently meet their limits in an increasingly complex medical environment (e.g., use of mechanical circulatory devices). The ANS is a new frontier in the management of ventricular arrhythmias. Before novel therapeutic strategies can be widely adopted in clinical practice, randomized clinical trials are needed to establish evidence of safety and efficacy (**Table 2**).

Given the myriad of new strategies to modulate the autonomic tone, there is a need to develop methods for individualizing treatment based on a given patient's triggers, comorbidities, and underlying pathology. Future therapies do not have to restrict themselves to secondary prevention nor a device-based approach to neuromodulation.

Recently published work has pioneered the use of optogenetic modulation of cardiac sympathetic nerve activity to prevent ventricular arrhythmias (126). Optogenetics is a relatively novel technology applied in neuroscience to silence or enhance neural activity via targeted genetic modification. Viral vectors are used to introduce an inhibitory light sensitive opsin into stellate ganglion neurons to silence them (127). When ArchT (inhibitory light-sensitive opsin) is genetically expressed in targeted cells, it can be activated via illumination using characteristic wavelength. Activation leads to cell hyperpolarization via activation of ionic channels and as a result silences target cells (128,129).

In a canine model, optogenetic (and reversible) stellate ganglia inhibition was protective against myocardial ischemia-induced ventricular arrhythmias (126). This work builds on prior attempts to modulate norepinephrine release from cardiac neurons via optogenetic modification (130). Targeted

genetic modulation resulted in a desired increase in norepinephrine release with consequent stimulation in cardiac function. Arguably, if this technology can be applied in man (cardiac plexus, stellate ganglia, thoracic sympathetic ganglia, and vagus nerve) it could be used as a preventative tool for high-risk patients with ventricular arrhythmias and as a therapeutic tool for patients with recurrent ventricular arrhythmias. The unique on/off property of the optogenetic modification is the central strength of this technology. A major limitation is the current need for direct application to the target nerve structure via injection for example.

The use of autonomic modulation for primary prevention is currently under investigation and if successful could have potentially far-reaching implications. An ongoing prospective randomized clinical trial is exploring the use of surgical sympathetic denervation for primary prevention of sudden cardiac death in patients with heart failure (131).

CONCLUSIONS

Over the past several decades, there has been increasing recognition of the importance of interactions between the heart and the ANS in the pathophysiology of arrhythmias. There are now a multiplicity of potential therapies under development to target several different neurologic targets and structures for both atrial and ventricular arrhythmias. Moving forward, randomized clinical trials will be essential to establish the safety, efficacy, and comparative effectiveness of these new and promising interventions.

ADDRESS FOR CORRESPONDENCE: Dr. Jonathan P. Piccini, Electrophysiology Section, Duke University Medical Center, Duke Clinical Research Institute, PO Box 17969, Durham, North Carolina 27710. E-mail: jonathan.piccini@duke.edu.

REFERENCES

1. Hanna P, Rajendran PS, Ajijola OA, et al. Cardiac neuroanatomy — imaging nerves to define functional control. Auton Neurosci 2017;207:48–58.

2. Beissner F, Meissner K, Bar KJ, Napadow V. The autonomic brain: an activation likelihood estimation meta-analysis for central processing of autonomic function. J Neurosci 2013;33:10503–11.

3. McDougall SJ, Munzberg H, Derbenev AV, Zsombok A. Central control of autonomic functions in health and disease. Front Neurosci 2014;8:440.

4. Shen MJ, Zipes DP. Role of the autonomic nervous system in modulating cardiac arrhythmias. Circ Res 2014;114:1004–21.

5. Armour JA, Murphy DA, Yuan BX, Macdonald S, Hopkins DA. Gross and microscopic anatomy of the human intrinsic cardiac nervous system. Anat Rec 1997;247:289–98.

6. Hou Y, Scherlag BJ, Lin J, et al. Ganglionated plexi modulate extrinsic cardiac autonomic nerve input: effects on sinus rate, atrioventricular conduction, refractoriness, and inducibility of atrial fibrillation. J Am Coll Cardiol 2007;50:61–8.

7. Pistoia F, Sacco S, Tiseo C, Degan D, Ornello R, Carolei A. The epidemiology of atrial fibrillation and stroke. Cardiol Clin 2016;34:255–68.

8. Krijthe BP, Kunst A, Benjamin EJ, et al. Projections on the number of individuals with atrial fibrillation in the European Union, from 2000 to 2060. Eur Heart J 2013;34:2746–51.

9. European Heart Rhythm A, European Association for Cardio-Thoracic S, Camm AJ, et al. Guidelines for the management of atrial fibrillation: the Task Force for the Management of Atrial Fibrillation of the European Society of Cardiology (ESC). Eur Heart J 2010;31:2369–429.

10. Ganesan AN, Chew DP, Hartshorne T, et al. The impact of atrial fibrillation type on the risk of thromboembolism, mortality, and bleeding: a systematic review and meta-analysis. Eur Heart J 2016;37:1591–602.

11. Chen LY, Chung MK, Allen LA, et al. Atrial fibrillation burden: moving beyond atrial fibrillation as a binary entity: a scientific statement from the American Heart Association. Circulation 2018;137:e623–44.

12. Oh S, Choi EK, Zhang Y, Mazgalev TN. Botulinum toxin injection in epicardial autonomic ganglia temporarily suppresses vagally mediated atrial fibrillation. Circ Arrhythm Electrophysiol 2011;4:560–5.

13. Chen PS, Tan AY. Autonomic nerve activity and atrial fibrillation. Heart Rhythm 2007;4:S61–4.

14. Oliveira M, da Silva MN, Timoteo AT, et al. Inducibility of atrial fibrillation during electrophysiologic evaluation is associated with increased dispersion of atrial refractoriness. Int J Cardiol 2009;136:130–5.

15. Patterson E, Lazzara R, Szabo B, et al. Sodium-calcium exchange initiated by the Ca2+ transient: an arrhythmia trigger within pulmonary veins. J Am Coll Cardiol 2006;47:1196–206.

16. Zipes DP, Mihalick MJ, Robbins GT. Effects of selective vagal and stellate ganglion stimulation of atrial refractoriness. Cardiovasc Res 1974;8:647–55.

17. Sharifov OF, Fedorov VV, Beloshapko GG, Glukhov AV, Yushmanova AV, Rosenshtraukh LV. Roles of adrenergic and cholinergic stimulation in spontaneous atrial fibrillation in dogs. J Am Coll Cardiol 2004;43:483–90.

18. Tan AY, Zhou S, Ogawa M, et al. Neural mechanisms of paroxysmal atrial fibrillation and paroxysmal atrial tachycardia in ambulatory canines. Circulation 2008;118:916–25.

19. Bettoni M, Zimmermann M. Autonomic tone variations before the onset of paroxysmal atrial fibrillation. Circulation 2002;105:2753–9.

20. Agarwal SK, Norby FL, Whitsel EA, et al. Cardiac autonomic dysfunction and incidence of atrial fibrillation: results from 20 years follow-up. J Am Coll Cardiol 2017;69:291–9.

21. Baykaner T, Zografos TA, Zaman JAB, et al. Spatial relationship of organized rotational and focal sources in human atrial fibrillation to autonomic ganglionated plexi. Int J Cardiol 2017;240:234–9.

22. Mann SJ. Redefining beta-blocker use in hypertension: selecting the right beta-blocker and the right patient. J Am Soc Hypertens 2017;11:54–65.

23. Pison L, Tilz R, Jalife J, Haissaguerre M. Pulmonary vein triggers, focal sources, rotors and atrial cardiomyopathy: implications for the choice of the most effective ablation therapy. J Intern Med 2016;279:449–56.

24. Kurotobi T, Shimada Y, Kino N, et al. Features of intrinsic ganglionated plexi in both atria after extensive pulmonary isolation and their clinical significance after catheter ablation in patients with atrial fibrillation. Heart Rhythm 2015;12:470–6.

25. Straznicky NE, Grima MT, Sari CI, et al. Neuroadrenergic dysfunction along the diabetes continuum: a comparative study in obese metabolic syndrome subjects. Diabetes 2012;61:2506–16.

26. Somers VK, Dyken ME, Clary MP, Abboud FM. Sympathetic neural mechanisms in obstructive sleep apnea. J Clin Invest 1995;96:1897–904.

27. Friedman DJ, Liu P, Barnett AS, et al. Obstructive sleep apnea is associated with

increased rotor burden in patients undergoing focal impulse and rotor modification guided atrial fibrillation ablation. Europace 2018;20:f337–42.

28. Linz D, Elliott AD, Hohl M, et al. Role of autonomic nervous system in atrial fibrillation. Int J Cardiol 2019;287:181–8.

29. Holmqvist F, Guan N, Zhu Z, et al. Impact of obstructive sleep apnea and continuous positive airway pressure therapy on outcomes in patients with atrial fibrillation-Results from the Outcomes Registry for Better Informed Treatment of Atrial Fibrillation (ORBIT-AF). Am Heart J 2015;169:647–54.e2.

30. Deng F, Raza A, Guo J. Treating obstructive sleep apnea with continuous positive airway pressure reduces risk of recurrent atrial fibrillation after catheter ablation: a meta-analysis. Sleep Med 2018;46:5–11.

31. Piccini JP, Pokorney SD, Anstrom KJ, et al. Adaptive servo-ventilation reduces atrial fibrillation burden in patients with heart failure and sleep apnea. Heart Rhythm 2019;16:91–7.

32. Danik S, Neuzil P, d'Avila A, et al. Evaluation of catheter ablation of periatrial ganglionic plexi in patients with atrial fibrillation. Am J Cardiol 2008;102:578–83.

33. Katritsis D, Giazitzoglou E, Sougiannis D, Goumas N, Paxinos G, Camm AJ. Anatomic approach for ganglionic plexi ablation in patients with paroxysmal atrial fibrillation. Am J Cardiol 2008;102:330–4.

34. Katritsis DG, Pokushalov E, Romanov A, et al. Autonomic denervation added to pulmonary vein isolation for paroxysmal atrial fibrillation: a randomized clinical trial. J Am Coll Cardiol 2013;62:2318–25.

35. Pokushalov E, Romanov A, Katritsis DG, et al. Ganglionated plexus ablation vs linear ablation in patients undergoing pulmonary vein isolation for persistent/long-standing persistent atrial fibrillation: a randomized comparison. Heart Rhythm 2013;10:1280–6.

36. Driessen AHG, Berger WR, Krul SPJ, et al. Ganglion plexus ablation in advanced atrial fibrillation: the AFACT study. J Am Coll Cardiol 2016;68:1155–65.

37. Knuepfer MM, Schramm LP. The conduction velocities and spinal projections of single renal afferent fibers in the rat. Brain Res 1987;435:167–73.

38. Barajas L, Wang P. Myelinated nerves of the rat kidney. A light and electron microscopic autoradiographic study. J Ultrastruct Res 1978;65:148–62.

39. DiBona GF, Kopp UC. Neural control of renal function. Physiol Rev 1997;77:75–197.

40. Kopp UC. Role of renal sensory nerves in physiological and pathophysiological conditions. Am J Physiol Regul Integr Comp Physiol 2015;308:R79–95.

41. Kopp UC, Cicha MZ, Smith LA, Mulder J, Hokfelt T. Renal sympathetic nerve activity modulates afferent renal nerve activity by PGE2-dependent activation of alpha1- and alpha2-adrenoceptors on renal sensory nerve fibers. Am J Physiol Regul Integr Comp Physiol 2007;293:R1561–72.

42. Pokushalov E, Romanov A, Corbucci G, et al. A randomized comparison of pulmonary vein isolation with versus without concomitant renal artery denervation in patients with refractory symptomatic atrial fibrillation and resistant hypertension. J Am Coll Cardiol 2012;60:1163–70.

43. Gal P, de Jong MR, Smit JJ, Adiyaman A, Staessen JA, Elvan A. Blood pressure response to renal nerve stimulation in patients undergoing renal denervation: a feasibility study. J Human Hypertens 2015;29:292–5.

44. Chinushi M, Izumi D, Iijima K, et al. Blood pressure and autonomic responses to electrical stimulation of the renal arterial nerves before and after ablation of the renal artery. Hypertension 2013;61:450–6.

45. Lu J, Wang Z, Zhou T, et al. Selective proximal renal denervation guided by autonomic responses evoked via high-frequency stimulation in a preclinical canine model. Circ Cardiovasc Interv 2015;8. pii:e001847.

46. Fudim M, Sobotka AA, Yin YH, et al. Selective vs. global renal denervation: a case for less is more. Curr Hypertens Rep 2018;20:37.

47. Linz D, Hohl M, Elliott AD, et al. Modulation of renal sympathetic innervation: recent insights beyond blood pressure control. Clin Auton Res 2018;28:375–84.

48. Yamada S, Fong MC, Hsiao YW, et al. Impact of renal denervation on atrial arrhythmogenic substrate in ischemic model of heart failure. J Am Heart Assoc 2018;7. pii:e007312.

49. Linz D, van Hunnik A, Hohl M, et al. Catheter-based renal denervation reduces atrial nerve sprouting and complexity of atrial fibrillation in goats. Circ Arrhythm Electrophysiol 2015;8:466–74.

50. Wang X, Huang C, Zhao Q, et al. Effect of renal sympathetic denervation on the progression of paroxysmal atrial fibrillation in canines with long-term intermittent atrial pacing. Europace 2015;17:647–54.

51. Kiuchi MG, Chen S, Hoye NA, Purerfellner H. Pulmonary vein isolation combined with spironolactone or renal sympathetic denervation in patients with chronic kidney disease, uncontrolled hypertension, paroxysmal atrial fibrillation, and a pacemaker. J Interv Card Electrophysiol 2018;51:51–9.

52. Pokushalov E, Romanov A, Katritsis DG, et al. Renal denervation for improving outcomes of catheter ablation in patients with atrial fibrillation and hypertension: early experience. Heart Rhythm 2014;11:1131–8.

53. Romanov A, Pokushalov E, Ponomarev D, et al. Pulmonary vein isolation with concomitant renal artery denervation is associated with reduction in both arterial blood pressure and atrial fibrillation burden: Data from implantable cardiac monitor. Cardiovasc Ther 2017;35.

54. Feyz L, Theuns DA, Bhagwandien R, et al. Atrial fibrillation reduction by renal sympathetic denervation: 12 months' results of the AFFORD study. Clin Res Cardiol 2018.

55. McLellan AJ, Schlaich MP, Taylor AJ, et al. Reverse cardiac remodeling after renal denervation: atrial electrophysiologic and structural changes associated with blood pressure lowering. Heart Rhythm 2015;12:982–90.

56. Lo LW, Chang HY, Scherlag BJ, et al. Temporary suppression of cardiac ganglionated plexi leads to long-term suppression of atrial fibrillation: evidence of early autonomic intervention to break the vicious cycle of "AF begets AF." J Am Heart Assoc 2016;5:e003309.

57. Nazeri A, Ganapathy AV, Massumi A, et al. Effect of botulinum toxin on inducibility and maintenance of atrial fibrillation in ovine myocardial tissue. Pacing Clin Electrophysiol 2017;40:693–702.

58. Mathew JP, Fontes ML, Tudor IC, et al. A multicenter risk index for atrial fibrillation after cardiac surgery. JAMA 2004;291:1720–9.

59. LaPar DJ, Speir AM, Crosby IK, et al. Postoperative atrial fibrillation significantly increases mortality, hospital readmission, and hospital costs. Ann Thorac Surg 2014;98:527–33.

60. Pokushalov E, Kozlov B, Romanov A, et al. Botulinum toxin injection in epicardial fat pads can prevent recurrences of atrial fibrillation after cardiac surgery: results of a randomized pilot study. J Am Coll Cardiol 2014;64:628–9.

61. Pokushalov E, Kozlov B, Romanov A, et al. Long-term suppression of atrial fibrillation by botulinum toxin injection into epicardial fat pads in patients undergoing cardiac surgery: one-year follow-up of a randomized pilot study. Circ Arrhythm Electrophysiol 2015;8:1334–41.

62. Romanov A, Pokushalov E, Ponomarev D, et al. Long-term suppression of atrial fibrillation by botulinum toxin injection into epicardial fat pads in patients undergoing cardiac surgery: three-year follow-up of a randomized study. Heart Rhythm 2019;16:172–7.

63. Waldron NH, Cooter M, Haney JC, et al. Temporary autonomic modulation with botulinum toxin type A to reduce atrial fibrillation after cardiac surgery. Heart Rhythm 2019;16:178–84.

64. Ogawa M, Tan AY, Song J, et al. Cryoablation of stellate ganglia and atrial arrhythmia in ambulatory dogs with pacing-induced heart failure. Heart Rhythm 2009;6:1772–9.

65. Leftheriotis D, Flevari P, Kossyvakis C, et al. Acute effects of unilateral temporary stellate ganglion block on human atrial electrophysiological properties and atrial fibrillation inducibility. Heart Rhythm 2016;13:2111–7.

66. Connors CW, Craig WY, Buchanan SA, Poltak JM, Gagnon JB, Curry CS. Efficacy and efficiency of perioperative stellate ganglion blocks in cardiac surgery: a pilot study. J Cardiothorac Vasc Anesth 2018;32:e28–30.

67. Chen PS, Chen LS, Fishbein MC, Lin SF, Nattel S. Role of the autonomic nervous system in atrial fibrillation: pathophysiology and therapy. Circ Res 2014;114:1500–15.

68. Patterson E, Po SS, Scherlag BJ, Lazzara R. Triggered firing in pulmonary veins initiated by

in vitro autonomic nerve stimulation. Heart Rhythm 2005;2:624–31.

69. Shen MJ, Hao-Che C, Park HW, et al. Low-level vagus nerve stimulation upregulates small conductance calcium-activated potassium channels in the stellate ganglion. Heart Rhythm 2013;10:910–5.

70. Chinda K, Tsai WC, Chan YH, et al. Intermittent left cervical vagal nerve stimulation damages the stellate ganglia and reduces the ventricular rate during sustained atrial fibrillation in ambulatory dogs. Heart Rhythm 2016;13:771–80.

71. Jiang Z, Zhao Y, Tsai WC, et al. Effects of vagal nerve stimulation on ganglionated plexi nerve activity and ventricular rate in ambulatory dogs with persistent atrial fibrillation. J Am Coll Cardiol EP 2018;4:1106–14.

72. Stavrakis S, Humphrey MB, Scherlag B, et al. Low-level vagus nerve stimulation suppresses post-operative atrial fibrillation and inflammation: a randomized study. J Am Coll Cardiol EP 2017;3:929–38.

73. Chen M, Yu L, Liu Q, et al. Low level tragus nerve stimulation is a non-invasive approach for anti-atrial fibrillation via preventing the loss of connexins. Int J Cardiol 2015;179:144–5.

74. Clancy JA, Mary DA, Witte KK, Greenwood JP, Deuchars SA, Deuchars J. Non-invasive vagus nerve stimulation in healthy humans reduces sympathetic nerve activity. Brain Stimul 2014;7:871–7.

75. Stavrakis S, Humphrey MB, Scherlag BJ, et al. Low-level transcutaneous electrical vagus nerve stimulation suppresses atrial fibrillation. J Am Coll Cardiol 2015;65:867–75.

76. Suarez-Roca H, Klinger RY, Podgoreanu MV, et al. Contribution of baroreceptor function to pain perception and perioperative outcomes. Anesthesiology 2019;130:634–50.

77. Heusser K, Tank J, Engeli S, et al. Carotid baroreceptor stimulation, sympathetic activity, baroreflex function, and blood pressure in hypertensive patients. Hypertension 2010;55:619–26.

78. Linz D, Mahfoud F, Schotten U, et al. Effects of electrical stimulation of carotid baroreflex and renal denervation on atrial electrophysiology. J Cardiovasc Electrophysiol 2013;24:1028–33.

79. Liao K, Yu L, Zhou X, et al. Low-level baroreceptor stimulation suppresses atrial fibrillation by inhibiting ganglionated plexus activity. Can J Cardiol 2015;31:767–74.

80. Zheng ZJ, Croft JB, Giles WH, Mensah GA. Sudden cardiac death in the United States, 1989 to 1998. Circulation 2001;104:2158–63.

81. Burgess MJ, Haws CW. Effects of sympathetic stimulation on refractory periods of ischemic canine ventricular myocardium. J Electrocardiol 1982;15:1–8.

82. Martins JB, Zipes DP. Effects of sympathetic and vagal nerves on recovery properties of the endocardium and epicardium of the canine left ventricle. Circ Res 1980;46:100–10.

83. Taggart P, Sutton P, Chalabi Z, et al. Effect of adrenergic stimulation on action potential duration restitution in humans. Circulation 2003;107:285–9.

84. Zaza A, Malfatto G, Schwartz PJ. Sympathetic modulation of the relation between ventricular repolarization and cycle length. Circ Res 1991;68:1191–203.

85. Opthof T, Coronel R, Vermeulen JT, Verberne HJ, van Capelle FJ, Janse MJ. Dispersion of refractoriness in normal and ischaemic canine ventricle: effects of sympathetic stimulation. Cardiovasc Res 1993;27:1954–60.

86. Vaseghi M, Yamakawa K, Sinha A, et al. Modulation of regional dispersion of repolarization and T-peak to T-end interval by the right and left stellate ganglia. Am J Physiol Heart Circ Physiol 2013;305:H1020–30.

87. Ben-David J, Zipes DP. Differential response to right and left ansae subclaviae stimulation of early afterdepolarizations and ventricular tachycardia induced by cesium in dogs. Circulation 1988;78:1241–50.

88. Ajijola OA, Yagishita D, Reddy NK, et al. Remodeling of stellate ganglion neurons after spatially targeted myocardial infarction: neuropeptide and morphologic changes. Heart Rhythm 2015;12:1027–35.

89. Han S, Kobayashi K, Joung B, et al. Electroanatomic remodeling of the left stellate ganglion after myocardial infarction. J Am Coll Cardiol 2012;59:954–61.

90. Saddic LA, Howard-Quijano K, Kipke J, et al. Progression of myocardial ischemia leads to unique changes in immediate early gene expression in the spinal cord dorsal horn. Am J Physiol Heart Circ Physiol 2018;15:H1592–601.

91. Gao C, Howard-Quijano K, Rau C, et al. Inflammatory and apoptotic remodeling in autonomic nervous system following myocardial infarction. PLoS One 2017;12:e0177750.

92. Li C, Huang D, Tang J, et al. ClC-3 chloride channel is involved in isoprenaline-induced cardiac hypertrophy. Gene 2018;642:335–42.

93. Fukuda K, Kanazawa H, Aizawa Y, Ardell JL, Shivkumar K. Cardiac innervation and sudden cardiac death. Circ Res 2015;116:2005–19.

94. Chatzidou S, Kontogiannis C, Tsilimigras DI, et al. Propranolol versus metoprolol for treatment of electrical storm in patients with implantable cardioverter-defibrillator. J Am Coll Cardiol 2018;71:1897–906.

95. Schwartz PJ, Snebold NG, Brown AM. Effects of unilateral cardiac sympathetic denervation on the ventricular fibrillation threshold. Am J Cardiol 1976;37:1034–40.

96. Schwartz PJMM, Pollavini G, Lotto A, et al. Prevention of sudden cardiac death after a first myocardial infarction by pharmacologic or surgical antiadrenergic interventions. J Cardiovasc Electrophysiol 1992;3:1–16.

97. Wilde AA, Bhuiyan ZA, Crotti L, et al. Left cardiac sympathetic denervation for catecholaminergic polymorphic ventricular tachycardia. N Engl J Med 2008;358:2024–9.

98. Ajijola OA, Lellouche N, Bourke T, et al. Bilateral cardiac sympathetic denervation for the management of electrical storm. J Am Coll Cardiol 2012;59:91–2.

99. Puddu PE, Jouve R, Langlet F, Guillen JC, Lanti M, Reale A. Prevention of postischemic ventricular fibrillation late after right or left stellate ganglionectomy in dogs. Circulation 1988;77:935–46.

100. Vaseghi M, Gima J, Kanaan C, et al. Cardiac sympathetic denervation in patients with refractory ventricular arrhythmias or electrical storm: intermediate and long-term follow-up. Heart Rhythm 2014;11:360–6.

101. Vaseghi M, Barwad P, Malavassi Corrales FJ, et al. Cardiac sympathetic denervation for refractory ventricular arrhythmias. J Am Coll Cardiol 2017;69:3070–80.

102. Hayase J, Patel J, Narayan SM, Krummen DE. Percutaneous stellate ganglion block suppressing VT and VF in a patient refractory to VT ablation. J Cardiovasc Electrophysiol 2013;24:926–8.

103. Tan AY, Abdi S, Buxton AE, Anter E. Percutaneous stellate ganglia block for acute control of refractory ventricular tachycardia. Heart Rhythm 2012;9:2063–7.

104. Fudim M, Boortz-Marx R, Ganesh A, et al. Stellate ganglion blockade for the treatment of refractory ventricular arrhythmias: A systematic review and meta-analysis. J Cardiovasc Electrophysiol 2017;28:1460–7.

105. Nademanee K, Taylor R, Bailey WE, Rieders DE, Kosar EM. Treating electrical storm: sympathetic blockade versus advanced cardiac life support-guided therapy. Circulation 2000;102:742–7.

106. Fudim M, Boortz-Marx R, Patel CB, Sun AY, Piccini JP. Autonomic modulation for the treatment of ventricular arrhythmias: therapeutic use of percutaneous stellate ganglion blocks. J Cardiovasc Electrophysiol 2017;28:446–9.

107. Meissner A, Eckardt L, Kirchhof P, et al. Effects of thoracic epidural anesthesia with and without autonomic nervous system blockade on cardiac monophasic action potentials and effective refractoriness in awake dogs. Anesthesiology 2001;95:132–8. discussion 6A.

108. Kamibayashi T, Hayashi Y, Mammoto T, Yamatodani A, Taenaka N, Yoshiya I. Thoracic epidural anesthesia attenuates halothane-induced myocardial sensitization to dysrhythmogenic effect of epinephrine in dogs. Anesthesiology 1995;82:129–34.

109. Bourke T, Vaseghi M, Michowitz Y, et al. Neuraxial modulation for refractory ventricular arrhythmias: value of thoracic epidural anesthesia and surgical left cardiac sympathetic denervation. Circulation 2010;121:2255–62.

110. Do DH, Bradfield J, Ajijola OA, et al. Thoracic epidural anesthesia can be effective for the short-term management of ventricular tachycardia storm. J Am Heart Assoc 2017;6. pii:e007080.

111. Wang S, Zhou X, Huang B, et al. Spinal cord stimulation protects against ventricular arrhythmias by suppressing left stellate ganglion neural activity in an acute myocardial infarction canine model. Heart Rhythm 2015;12:1628–35.

112. Odenstedt J, Linderoth B, Bergfeldt L, et al. Spinal cord stimulation effects on myocardial ischemia, infarct size, ventricular arrhythmia, and

noninvasive electrophysiology in a porcine ischemia-reperfusion model. Heart Rhythm 2011;8:892–8.

113. Grimaldi R, de Luca A, Kornet L, Castagno D, Gaita F. Can spinal cord stimulation reduce ventricular arrhythmias? Heart Rhythm 2012;9:1884–7.

114. Zipes DP, Neuzil P, Theres H, et al. Determining the feasibility of spinal cord neuromodulation for the treatment of chronic systolic heart failure: the DEFEAT-HF study. J Am Coll Cardiol HF 2016;4:129–36.

115. Janes RD, Brandys JC, Hopkins DA, Johnstone DE, Murphy DA, Armour JA. Anatomy of human extrinsic cardiac nerves and ganglia. Am J Cardiol 1986;57:299–309.

116. Assis FR, Yu DH, Zhou X, et al. Minimally invasive transtracheal cardiac plexus block for sympathetic neuromodulation. Heart Rhythm 2019;16:117–24.

117. Sobotka PA, Harrison DG, Fudim M. The endpoint on measuring the clinical effects of renal denervation: what are the best surrogates. In: Heuser R, Schlaich M, Sievert H, editors. Renal Denervation. London: Springer, London, 2015.

118. Linz D, Wirth K, Ukena C, et al. Renal denervation suppresses ventricular arrhythmias during acute ventricular ischemia in pigs. Heart Rhythm 2013;10:1525–30.

119. Remo BF, Preminger M, Bradfield J, et al. Safety and efficacy of renal denervation as a novel treatment of ventricular tachycardia storm in patients with cardiomyopathy. Heart Rhythm 2014;11:541–6.

120. Ukena C, Mahfoud F, Ewen S, et al. Renal denervation for treatment of ventricular arrhythmias: data from an International Multicenter Registry. Clin Res Cardiol 2016;105:873–9.

121. Armaganijan LV, Staico R, Moreira DA, et al. 6-Month outcomes in patients with implantable cardioverter-defibrillators undergoing renal sympathetic denervation for the treatment of refractory ventricular arrhythmias. J Am Coll Cardiol Intv 2015;8:984–90.

122. Kandzari DE, Bohm M, Mahfoud F, et al. Effect of renal denervation on blood pressure in the presence of antihypertensive drugs: 6-month efficacy and safety results from the SPYRAL HTN-ON MED proof-of-concept randomised trial. Lancet 2018;391:2346–55.

123. Yu L, Wang S, Zhou X, et al. Chronic intermittent low-level stimulation of tragus reduces cardiac autonomic remodeling and ventricular arrhythmia inducibility in a post-infarction canine model. J Am Coll Cardiol EP 2016;2:330–9.

124. Myers RW, Pearlman AS, Hyman RM, et al. Beneficial effects of vagal stimulation and bradycardia during experimental acute myocardial ischemia. Circulation 1974;49:943–7.

125. Vanoli E, De Ferrari GM, Stramba-Badiale M, Hull SS Jr., Foreman RD, Schwartz PJ. Vagal stimulation and prevention of sudden death in conscious dogs with a healed myocardial infarction. Circ Res 1991;68:1471–81.

126. Yu L, Zhou L, Cao G, et al. Optogenetic modulation of cardiac sympathetic nerve activity to prevent ventricular arrhythmias. J Am Coll Cardiol 2017;70:2778–90.

127. Deisseroth K. Optogenetics: 10 years of microbial opsins in neuroscience. Nat Neurosci 2015;18:1213–25.

128. Tsunematsu T, Tabuchi S, Tanaka KF, Boyden ES, Tominaga M, Yamanaka A. Long-lasting silencing of orexin/hypocretin neurons using archaerhodopsin induces slow-wave sleep in mice. Behav Brain Res 2013;255:64–74.

129. Chow BY, Han X, Dobry AS, et al. High-performance genetically targetable optical neural silencing by light-driven proton pumps. Nature 2010;463:98–102.

130. Wengrowski AM, Wang X, Tapa S, Posnack NG, Mendelowitz D, Kay MW. Optogenetic release of norepinephrine from cardiac sympathetic neurons alters mechanical and electrical function. Cardiovasc Res 2015;105:143–50.

131. Chin A, Ntsekhe M, Viljoen C, Rossouw J, Pennel T, Schwartz PJ. Rationale and design of a prospective study to assess the effect of left cardiac sympathetic denervation in chronic heart failure. Int J Cardiol 2017;248:227–31.

132. Bradfield JS, Ajijola OA, Vaseghi M, Shivkumar K. Mechanisms and management of refractory ventricular arrhythmias in the age of autonomic modulation. Heart Rhythm 2018;15:1252–60.

133. Chatterjee NA, Singh JP. Novel interventional therapies modulate the autonomic tone in heart failure. J Am Coll Cardiol HF 2015;3:786–802.

KEY WORDS arrhythmia, atrial fibrillation, autonomic nervous system, ganglionated plexi, neuromodulation, ventricular arrhythmias

Go to http://www.acc.org/jacc-journals-cme to take the CME/MOC/EME quiz for this article.

JACC: BASIC TO TRANSLATIONAL SCIENCE VOL. 4, NO. 4, 2019

ISSN 2452-302X

Letters

Unsaturated Fatty Acids to Improve Cardiorespiratory Fitness in Patients With Obesity and HFpEF

The UFA-Preserved Pilot Study

Heart failure with preserved ejection fraction (HFpEF) and obesity are 2 common and often coexisting conditions that reduce cardiorespiratory fitness (CRF) (1,2).

Intake of unsaturated fatty acids (UFAs), which consist of monounsaturated fatty acids (MUFAs) and polyunsaturated fatty acids (PUFAs), has recently been associated with favorable CRF, body composition, and cardiac diastolic function in patients with obesity and HFpEF (3). A high UFA diet also prevented weight gain and cardiac diastolic dysfunction (3) in a mouse model of Western diet-induced cardiac dysfunction (4), despite similar total caloric and total fats intake. However, the feasibility of a dietary intervention aimed at increasing daily UFA intake in a prospective trial is required in this population to test its potential efficacy in a large randomized controlled trial.

We hypothesized that a 12-week dietary intervention aimed at increasing UFA consumption was feasible in patients with obesity and HFpEF, and would result in increased consumption of UFAs at 12 weeks (primary endpoint), as assessed by both dietary recall and biomarkers. To test this hypothesis, we performed a proof-of-concept trial and enrolled 9 patients with obesity, symptomatic HFpEF (i.e., dyspnea, fatigue), and reduced CRF (<80% of predicted) measured with maximal cardiopulmonary exercise testing, in a single-arm dietary intervention. All study participants provided written consent (NCT03310099).

Dietary intervention consisted of an individualized, in-person meeting with a dietitian at baseline and every 4 weeks thereafter, with a weekly telephone call to support dietary adherence. Dietary intervention was aimed at consuming a recommended daily amount (or more, without upper limit for consumption) of UFA-rich foods: extra-virgin olive oil (54 g), canola oil (54 g), unsalted or lightly salted mixed dry tree nuts (walnuts, hazelnuts, almonds, pecans), and peanuts (28 g), without providing recommendations on caloric intake. In patients who could not consume the recommended foods for personal and/or cultural preferences, the following foods were recommended: unsalted mixed seeds (28 g), Hass avocado (50 g), and fatty fish (salmon, tuna, trout, mackerel, sardines) (170 g). We provided $100 of financial support to purchase the recommended UFA-rich foods at baseline and 12-week visits, as well as $50 at 4- and 8-week visits. At each visit, a standardized 5-pass, 24-h dietary recall (3) was administered by a dietitian and nonfasting plasma UFA (oleic acid [MUFA], α-linolenic acid, and linoleic acid [PUFA]) levels were measured (Salveo Diagnostics Inc., Henrico, Virginia). We also measured exercise time, peak oxygen consumption (VO_2) and peak oxygen (O_2) pulse at baseline and at 12 weeks using a metabolic cart interfaced with a treadmill using a conservative ramping protocol. Physical activity was assessed using the International Physical Activity Questionnaire-short version (IPAQ) to calculate the cumulative metabolic equivalent of task-minutes per week (MET-min/week). The Shapiro-Wilk test was used to assess deviation from a Gaussian distribution with paired Student's *t*-tests and Pearson's rank test with mean ± SD used to examine changes between baseline and 12 weeks for normally distributed variables. Wilcoxon's test and Spearman's rank test with median and interquartile ranges were used to compare abnormally distributed variables, respectively. Statistical analysis was performed using SPSS version 24.0 (IBM, Armonk, New York).

Of 9 patients (6 African American) enrolled, 5 were women; mean age was 54 ± 5 years. All patients had arterial hypertension, and 5 had type 2 diabetes mellitus. Baseline left ventricular EF, N-terminal pro-brain natriuretic peptide, E/e′ ratio, and left atrial volume were 58 ± 4%, 29 pg/ml (range 17.5 to 54 pg/ml), 8.7 ± 2.9, and 57.9 ± 29.7 ml/m^2, respectively. Baseline peak VO_2 was 16.3 ± 5.9 ml/kg^1/min^1 or 53 ± 12% of predicted according to age, sex, height, and ideal body weight. Baseline exercise time and O_2 pulse

FIGURE 1 Dietary and Plasma Level of UFAs, MUFAs, and PUFAs

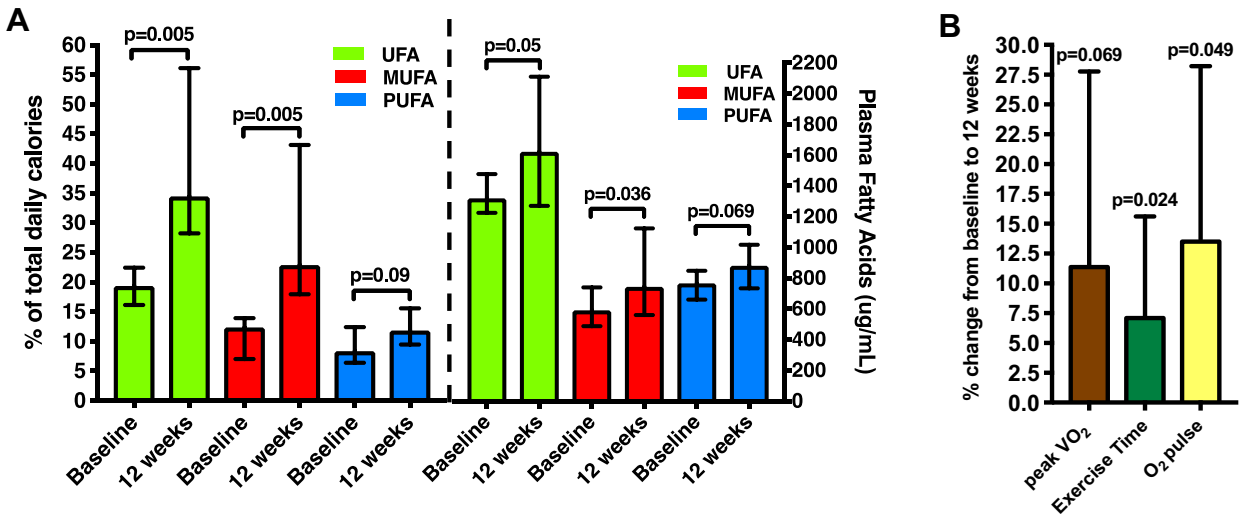

(A) Dietary and plasma level of unsaturated fatty acids (UFAs) (monounsaturated fatty acids [MUFAs], polyunsaturated fatty acids [PUFA]) and **(B)** changes in peak oxygen consumption (VO_2), exercise time, and O_2 pulse.

were 10.7 ± 3.2 min and 12.8 ± 4.8 ml/beat, respectively.

After 12 weeks, patients reported a significant increase in the proportion of daily calories derived from dietary UFAs and demonstrated an increase in plasma UFA biomarkers (Figure 1A). In addition to increased UFA consumption, we observed a significant increase in proportion of calories from total fat consumption ($p = 0.007$), but not a proportion of calories from saturated fatty acids, protein, total calories and milligrams of sodium intake (all $p > 0.05$). We found a significant reduction in the proportion of calories from total carbohydrates ($p = 0.011$) and fructose ($p = 0.02$).

Baseline plasma UFAs, MUFAs, and PUFAs were positively associated with peak VO_2 ($R = +0.79$; $p = 0.036$; $R = +0.75$; $p = 0.052$; $R = +0.79$; $p = 0.036$, respectively) and O_2 pulse ($R = +0.86$; $p = 0.014$; $R = +0.89$; $p = 0.007$; $R = +0.86$; $p = 0.014$, respectively). After 12 weeks of UFA supplementation, we observed a significant improvement in exercise time and O_2 pulse (Figure 1B) with a trend toward a significant increase in peak VO_2 ($p = 0.069$), without significant changes in the respiratory exchange ratio (1.09 ± 0.09 to 1.07 ± 0.11; $p = 0.44$), body mass index (40.0 to 40.2 kg/m^2; $p = 0.21$) or IPAQ-estimated physical activity (1,155 to 1,030 MET-min/wk; $p = 0.67$). Changes in peak VO_2 tended to associate with changes in plasma UFAs ($R = +0.71$; $p = 0.071$), MUFAs ($R = +0.75$; $p = 0.052$), and PUFAs ($R = +0.71$; $p = 0.071$), although the associations did not reach statistical significance ($p < 0.05$).

Although limited by the small sample size and single-arm intervention, for the first time, we showed that a dietary intervention aimed at increasing UFA consumption was feasible and had the potential to improve CRF in patients with severe obesity and HFpEF. Larger randomized controlled trials to test the efficacy of UFA supplementation on CRF and clinical outcomes, as well as understanding the mechanisms through which UFAs may exert these beneficial effects are clearly warranted. Finally, understanding whether the improvements in CRF induced by increased UFA consumption result from improvement in cardiac function or noncardiac factors, such as favorable changes in body composition (5), remains a critical question to investigate in future studies.

*Salvatore Carbone, PhD
Hayley E. Billingsley, RD
Justin M. Canada, PhD
Dinesh Kadariya, MD
Horacio Medina de Chazal, MD
Brando Rotelli, BA
Nicola Potere, MD
Bishal Paudel, BS
Roshi Markley, MD

Dave L. Dixon, PharmD
Cory R. Trankle, MD
Benjamin W. Van Tassell, PharmD
Francesco S. Celi, MD, MHSc
Antonio Abbate, MD, PhD

*VCU Pauley Heart Center
Virginia Commonwealth University
West Hospital
5th Floor, Room 529b
1200 East Broad Street
P.O. Box 980204
Richmond, Virginia 23298
E-mail: salvatore.carbone@vcuhealth.org

https://doi.org/10.1016/j.jacbts.2019.04.001

Please note: The study was supported by the VCU Department of Internal Medicine Pilot Project Grant Program 2017 and by the VCU Pauley Heart Center Pilot Project Grant Program 2017. All authors have reported that they have no relationships relevant to the contents of this paper to disclose.

All authors attest they are in compliance with human studies committees and animal welfare regulations of the authors' institutions and Food and Drug Administration guidelines, including patient consent where appropriate. For more information, visit the *JACC: Basic to Translational Science* author instructions page.

REFERENCES

1. Carbone S, Canada JM, Buckley LF, et al. Obesity contributes to exercise intolerance in heart failure with preserved ejection fraction. J Am Coll Cardiol 2016;68:2487–8.

2. Obokata M, Reddy YNV, Pislaru SV, Melenovsky V, Borlaug BA. Evidence supporting the existence of a distinct obese phenotype of heart failure with preserved ejection fraction. Circulation 2017;136:6–19.

3. Carbone S, Canada JM, Buckley LF, et al. Dietary fat, sugar consumption, and cardiorespiratory fitness in patients with heart failure with preserved ejection fraction. J Am Coll Cardiol Basic Transl Sci 2017;2:513–25.

4. Carbone S, Mauro AG, Mezzaroma E, et al. A high-sugar and high-fat diet impairs cardiac systolic and diastolic function in mice. Int J Cardiol 2015;198:66–9.

5. Del Buono MG, Arena R, Borlaug BA, et al. Exercise intolerance in patients with heart failure. *JACC* State-of-the-Art Review. J Am Coll Cardiol 2019;73:2209–25.

JACC: BASIC TO TRANSLATIONAL SCIENCE VOL. 4, NO. 4, 2019

EDITOR'S PAGE

JACC: Basic to Translational Science

The End of the Beginning

Douglas L. Mann, MD, *Editor-in-Chief: JACC: Basic to Translational Science*

This is not the end. It is not even the beginning of the end. But it is, perhaps, the end of the beginning.

—Winston Churchill (1)

JACC: Basic to Translational Science was launched in February 2015, with a journalistic vision of providing a literary home for those committed to developing new therapies to improve the outcomes of patients afflicted with cardiovascular disease. Over the ensuing 4 years, the journal has sought to publish papers that have a clear translational vector, which the Editorial Board defines as any research that will lead to the development of new therapy. I am excited to announce that beginning with the August issue, *JACC: Basic to Translational Science* will be published monthly. Given that *JACC: Basic to Translational Science* is an open access journal, authors will now be able to have their work disseminated worldwide, within months of the final acceptance of their manuscript.

As Editor-in-Chief, I recognize that journals do not exist in a vacuum, and that any journalistic undertaking takes a village. Accordingly, I would like to acknowledge a number of individuals who have been critical to the journey thus far. First and foremost, I would like to thank the Editorial Board for their commitment to the mission of the journal: Kristen Newby (Deputy Editor), Brian Annex, Nanette Bishopric, Dan Kelly, Juan Granada (Guest Editor), Peter Libby (who coined the term translational vector), W. Robb MacLellan, Geoff Pitt, Robert Roberts (Guest Editor-in-Chief), Eva van Rooij; our woke social media editors, Meena Mathur and Reza Ardehali; Cindy Green, our statistical editor; and Amanda Coniglio, Michelle Kelsey, and Vishal Rao, our talented CME Editors. A very special shout out to Kim Trevey (Managing Editor) for keeping everyone (especially me) organized and on time. I would be remiss if I did not acknowledge the support of our Editorial Consultants (http://basictranslational.onlinejacc.org/content/editorial-board) and the amazing reviewers who have provided fair and balanced reviews in a timely manner. Last, I would like to thank the authors who have entrusted their life's work to a new journal, as well as the awesome readership of *JACC: Basic to Translational Science,* without whose enthusiastic support we would not exist.

Going forward, we are committed to improving the timeliness of our review process, as well as expanding the content of the journal by soliciting targeted reviews and commentaries on topics that are relevant to the field of cardiovascular translational medicine, in order to fulfill our mandate to become *the* forum and learning center for translational cardiovascular investigators in academia and industry, patients and families impacted by heart disease, the National Heart, Lung, and Blood Institute, and the U.S. Food and Drug Administration. As always, we welcome your thoughts about ways we can improve the journal and the kind of content you would like to read in the journal, either through social media (*#JACC:BTS*) or by email (jaccbts@acc.org).

ADDRESS FOR CORRESPONDENCE: Dr. Douglas L. Mann, Editor-in-Chief, *JACC: Basic to Translational Science,* American College of Cardiology, Heart House, 2400 N Street NW, Washington, DC 20037. E-mail: JACC@acc.org.

REFERENCE

1. Churchill W. The End of the Beginning. Available at: http://www.churchill-society-london.org.uk/EndoBegn.html. Accessed July 16, 2019.

ISSN 2452-302X https://doi.org/10.1016/j.jacbts.2019.07.003